University of Nottingham
UK | CHINA | MALAYSIA

Magnetic Resonance Imaging and Spectroscopy Methods for Studying Obesity: Applications for Bariatric Surgery.

ABI SPICER

Thesis submitted the University of Nottingham for the degree of Doctor of Philosophy

SEPTEMBER 2024

Abstract

The prevalence of obesity in the population is increasing globally, leading to a rise in metabolic disorders such as Type-II Diabetes (T2D). Magnetic Resonance Imaging (MRI) and Spectroscopy (MRS) provide safe non-invasive techniques for investigating the physiology and metabolism of the human body. Whilst multinuclear MRS allows metabolic pathways that cannot be measured using ^{1}H methods to be probed, in this thesis ^{13}C and ^{31}P MRS are used to study liver metabolism.

This thesis first provides an outline of the necessary biology and NMR theory to introduce the four experimental chapters. The first experimental chapter, Chapter 3 describes a clinical study using multiparametric ^{1}H MRI and MRS to investigate the changes that occur in T2D and pre-diabetic patients across the bariatric surgery journey. Participants are scanned at 4 timepoints: baseline, following a Very-Low Calorie Diet (VLCD) that precedes surgery, and 6 weeks and 24 weeks post-surgery. MRI findings of the changes in the volume of Subcutaneous Adipose Tissue (SAT) together with volume, fat fraction and MR relaxometry of the liver, spleen, and pancreas measures, are discussed.

The field of multinuclear MRS is ever-growing. However, there are many challenges to applying this research technique to clinical groups with further challenges in obese individuals. Chapter 4 describes the optimisation of RF excitation pulses for abdominal multinuclear MRS using a single-loop surface coil. Block and Half-Passage Hyperbolic Secant pulses for non-localised ^{13}C and 1D ISIS ^{31}P MRS acquisitions are

explored including B_1 field simulations. Simulations using ^{13}C were compared to experimental data taken in a phantom. ^{31}P MRS measures are then tested *in vivo* to study the change in Signal-to-Noise Ratio (SNR) with distance from the surface coil. Methods are then used to inform ^{31}P MRS saturation transfer experiments investigating changes to ATP flux in the liver in two intervention studies, the first on the effect of consuming Inulin Propionate Ester (IPE), a dietary fibre, and the second studying changes following bariatric surgery.

A high Number of Signal Averages are needed for natural abundance multinuclear MRS due to low SNR, resulting in spectra typically acquired whilst free breathing. Chapter 5 explores the effects of respiration on liver ^{1}H spectra as an analogue for understanding the effect of respiration on multinuclear MRS. The shifts in the ^{1}H MRS liver water peak central frequency, Full-Width Half Maximum and amplitude are evaluated and compared to shifts seen in imaging-based dynamic and breath-held liver B_0 maps. Implications of the results for multinuclear MRS are discussed.

Ensuring the reproducibility of any data is key to its scientific value. In the final experimental chapter, Chapter 6, the reproducibility of ^{13}C liver MRS after a tailored meal and overnight fast is assessed. Measures of inter-subject and intra-subject reproducibility are assessed, as well as intra-rater and inter-rater reproducibility, for two raters and an automatic analysis pipeline.

Finally, a summary of key findings and proposals for future work are provided.

Acknowledgements

I would like to thank Professor Penny Gowland and Professor Susan Francis for all the guidance they have given throughout my PhD. Their encouragement was invaluable, and the support they provided through the many challenges that arose was unwavering. I would also like to thank Dr Stephen Bawden, Dr Elizabeth Simpson and Dr Chris Bradley whose knowledge and experience helped me navigate many new challenges. Thank Professor Guru Aithal, Professor Iskandar Idris and Dr Rebekah Wilmington, who collaborated and contributed to projects within this thesis. Thank you to the Medical Research Council IMPACT doctoral training programme for funding my studies. I particularly thank Vikki Harrison and Dr Karen Robinson for their continued support during my studentship. Thank you to the BRC for their funding contributions for the Bariatric Surgery Study.

Thank you to all of the SPMIC for providing me with a space to grow and learn. Many people within or associated with the SPMIC have collaborated or advised on work within this thesis, and I would not have been able to achieve so much without them. Thank you to some new friends, Amy Turnbull, Dr. Rebecca Dewey, Dr. Alex Daniel, Dr. Caitlin Connolly and Dr. Daniel Cocking for allowing me to be a distraction and making completing a PhD an enjoyable process.

Thank you to old friends, Professor Rob Morris, Dr Nicasio Geraldi, Kerry Worton, Kieran Hall, Edward Monkton and Jim Hall for pushing me to new horizons. Your belief in me helped me to believe in myself, and your continued advice and support were not unnoticed.

This PhD is one of the hardest things I have ever done, and without my family, I would not be where I am today. An immense amount of support came from my parents. Thank you to my Mum and Dad, who were always keen to hear about my progress, feed me, and gave me their dog when I was struggling with isolation during the pandemic (which I never gave back). To my brother and sisters Alex, Zoe and Hollie you ensured I remained myself and were always there when I needed to take a break to laugh or complain. Thank you to Richelle (and the other) Nicholls, who provided me with an escape and a home to write my thesis when I needed one.

Thank you to my partner, Jack, who held me up through every down that came with this PhD. You ensured that home was always a safe space to come back to and forced me to take care of myself when I needed it. Your love and support mean the world to me.

There are many more people to thank, and I cannot name them all. I will end with a thank you that cannot be heard. Thank you to Joyce Bywater, a kind neighbour who was my dyslexia tutor for seven years. Before her interventions, I could barely read or write. So, it suffices to say that without her, none of this would be possible.

"Here's to strong women, may we know them, may we be them, may we raise them."

- Amy Rees Anderson

Contents

Acronyms

^{13}C	**Carbon-13**
1D	1-Dimension
^{1}H	Hydrogen-1
^{31}P	Phosporous-31
ADC	Apparent Diffusion Coefficient
ADP	Adenosine DiPhosphate
AFI	Actual Flip Angle
AMARES	Advanced Method for Accurate, Robust and Efficient Spectral fitting
AO	AOrtic
AP	Anterior-Posterior
ATP	Adenosine TriPhosphate
AUC	Area Under the Curve
BARI	BARIatric
bFFE	balanced - Fast Field Echo
BH	Breath Hold
BL	BaseLine
BMI	Body Mass Index
BSA	Body Surface Area
bSSFP	balanced Steady-State Free Precession
BW	Bandwidth
CEST	Chemical Exchange Saturation Transfer
CHESS	CHEmically Selective Saturation
COV	Coefficient Of Variation
CRF	Clinical Research Form
CS	Compressed Sense
CSI	Chemical Shift Imaging
CVD	Cardio Vascular Disease
DDPIV	DipeptiDyl Peptidase 4
DREAM	Dual Refocusing Echo Acquisition Mode
DWI	Diffusion Weighted Imaging
ELISA	Enzyme-Linked Immunosorbent Assay
EPI	Echo Planar Imaging
FA	Flip Angle
F_{ATP}	Forward Flux Rate (ATP)
FB	Free Breathing
FFE	Fast Field Echo
FF_{MRI}	Fat Fraction - MRI
FF_{MRS}	Fat Fraction - MRS
FFT	Fast Fourier Transform

FHWM	Full-Width Half Maximum
FID	Free Induction Decay
FOV	Field Of View
FWHM	Full Width Half Maximum
GE	Gradient Echo
GIP	Gastric Inhibitory Polypeptide
GLP-1	Glucagon-Like Peptide 1
GRASE	Gradient Spin-Echo
HbA1c	Haemoglobin A1c
HIV	Human Immunodeficiency Virus
HPC	High Performance Cluster
HPHS	Half-Passage Hyperbolic Secant
HV	Healthy Volunteer
ICC	Intra-class Correlation Coefficient
IPE	Inulin Propionate Ester
IR	Inversion Recovery
ISIS	Image-Selected In vivo Spectroscopy
ISMRM	International Society for Magnetic Resonance in Medicine
IVIM	IntraVoxel Incoherent Motion
LV	Liver Volume
MMT	Mixed Meal Test
MOIST	Multiple Optimisation Insensitive Suppression Train
MOLLI	MOIdified Look Locker
MR	Magnetic Resonance
MRE	Magnetic Resonance Elastography
MRI	Magnetic Resonance Imaging
MRS	Magnetic Resonance Spectroscopy
MT	Magnetisation Transfer
NADH	Nicotinamide adenine dinucleotide
NAFLD	Non-Alcoholic Fatty Liver Disease
NASH	Non-Alcoholic SteatoHepatitis
NHS	National Health Service
NMR	Nuclear Magnetic Resonance
NSA	Number of Signal Averages
NWS	Non-Water Suppressed
PCr	PhosphoCreatine
PE	Phase Encoding
PIS	Participant Information Sheet
PLD	Post Low-calorie Diet
PPM	Parts Per Million
PRESS	Point RESolved Spectroscopy

PROMET	PROpionate METabolism study
PS	Post Surgery
PV	Pancreatic Volume
REC	Research Ethics Committee
RF	Radio Frequency
RL	Right-Left
ROI	Region Of Interest
RYGB	Roux-en-Y Gastric Bypass
SAR	Specific Absorption Ratio
SAT	Subcutaneous Adipose Tissue
SAT	Subcutaneous Adipose Tissue
SCP	Scan control parameter
SD	Standard Deviation
SD	Standard Deviation
SE	Spin Echo
SENSE	SENSitivity Encoding
SEPS	Spin Echo Phase-Sensitive
SG	Sleeve Gastrectomy
SNR	Signal-to-Noise Ratio
SPIR	Spectral Pre-saturation with Inversion Recovery
SPMIC	Sir Peter Mansfield Imaging Centre
SPMIC	Sir Peter Mansfield Imaging Centre
ST	Saturation Transfer
STE	STimulated Echo
STEAM	STimulated Echo Acquisition Mode
SVS	Single Voxel Spectroscopy
T1D	Type I Diabetes Mellitus
T2D	Type II Diabetes Mellitus
T_{AM}	Morning time point
TCA	TriCarboxylic Acid
TE	Echo Time
TI	Inversion Time
TM	Mixing Time
T_{PM}	Afternoon time point
TR	Repetition Time
UDP-Glucose	Uridine DiPhosphate Glucose
UK	United Kingdom
V1	Visit one
V2	Visit two
VAPOUR	VAriable Power radiofrequency pulses with Optimized Relaxation delay
VAT	Visceral Adipose Tissue

VLCD	Very-Low Calorie Diet
VOI	Volume Of Interest
WHO	World Health Organisation
WS	Water Supressed
YSI	Yellow Springs Instruments

1 Introduction

Obesity is the accumulation of excess body fat which is characterised by a Body Mass Index (BMI) of over 30 kgm^{-2}. The prevalence of obesity is increasing worldwide for both adults and children, with it being considered a form of malnutrition that often poses a risk to a person's health. Obesity is a risk factor for many diseases, including Type-II-Diabetes (T2D), heart disease, stroke and some cancers (1). Magnetic Resonance Imaging (MRI) and Magnetic Resonance Spectroscopy (MRS) are valuable tools for understanding the physiological and metabolic changes that occur in obesity and during weight loss.

This Chapter will give a brief background of the physiology and metabolism studied in this thesis, including the role of the liver, pancreas and spleen in the body. This is followed by the metabolic pathways in the liver, including the role of Adenosine TriPhosphate (ATP) and an overview of T2D. Finally, the aims of this thesis and an overview of the work covered will be provided.

1.1 Physiology and Metabolism

Much of the work in this thesis focuses on metabolism and the study of the liver using MRI and MRS techniques. Chapter 3 studies the physiological changes to the liver, pancreas and spleen over the bariatric surgery journey. The liver sits below the heart in the abdominal cavity, the pancreas below the left lobe of the liver, and the spleen behind the stomach on the opposite side of the body to the liver, as shown in Figure 1.1.

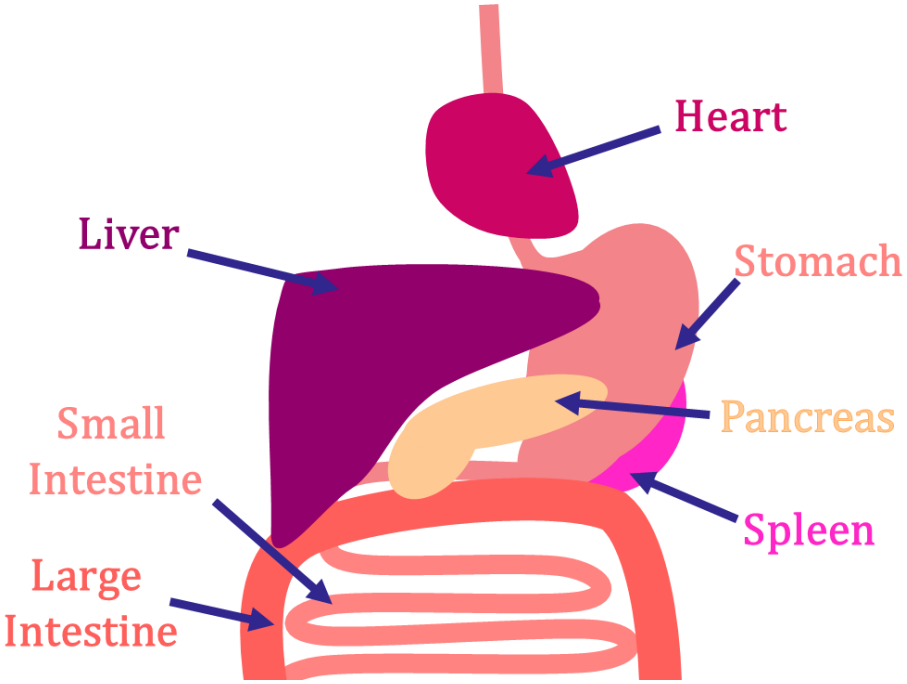

Figure 1.1 - Schematic of organ locations in the chest and upper abdominal region showing the heart, stomach, liver, spleen, pancreas and small/large intestine.

1.1.1 The Liver

The liver is the largest organ in the human body, comprising around 2% of an adult's body weight, and is critical to many basic functions (2). The liver is divided into two lobes (a large right lobe and a smaller left lobe), with approximately 85% of liver tissue being of one cell type, hepatocytes (3). The liver has two blood supplies, one from the portal vein which supplies nutrient-rich blood to the liver, and one from the hepatic artery which supplies oxygen-rich blood. Nutrients derived from food brought to the liver through the portal vein, enter the hepatocytes through active transport or diffusion. Inside the cells, metabolic processes occur, including those related to energy storage. The liver is the primary organ studied in this thesis, with

investigations of the two main forms of energy storage in the liver, lipids and glycogen, as well as investigations into energy production through ATP Flux.

1.1.2 The Pancreas

The pancreas plays a key role in the endocrine system, producing hormones that regulate blood sugar and glandular secretions. The pancreas is divided into three sections: the head, body and tail. It has a lobular structure, with around 80% of the organ's mass made of secretory vesicles. The islet cells are cell clusters inside the pancreas which produce hormones such as insulin, C-peptide and glucagon, all of which play a key role in regulating blood sugar. Insulin (produced by beta-cells within the islets) triggers the liver to begin the process of converting glucose to glycogen for storage, reducing blood glucose concentration, whilst glucagon triggers the liver to convert stored glycogen back to glucose, raising blood glucose concentration. There are multiple diseases that can be linked to issues with pancreatic function, including coeliac disease, cystic fibrosis, as well as obesity and diabetes (4).

1.1.3 The Spleen

The spleen has important functions, including fighting invading germs in the blood, controlling the level of blood cells (white blood cells, red blood cells and platelets), and filtering the blood. Spleen tissue can be split into two categories; lymphoid tissue containing white pulp and blood filtering red pulp. The role of the red pulp is to filter the blood and remove old or damaged red blood cells and recycle iron. The white pulp produces white blood cells which produce antibodies to fight infections.

The spleen can become enlarged when there is an infection in the body or if cirrhosis is present in the liver, important considerations for the study of bariatric patients in Chapter 3 (5,6).

1.1.4 Obesity and Fat Storage

Fat is the body's primary long-term energy store. Much of the fat stored in the body is Subcutaneous Adipose Tissue (SAT) which is the fat that lives between the skin and muscles, but fat can also be found as Visceral Adipose Tissue (VAT) within the abdominal cavity surrounding the organs which is more dangerous to health. The distribution of SAT and VAT are shown in Figure 1.2.

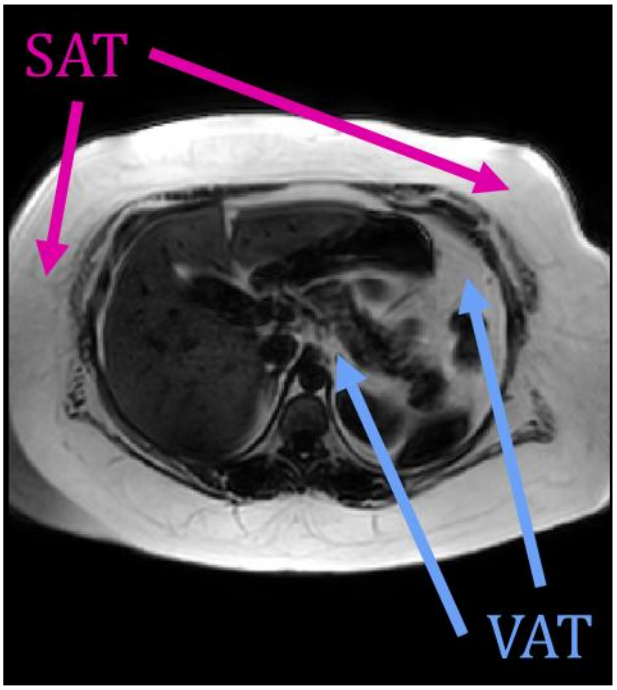

Figure 1.2 – Cross-sectional MRI of the body showing stored Subcutaneous Adipose Tissue (SAT) and Visceral Adipose Tissue (VAT)

The primary purpose of fat is to act as an energy store for the body, though it also provides insulation. Hepatocytes and other cells metabolise the fat through different processes. Fats can also be synthesised by the body or obtained from food; fatty acid synthesis is explored further in Section 1.2.3.

1.1.5 Diabetes

The World Health Organisation (WHO) reported that 8.5% of people over the age of 18 had diabetes in 2014 and that in 2019 diabetes was a direct cause of death for 1.5 million people (7). Diabetes is the dysregulation of blood glucose, and there are three main types: Type I, Type II and gestational. In Type I diabetes, there is a deficiency in insulin production, it is classified as an autoimmune condition with no known cause or prevention; gestational diabetes occurs during pregnancy.

95% of people with diabetes have Type II diabetes (T2D) (4). T2D is caused by the combination of reduced tissue sensitivity to insulin and insufficient insulin secretion by the pancreatic beta cells, both of which lead to continued raised blood glucose concentration. A clinical diagnosis of diabetes is achieved by measuring the degree of glycation of blood haemoglobin (Hemoglobin A1c, HbA1c), which provides an index for the average blood sugar concentration in the past 90 days. Glucose binds to the hemoglobin protein, the higher the prevailing blood glucose concentration in the blood, the more that becomes bound over time, increasing the HbA1c levels. HbA1c values between 5.7% and 6.4% are considered pre-diabetic and 6.5% or higher are diabetic (8).

The risk factors for T2D include ethnicity and lifestyle factors, such as diet, physical activity and obesity. Though the mechanisms behind the link between obesity and T2D are not fully elucidated, there is evidence that it occurs on a cellular level and across organs (9). A particular risk factor for T2D is a high proportion of VAT in the abdominal region. The organs impacted by T2D include the liver, pancreas, skeletal muscle, kidneys, brain, and small intestine (10,11).

1.2 Energy Storage and Production

Energy storage and production are key to maintaining homeostasis in the body. The energy used in the human body is derived from digested food, which is then used in cells or stored. Both the liver and pancreas play key roles in this storage and energy production as shown in Figure 1.3. Food consumed is metabolised to ultimately produce Adenosine TriPhosphate (ATP), used as the body's energy currency within cells. This section discusses the metabolic pathways behind storage and energy production, including glycolysis/ gluconeogenesis, glycogenesis/glycogenolysis, fatty acid synthesis and the TriCarboxylic Acid (TCA) cycle.

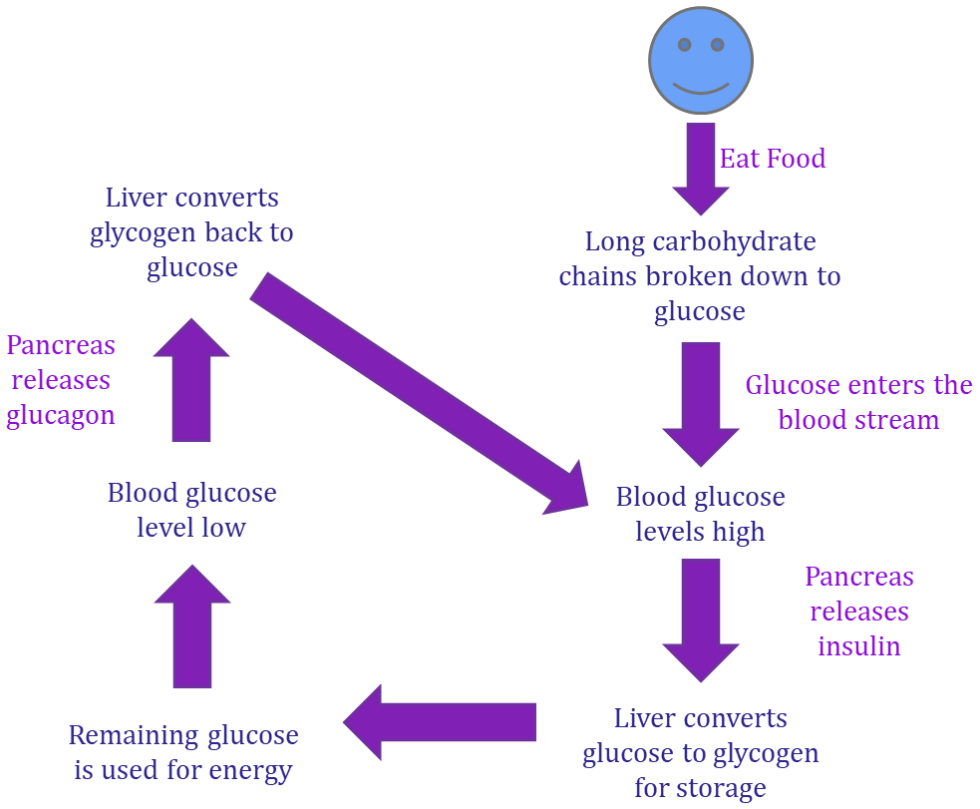

Figure 1.3 - Role of Insulin, Glucagon and Glycogen in energy storage

In the stomach and small intestine, carbohydrates (polysaccharides made up of long chains of sugar units) are broken down into monosaccharides. Glucose, among other monosaccharides, enters the bloodstream and flows into the liver via the portal vein. Inside the liver, monosaccharides are converted into pyruvate through glycolysis (a precursor to ATP production for energy usage), built up to form glycogen (glycogenesis) or converted to lipids for storage as shown in Figure 1.4.

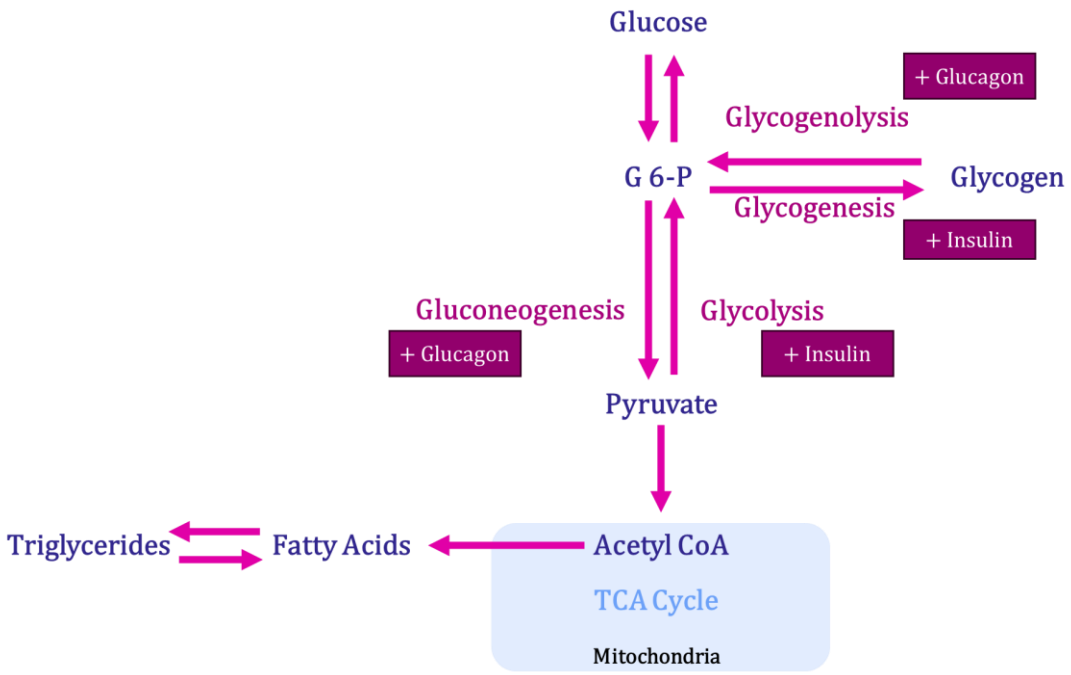

Figure 1.4 - Simplified schematic of metabolic pathways that occur in hepatocytes. G-6-P is glucose-6-phosphate.

1.2.1 Glycolysis and Gluconeogenesis

Glycolysis is the process of converting monosaccharides into pyruvate for use in the TCA cycle and other metabolic pathways. It occurs in hepatocytes and other cells around the body to produce ATP for energy use. In the initial stages of glycolysis, energy is consumed through the breakdown of ATP to Adenosine DiPhosphate (ADP) to phosphorylate glucose. In the later stages of glycolysis, energy is produced through the conversion of ADP to ATP when the phosphorylated intermediary metabolites form pyruvate. Through these processes, one glucose molecule produces two pyruvate and a net production of two ATP (2 destroyed, 4 created). Gluconeogenesis is the opposing pathway to glycolysis. In the liver, it is possible to

reverse the phosphorylation of glucose-6-phosphate to release glucose out of the cell for use elsewhere in the body, such as the brain.

Insulin and glucagon play key roles in regulating this metabolic pathway. Insulin stimulates glucose uptake within the cells, lowering blood sugar concentration, however, insulin does not directly affect glucose uptake in the liver. As previously discussed, insulin plays a key role in T2D, which is explored in Chapter 3. Low blood glucose concentration can initiate hepatic metabolic pathways and stimulate glucagon release from the pancreas. Glucagon stimulates the liver's conversion of stored glycogen into glucose for use in energy production and, when present, allows the body to use fats as an energy source.

1.2.2 Glycogenesis and Glycogenolysis

Glycogenesis is the process of converting glucose into glycogen for storage. Glycogen storage in the liver is explored in Chapter 6. When energy is needed, glycogen is quickly broken down through glycogenolysis. Glycogenesis converts phosphorylated glucose into precursor molecules (such as UDP-glucose), which attach to the first glucosyl unit via a primer molecule, glycogenin. Synthesis continues by adding the glucose molecules to the chain, the glycogenin remains bound at all stages. The breakdown of glycogen is triggered by glycogen phosphorylase, which removes glucose molecules from the chain. The rates of glycogenesis and glycogenolysis are regulated by the enzymes glycogen synthase and glycogen phosphorylase respectively, which are in turn regulated by insulin and glucagon as well as the rate of phosphorylation.

1.2.3 Fatty Acid Synthesis and β-oxidation

In the body, fat is primarily stored as triglycerides which are formed of three fatty acid chains attached to a glycerol backbone. Fatty acids are either saturated (only have single hydrogen bonds) or unsaturated (contain at least one double bond reducing the amount of hydrogen atoms in the chain), as shown in Figure 1.5.

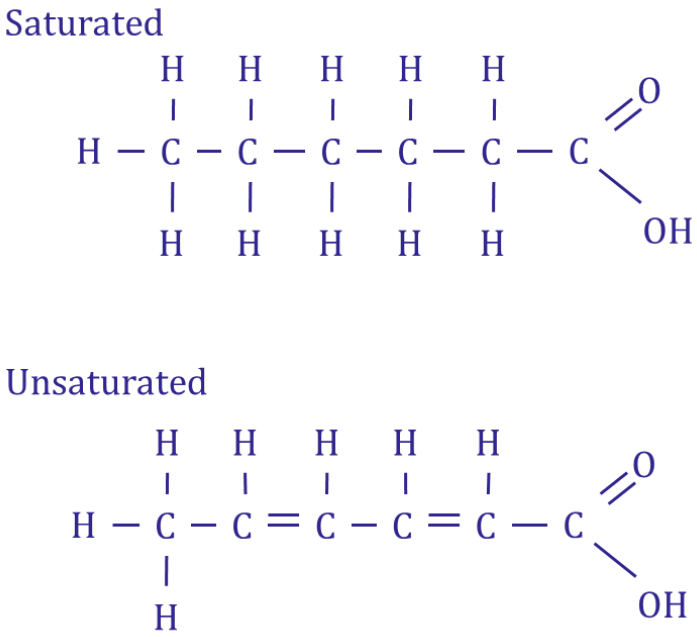

Figure 1.5 Example of a saturated (top) and unsaturated (bottom) fatty acid chain.

Triglycerides cannot be released directly back into the body once they are stored in cells and instead need to be broken down into the fatty acid and glycerol components via lipolysis. During lipolysis enzymes work to break down lipids into free fatty acids. Lipase catalyses this reaction within cells. Once free fatty acids are formed, they are often converted to fatty Acyl-CoA within a cell. Fatty Acyl-CoA

undergoes β-oxidation inside the mitochondria to produce Acetyl-CoA (which can be used in the TCA cycle) yielding ~14 ATP molecules.

1.2.4 TCA Cycle

The TCA cycle occurs in the cell's mitochondria and generates energy through the oxidation of Acetyl CoA which can be created from pyruvate. An illustration of the TCA cycle is shown in Figure 1.6. Many of the steps in the TCA cycle will not be discussed in depth in this thesis. However, much of the energy from the oxidative steps in the TCA cycle are used to form NADH from NAD^+ (Nicotinamide adenine dinucleotide). NADH can later be used to produce ATP from ADP through oxidative phosphorylation.

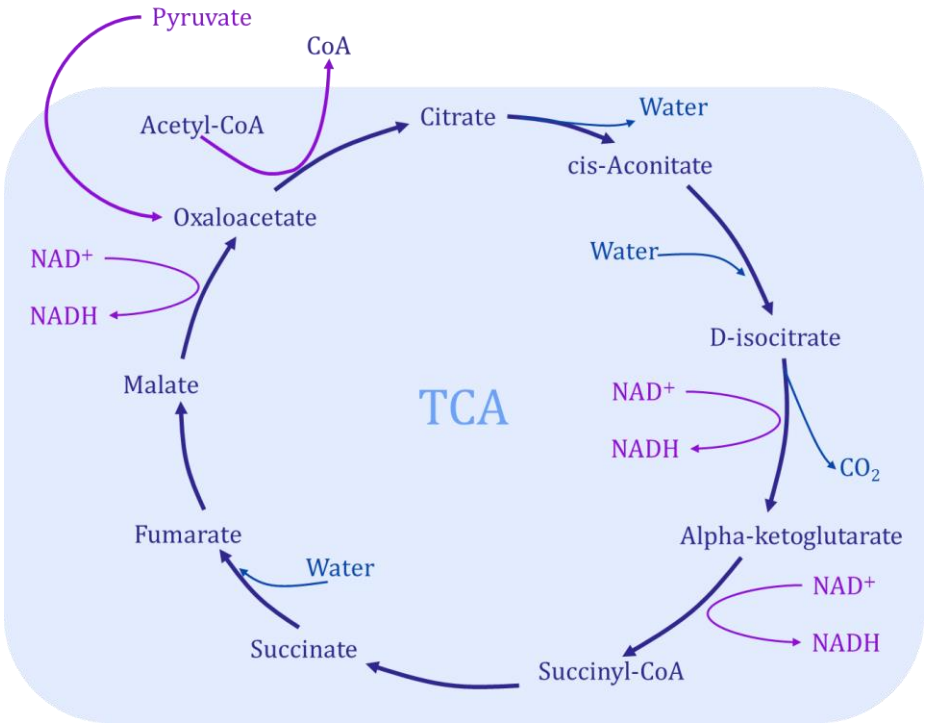

Figure 1.6 - The TCA cycle

1.2.5 Adenosine Triphosphate

Fats and carbohydrates are broken down to make energy for the cells. It is said that ATP is the body's energy currency, with energy is transferred and stored as ATP within cells. ATP is formed from the addition of a phosphate to ADP, from a phosphate donor such as inorganic phosphate (Pi) Figure 1.7.

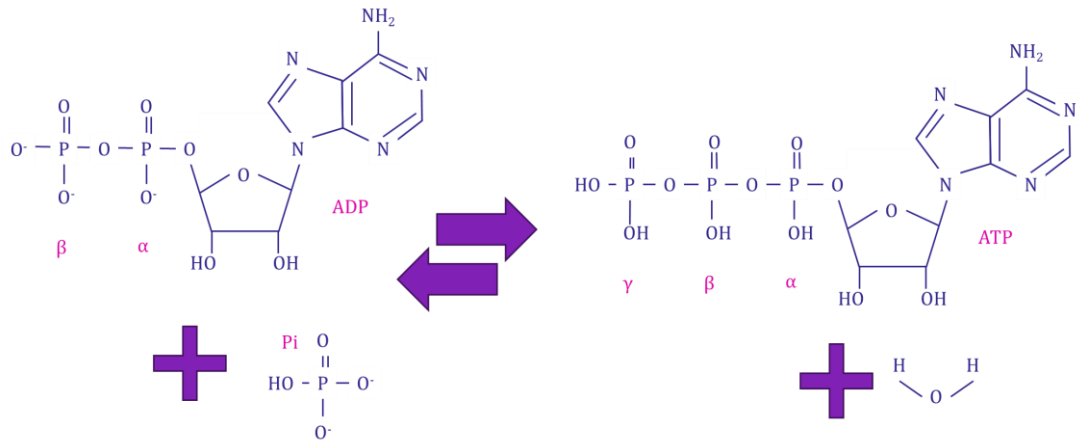

Figure 1.7 - Creation of ATP from ADP and Pi, and the reverse, the conversion of ATP to ADP through hydrolysis

When a cell uses ATP for energy, the bonds between the phosphate tails are broken forming ADP and Pi. This constant exchange between molecules for the formation and destruction of ATP to ADP and Pi is known as ATP Flux and is explored in the liver in Chapter 4. The enzyme AMPK regulates this process through many pathways, including glucose uptake, glycolysis, and glycogen synthesis, to increase or decrease the rate of production as needed. This is the process of ATP homeostasis in cells.

1.3 Thesis Overview

1.3.1 Thesis Aims

This thesis aims to study the metabolic and physiological changes in the body with obesity using Magnetic Resonance Imaging (MRI) and Magnetic Resonance Spectroscopy (MRS), including multinuclear (^{13}C and ^{31}P) MRS, and to optimise the use of these techniques for children and obese individuals.

1.3.2 Thesis Overview

Chapter 2 provides an outline of NMR theory, Magnetic Resonance Imaging and Spectroscopy, as well as safety considerations. This is followed by four experimental chapters of original work.

Chapter 3 describes using MRI and ^{1}H MRS in a bariatric surgery intervention study, where participants were scanned at 4 visits throughout their surgical journey. The goal of this study is to understand the physiological and metabolic changes that occur from the Very Low-Calorie Diet that precedes bariatric surgery, as well as the short (6 weeks) and long (6 months) term effects of bariatric surgery.

Chapter 4 covers the optimisation of ^{31}P MRS for two intervention studies using computational modelling and experimental data. The first intervention study investigates the effects of consuming Inulin Propionate Ester on ATP flux using ^{31}P saturation transfer experiments. The second intervention study is a pilot arm from

Chapter 3 investigating the changes to ATP flux before and after bariatric surgery using ^{31}P saturation transfer experiments.

Chapter 5 studies the consequences of the free-breathing acquisitions on ^{1}H liver MRS, this is then related to the consequences of free-breathing for multinuclear spectroscopy.

The final experimental chapter, Chapter 6, studies the reproducibility of ^{13}C liver MRS in children, exploring both inter- and intra-rater as well as inter- and intrasubject variability.

This work is then discussed in the conclusion chapter (Chapter 7) along with directions for future work.

2 Magnetic Resonance

2.1 Overview

This chapter provides an overview of Nuclear Magnetic Resonance (NMR) theory followed by an introduction to Magnetic Resonance Imaging (MRI) and Magnetic Resonance Spectroscopy (MRS) methods. These techniques are then outlined in more detail across the various experimental chapters. The chapter concludes with a discussion of safety aspects related to MR.

2.2 Nuclear Magnetic Resonance

Nuclear Magnetic Resonance (NMR) requires nuclei with an odd number of protons, neutrons, or both, as these have an inherent property of spin (*I*). The relative sensitivity and natural abundance of different nuclei that can be investigated with NMR are shown in Table 2.1. The relative sensitivity is determined by comparing the signal produced by a given nuclei under investigation to that from hydrogen (^{1}H), whilst the natural abundance describes how much (as a percentage) of the nucleons present are of an NMR-active isotope. In this thesis, NMR studies using ^{1}H, ^{13}C and ^{31}P nuclei are described.

Nucleus	Spin I	Gyromagnetic Ratio ($MHzT^{-1}$)	Relative Sensitivity	Natural Abundance (%)
^{1}H	$^{1}/_{2}$	42.58	1.00	99.99
^{3}He	$^{1}/_{2}$	32.43	0.442	0.0001
^{13}C	$^{1}/_{2}$	10.71	0.016	1.108
^{19}F	$^{1}/_{2}$	40.06	0.833	100
^{23}Na	$^{3}/_{2}$	11.26	0.083	100
^{31}P	$^{1}/_{2}$	17.24	0.066	100
^{129}Xe	$^{1}/_{2}$	11.78	0.021	26.44

Table 2.1 - Properties of NMR active nuclei showing the spin, gyromagnetic ratio, relative sensitivity and natural abundance.

A nucleus with spin has angular momentum ($\boldsymbol{J}$) as it rotates leading to an associated magnetic moment, $\boldsymbol{\mu}$, defined as,

$$\boldsymbol{\mu} = \gamma \boldsymbol{J}$$

Equation 2.1

where γ is the gyromagnetic ratio in units of $MHzT^{-1}$, which is nucleus-specific as outlined in Table 2.1, and describes how a nucleon will interact with an external magnetic field.

The angular momentum of the spin is a vector quantity whose magnitude is defined by,

$$|\boldsymbol{J}| = \hbar\sqrt{I(I+1)}$$

Equation 2.2

where $\hbar$ is Planck's constant (h) divided by 2π and I is the spin angular momentum quantum number. The direction of $\boldsymbol{J}$ is reflected in the magnetic spin quantum number, m_I. When an external field ($\boldsymbol{B}$) is applied, there are $(2I+1)$ possible values for m_I. Thus, for spin ½ nuclei such as ^{1}H, ^{13}C and ^{31}P the value of m_I can take values of ± ½, where spins with m_I = -½ align parallel with the B_0 field and spins with m_I = ½ are antiparallel to the B_0 field.

The potential energy (E) of a magnetic moment in an external field is defined by,

$$E = -\boldsymbol{\mu} \cdot \boldsymbol{B}$$

Equation 2.3

Thus, when a nucleus is placed in an external magnetic field aligned in the z-direction (B_0), the energy E can take two possible values as illustrated in Figure 2.1 given by,

$$E = -J_z B_0 = \pm\frac{1}{2}\gamma\hbar B_0$$

Equation 2.4

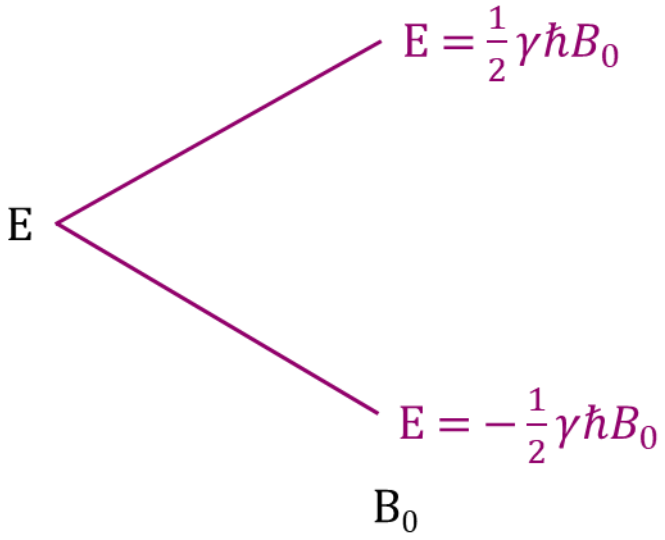

Figure 2.1 - Energy states for a spin 1/2 nucleus in the presence of an external magnetic field B_0

The difference in energy levels between the two spin states is termed the Zeeman energy. As shown in Equation 2.5, this can be related to Planck's constant multiplied by the frequency (ω_0) of a photon that, through the absorption or emission, can modulate the spin system.

$$\Delta E = \gamma \hbar B_0 = \omega_0 h$$

Equation 2.5

ω_0 Is known as the Larmor frequency (typically described in MHz) and is given by the Larmor equation (Equation 2.6) through the strength of the external magnetic field multiplied by the gyromagnetic ratio.

$$\omega_0 = \gamma B_0$$

Equation 2.6

The Boltzmann distribution describes the ratio of spins between the high (spin-up, ½) and low (spin-down, -½) energy states with the two energy levels described according to

$$\frac{N_{high}}{N_{low}} = e^{-\frac{\Delta E}{k_B T}} = e^{-\frac{\gamma \hbar B_0}{k_B T}}$$

Equation 2.7

where *N* is the number of spins in the high (N_{high}) and low (N_{low}) energy states respectively, k_B is the Boltzmann constant, and *T* is the temperature of the system. In the case of the high-temperature limit, where $k_b T \gg \gamma \hbar B_0$, this reduces to,

$$\frac{N_{high}}{N_{low}} \approx 1 - \frac{\gamma \hbar B_0}{k_B T}$$

Equation 2.8

The difference in the populations between two spin states, N_s, leads to a net equilibrium magnetisation (M_0) along the z-axis given by,

$$M_0 \approx \frac{\gamma^2 \hbar^2 B_0 N_s}{4 k_b T}$$

Equation 2.9

which can be seen to be proportional to the external magnetic field (B_0) and inversely proportional to the temperature (T). For protons in a 3 Tesla external magnetic field the population difference N_s is of the order of 10 parts per million (ppm).

The angular momentum of the spins will experience a torque causing precession around the applied field at the Larmor frequency and resulting precession of the net magnetisation vector as shown in Figure 2.2. This precession of magnetisation ***(M)*** in the presence of an applied field ($\boldsymbol{B_0}$) is described by,

$$\frac{d\boldsymbol{M}}{dt} = \gamma(\boldsymbol{M} \times \boldsymbol{B_0})$$

Equation 2.10

.

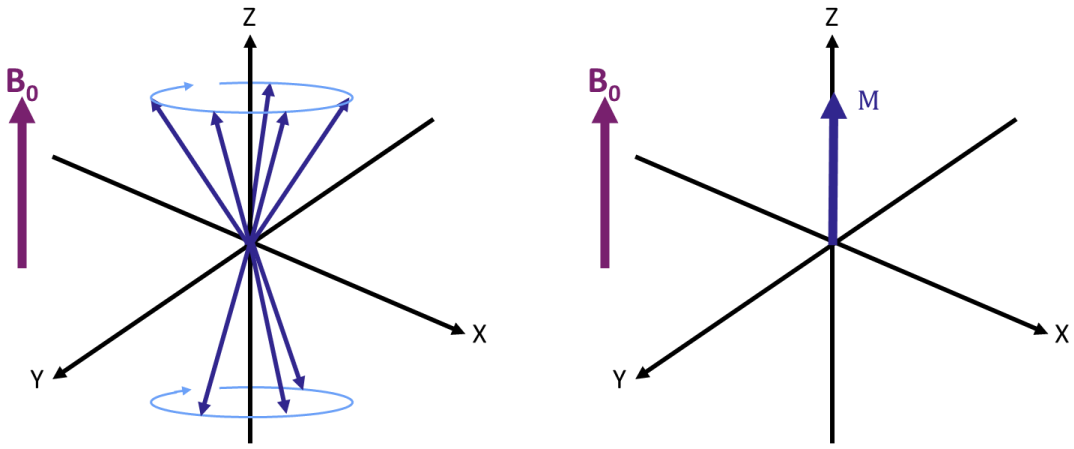

Figure 2.2 - Left - the magnetisation vectors from individual spins, with schematic showing more spins in the low energy state (spin-up) than high energy state (spin-down), giving a net magnetisation vector, M_0 (Right). Note that in practice this difference is of approximately 10 parts per million for protons at 3T.

Typical B_0 field strengths of clinical MR systems are 1.5 and 3 Tesla (T), with research-based human scanners at ultra-high field of 7 T, 9.4 T and most recently reaching 11.7 T, there has also been a recent push towards lower field, with 0.5 and 0.1 T systems which provide more accessibility. In this thesis, data is collected at 3 T on both a Philips Achieva and a wide-bore Philips Ingenia scanner (Philips Medical), as shown in Figure 2.3.

Figure 2.3 - University of Nottingham Left - 3T Philips Achieva and Right- Wide-bore 3T Philips Ingenia (12,13)

2.2.1 Excitation

The next component is the application of a radiofrequency (RF) magnetic field (termed the $\mathbf{B_1}$ field) at a frequency closely matched to the Larmor frequency of the precession of the spins. The $\mathbf{B_1}$ is needed to induce phase coherence within the spins and tip the magnetisation into the transverse forming the net magnetisation **M** for measurement, or otherwise manipulate the nuclear magnetisation.

The RF field is transmitted using an RF coil, sometimes the same coil is used to both transmit and receive the MR signal. In Chapters 4 and 6 a single-loop coil, the simplest form of a surface coil, is used for both transmit (Tx) and receive (Rx) when studying ^{13}C and ^{31}P measures. In Chapter 5 a butterfly Tx/Rx loop is used for ^{1}H measures. In Chapter 3, the body RF coil is used for ^{1}H measures with a separate receive coil for signal detection.

When assessing the effect of the $\mathbf{B_1}$ field on the net magnetisation vector, there are two frames of reference that can be considered: the laboratory reference frame (X, Y, Z) or the rotating reference frame (X', Y', Z' = Z), as shown in Figure 2.4. The

rotating reference frame rotates at the same frequency as the Larmor frequency defined by the main magnetic field (ω_0). Considering the effect of an RF pulse applied at a frequency ω_1 matched to ω_0, the 'on-resonance' condition, in the laboratory reference frame the net magnetisation will precess around the z-axis as it is tipped about the x-axis. However, when viewing in the rotating frame of reference of $\omega_1 = \omega_0$, the precession of the net magnetisation ***M*** about z is removed, allowing simple visualisation of the net magnetisation being tipped about the x'-axis.

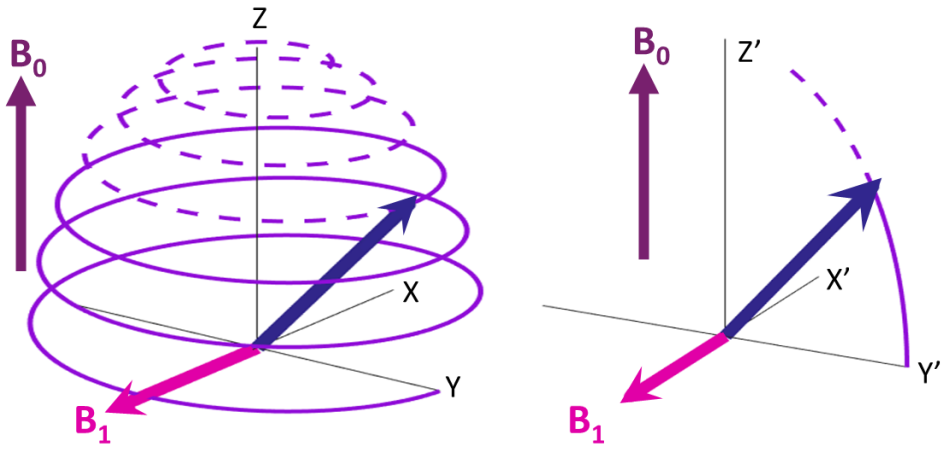

*Figure 2.4 – Precession of magnetisation vector **M** (shown by the blue arrow) in the (left) laboratory reference frame (X,Y,Z) and (right) rotating reference frame (X',Y',Z' = Z).*

The amplitude and duration of the shaped RF pulse determines how much energy is transferred to the spins and, hence, how much they are tipped from the z-axis, these factors are discussed further in Section 2.4.4. The amount of tip is known as the flip angle (α) and is given by the integral,

$$\alpha = \int_0^T \gamma B_1(t)\, dt$$

Equation 2.11

A flip angle of 90° refers to when the spins are tipped into the x-y plane perpendicular to $\mathbf{B_0}$, whilst a 180° pulse is used to invert the spins about the z-axis or to form an echo (see Section 2.2.3).

The shape of the RF pulse determines the excitation profile, which can be approximated using the Fourier transform, Figure 2.5 (14).

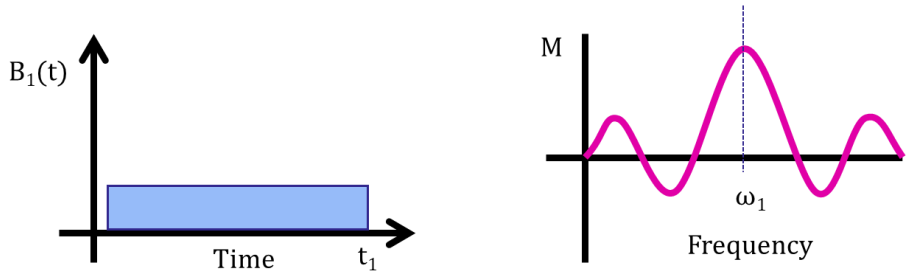

Figure 2.5 – (left) block RF pulse and (right) its frequency profile, The width of the central excitation frequency (ω_1) is dependent on $1/t_1$, where t_1 is the pulse duration.

2.2.1.1 Off- Resonance Effects

The tipping of the magnetisation vector described above holds true for spins oscillating at a Larmor frequency matched to the frequency of the applied RF pulse, i.e. 'on-resonance' for which $\omega_1 = \omega_0$. However, in practice, many factors can lead to B_0 field inhomogeneity, thus leading to a non-uniform precession frequency of the

spins, and this is called 'off-resonance'. Further, no B_1 field is perfect and hence even when exactly the Larmor frequency is desired there are portions of the image or sample that may not experience exactly this and instead receive an 'off-resonance' frequency (as illustrated by the Fourier transform of RF pulses shown above in Figure 2.5).

The following considers what happens when B_1 is applied at a frequency ω_1 that is not exactly matched to the Larmor frequency ω_0. If the rotating frame is now locked to the 'off-resonance' frequency of the RF pulse, ω_1 (so $\omega_1 \neq \omega_0$) the B_0 field does not disappear but has a residual component $\mathbf{B_z'}$,

$$B_z' = \frac{\omega_0 - \omega_1}{\gamma}$$

Equation 2.12

In this rotating frame $\mathbf{B_z'}$ and $\mathbf{B_1}$ vectorially add together resulting in an effective field $\mathbf{B_{eff}}$ which the spins will rotate about, as shown in Figure 2.6). The angle between $\mathbf{B_1}$ and $\mathbf{B_{eff}}$ is minimised when $B_1 \gg B_z'$, as is achieved using high-power RF pulses.

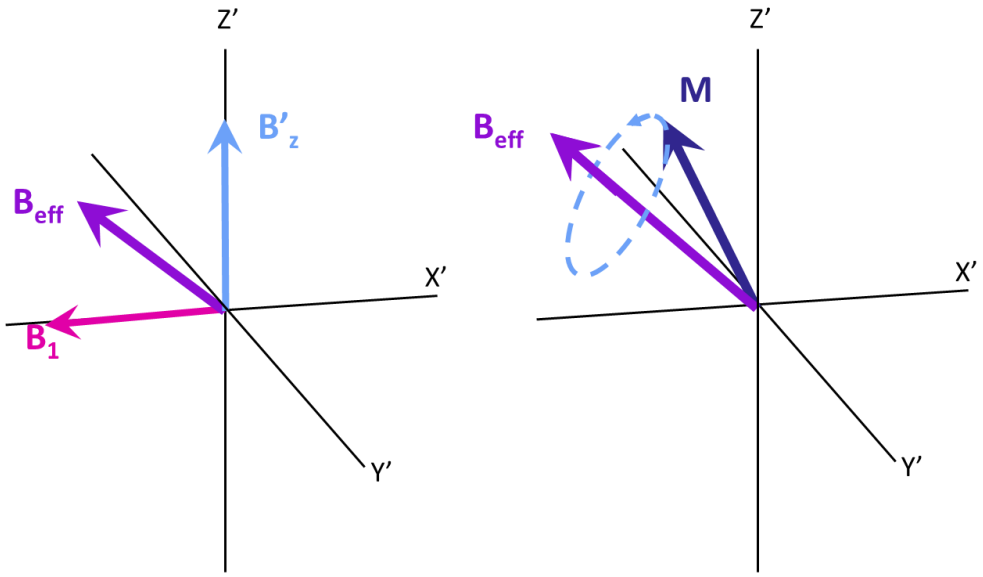

Figure 2.6 – (Left)The formation of $\boldsymbol{B_{eff}}$ *from* B_1 *and* B'_z*. (Right) The precession of* $\boldsymbol{M}$ *around* $\boldsymbol{B_{eff}}$ *when* $\omega_0 \neq \omega_1$

There are a number of interesting MR techniques in which the B_1 frequency is purposely offset from resonance or swept through frequencies on either side of the Larmor frequency. For nuclei such as ^{13}C and ^{31}P, the spectra span a large range of chemical shifts. For these nuclei, off-resonance effects need to be accounted for using advanced techniques such as specialised RF pulse shapes as is discussed in Chapter 4.

2.2.2 Signal Detection

After the application of a 90^0 RF pulse, the magnetisation will be tipped into the xy-plane. In keeping with Faraday's law, if a loop of wire is placed near an oscillating or, in this case, precessing field, it will induce an oscillating current at the Larmor frequency with a decay envelope given by the transverse relaxation time constant

T_2* (see Section 2.13). This oscillating current is detected to provide the simplest form of the MR signal termed the Free Induction Decay (FID) (Figure 2.7).

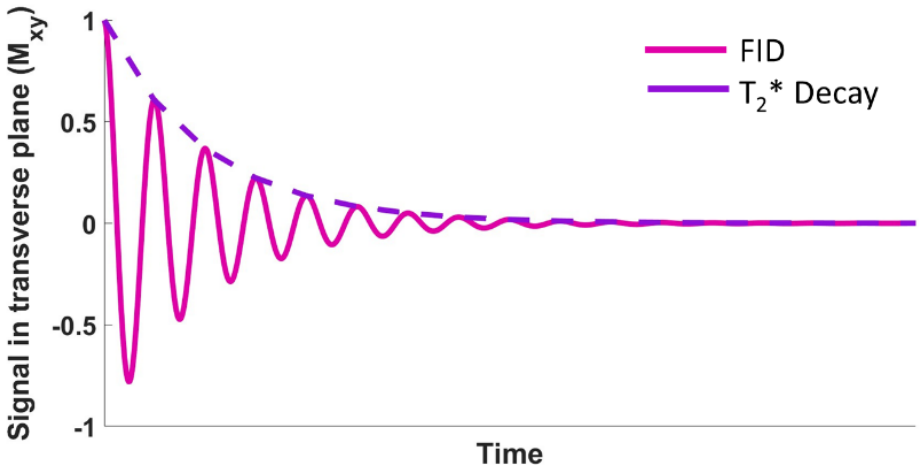

*Figure 2.7 - The free induction decay (FID) following a 90° RF pulse oscillating at the Larmor frequency with an exponential decay envelop determined by the transverse relaxation time constant T_2**

2.2.3 MR relaxation

Once the RF pulse ceases, the energy that was absorbed is re-emitted as the spins return to equilibrium through relaxation, and the magnetisation will relax back to alignment with B_0 and dephase through longitudinal and transverse relaxation processes. This relaxation process is described by the Bloch equations:

$$\frac{dM_z}{dt} = -\frac{(M_z - M_0)}{T_1}$$

$$\frac{dM_x}{dt} = -\frac{M_x}{T_2} + \gamma M_y B_0$$

$$\frac{dM_y}{dt} = -\frac{M_y}{T_2} - \gamma M_x B_0$$

Equations 2.13

where T_1 is the longitudinal relaxation time and T_2 is the transverse relaxation time. Relaxation mechanisms form the basics of MR contrast as relaxation times are dependent on tissue type and the chemical environments the spins exist within.

The origin of the longitudinal relaxation is caused by dipole-dipole interactions. Molecules within any medium are constantly in motion, the rate at which the molecules move is determined by how bound they are and the temperature. As the molecules move, the magnitude and the direction of the magnetic field associated with each spin will vary, causing shifts in the effect on its neighbour. Solids have more bound molecules compared to liquids. With higher temperatures, the molecules move faster compared to colder temperatures; this leads to relaxation effects being dependent on temperature as shown in Figure 2.8. How well matched the molecular movement rate is to the Larmor frequency (ω_0) determines the efficiency of the longitudinal relaxation (T_1) process, with a much faster relaxation (and so shorter relaxation time) when the rates are well matched.

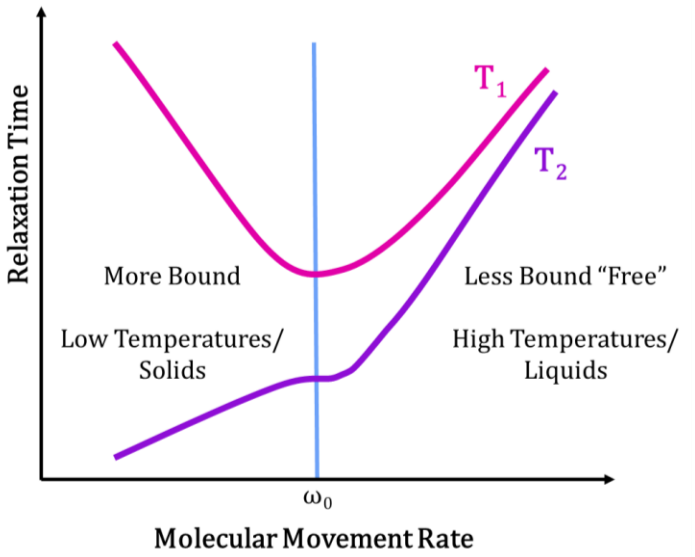

Figure 2.8 - Relationship between molecular movement rate and MR relaxation time. When the molecular movement rate matches the Larmor frequency (ω_0) of spins matches this results in the shortest longitudinal (T_1) relaxation time.

2.2.3.1 Longitudinal relaxation

The longitudinal recovery of magnetisation along the z-axis is governed by the longitudinal relaxation time, also known as the spin-lattice relaxation time.

The longitudinal magnetisation recovery is described by,

$$\frac{dM_z(t)}{dt} = -\frac{(M_z(t) - M_0)}{T_1}$$

Equation 2.14

where T_1 is the time constant for longitudinal relaxation. If a 90° RF pulse is applied, Equation 2.14 can be solved to determine the recovery of M_z after a 90° RF pulse resulting in,

$$M_z(t) = M_0\left(1 - e^{-\frac{t}{T_1}}\right)$$

Equation 2.15

this is termed a saturation recovery, T_1 is defined as the time it takes for M_z to recover to ~63% (1 – 1/e) of M_0.

To measure T_1, a 180° inversion RF pulse is commonly applied (such that $M_z(0) = -M_0$) as this provides a larger dynamic range for the measurement of the longitudinal signal recovery. The solution for M_z following an inversion pulse is given by

$$M_z(t) = M_0\left(1 - 2e^{-\frac{t}{T_1}}\right)$$

Equation 2.16

Figure 2.9 shows example saturation and inversion recovery signal curves. To measure T_1, multiple sample points are collected along the recovery curve and fit. T_1 mapping schemes are discussed further in Chapter 3.

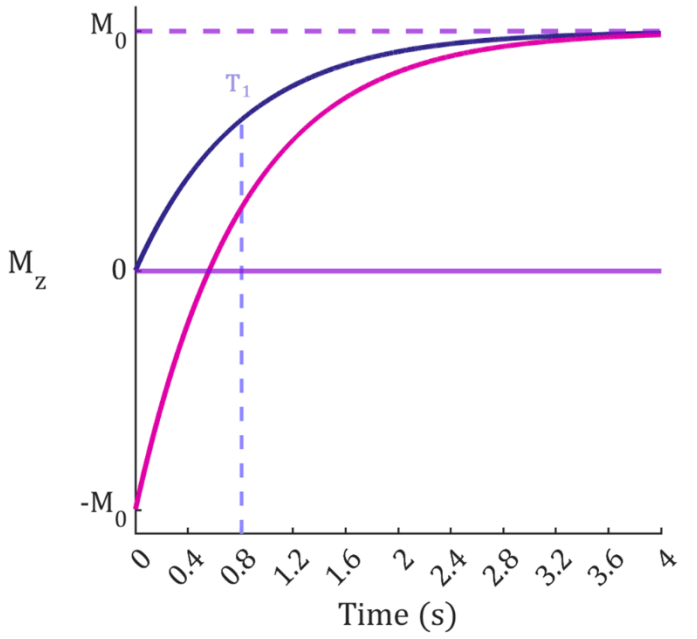

Figure 2.9 –Simulated longitudinal magnetisation (M_z) after a 90° excitation pulse (blue) and a 180° inversion pulse (pink) pulse shown for a T_1 of 809 ms to represent liver at 3 T. The dashed blue line shows for a saturation recovery that T_1 can be measured from the time it takes for M_z to recover to ~63% of M_0. Note, for the longitudinal magnetisation to fully recover this takes approximately 5 times the T_1 of the tissue.

Note, for the longitudinal magnetisation to fully recover, this takes approximately 5 times the T_1 of the tissue, and so this time needs to be allowed between repeats when performing T_1 mapping or the effect of incomplete recovery needs to be considered in the fitting.

2.2.3.2 Transverse relaxation

The source of transverse relaxation is inhomogeneities in the magnetic field, including extrinsic imperfections in the applied field, susceptibility issues within tissue and intrinsic spin-spin interactions, with the dominant effect from dipole-dipole interactions between spins. Hence, transverse relaxation is also known as spin-spin relaxation. The transverse components of the coupled Bloch equations related to relaxation are,

$$\frac{dM_x(t)}{dt} = -\frac{M_x(t)}{T_2}$$

Equation 2.17

$$\frac{dM_y(t)}{dt} = -\frac{M_y(t)}{T_2}$$

Equation 2.18

which can be solved for the transverse magnetisation M_{xy} to give

$$M_{xy}(t) = M_{xy}(0)e^{-\frac{t}{T_2}}$$

Equation 2.19

where $\mathrm{M_{xy}}(0)$ is transverse magnetisation at t = 0, and $\mathrm{T_2}$ is the transverse relation time constant, defined as the time it takes for the signal to decay by ~37 % (1/e) of its initial value Figure 2.10.

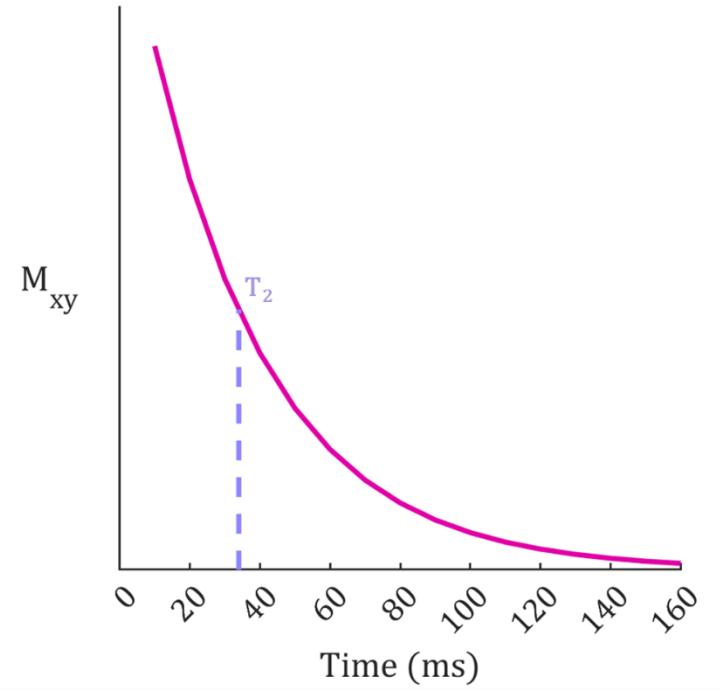

Figure 2.10 –Transverse signal (M_{xy}) signal decay simulated for a T_2 of 34 ms to represent liver tissue. The T_2 measures at 37% of its initial value is marked with a dashed line.

As described by the Larmor equation, the rate of precession of spins is dependent on the strength of the field experienced; local changes in field strength will cause spins to precess at different rates, and over time, they come out of phase with each other.

In practice, the measured signal decay time of an FID does not match the T_2 relaxation as this does not account for the effects from the inhomogeneities in B_0. The inhomogeneities caused by imperfections in the applied static field and susceptibility difference across a tissue cause a secondary effect (T_2'), which, when

combined with T_2 as described in Equation 2.17, gives T_2*. T_2* can be measured as the envelope of the FID, Figure 2.11 and is related to T_2 through,

$$\frac{1}{T_2^*} = \frac{1}{T_2} + \frac{1}{T_2'}$$

Equation 2.20

The T_2 relaxation time can be measured using a Spin Echo (SE) pulse sequence, as shown in Figure 2.11. In a SE sequence, following an initial 90° pulse the FID will decay with T_2* time constant. But if a 180° refocusing pulse is applied at time (TE/2), then an echo will be formed at time TE, which is dependent on the T_2 envelope. Applying a refocussing 180^0x RF pulse flips the spins about the x-axis to refocus the spins. By repeating this measurement with different echo times the signals can then be used to determine T_2. T_2 mapping is further described in Chapter 3 where it is applied to study changes that occur following bariatric surgery.

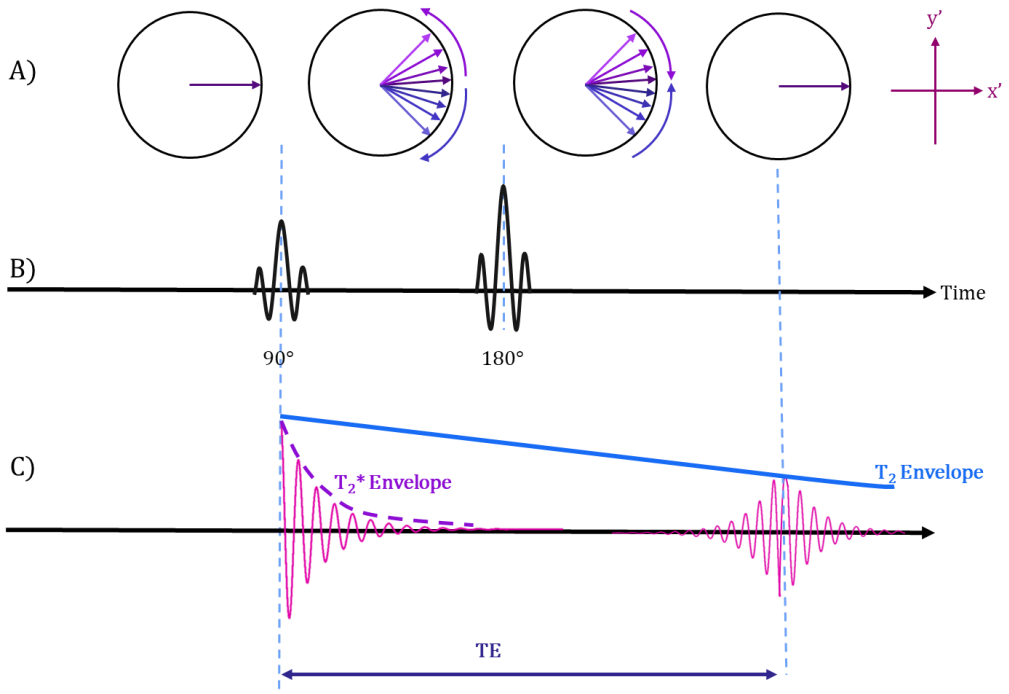

Figure 2.11 - A spin echo sequence. A) Spin isochromats shown in the rotating frame of reference (x', y') with de-phasing after the 90° excitation pulse and rephasing after the 180° RF pulse, with RF pulses shown in B) and the resulting C) signals with T_2 (purple) and T_2 (blue) and decay envelopes.*

2.2.3.3 Relaxation times in abdominal tissue

Typical values for ^{1}H T_1 and T_2 relaxation times in healthy abdominal tissue are provided in Table 2.2, with values increasing in organs when more free water is present.

Organ/Tissue	**^{1}H T_1 (ms)**	**^{1}H T_2 (ms)**
Liver	809 ±71	34 ±4
Spleen	1328 ±31	61 ±9
Kidney Cortex	1142 ±154	76 ±7
Kidney Medulla	1545 ±142	81 ±8
Pancreas	725 ±71	43 ±7

Table 2.2 – ^{1}H T_1 and T_2 relaxation for healthy abdominal organs at 3 T (15)

Disease will alter the tissue T_1 and T_2 values. T_1 has been shown to increase with kidney, liver and pancreas disease severity due to fibrosis, which alters the molecular environment due to the associations of collagen with supersaturated hydrogel, and due to inflammation, from interstitial oedema and cellular swelling. In liver disease, the iron content of the liver tissue can increase resulting in increased field inhomogeneities and a decrease in T_2*, whilst inflammation often causes an increase of fluid in tissue (oedema) leading to an increase in T_2 and T_2* decay times.

T_1 and T_2 of abdominal tissues are mapped in Chapter 3 when studying the effect of bariatric surgery.

2.3 Magnetic Resonance Imaging (MRI)

The following section outlines the basics of MR Imaging (MRI). Imaging is used predominantly in experimental Chapters 3 and 5.

2.3.1 Gradients

The application of a spatially varied magnetic field or gradient (G) (in units of mTm^{-1}) is key for localisation in MRI. Inside an MR scanner, there are three gradient coils to produce a spatially varying field in each of the x, y, and z directions (Figure 2.12).

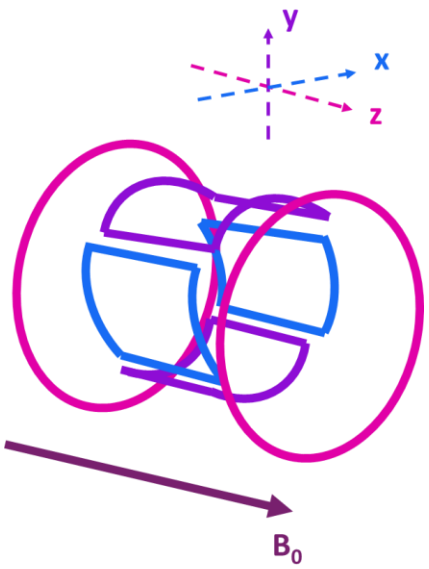

Figure 2.12 - Schematic of the x, y and z gradient coils inside the bore of an MR scanner

A gradient causes known spatially dependent changes in B_0,

$$B_z(x) = B_0 + G_x \cdot x \qquad B_z(y) = B_0 + G_y \cdot y \qquad B_z(z) = B_0 + G_z \cdot z$$

Equations 2.21

and thus, an associated spatial dependence in the Larmor frequency (ω),

$$\omega(x) = \gamma(B_0 + G_x \cdot x) \qquad \omega(y) = \gamma(B_0 + G_y \cdot y) \qquad \omega(z) = \gamma(B_0 + G_z \cdot z)$$

Equations 2.22

2.3.1.1 Gradient Echoes

In a gradient-echo (GE) sequence, after the RF excitation pulse, a negative 'dephasing' gradient is applied, causing local changes in net magnetisation and, hence, resonance frequencies. This, in turn, causes rapid dephasing of the FID. An equal and opposite positive 'rephasing' gradient is then applied, reversing the dephasing of the spins, which begin to refocus producing a gradient echo (Figure 2.13). This refocusing only corrects the additional dephasing introduced by the gradients and does not reverse dephasing caused by T_2* relaxation. Hence, the signal measured is heavily dependent on T_2* decay, and this sequence can be used for T_2* mapping.

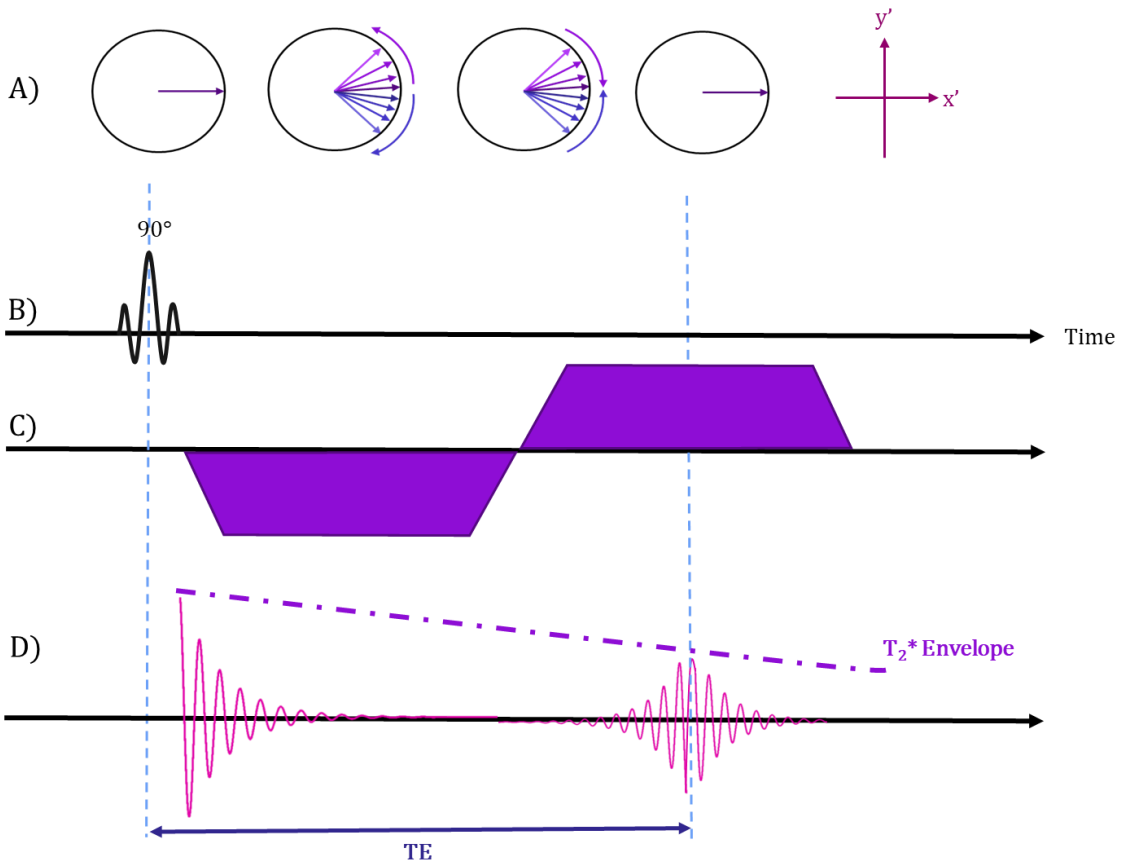

Figure 2.13 - Spins dephasing after applying a (B) 90° RF pulse and (C) negative gradient and rephasing from applying the positive gradient. D) shows the signal produced and the T_2 envelope (purple).*

2.3.2 Image Formation

This section will describe how localisation occurs first through plane using slice selection, followed by in-plane using the concepts of phase and frequency encoding.

2.3.2.1 Slice Selection

If the RF excitation pulse of a select bandwidth (Δω) of frequencies centered at the Larmor frequency (ω_0) (as shown in Section 2.3.1) is applied at the same time as a

gradient (of strength G_z), then a slice of a select range of spins will be excited in a given slice thickness (Δz), as described in Equation 2.23 and illustrated in Figure 2.14. By altering the bandwidth of the RF pulse or strength of the gradient, G_z, the slice thickness can be varied.

$$\Delta z = \frac{\Delta\omega}{\gamma G_z}$$

Equation 2.23

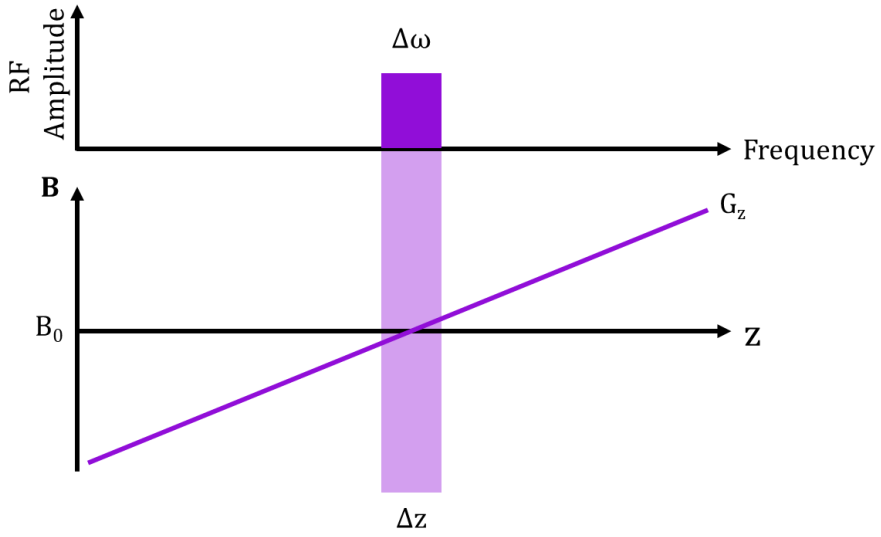

Figure 2.14 - Illustration of how the slice thickness (Δz) is related to the RF pulse bandwidth (Δω) and gradient strength (Gz).

The application of the slice selective gradient will itself induce dephasing of the spins, to correct this, a slice selective gradient is immediately followed by a refocusing gradient of half the area of the slice select gradient, as shown in Figure 2.15.

2.3.2.2 Phase and Frequency Encoding

To encode in-plane, a second gradient is applied along the y-axis, known as the phase encoding gradient. The spins will precess at a spatially dependent frequency ω(y) which causes a phase shift (Δϕ) given by:

$$\Delta\phi = \gamma G_y ty$$

Equation 2.24

which is dependent on the position in *y,* the strength (*Gy)* and duration (t) of the gradient. To sample the entirety of k-space, the amplitude and/or duration of the gradient needs to be varied with each repeat sampling (Figure 2.15). To encode in the third dimension, the frequency encoding gradient is conventionally applied along the x-axis during signal readout (Figure 2.15). Spins will precess according to ω(x) with spins at the center of the gradient precessing at the Larmor frequency with faster or slower precession occurring in stronger and weaker fields, respectively.

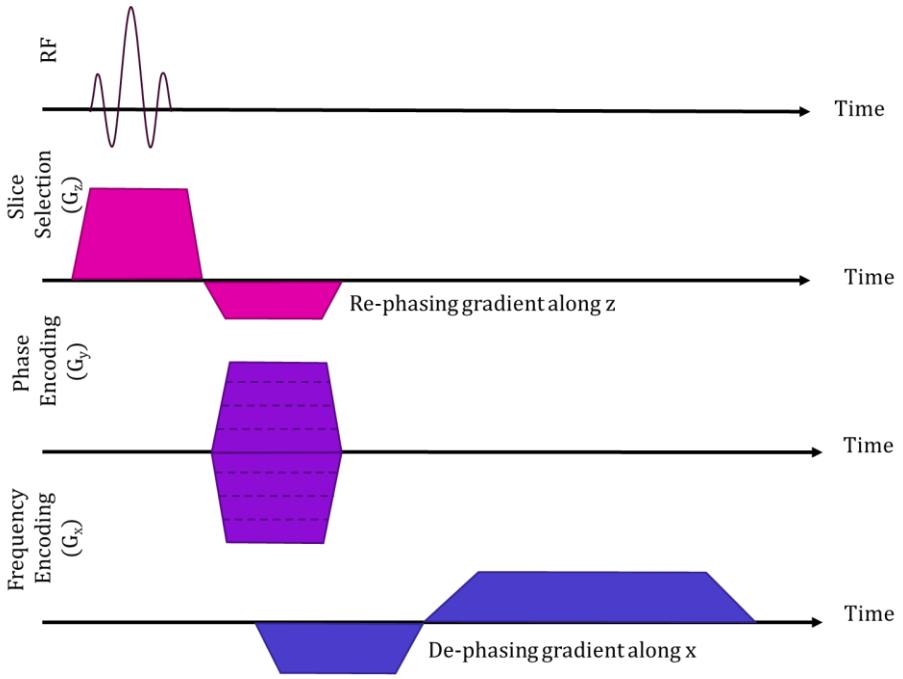

Figure 2.15 - Example pulse sequence diagram showing spatial encoding gradients following a 90° excitation. The dotted lines represent the different gradient steps.

2.3.2.3 k-space

The frequency domain, known as k-space, comprises k_x and k_y, which represent the spatial frequencies in the x and y directions, respectively. Each point in k-space is a combination of signals from k_x and k_y given by,

$$k_x = \gamma G_x t_x$$

Equation 2.25

$$k_y = \gamma G_y t_y$$

Equation 2.26

where t_x and t_y are the duration of the x and y gradients, respectively. The difference between points in k-space (Δk_x, Δk_y) is inversely proportional to the field of view (the size of the imaging window), whilst the amount of sampling points is proportional to the spatial resolution of the image. The edges of the k-space provide information on the structure of an image, whilst the center provides information on the image contrast. Therefore, the way k-space is sampled, and the density of the sampling affect the resulting image quality.

There are many ways to sample k-space, some faster than others. Simple schemes such as spin-warp imaging use gradient echoes to sample one k-space line per excitation. Each excitation applies a unique phase-encoded gradient that moves through k_y, the signal is acquired simultaneously with the application of a frequency-encoded gradient, Figure 2.16. However, this process can take a long time (minutes). Echo-planar imaging (EPI) is much faster (image acquired in 10's of ms) as all k-space lines are acquired from one excitation as small phase encoding gradients are applied during the acquisition to move through k_y, Figure 2.16 (16). k-space data can be transformed into an image via a Fourier transformation.

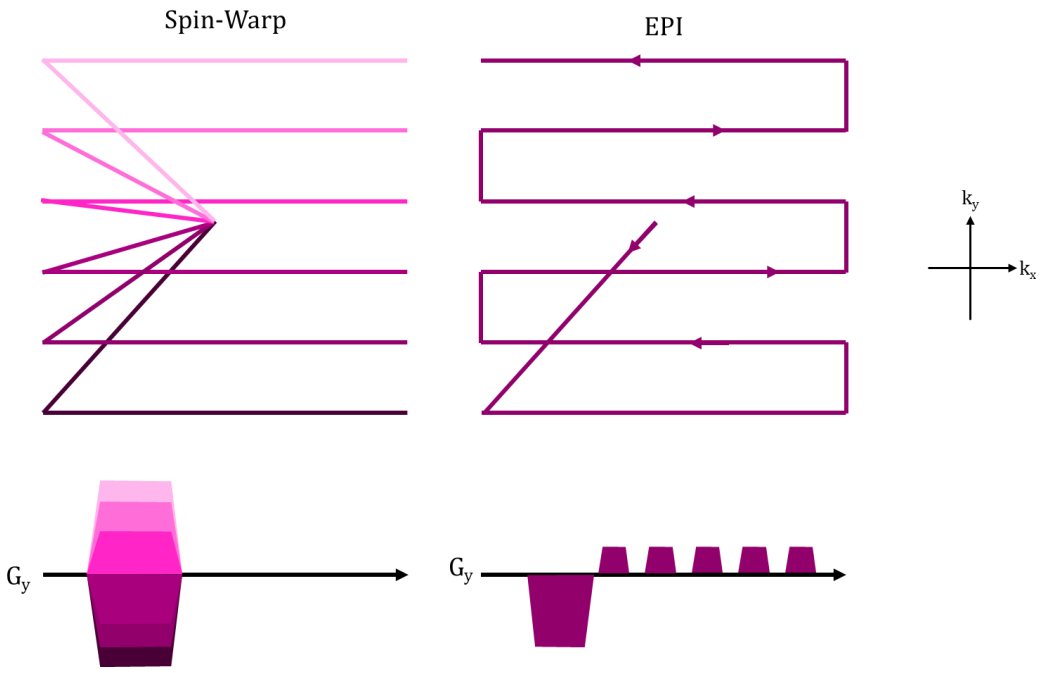

Figure 2.16 - Example k-space trajectories for (left) spin-warp and (right) echo-planar imaging techniques and their respective G_y gradients. For spin-warp imaging the coloured gradients match the colours of the lines of k-space

It is often the case that MR signals are measured in quadrature. When Fourier transformed, this produces a complex image with real and imaginary components. These real and imaginary signals can then be combined to obtain magnitude (MAG) and phase (ϕ) images given by

$$MAG = \sqrt{real^2 + imaginary^2}$$

Equation 2.27

$$\phi = \tan^{-1}\left(\frac{imaginary}{real}\right)$$

Equation 2.28

2.4 Magnetic Resonance Spectroscopy (MRS)

MRS is performed in all experimental chapters of this thesis. Nuclei resonate at the Larmor frequency which is dependent on the strength of the magnetic field it experiences and the gyromagnetic ratio of the nucleus, as described in Equation 2.6. Spins also precess at different frequencies depending on the chemical environment they experience within a molecule. These variations are unique for different groups of molecules and can be observed using an NMR spectrum.

2.4.1 Chemical Shift Scale

Nuclei are often part of larger, more complex molecules such as hydrogen in the hydrocarbon chains of fat, phosphorous within adenosine triphosphate (ATP) and carbon within glycogen. The other chemicals that the nuclei bond with cause shielding effects, altering the local magnetic field and, therefore, the resonant frequency; this is known as chemical shift, δ. Chemical shift is defined as the relative difference in frequency between the spin under investigation (ν_{sample}) and a reference compound ($\nu_{reference}$) normalised by the reference frequency and converted to parts per million (ppm), Equation 2.29.

$$\delta\ (ppm) = \frac{\nu_{sample} - \nu_{reference}}{\nu_{reference}} \cdot 10^6$$

Equation 2.29

For the ppm scale, shifts are equivalent across all atomic species. On an NMR spectrum the Area Under the Curve (AUC) of a peak represents how many spins of

the investigated atomic species are in an environment and the position along the x-axis represents the chemical shift, Figure 2.17.

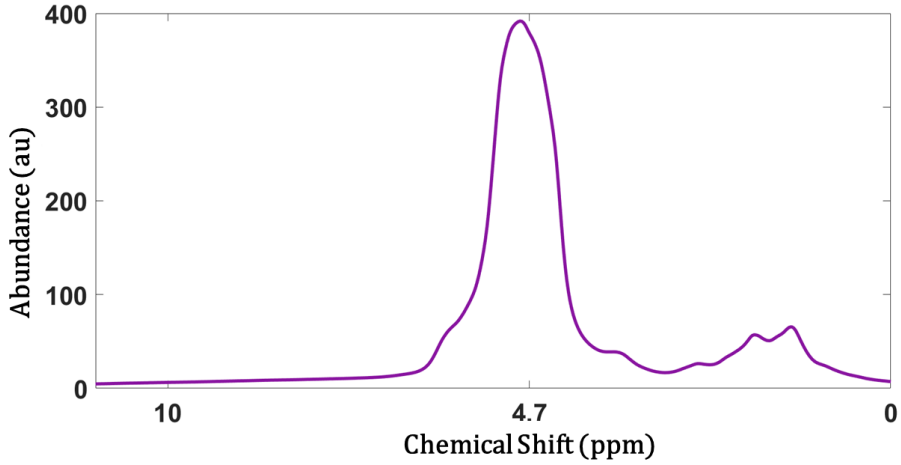

Figure 2.17 - ^{1}H spectra of the liver, showing the water peak at ~4.7 ppm and fat peaks at ~2 ppm.

2.4.2 Localisation Techniques

Though it is possible to acquire spectra with no localisation, to gain clinically relevant information, it is important to specify the tissue from which the spectra are being collected. In some multinuclear acquisitions, such as ^{13}C liver, localisation from the signal detected from a single loop RF coil is sufficient. However, this is not always the case; for ^{1}H and ^{31}P spectroscopy, the user may wish to select a specific tissue under the coil's active region. Localisation can reduce the received signal to a slab, a single voxel MRS or in Chemical Shift Imaging (CSI), multiple voxels are encoded across a region of interest. This section will cover the basics of localisation in spectroscopy, including STEAM for ^{1}H spectroscopy and ISIS which is used for ^{31}P spectroscopy, and which are used in this thesis.

2.4.2.1 ^{1}H Spectroscopy

In this thesis, ^{1}H MRS is used in Chapters 3 and 5. There are a number of possible localisation techniques with common methods being Point RESolved Spectroscopy (PRESS) and STimulated Echo Acquisition Mode (STEAM). In both techniques three slice selective RF pulses are applied with simultaneous orthogonal gradients. The resulting echo originates from spins that experience all 3 gradients, creating a single voxel MRS measure.

PRESS uses three RF pulses of 90°, 180°, and 180°, which produce an asymmetric spin echo. This technique is often used within CSI as a localisation technique. The large RF pulses lead to long echo times, which is the main disadvantage of this technique and made it unsuitable for use in this thesis. STEAM uses three 90° RF pulses, the first two RF pulses are separated by TE/2 with a stimulated echo occurring at TE/2 after the third pulse (Figure 2.18). The time between the second and third slice select gradient is known as the mixing time (TM); during this, the magnetisation is preserved along the z-axis, experiencing only T_1 relaxation. TM is kept as short as possible and is not included in the total TE, leading to STEAM having shorter echo times than other methods, making it a key technique for hepatic fat fraction quantification.

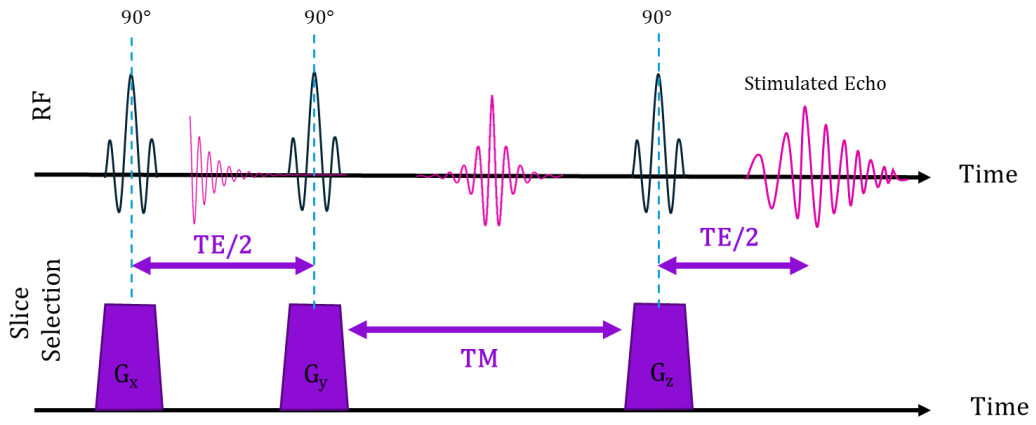

Figure 2.18 - Simplified Pulse sequence diagram for a STEAM (STimulated Echo Acquisition Mode) technique showing the RF pulses, slice selective gradients and resultant echoes.

2.4.2.2 ^{31}P Spectroscopy

Although it is possible to perform STEAM for ^{31}P MRS, Image-Selected In vivo Spectroscopy (ISIS) is often the favoured scheme. ISIS works similarly to STEAM and PRESS as multiple slice selective regions produce localisation. However, in ISIS, multiple acquisitions are collected with the same ROI, inverted or otherwise, which are then summed or subtracted from each other to define the final MRS signal region. Due to the separate acquisitions used in ISIS, the time from excitation to read out is reduced, making ISIS good for measuring metabolites with short T_2's, such as those in ^{31}P. In this thesis 1D ISIS is used, for which 2 cycles (S_1 and S_2) are collected and subtracted to give a signal region that is a slab parallel to the RF coil, a diagram illustrating this sequence is shown in Figure 2.19.

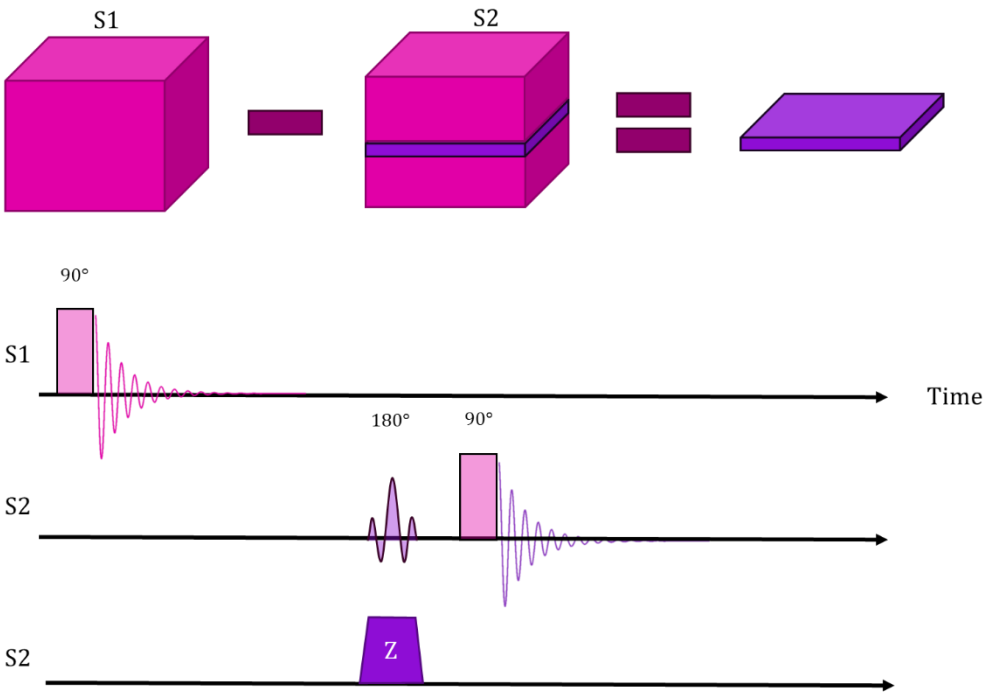

Figure 2.19 - ISIS Slice Selection. In the first cycle, the whole region is excited, and the FID represents all spins. In the second cycle, the spins of the middle slab are selectively inverted prior to excitation. When the FID generated from the 2nd cycle is subtracted from that from the 1st cycle the signal from the middle slab remains.

2.4.3 Saturation of Unwanted Signals

2.4.3.1 Water Suppression

Although the large amounts of water in the body benefit MR imaging, the dominant water peak often dwarfs other metabolites in MRS, making them hard to quantify. To adequately quantify these metabolites, water suppression is performed, for example, using CHEmically Selective Saturation (CHESS). CHESS uses a frequency-encoded RF pulse to tip the water magnetisation into the transverse plane, where it is immediately dephased using a spoiler gradient. This process is repeated a

minimum of three times to ensure the signal is fully saturated with the quantity of pairings, depending on the technique used. In this thesis VAriable Power radiofrequency pulses with Optimized Relaxation delays (VAPOUR) water suppression is used. VAPOUR uses 8 RF-spoiler gradient pairings (Figure 2.20). Each CHESS set requires 20-30 ms, so though more may improve the water suppression, this comes at the cost of an increased TR.

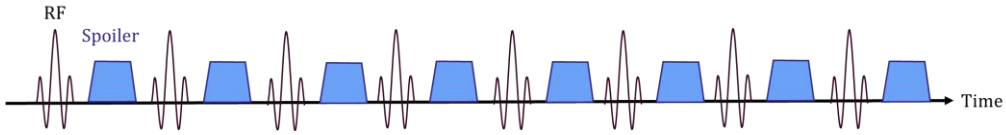

Figure 2.20 -VAPOUR water-suppression with 8 RF pules' and spoiler gradients.

An example of spectra acquired in the liver using STEAM with and without water suppression is shown in Figure 2.21.

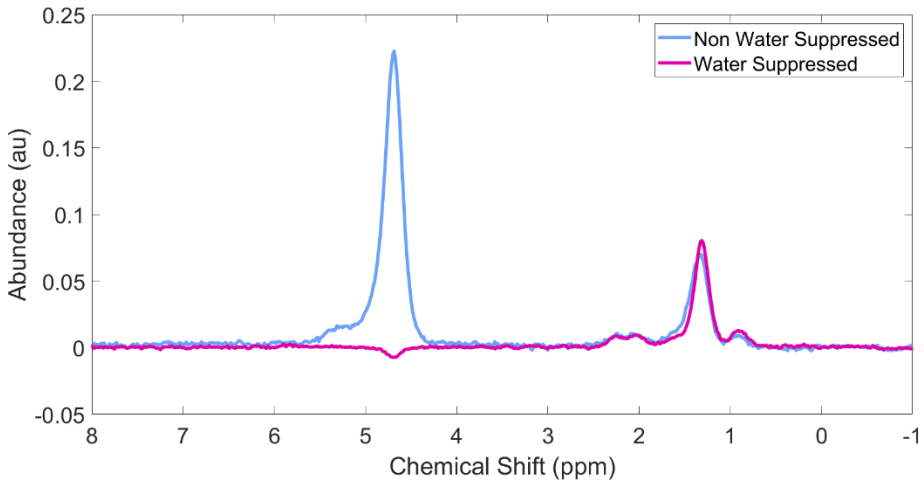

Figure 2.21 - Example STEAM spectra of the liver with (pink) and without (blue) water-suppression

2.4.3.2 Saturation Transfer in ^{31}P

Saturation transfer experiments allow the investigation of the exchange between molecules. For a Saturation Transfer (ST) experiment, an extra frequency-encoded RF pulse is used compared to standard spectroscopy. The frequency-encoded RF pulse is applied to one of the peaks corresponding to molecules that are in flux with each other; this nulls or saturates the transverse magnetisation. Due to the exchange between the two molecules, this saturation is transferred to the other molecule. In the resulting spectra, the target peak is completely saturated, and the signal from the exchanging molecule is reduced. Although the saturation pulse is frequency encoded, a large bandwidth is often used to ensure the targeted magnetisation is fully saturated. This can lead to saturation leaking into other metabolite peaks. For this reason, a second set of spectra is acquired where the saturation pulse is applied, mirrored around the exchange peak. This is the unsaturated spectra. In the case of ^{31}P ST experiments, the saturation pulse is applied to the γATP peak, which will, in turn, reduce the signal from the inorganic phosphate (Pi) peak due to the exchange described in Chapter 1. In unsaturated spectra, the saturation pulse is applied mirrored around the Pi peak, as shown in Figure 2.22 (17,18).

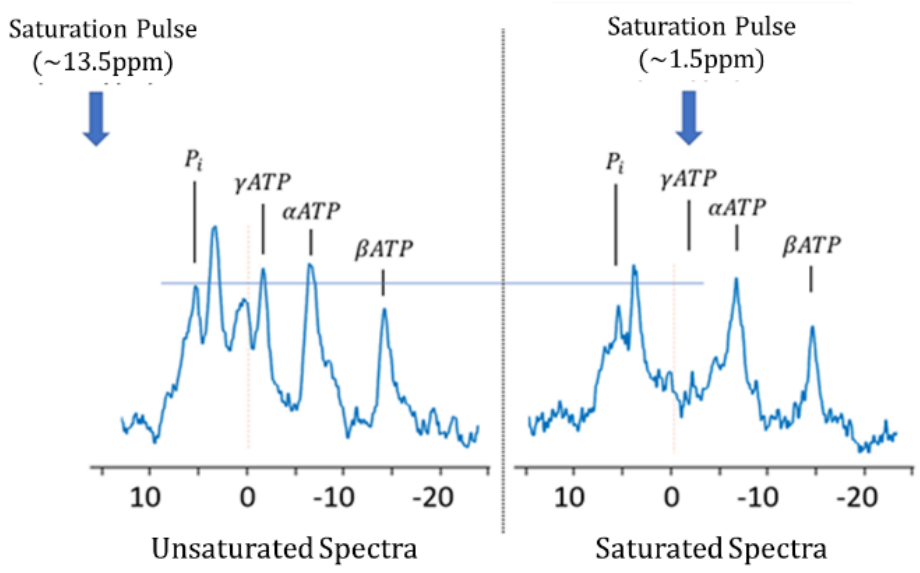

Figure 2.22 - Location of saturation pulses in ^{31}P saturation transfer experiments. The horizontal line shows the drop in the Pi signal in unsaturated spectra.

From this, the exchange rate constant (k) can be calculated using

$$k\ (s^{-1}) = \frac{1}{T_1^{app}}\left(1 - \frac{A_s}{A_0}\right)$$

Equation 2.30

where A_s and A_0 are the areas of the Pi peak in the saturated and unsaturated spectra, respectively and T_1^{app} is the apparent T_1 of Pi. The forward flux rate can be calculated by multiplying k by the concentration Pi. Due to multiple factors, such as too narrow bandwidth for the saturation pulse or not targeting the central frequency of the peak, the saturation of the γATP peak could be incomplete. A correction factor can be used to account for this (19,20). The exchange rate constant then expands to

$$k\ (s^{-1}) = \frac{A_0^{Pi} - A_s^{Pi}}{A_s^{Pi} \cdot T1_{Pi}^{app}} \times \frac{A_0^{ATP}}{A_0^{ATP} - A_S^{ATP}}$$

Equation 2.31

where A_0 and A_S hold the same meaning as above, A^{ATP} and A^{Pi} refer to the area from the γATP and Pi peaks, respectively, and $T1_{Pi}^{app}$ is apparent T_1 of Pi (13).

2.4.4 Choice of RF pulse for MRS

As described in Section 2.2.1, the excitation profile of a RF pulse can be approximated from the Fourier transform (14). For a rectangular (or block) pulse this leads to a reduction in the range of excitation frequencies as the pulse duration increases, as shown in Figure 2.23. This can cause issues in broader bandwidth spectra, such as ^{13}C MRS. To excite a large bandwidth but maintain the same tip in magnetisation, the power (B_1(T)) of the pulse must be increased proportionally to the reduction in duration; that is, the area of the pulse must be maintained.

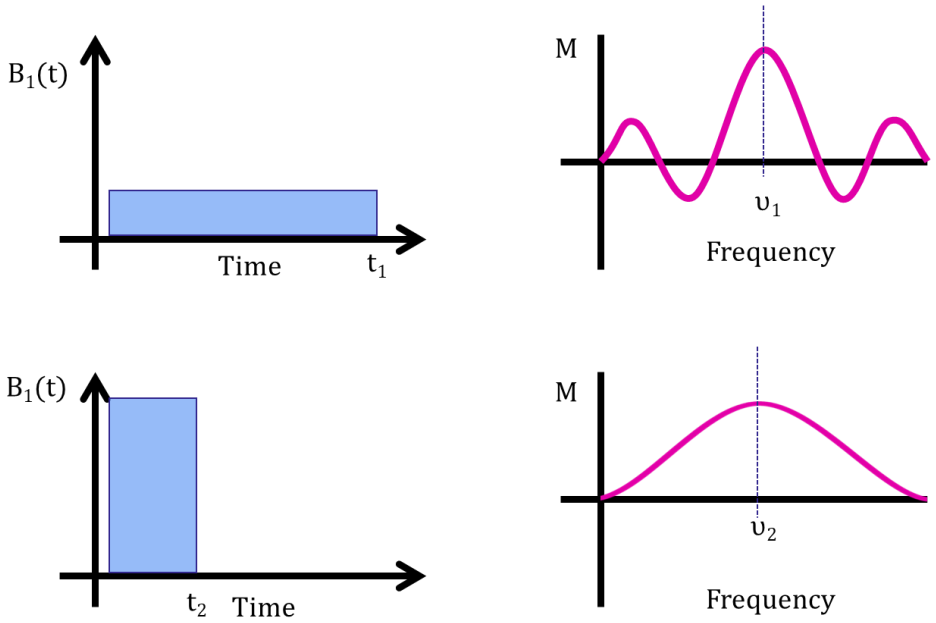

Figure 2.23 - Left - RF Pulse and Right- the respective excitation profiles for two block pulses. The width of the excitation frequency (υ) is dependent on 1/t, where t is the pulse duration.

The off-resonance effects described in Section 2.2.1.1 can mean that even excitation across all frequencies from a block pulse is not desirable. Another way to excite a broad range of frequencies is to use an adiabatic pulse (22). These pulses use frequency and amplitude modulation that vary with B_{eff} intending to provide a more even excitation across a specified range of B_1. In this thesis, a type of adiabatic pulse known as a hyperbolic secant is used. For this pulse type amplitude modulation is performed using the function $(F_1(t))$

$$F_1(t) = \operatorname{sech}(\beta t)$$

Equation 2.32

where β is the frequency of the RF pulse. The frequency modulation is performed using the function $(\mathrm{F_2(t)})$

$$F_2(t) = \frac{\tanh(\beta t)}{\tanh(\beta)}$$

Equation 2.33

this increases the net magnetisation across the bandwidth compared to using a block pulse. A traditional hyperbolic secant pulse inverts the magnetisation; to achieve a 90° tip, a half-passage hyperbolic secant can be used. The comparison of block and Half-Passage Hyperbolic Secant pulses is explored further in Chapter 4.

2.5 RF Safety

There are many considerations to be made when performing MRI and MRS studies in human subjects, especially as performed in this thesis in complex participant groups of children and bariatric (overweight) participants. Below are RF-specific safety considerations.

When an RF pulse is absorbed by the tissue, it causes a heating effect. The first level limit of RF heating allowed is 1°C at the centre of the abdomen. The Specific Absorption Ratio (SAR) is used to measure the effects of RF heating in the body and is calculated using,

$$SAR = 0.5\sigma\frac{E}{\rho}$$

Equation 2.34

where E is the induced electric field and ρ is the density of tissue in Wkg^{-1}. The SAR limit for whole-body imaging is 4 Wkg^{-1} averaged over 15 minutes and 8-10 Wkg^{-1} for abdominal imaging per gram of tissue; this is automatically calculated by the scanner during operation. It is key to note that for larger participants, more energy needs to be deposited to penetrate deep enough into the tissue and achieve the same level of signal as in a slimmer person; this means that more heating will occur in an obese participant group. For larger participants and/or diabetic participants, it's often more difficult to regulate the temperature. For these groups, it's key that they are regularly monitored and that the inbuilt fans of the MR scanner are used to assist in participant cooling.

According to Faraday's Law, an alternating magnetic field will generate small electrical currents (eddy currents) in conductive materials. Provided the scanner is ran within safety limits, the body is generally able to overcome the heating effects caused by currents induced in the tissue. However, if the currents are induced in metal or across high-resistance skin-to-skin contact, significant heating can occur. In these scenarios, or if a participant has a reduced capacity for thermoregulation, the body's cooling mechanisms may not be efficient enough, and burns can occur. To mitigate the risk from clothing, participants are asked to ensure there are no zips, metallic buttons or fasteners or are requested to change into paper scrubs provided.

To prevent burns from the bore or coil, 1 cm thick foam padding or blankets are placed at each point of contact. Participants are also instructed not to make loops with their limbs; hence, avoid skin-to-skin contact.

3 Investigating the Effects of Bariatric Surgery on Type II Diabetic and Pre-diabetic Patients

3.1 Overview

Obesity rates are climbing worldwide leading to a rise in obesity-related complications such as Type-2 Diabetes (T2D), pre-diabetes and cardiovascular diseases (CVD). These conditions have inherent mortality, risk of functional decline, hospitalisation and loss of independence, especially in the morbidly obese subjects. Over the last decade, bariatric surgery has emerged as a safe and proven method for better, more sustained weight loss compared to exercise and dietary measures. The bariatric surgery procedures most commonly performed in the UK and worldwide are Roux-en-Y Gastric Bypass (RYGB) and Sleeve Gastrectomy (SG). Prior to such bariatric surgery procedures, all patients undergo a Very Low-Calorie Diet (VLCD) for a period of typically 6 weeks to reduce the size of the liver, thus allowing surgeons easier access to the digestive tract. The VLCD has been shown to independently reduce blood glucose levels and, in some cases, induce diabetes remission.

The goal of this study is to use Magnetic Resonance Imaging (MRI) and Spectroscopy (MRS) to assess the multiorgan changes that occur over the time course of the bariatric surgery journey which may lead to diabetes remission.

This work was presented as a power pitch and digital poster 'Multiparametric MRI to study changes across the Surgical Journey in Bariatric Patients with Type 2 diabetes or Prediabetes' and at the International Society of Magnetic Resonance in Medicine, Singapore, 2024.

3.2 Introduction

This section outlines the role of the Very-Low Calorie Diet (VLCD) and the different surgical options available to patients who are undergoing bariatric surgery. This includes a review of the existing literature of applying MRI and MRS in the abdomen to study patients undergoing bariatric surgery, followed by a review of the key MRI and MRS acquisition methods used in this chapter to study changes that occur over the bariatric surgery journey. The work aims to provide increased understanding of the distribution of body fat and the changes in the volume and degree of inflammation of critical metabolic abdominal organs. This, together with clinical measures, has the potential to increase understanding of the mechanism for an improved glycaemic profile, including diabetic remission following bariatric surgery or return to euglycaemia from pre-diabetic states, and their effects on weight loss or changes in gut hormone levels.

3.2.1 Role of the Very Low-Calorie Diet

In the UK and in many parts of the world, prior to undergoing bariatric surgery, patients are required to undergo a period of Very Low-Calorie Diet (VLCD). It has been described that the VLCD leads to weight loss and liver shrinkage with a debate on whether this reduces surgical complexity and improves outcomes (23–26). In clinical practice, the VLCD is typically restricted to up to 800 calories and 2 litres of fluids consumed daily. The provision of VLCD within routine NHS practice can range from using meal replacements, a standardised plan or calorie counting. An example

of the recommended daily food intake for people on a VLCD is shown in Figure 3.1 (27).

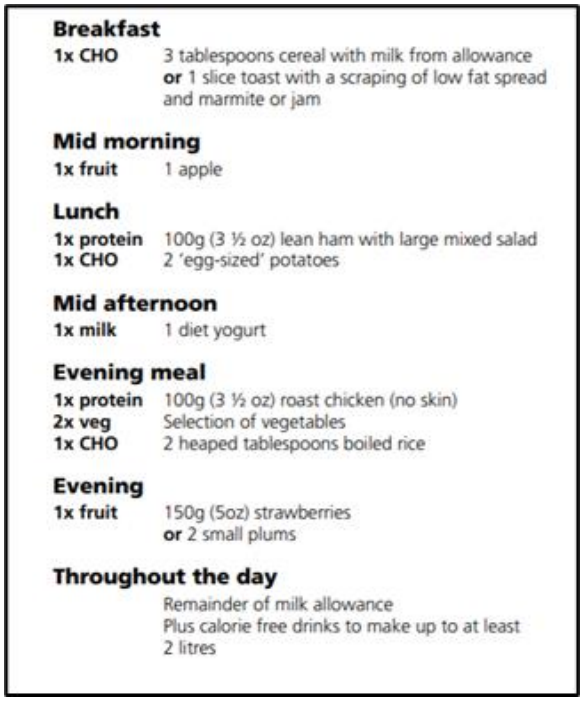

Figure 3.1 - Example of the daily food intake recommended for people on a VLCD, taken from the NHS website (5).

Diabetic remission has been linked to the reduction of fatty acids within the liver and pancreas, with a reduction in caloric intake shown to reduce the fat deposition and fatty acids in organs including the liver, pancreas, and muscles, which regulate glucose metabolism (28–32). It follows that the VLCD can induce diabetic remission without the need for bariatric surgery, and this has been shown in previous literature (29,33–35). However, there are known compliance issues with diet interventions. Vijan *et al.* (36) surveyed 446 diabetic patients and held patient focus groups to explore the barriers to diet compliance, reporting results using a seven-

point scoring system. They found that a moderate diet (reduction in fat/sugar but little reduction in calories) was a greater burden than oral medication but less than twice daily injections of insulin (median 1, 0, and 4 points respectively, diet vs. oral $p=0.001$, diet vs. insulin $p<0.001$), whilst a strict diet (reduced sugar/fat and calorie intake aimed at weight loss) was rated equal to insulin (median 4 points). The paper noted that burden level did not necessarily link to compliance, as insulin compliance was self-reported higher than moderate diet. The most common factors raised in the focus groups to diet compliance were cost, portion size, family issues (such as lack of support) and quality of life/lifestyle maintenance (36).

There are many articles that describe the VLCD as a cure for diabetes, and one cannot argue with the success seen in literature. However, the controlled environment of trials and type of individuals willing to participate likely do not provide an accurate reflection of the real-world situation and cannot encompass the factors that may affect many individuals.

3.2.2 Surgical Procedures: Roux-en-Y Gastric Bypass Vs. Sleeve Gastrectomy

The two most common types of bariatric surgery performed globally are Roux-en-Y Gastric Bypass (RYGB) and Sleeve Gastrectomy (SG). Both surgical procedures have been shown to achieve a large and sustained weight loss, with improvements in insulin sensitivity and improved beta cell function (31,37). They have been associated with a high-resolution rate of Type-II-Diabetes Mellitus (T2D) or

achievement of normoglycaemia (normal glucose concentration in the blood) in pre-diabetic states (38–40).

Both procedures are performed laparoscopically. In the SG procedure, ~80% of the stomach is removed, the remaining stomach volume is then sewn up leaving patients with a drastically reduced consumption capacity. In the RYGB procedure, at the end of the oesophagus a small pouch of is created which is anastomosed to the distal small bowel, the stomach remains and continues to produce digestive juices which empty into the intestine, this results in food 'skipping' the stomach, duodenum and upper small intestine, resulting in a consumption restriction. These two procedures are shown schematically in Figure 3.2.

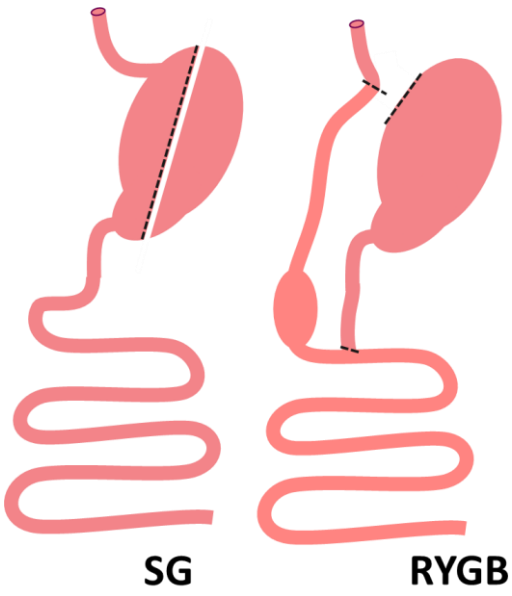

Figure 3.2 -Schematic of Sleeve Gastrectomy (SG) and Roux-en-Y Gastric Bypass (RYGB) procedures.

Filip *et al.* (41) and Pucci *et al*. (42) have both concisely reviewed the theories behind what makes bariatric surgery more successful than lifestyle changes alone and compared the surgical success. Pucci *et al.* (42) concluded that the mechanisms were not fully understood yet, but long-term studies (~3 years) favored RYGB when it came to weight loss (42). Filip *et al.* (41) concluded that the sudden change to a caloric intake much lower than required by the body is the predominant cause for metabolic changes that occur following both SG and RYGB procedures, and that the re-wiring of the digestive tract in RYGB leads to an increased Glucagon-like peptide-1 (GLP-1) response(41). GLP-1 is a hormone released by the gut at 10-15 minutes post ingestion of food that helps trigger insulin secretion from pancreatic beta-cells. GLP-1 is often referred to as the satiety hormone and is believed to be responsible for making an individual feel full; a lower response means satiety dissipates quicker, causing greater energy consumption (43,44). It is believed that GLP-1 is predominantly released when glucose is up taken through the small intestine, so patients who undergo RYGB will have a shorter time period before GLP-1 release and so feel fuller faster. This, combined with other metabolic changes is speculated to be one of the reasons why patients who undergo RYGB have diabetic remission before significant weight-loss (45).

3.3 Scope of Existing MRI and MRS Research in Bariatric Surgery

To date, there are several studies that have applied MRI or MRS to investigate the effects of bariatric surgery on the body; often, the time points of the measurements overlook the precursor diet, with there being little consensus on the timepoints to collect post-surgery. A summary of the literature which is outlined in this section is provided in Table 3.1, including the participant groups and endpoints. These studies often have a limited scope, focusing on using MRI to investigate the physical changes to fat deposition as a marker to assess improvements from baseline (BL) to post-surgery (PS), as such overlooking the specific changes that occur post-VLCD (29,41,46–48). The most common method for assessment of Liver Fat (LF) uses the DIXON MRI sequence (Section 3.4.2.1) to generate Fat Fraction (FF) maps which are interrogated either using small Regions Of Interest (ROI) (49) or using whole liver masks (50,51). To date, few studies have used ^{1}H MR spectroscopy to study changes in LF in a bariatric cohort (52). Other than the assessment of LF, studies also measure Liver Volume (LV), Pancreatic Fat (PF), abdominal Subcutaneous Adipose Tissue (SAT) and Visceral Adipose Tissue (VAT) volume/area.

Study	Participants	Study Timepoints (numbers indicate weeks after surgery)	Endpoint Measurements
Hedderich *et al.* (2017) (50)	N = 19, RYGB = 17, SG =2 NAFLD, non-diabetic	BL, 6, 12, 24 (No VLCD)	LF, LV, SAT volume, VAT volume
Meyer-Gerspach *et al.* (2019) (51)	N = 16 RYGB = 12, SG = 4 Obese, non-diabetic	BL, 12, 24, and 1 and 2 years (No VLCD)	LF, LV, SAT volume, VAT volume
Hui *et al.* (2019) (52)	N = 12 RYGB = 2, SG = 8, Other = 2 Obese, metabolic conditions included	BL,24, and 1 year (No VLCD)	PF, Pancreas T_2*, SAT volume, VAT volume
Lehmann *et al.* (2018) (49)	N = 23 All RYGB	BL,4 (No VLCD)	VAT volume, $T_{1\text{-Vat}}$, $T_{1\text{-SAT}}$, FF_{VAT}, FF_{SAT}
Li *et al.* (2024) (53)	N = 514 RYGB = 203, T2D SG = 311 (comparison cohort, T2D = 143)	BL, 24, 52, and 2 ,3 ,4 ,5 years (No VLCD)	SAT area, VAT area
Tan *et al.* (2023) (54)	N = 9 All SG Obese	BL, 4, 24 (No VLCD)	T_1 MOLLI, T_2*, LF, SAT area, VAT area, Magnetic Resonance Elastography
Chiyanika *et al.* (2024) (55)	N = 34 SG = 13, Lifestyle Modification = 21 NAFLD and metabolic issues	BL, 16	T_1 MOLLI, T_2*, LF, SAT volume, VAT volume
Luo *et al.* (2017) (56)	N = 124 (49 completing all timepoints) RYGB = 26, SG = 20, Other = 3	BL, Post-Diet, 4, 12, 24	LF, LV

	NAFLD		
Bai *et al.* (2023) (57)	N = 21 All SG Obese, non-diabetic	BL, 12, and 1 to 2 years) (No VLCD)	LF, LV, PF, Pancreatic Volume

Table 3.1 - Summary of studies using MRI and MRS to assess the effects of Bariatric Surgery. Details are provided on participant characteristics, study time points and endpoint measurements. BL = Baseline, 24 weeks = 6 months, NAFLD = Non-alcoholic fatty liver disease, VLCD = Very Low-Calorie Diet, LF = liver fat, LV = liver volume, SAT = Subcutaneous Adipose Tissue, VAT = Visceral Adipose Tissue, PF = pancreatic fat.

In non-diabetic cohorts of bariatric surgery patients with Non-Alcoholic Fatty Liver Disease (NAFLD), Hedderich *et al.* (50) used DIXON MRI to investigate the changes in LF, LV, SAT and VAT at 6 weeks, 12 weeks and 24 weeks post-surgery compared to a BL scan collected prior to surgery. Significant changes were seen in all measures at 24 weeks PS compared to BL, but no significant change was seen in LV or LF at 6 weeks or 12 weeks. They noted that the percentage of LF at BL had a significant effect on the change that subsequently occurred, with those participants who had a LF of > 10% dropping by ~85%, compared to a drop in LF of ~31% in those participants who had an initial LF of < 10% (with NAFLD defined as LF > 6.4% (58)).

Meyer-Gerspach *et al.* (51) studied 16 morbidly obese participants' measures of LF, LV, and abdominal SAT and VAT using DIXON MRI at BL and at 12, 24, 52, and 104 weeks after RYGB or SG. For abdominal SAT and VAT quantification, they

used a 2-point DIXON, and for LF measurement they used a 6-echo DIXON. The study did not compare the results from each surgery or absolute values from each time point. Instead, they investigated the rate of change in measures between subsequent time points, i.e. the decay coefficient. Abdominal SAT and VAT were shown to decrease at the same rate, whilst LF decreased significantly faster than both SAT and VAT ($p<0.001$). LV decreased from BL to 12 and 24 weeks PS, but increased from 24 weeks to 52 weeks and remained approximately constant between 52 and 104 weeks PS. In addition to the longitudinal changes, in this study the repeatability of fat quantification methods was also investigated by collecting repeat measurements at three visits prior to surgery; Intraclass Correlation Coefficients (ICC) values showed excellent agreement for LF, LV, SAT and VAT (51).

In a small study of 12 participants with morbid obesity at high risk of developing T2D, Hui *et al.* (52) investigated the changes to LF, PF, SAT and VAT from BL to 24 and 52 weeks PS. In this study the measurement of LF was made using MRS with a STEAM sequence to estimate intrahepatic triglyceride, while PF was measured by interrogating multiple regions of interest drawn on a single-slice Philips mDIXON fat fraction image fit with the multi-peak spectral model of fat. LF was significantly reduced 24 weeks after surgery ($p=0.005$), and PF decreased by approximately 25% at 24 weeks PS, but this was not significant; a significant decrease was seen in all measures from BL to 52 weeks PS (52). With a focus on changes to fat, Lehmann *et al.* (49) investigated the changes to abdominal SAT

and VAT volume using DIXON MRI at 4 weeks after RYGB. VAT volume decreased by 11% PS; SAT volume could not be evaluated due to incomplete data due to restrictions with the Field of View (FOV). T_1 changes were also measured in the SAT and VAT using MOLLI T1 mapping (see Section 3.4), with a decrease of 0.9% and an increase of 4.4% for SAT and VAT T_1, respectively, but the changes seen were not significant, and this was suggested to be due to restrictions with the method used such as MOLLI's sensitivity to fat and too few/short TIs used (49).

Li *et al.* (53) performed a large cohort longitudinal study on 203 T2D RYGB patients at BL, 24 weeks and 1, 2, 3, 4 and 5-years PS to understand the correlation of BL body fat percentage with diabetes remission. It is important to note that in this study not all the participants completed all of the time points; for RYGB, there were N=70 who completed scans at Year 5. Results were compared to a cohort of 311 SG patients (N = 168 T2D) with time points at 24 weeks, 1 and 2 year PS. This study was not primarily an MR study, and body fat percentage was calculated using a participant's Body Mass Index (BMI), age and sex and diabetes remission was assessed using blood tests. A single slice MRI was acquired at the 3rd lumbar vertebrae to assess the SAT and VAT area. A significant drop compared to BL was seen on SAT and VAT area at all time points for both male and female participants in both the diabetic remission and non-remission groups ($p<0.001$). Still, no significant difference was seen between the males and females or remission and non-remission in these measures. Diabetes remission significantly correlated with all body measures; they noted that changes to body

fat percentage at 24 weeks were an excellent predictor of diabetes remission and that the largest changes to body composition occurred in the first 24 weeks (53). Tan *et al*. (54) investigated the changes to iron-corrected liver MOLLI T_1 (cT_1) and T_2*, LF, SAT, VAT and Magnetic Resonance Elastography (MRE) liver stiffness in 9 participants undergoing SG at BL, 4 and 24 weeks PS. 67% of the participants had T2D. SAT and VAT volumes were not calculated; instead, the SAT and VAT area at the 3rd Lumbar vertebrae was used. A significant drop was seen at 4 and 24 weeks PS in LF ($p = 0.0159$ and 0.0018, respectively) and VAT ($p = 0.0021$ and 0.0006, respectively), and in cT_1 MOLLI at 4 weeks PS ($p = 0.0473$) and SAT at 24 weeks PS ($p = 0.0256$). A significant increase was also seen in liver T_2* at 24 weeks PS ($p = 0.0355$). No significant change was seen in the MRE liver stiffness, possibly due to the time points chosen being too early for the reversal of fibrosis (54). Chiyanika *et al.* (55) investigated the effectiveness of iron-corrected MOLLI T_1 (cT_1) in assessing NAFLD progression in bariatric surgery and lifestyle modification cohorts. The study performed MOLLI T_1 and DIXON MRI at BL and 16 weeks PS; 13 participants underwent SG (8 T2D), and 21 underwent lifestyle modification (17 T2D). Semi-automatic segmentation was performed on the liver maps for LF, liver cT_1 and 3 ROIs were placed in the liver T_2* maps to calculate the average values used for the MOLLI T_1 correction. Using automatic segmentation, SAT and VAT volumes were also assessed using the DIXON MRI. At BL, there was no significant difference between the SG and lifestyle modification groups for LF, liver cT_1 and T_2* and VAT; however, the SG group had a

significantly higher SAT volume (p=0.031). For the SG group, a significant decrease was seen in LF, liver cT_1 and SAT with a significant increase in liver T_2* (p = 0.012, 0.025, 0.018 and 0.017, respectively) from BL to 16 weeks PS. No significant change was seen in VAT. A significant decrease was seen in LF (p = 0.012) for the lifestyle modification group, and no significant change was seen in liver cT_1 and liver T_2*, SAT or VAT. At 16 weeks PS, the SG group had significantly lower LF and SAT (p < 0.001, p = 0.032, respectively) than the lifestyle modification group. However, there was no significant difference between the lifestyle modification and SG groups in liver cT1, liver T2* and VAT. It was noted that three participants in the lifestyle modification group had an increase in liver cT_1 at 16 weeks PS, indicating worsening liver health, whilst all SG patients showed a reduction in liver cT_1. The study found that liver cT_1 significantly correlated with a non-alcoholic steatohepatitis activity score used for grading the degree of NAFLD (p = 0.008) and was comparable to the use of LF in staging the disease (55).

For the above studies, the percentage reduction from baseline in common endpoints at 12 and 24 weeks PS are summarised in Table 3.2

STUDY	Liver Volume (LV)		Liver Fat (LF)		Subcutaneous Adipose Tissue (SAT)		Visceral Adipose Tissue (VAT)	
Post Surgery Weeks	***12***	***24***	***12***	***24***	***12***	***24***	***12***	***24***
Meyer-Gerspach *et al. (2019)* (51)	21	26	64	74				
Hedderich et al. (2017) (50)	9	8	42	68	20	41	36	52
Hui et al. (2019) (52)			85		30		46	
Li et al. (2024) (53)						* 51.5(M) *41.7 (F) 42.2 (M) 40.0 (F)		*81.6 (M) *76.1 (F) 74.8 (M) 70.3 (F)
Tan et al. (2023) (54)				65		34		37

*Table 3.2 – Approximate percentage reduction from baseline to ~12 and ~24 weeks PS measured in bariatric studies. *shows diabetic remission group, M and F indicates Male and Female. SAT and VAT values from Hedderich et al. (2017) show a % reduction in volume, whilst those from Li et al. (2024) and Tan et al. (2023) describe a % rection in area.*

A study encompassing both RYGB and SG has been performed by Luo *et al.* (46) who investigated LF changes in 49 (26 RYGB, 20 SG, and 3 Gastric banding) participants at BL, post low-calorie diet (PLD) and 4, 12 and 24 weeks PS. They

showed a statistically significant reduction in LF between each successive timepoint, with a ~42% reduction seen from PLD to 4 weeks PS. No statistical significance was seen between the RYGB and SG groups for LV and LF decrease; however, the RYGB group had a significantly higher reduction in BMI at 24 weeks after surgery. Bai *et al.* (57) investigated the change to LF, PF, LV and Pancreatic Volume (PV) after SG in 21 non-diabetic participants. All underwent MRI scans prior to surgery, with 10 having scans 12 weeks PS and 11 having scans at 1-2 years PS. Fat and volume measurements in the liver and pancreas were made from DIXON MRI FF maps from manually drawn masks. LV and PV significantly decreased at 12 weeks PS and 1-2 years from BL ($P<0.01$ for all), but no significance was seen between 12 weeks and 1-2 years PS time points (though this comparison was across different participants). At BL, 81% of participants had fatty livers, and 38.1% of participants had a fatty pancreas; no patients had a fatty liver at 12 weeks PS and no fatty pancreas present at 1-2years PS, and no cut-off for these measures are stated in the paper (57).

Any issues that arise from a small field-of-view (FOV) in the imaging volume can be exacerbated in bariatric participants. Often, the maximum imaging FOV may not capture the entirety of the abdomen, making accurate SAT volume quantification difficult, as described by Lehmann et al. (28). Michel *et al.* (59) attempted to find surrogate methods to estimate SAT volume with data which had an incomplete imaging FOV to cover participants. Using data from 193 participants with Body Mass Index (BMI) ranging from 24.5 - 45 kgm^{-2} who had

FOV of sufficient coverage for complete data for SAT volume measures, the thickness of the abdominal wall fat or hip fat, and partial area and partial volume of SAT were tested as surrogate methods. Better agreement was seen for male participants compared to females across all methods. Partial volume assessment, using volumes of abdominal wall fat from a ROI between the femoral heads ($V_{p\text{-}FH}$) or anterior superior iliac spines ($V_{p\text{-}ASIS}$) was shown to be the most successful surrogate at estimating SAT volume. $V_{p\text{-}FH}$ was marginally more successful ($R^2 = 0.78$ compared to $R^2 = 0.69$) likely due to it encompassing a larger area, hence, giving more information to the algorithm (59).

3.4 MRI and MRS Sequences used in this study of Bariatric Surgery

This section provides an overview of the common artefacts resulting from the complications of imaging larger patients, and the MRI and MRS sequences used to collect the data shown in this chapter. First, the considerations for scanning participants of a larger size prior to their bariatric surgery are outlined. Following this the theory of the MRI and MRS sequences implemented are outlined.

3.4.1 Common Artefacts when Scanning Larger Participants

This section covers the common MRI artefacts, including the sources and possible mitigations needed that are relevant to the study of larger participant groups as assessed in this chapter.

3.4.1.1 Signal Wrap

Signal wrap occurs when anatomy outside of the FOV folds onto (or wraps over) anatomy inside the FOV; this can happen in either the phase or, less often, in the frequency encoding direction. In an ideal situation, only those frequencies from inside the FOV would be encoded. If the sampling of the frequencies in an echo does not follow the Nyquist theorem,

$$\nu_{sampling} = 2 \cdot \nu_{Nyquist}$$

Equation 3.1

where $\nu_{Nyquist}$ is the highest frequency present in the echo, then the frequencies are under sampled and can lead to a mischaracterisation of the echo. Frequency wrap then occurs from signal outside the FOV in the frequency encoding direction, which presents as overlayed anatomy. Phase can only take a value between 0 and 2π, meaning phase values will repeat along the phase encoding direction. The rate of phase repetition is dependent on the applied gradient used to encode them; if spins outside the FOV have identical phases to spins inside the FOV, then the signal will wrap.

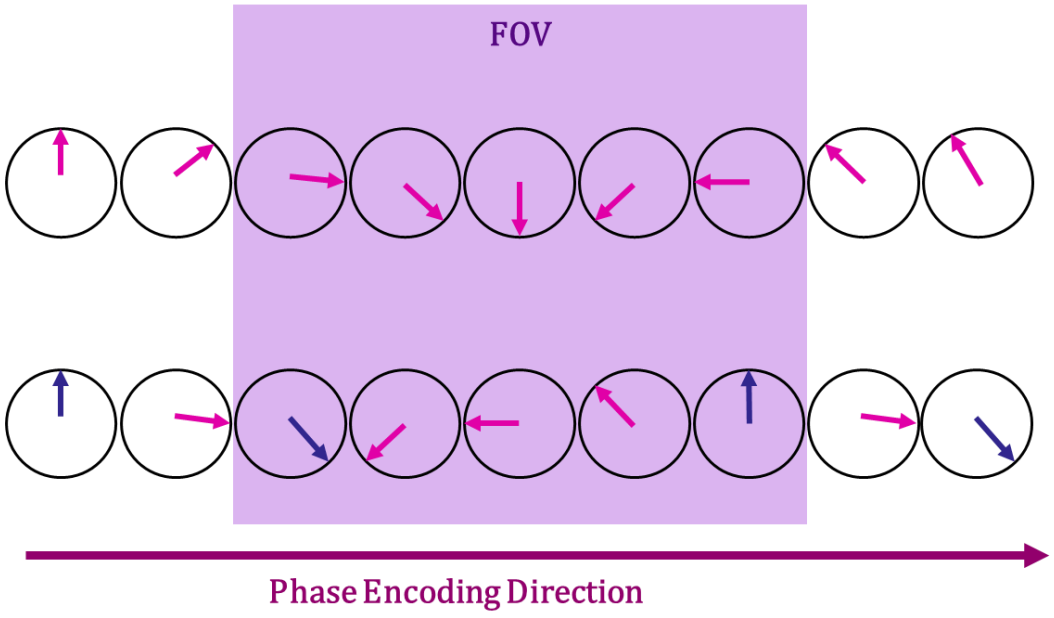

Figure 3.3 - How phase wrap occurs. Top row - No phase wrap; spins outside FOV all have different phases to spins inside FOV. Bottom row - Phase of spins outside FOV matches the phase of spins inside FOV. Spins with matching phase (blue arrows) will wrap.

3.4.1.2 Motion Artefacts

Motion during imaging causes a ghosting effect within the image, an effect which is most dramatic in the phase encoding (PE) direction. The prominence of the effect in the PE direction is due to the PE gradient changing with each TR, which can lead to the same location within a sample being phase encoded differently between repetitions.

There are many sources of motion that can lead to ghosting artefacts; these can be broadly categorised as bulk motion (patients become uncomfortable or bored and move) or physiological motion (cardiac motion, respiratory motion, and flow). To reduce the risk of bulk motion, the duration of scan visits should be kept as short as possible, and participants should be instructed to keep still. Physiological motion can be accounted for using the in-built triggering systems of the scanner. Respiratory motion can also be negated through breath-hold (BH) acquisitions. Larger patients often have trouble holding their breath for an extended period; in these situations, multiple BH acquisitions can be used for a given sequence. The BH can be performed at either inspiration or expiration. In the case of failed BHs, participants can be instructed that they should slowly release the hold and not gasp for breath, reducing the amount of motion that occurs.

3.4.1.3 Chemical Shift Artefacts

The signal from protons in fat and water precess at different Larmor frequencies with a chemical shift difference of ~3.5 ppm (440Hz difference at 3T). Under certain conditions this difference can lead to chemical shift artefacts in the frequency encoding direction.

The receive bandwidth (Δω) of an image is divided across the matrix size of the image; for example, for a 256 x 256 image matrix, if Δω = 32 kHz, each voxel spans 125 Hz, however with Δω = 64 kHz, each spans 250 Hz. Due to the chemical shift difference between fat and water, in the Δω = 64kHz image then fat and water appear to be from neighbouring voxels, but in the Δω = 32 kHz image the fat and water signals are separated by 2 voxels, as shown in Figure 3.4.

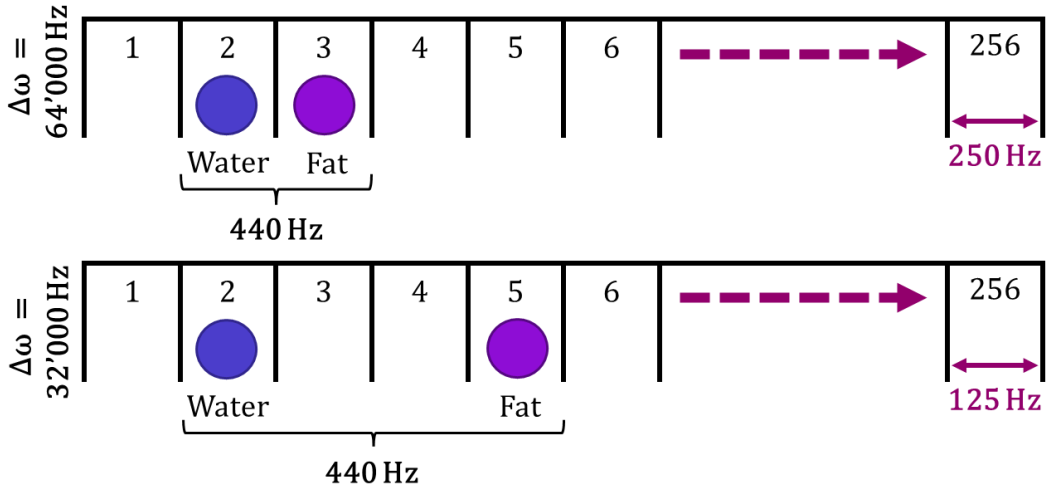

Figure 3.4 - Source of Chemical Shift Artefact - fat and water shift shown for two receive bandwidths.

This leads to bright and dark bands on the images at interfaces between areas of fat and water, Figure 3.5, this effect is more pronounced at higher field strength as the chemical shift in Hz increases.

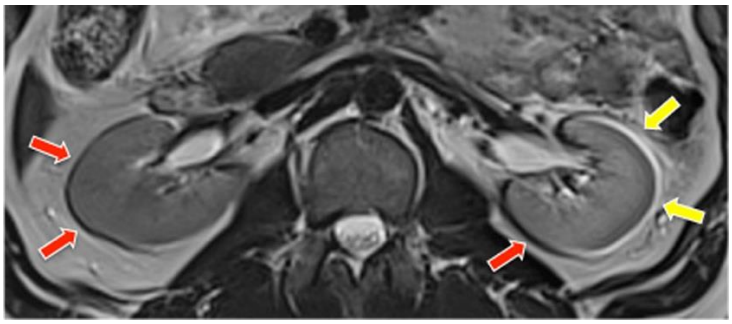

Figure 3.5 - Example of chemical shift artefact - taken from mriquestions.com (60)

3.4.2 MRI and MRS Sequences used in this bariatric surgery study

This section outlines the theory of the MRI and MRS sequences implemented in this chapter. Table 3.3 contains a list of all the sequences used in this study with the acquisition parameters, these are then expanded upon in the following sections.

Scan	Parameters			Arm A	Arm B
	Respiration (BH/FB)	Space (FOV, voxel size in mm)	Other		
Abdominal 6-point mDIXON Quant	BH	FOV = 450 x 450, Voxel = 2.5 x 2.5 x 6 Slices = 77 Orientation = Axial	SENSE = N TR = 5.7 ms TE = 0.98 ms ΔTE = 0.7 ms Duration = 16 s	X	X
Dual-echo B_0 mapping	BH	FOV = 440 x 357, Voxel = 6.8 x 6.8 x 6 Slices = 27 Orientation = Axial	SENSE = Y (2 AP) TR = 20 ms TE1 = 4.8 ms TE2 = 7.2 ms Duration = 17 s	X	X
DREAM B_1 mapping	BH	FOV = 440 x 374, Voxel = 3.5 x 3.5 x 6 Slices = 27 Orientation = Axial	SENSE = N TR = 4.5 ms TE1 = 1.5 ms TE2 = 2.4 ms Duration = 17 s	X	X
Pancreas eThrive	BH	FOV = 450 x 400, Voxel = 1.7 x 1.7 x 3 Slices = 82 Orientation = Axial	SENSE = Y (2.5 RL, 1.3 FH) TR = 2.7 ms TE = 1.3 ms Duration = 10 s	X	X
Abdominal T_1 MOLLI	5 x BH	FOV = 440 x 330, Voxel = 2.3 x 2.3 x 8 Slices = 5 Orientation = Axial	SENSE = Y (2 AP) TR = 2.4 ms TE = 1 ms FA = 35° Duration = 55 s	X	X
SVS STEAM ^{1}H liver MRS Water-Supressed and Non-water Supressed	BH	Voxel = 20 x 20 x 20	TR = 2500 ms TE = 15/30/45/90 ms BW = 2000 Hz FA = 90° Duration = 10 s (WS = MOIST, BW = 200 Hz)	X	X

Scan	Parameters			Arm A	Arm B
	Respiration (BH/FB)	Space (FOV, voxel size in mm)	Other		
^{1}H liver adipose tissue MRS	FB	Voxel = 20 x 20 x 20	TR = 2500 ms TE = 14 ms BW = 2000 Hz FA = 90° Duration = 15 s WS = N	X	X
Kidney T_2* 12-echo	BH	FOV = 384 x 384, Voxel = 1.5 x 1.5 x 5 Slices = 1 Orientation = Coronal	SENSE = Y (2 RL) TR = 80 ms TE = 4.6 ms ΔTE = 4.6 ms Duration = 11 s	X	X
Kidney T_1 5(3)3 MOLLI	BH	FOV = 384 x 384, Voxel = 1.5 x 1.5 x 5 Slices = 1 Orientation = Coronal	SENSE = Y (2 RL) TR = 3 ms TE = 1.5 ms FA = 20° Duration = 11 s	X	X
AO Flow	FB	FOV = 280 x 265, Voxel = 2 x 2 x 10 Slices = 1 Orientation = Axial	SENSE = Y (2 AP) TR = 3.8 ms TE = 2.5 ms Flow 300 mm/s FA = 15° Duration = 27 s	X	X
Abdominal GraSE T_2	Triggered	FOV = 420 x 420 Voxel = 3 x 3 x 5 Slices = 5 Orientation = Axial	SENSE = Y (3 AP) TR = 3000 ms TE = 12.9 ΔTE = 12.9 No. Echoes = 10 Duration = 290 s	X	

Scan	Parameters			Arm A	Arm B
	Respiration (BH/FB)	**Space (FOV, voxel size in mm)**	**Other**		
SE-EPI fat suppressed T_1 mapping	Triggered	FOV = 420 x 420 Voxel = 3 x 3 x 8 Slices = 9 Orientation = Axial	SENSE = Y (2 AP) TR = 8000 ms TI (ms) = 100, 125, 150, 200, 250, 300, 4 500, 600, 700, 800, 900, 1100, 1300, 1500 Duration = 130 s	X	
Diffusion Weighted Imaging	Triggered	FOV = 420 x 420 Voxel = 3 x 3 x 5 Slices = 9 Orientation = Axial	SENSE = Y (2 AP) TR = 898 ms TE = 66 ms b (s/mm^2) = 0, 5, 9, 10, 20, 30, 40, 49, 50, 69, 70, 100, 105, 200, 300, 400, 500 3 Directions Duration = 260 s	X	
2D Gradient Echo Magnetisation Transfer (CEST)	Triggered	FOV = 440 x 440 Voxel = 3 x 3 x 5 Slices = 1 Orientation = Axial	SENSE = CS (2) TR = 5 ms TE = 3.4 ms Freq. Offsets (Hz) = -10000, -7000, -5000, -3000, -2000, -1300, -800, -500, -450, -400, -300,0, 300, 400, 450, 500, 800,1300, 2000, 3000, 5000, 7000 Saturation BW = 1260 Hz Sweep = Full Duration = 90 s	X	
Scan	**Parameters**				

	Respiration (BH/FB)	Space (FOV, voxel size in mm)	Other	Arm A	Arm B
Whole body mDIXON	2 x BH 4 x FB	FOV = 400 x 360 Voxel = 2.5 x 2.5 x 6 Slices = 120 Stacks = 6 Orientation = Coronal	SENSE = Y (1 AP, 2 RL) TR = 5.4 ms TE = 0.9 ms ΔTE = 0.7 ms Duration = 160 s		X
Cardiac 2-chamber cine	BH	FOV = 300 x 300 Voxel = 2 x 1.6 x 8 Slices = 1	SENSE = Y (RL = 2) TR = 2.8 ms TE = 1.4 ms Duration = 7 s		X
Cardiac 4-chamber cine	BH	FOV = 300 x 300 Voxel = 2 x 1.6 x 8 Slices = 1	SENSE = Y (AP = 2) TR = 3 ms TE = 1.5 ms Duration = 8 s		X
Cardiac short-axis stack	BH	FOV = 300 x 300 Voxel = 2 x 1.6 x 8 Slices = 12	SENSE = Y (AP = 2.2) TR = 3 TE = 1.5 Duration = 13 s		X
^{31}P liver MRS x 2	FB	Slab Thickness = 60 mm	TR = 8000 ms NSA = 150BW = 4000 Hz Excitation FA = 180° Saturation FA = 100° Duration = 1208 s		X

Table 3.3 – Scans acquired across the bariatric study with acquisition parameters provided. Scans performed on both arms are shaded purple, scans for Arm A only are shown in pink and scans for Arm B only are shown in blue. BH – Breath-hold, FB – Free-Breathing.

3.4.2.1 DIXON MRI for study of organ fat fraction, T_2 and volume*

The DIXON MRI sequence (61) takes advantage of the chemical shift difference between water and fat (~3.5 ppm, equivalent to 440 Hz at 3 T). Separate images of fat and water can be created by collecting images at different echo times in which the fat and water spins are in-phase and out-of-phase (also termed opposed-phase) with each other (at 3 T, the difference in echo time (ΔTE) required between the two states is approximately 1.1 ms, with an out-of-phase image collected at a TE of 1.1 ms and an in-phase image at a TE of 2.2 ms). The in-phase signal (S_{ip}) originates from the sum of the water signal (S_w) and fat signal (S_f), and the out-of-phase signal (S_{op}) from the difference:

$$S_{ip} = S_w + S_f$$

Equation 3.2

$$S_{op} = S_w - S_f$$

Equation 3.3

By summing or differencing the in-phase and out-of-phase images, the water and fat signals can be isolated:

$$S_{op} + S_{ip} = (S_w + S_f) + (S_w - S_f) = 2S_w$$

Equation 3.4

$$S_{op} - S_{ip} = (S_w + S_f) - (S_w - S_f) = -2S_f$$

Equation 3.5

The simplest DIXON sequence uses two echo times when are set to in-phase and out-of-phase. However, if data is collected with multiple echoes which are not fixed to the in-phase and out-phase echo times (this is termed mDIXON and typically 6 echoes are used), it is possible to compute fat and water images whilst also correcting for B_0 inhomogeneities and fitting for fat fraction (FF, %) and T_2*. In this Chapter, a 3D 6-echo gradient echo mDIXON scan using the Philips mDIXON Quant product is collected, with the reconstructed water image then used for volumetric quantification of organs and the FF image used to assess fat within the organs, Figure 3.6.

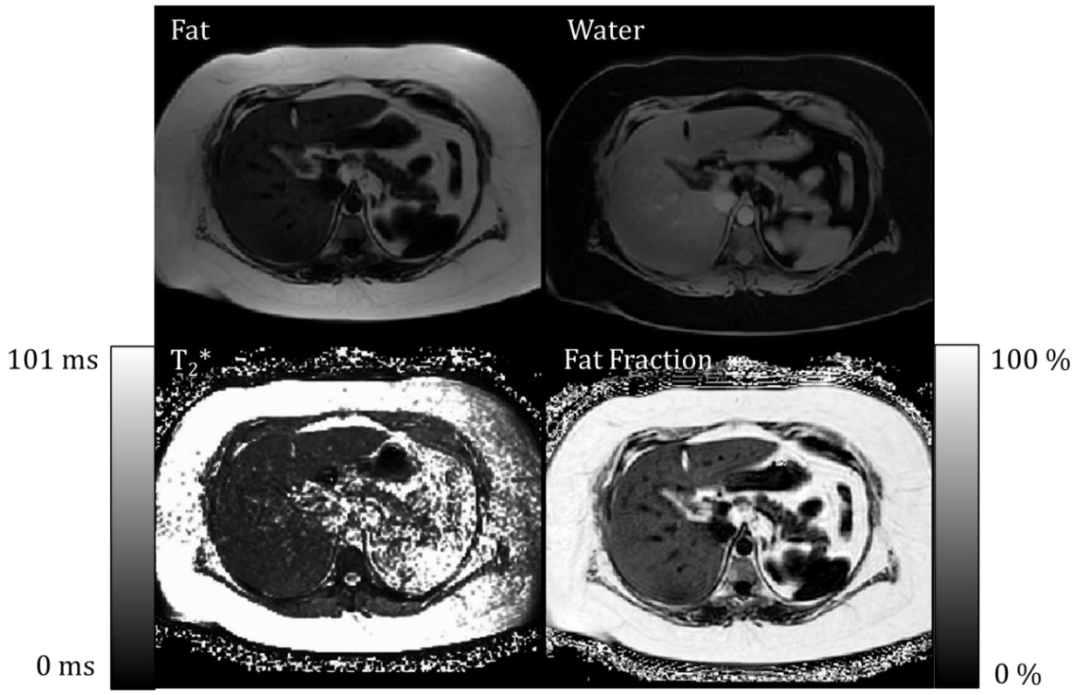

Figure 3.6 - Example of mDIXON outputs, showing the Fat, Water, T_2 and Fat Fraction images*

3.4.2.2 Proton MR Spectroscopy for assessment of liver fat fraction

Methods for acquiring and localising proton (^{1}H) spectra are outlined in Chapter 2. In this chapter, proton MRS is used to investigate the FF of liver tissue using a single voxel STEAM acquisition. The MRS fat fraction (FF_{MRS}) is calculated as the ratio of the sum of the signals of the fat peaks (S_f) compared to the signal from the water peak (S_w),

$$FF_{MRS}(\%) = \frac{S_f}{S_w + S_f} \times 100$$

Equation 3.6

and represented as a percentage. In ^{1}H MRS the water peak has a much larger amplitude than any other metabolite, in the case of fat some of the peaks are visible but dwarfed by the water peak whilst others are completely hidden. Therefore, to accurately quantify the fat MRS peaks, water suppression techniques must be used. One such method is CHEmical Shift Selective saturation (CHESS), which was described in Chapter 2. There are multiple versions of CHESS each named with a water theme, in this chapter the MRS acquisition used the VAPOUR water suppression method as described in Section 2.4.3.1.

3.4.2.3 T_1 Mapping of abdominal organs

In this chapter, two different T_1 mapping sequences are collected. The first is a MOdified Look-Locker Inversion recovery (MOLLI) sequence, which uses a balanced FFE (bFFE) readout (as termed on Philips, and also known as balanced Steady-State Free Precession (bSSFP), True Fast Imaging with Steady-state Precession (TruFISP), and FIESTA by various manufacturers) and results of this scheme are reported in this chapter. The second sequence is an Inversion Recovery (IR) fat-suppressed sequence with Spin-Echo EPI (SE-EPI) readout, but results for this method are not included in this thesis work.

In this chapter a 5(3)3 MOLLI implementation is used, as shown in Figure 3.7, this applies two inversion pulses over eight heart beats with a three-beat recovery period in between. For this work a physiological simulator is used to set a fixed beat

interval of 60 beat-per-minute (1s R-R interval), this results in the images shown in Figure 3.8.

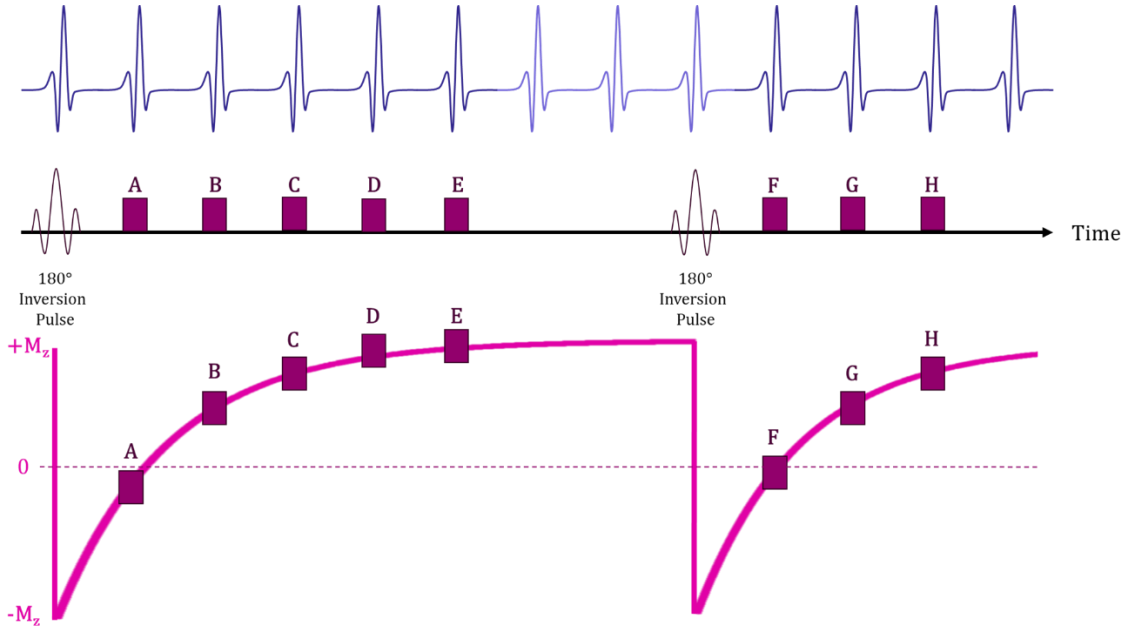

Figure 3.7 – Timings of a T_1 MOLLI 5(3)3 implementation and simulated heart rate

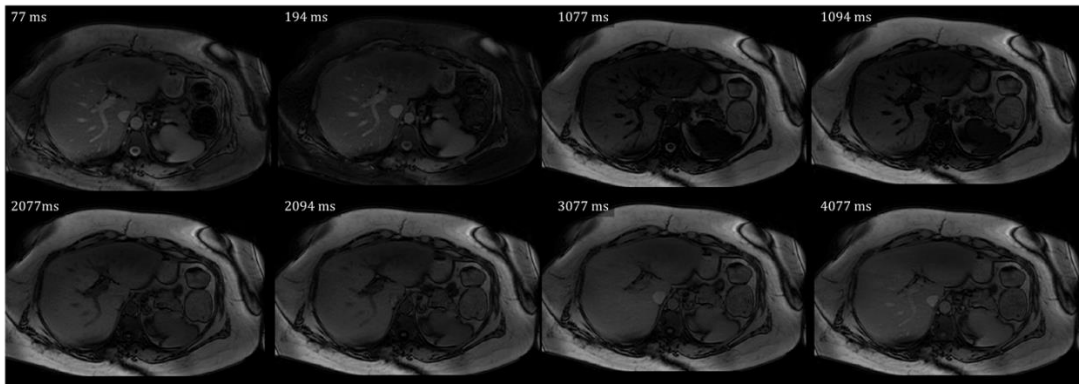

Figure 3.8 - Example MOLLI images of the abdomen acquired using a 5(3)3 sequence.

Data points in the MOLLI scheme can then be fit to the following equation

$$Signal = A - Be^{\left(\frac{-t}{T_1*}\right)}$$

Equation 3.7

where *A* and B are fitting parameters related to the equilibrium magnetisation and type of preparation, *t* is the time after the inversion pulse. Importantly for a MOLLI scheme, the RF pulses in the bFFE scheme used to acquire the image will affect the T_1 recovery curve, resulting in an apparent T_1 termed T_1* being fit which is not the same as the true T_1 for an undisturbed inversion recovery. This true T_1 relaxation time can be recovered by using the following approximation

$$T_1\ (ms) = \left(\frac{B}{A-1}\right) \cdot T_1^*$$

Equation 3.8

It should be noted that the T_1 values computed by the MOLLI bFFE scheme can also depend on other factors, including the bFFE TR, tissue T_2, off-resonance (B_0) and RF-homogeneity (B_1), as well as Fat Fraction (FF), as have been reported by Mozes *et al.* (62) Figure 3.9 shows a simulation taken from Mozes *et al.* which illustrates the dependence of MOLLI T_1 on FF, it can be seen that high FF leads to elevated measured MOLLI T_1 values. This is an important consideration in larger patients who are undergoing bariatric surgery and whose FF may change throughout their bariatric surgery journey.

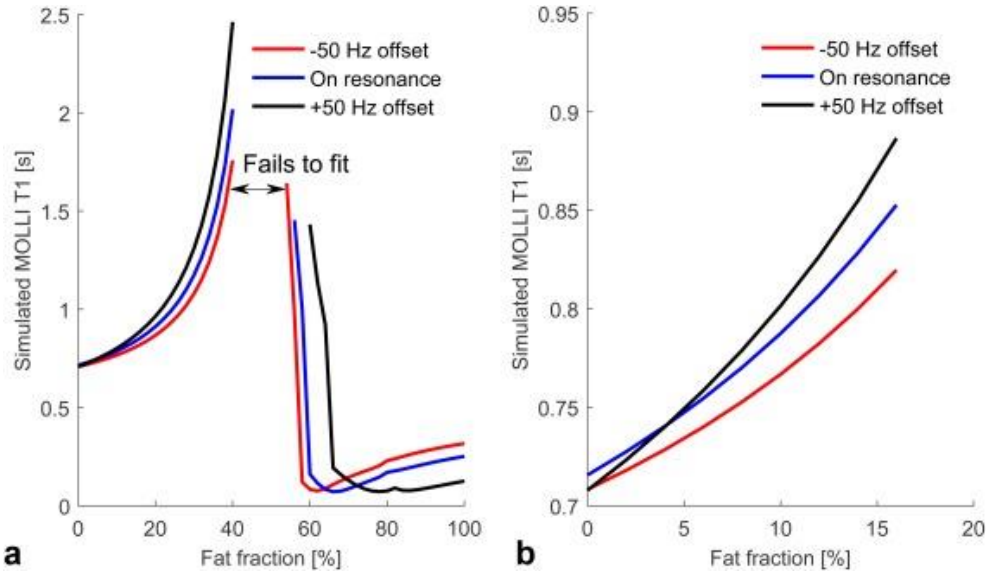

Figure 3.9 – Simulation of the effect of fat fraction (%) on MOLLI T_1 (s) taken from Mozes et al. (62) assuming a 5(3)3 MOLLI scheme with flip angle (FA) = 35°, TR/TE = 2.3/1.15 ms as used in this thesis chapter.

An Inversion Recovery (IR) scheme is the simplest method by which to evaluate the T_1 of a tissue, as described in Chapter 2. In a subset of participants, an IR-SE-EPI sequence was also collected. For this scheme, an inversion pulse is applied followed at an inversion time (TI) later by a SE-EPI readout, a period is then allowed for the spins to recover prior to repeating this process, Figure 3.11. This process is then repeated for a range of TIs and fitted to the solution of the Bloch equation for the longitudinal relaxation time. In the IR-SE-EPI scheme implemented in this thesis, non-selective inversion was applied, and multi-slice SE-EPI slices were obtained after the inversion pulse, leading to variations in TI across the slices, which is accounted for in the fit. Acquisitions are performed in both ascending (slice 1-9) and

descending (slice 9-1) slice ordering to increase the dynamic range of inversion times acquired for each slice, Figure 3.10.

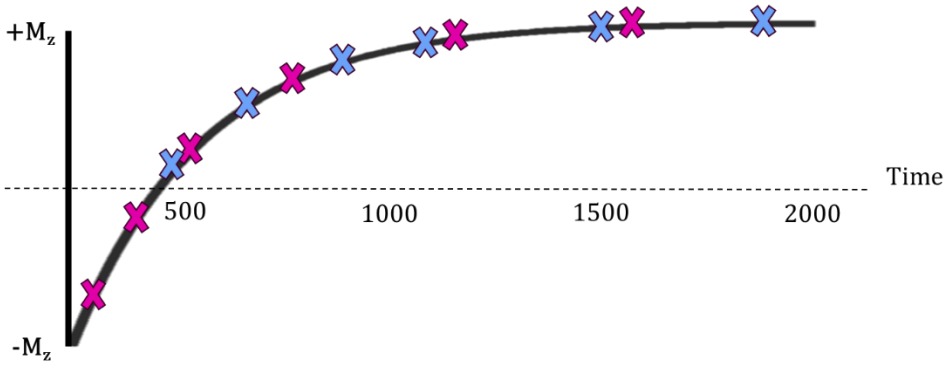

Figure 3.10 – Schematic of how acquiring data with ascending and descending slice ordering provides a larger range of inversion times for the multi-slice T_1 IR-SE-EPI sequence.

For the IR-SE-EPI scheme, a fat suppression RF pulse (using the chemical shift difference between fat and water (3.5 ppm) – Section 3.4.1.3) is applied prior to the image readout to remove any contamination from fat when measuring the tissue T_1, example images are shown in Figure 3.12. Note that the fat signal is suppressed in all images, unlike the T_1 MOLLI images shown in Figure 3.8. The results of this method are not reported in this chapter.

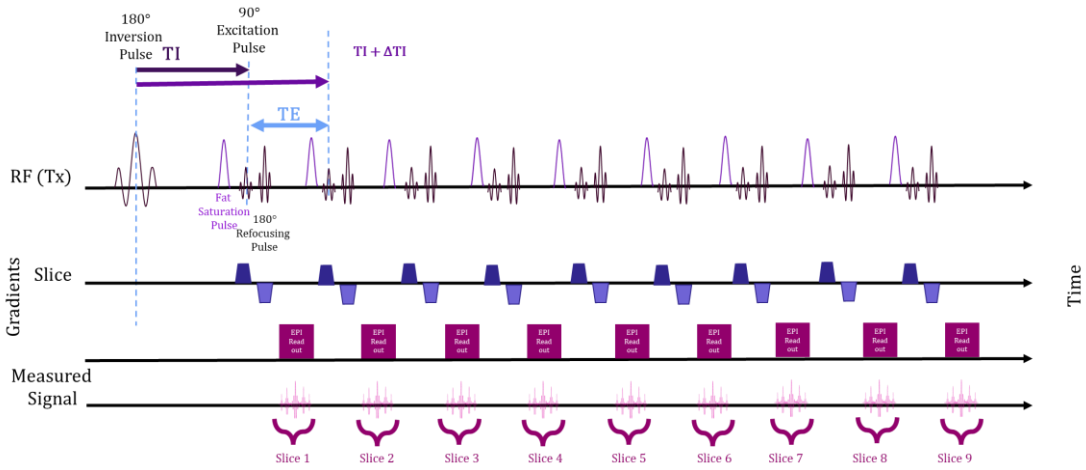

Figure 3.11 - Multi-slice inversion recovery SE-EPI T_1 mapping sequence. Inversion times across the slices vary as shown in purple. Note the EPI readout is shown schematically. The data is also collected with a fat suppression pulse prior to the EPI readout. This scheme is repeated for each inversion time (TI), where within each TI, slice 1 is collected at time = TI, slice 2 at time = TI +ΔTI … slice 9 at time = TI +8ΔTI. The entire scheme is then repeated for descending slice ordering.

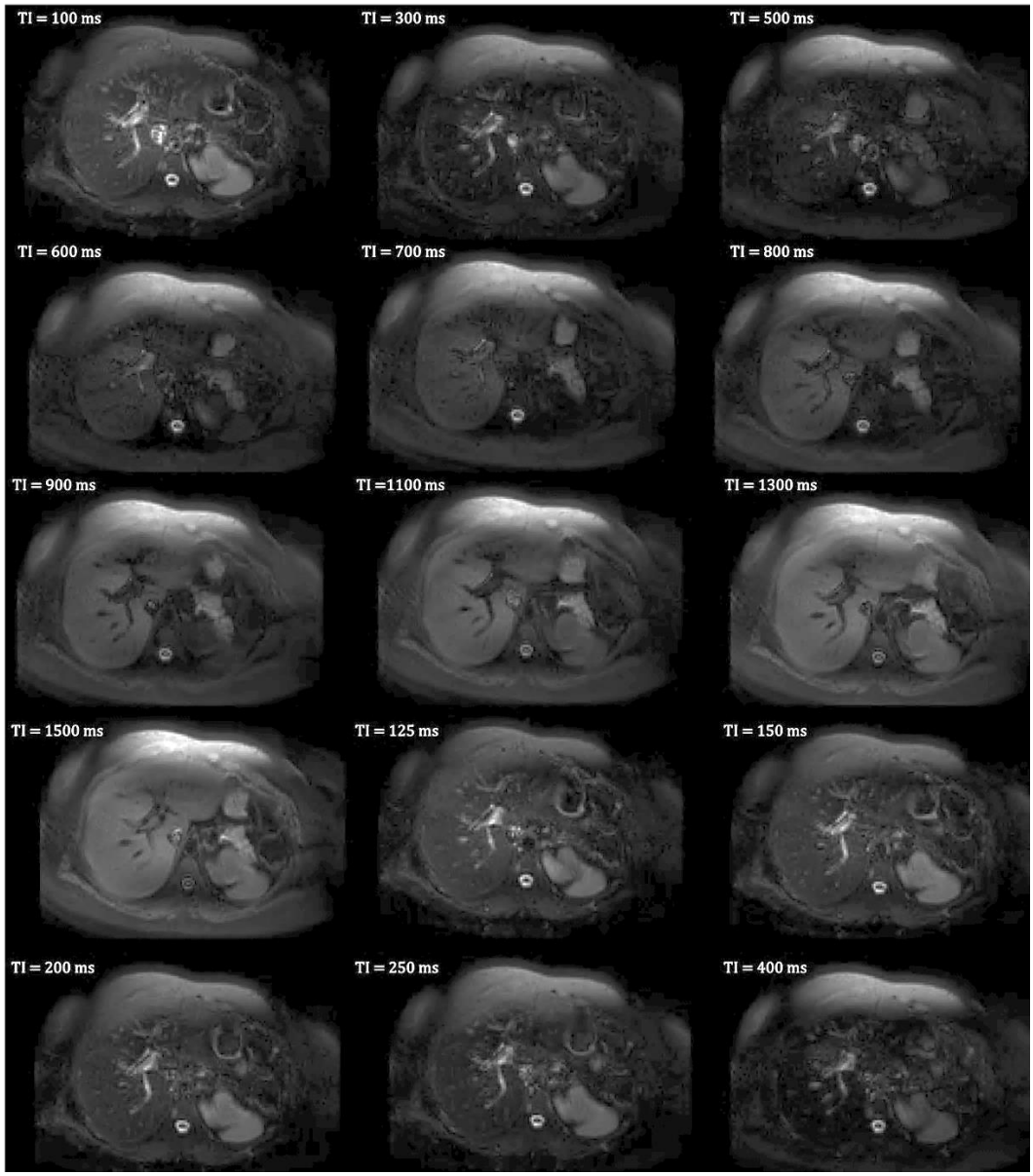

Figure 3.12 - Example IR-SE-EPI images shown for 1st slice in the 9 slice readout. Inversion times are shown for each image. Note the artefact in the anterior of the image due to fat (despite SPIR being used) as the fat suppression can fail on large subjects and is especially dependent on the accuracy of the shimming.

3.4.2.4 T_2 Mapping of abdominal organs

There are multiple methods to perform T_2 mapping (63–66), the Gradient Spin-Echo (GraSE) scheme with 10 echoes is used in this Chapter. In the GraSE scheme, multiple refocusing RF pulses are applied resulting in multiple gradient echo-readouts collected between, as shown in Figure 3.13. The first echo is discarded by the scanner to ensure a robust T_2 fitting measure. Example images can be seen in Figure 3.14.

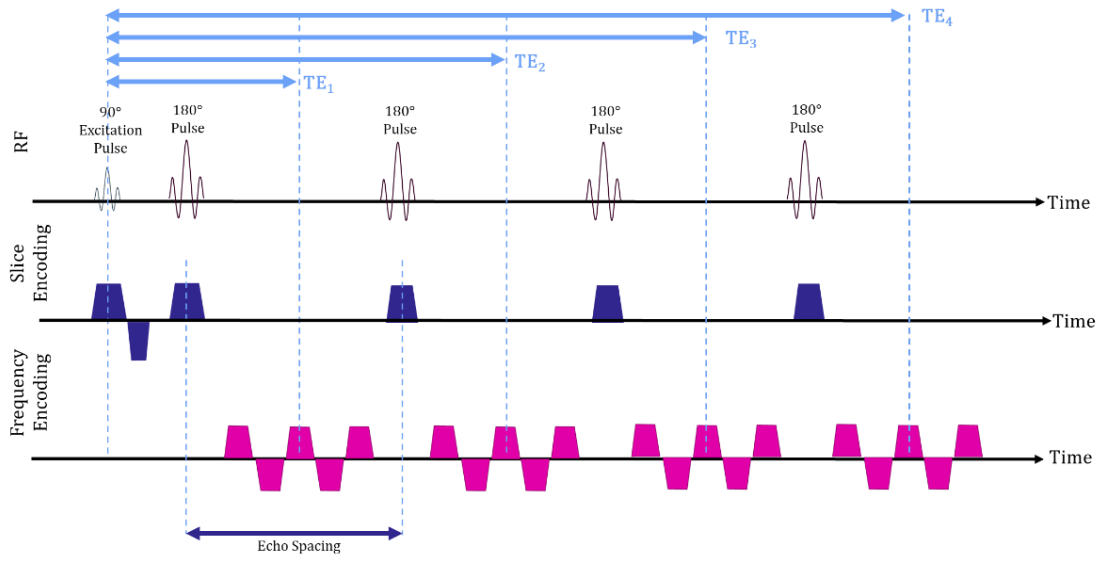

Figure 3.13 – Simplified pulse sequence diagram for a GraSE T_2 mapping showing the RF, slice encoding and frequency encoding gradients for 4 of 10 echoes.

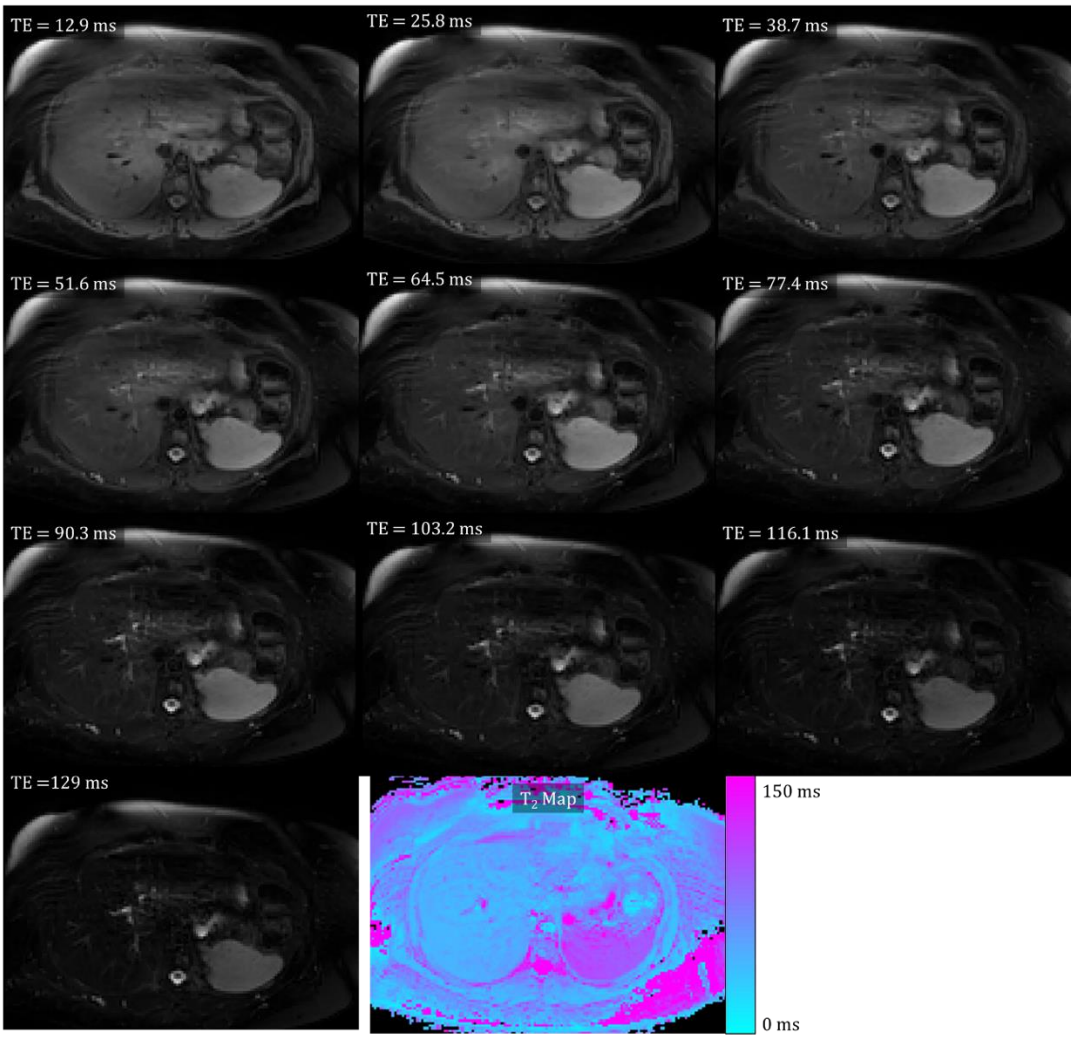

Figure 3.14 - Example of echoes (TE shown on image) and T_2 map (bottom middle) acquired using a GraSE sequence.

3.4.2.5 Diffusion-Weighted Imaging of abdominal organs

Diffusion Weighted Imaging (DWI) is a method for measuring the Brownian motion of water in tissues, both in cells and extracellular space within a voxel. The restriction of water in a tissue, as occurs in fibrosis, reduces the MR-measured apparent diffusion coefficient (ADC) parameter.

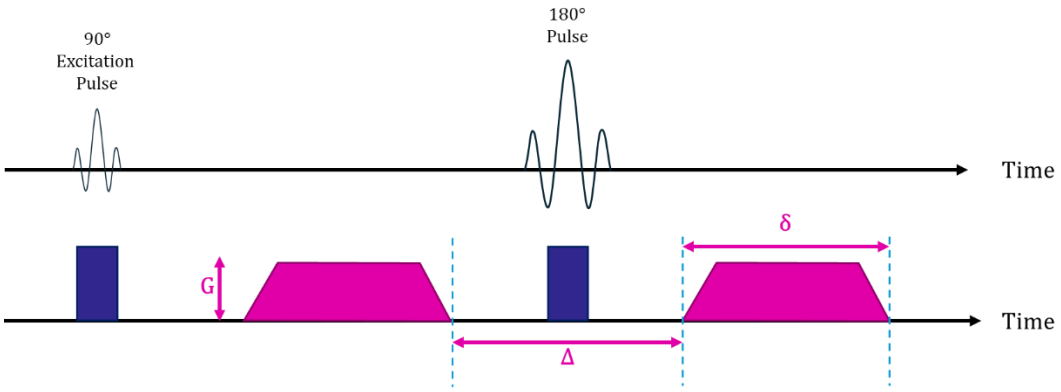

Figure 3.15 - RF pulse train, slice selection (blue) and diffusion gradients (pink) for diffusion-weighted imaging.

To perform DWI, strong diffusion gradients are applied either side of a 180° refocussing pulse and this is followed by a SE-EPI readout. The diffusion gradients can be applied in three perpendicular directions. The amount of diffusion weighting is dependent on the duration of the diffusion gradients (δ), the time between the gradients (Δ) and their amplitude (G) as shown in Figure 3.15. The b-value of each diffusion weighting is given by

$$b\ (smm^{-2}) = \gamma^2 G^2 \delta^2 \left(\Delta - {}^{\delta}/_{3}\right)$$

Equation 3.9

In DWI, images are collected at multiple b-values to assess the diffusion properties of tissue. Larger b-values require longer echo times (TE) to fit in the required gradients which exacerbates the effects of signal attenuation that occurs. Data from across the multiple b-value are then fit to,

$$S(b) = S_0 e^{-b \cdot ADC}$$

Equation 3.10

where S_0 is the signal when b = 0 and ADC is the Apparent Diffusion Coefficient given in mm^2s^{-1}, with ADC mapped and interrogated to assess tissue microstructure. Example DW images are shown in Figure 3.16. Results on DWI are not reported within this thesis.

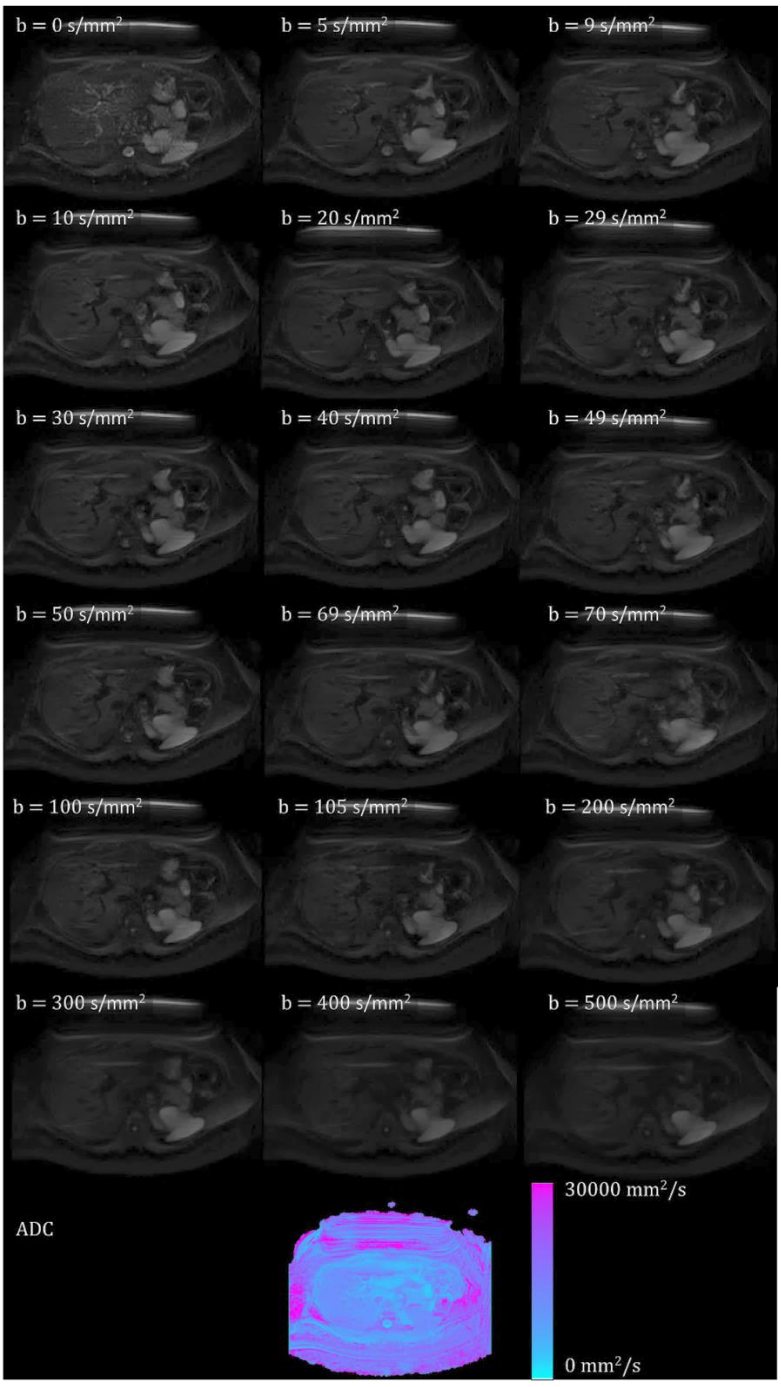

Figure 3.16 - Images produced from the DWI sequence. Respective b-values are displayed in the top left corner of each image. The corresponding ADC map is shown on the bottom row.

3.4.2.6 Field mapping

Field mapping provides a measure of B_0 field inhomogeneities and the B_1 field describing the penetration of RF into the tissue. As the size of or distance to the sample being investigated increases, for example, when scanning larger participants, the RF penetration is reduced and understanding the degree of this is important, especially in larger subjects, further the effect field inhomogeneities can also be exacerbated. These B_0 and B_1 effects can affect values in the quantitative maps created, especially in larger participants as studied in this chapter.

3.4.2.6.1 B_0 Mapping

B_0 mapping uses two gradient echo acquisitions collected at different echo times separated by a small echo spacing compared to T_2*, a ΔTE~ 2.3 ms is typically chosen in the body to ensure no change in the fat-water shift between the echoes. From the phase data at each echo time, it is then possible to calculate voxel wise the variations in B_0 field (ΔB_0, Hz) from the Larmor frequency given by

$$\Delta B_0 = \frac{\Delta\phi}{\gamma \Delta TE}$$

Equation 3.11

where $\Delta\phi$ is the phase shift. To maintain accurate phase across the echoes on a Philips scanner the Scan Control Parameter 'echo phase determination' must be set to 'OFF', operators were given a manual to ensure this change was made (Appendix 9.1). An example B_0 map made using this dual echo technique which shows a large

dispersion in the B_0 field can be seen in Figure 3.17. Note B_0 field mapping is also studied extensively later in this thesis in Chapter 5, where it is used to study respiration effects of free breathing on Magnetic Resonance Spectroscopy.

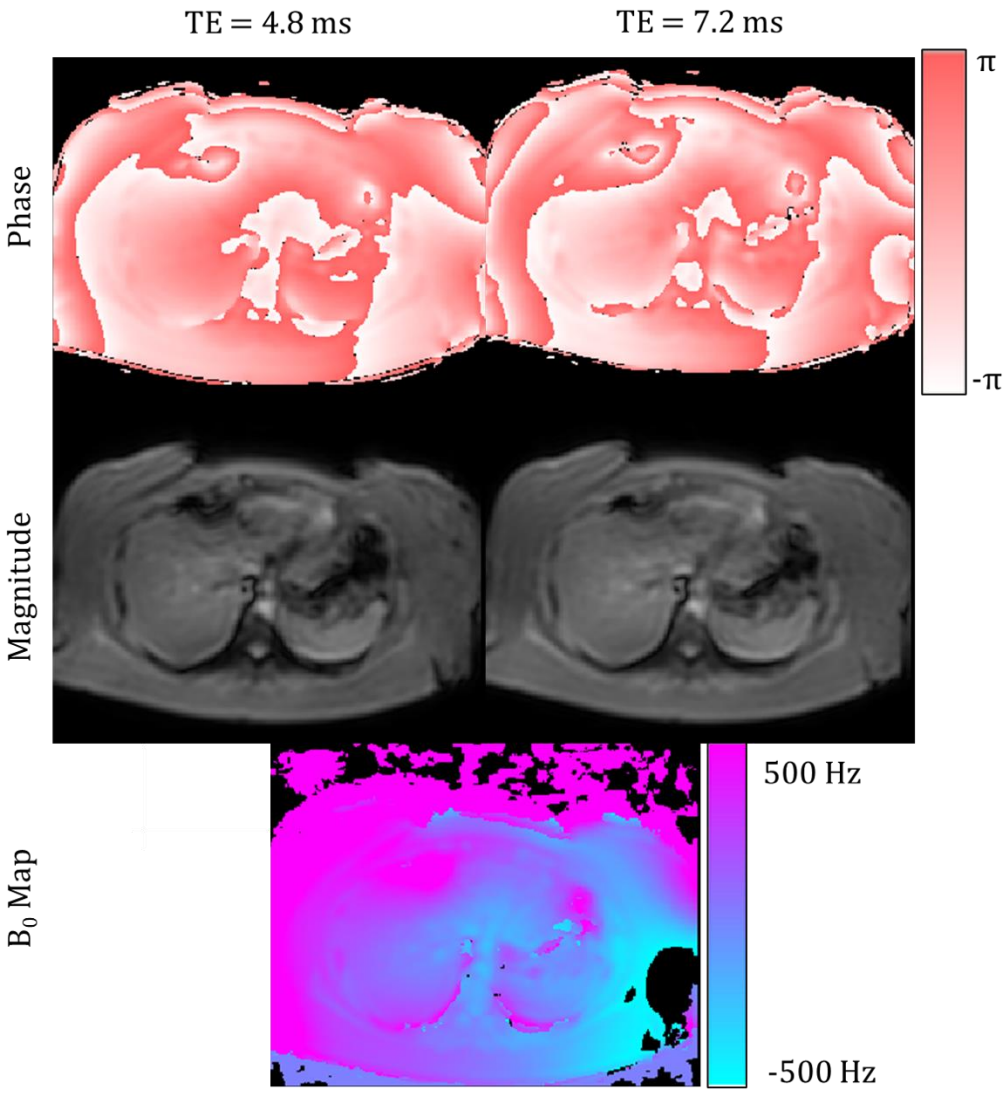

Figure 3.17 - (left) magnitude image from B_0 and (right) the respective map

3.4.2.6.2. B_1 Mapping

Multiple phase and magnitude based methods are available for estimating the B_1 field. Magnitude-based methods include the Double Angle (DA), Actual Flip Angle (AFI), and Dual Refocusing Echo Acquisition Mode (DREAM) methods, and phase methods include the Spin Echo Phase-Sensitive (SEPS) method. In this chapter, the DREAM method is used, in which a STEAM preparation sequence is followed by a low-angle gradient echo train, Figure 3.18 (67).

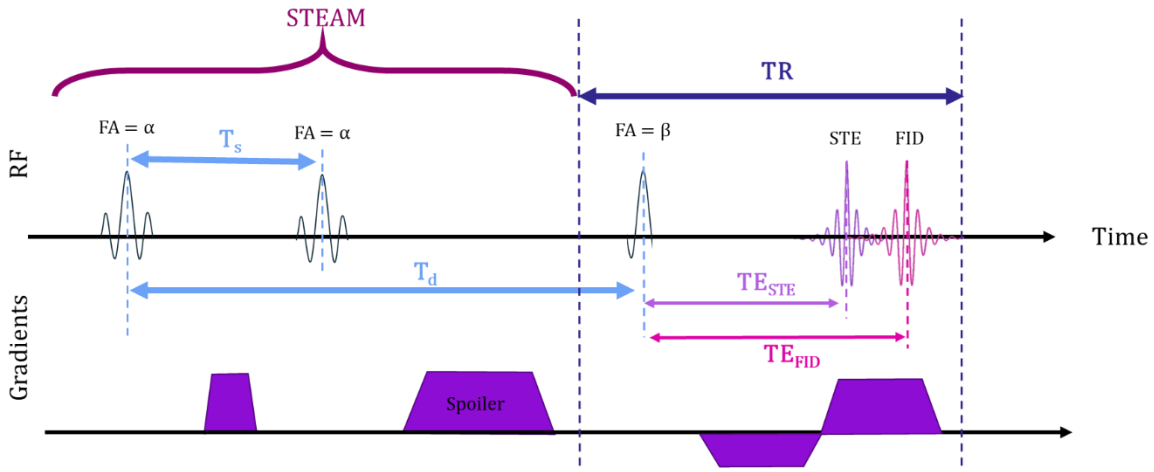

Figure 3.18 – Pulse sequence diagram for DREAM B_1 mapping sequence.

The signal from the STimulated Echo (STE) (S_{STE}) and the FID (S_{FID}) are given by,

$$S_{STE} = \sin(\beta)\, M_{z,STE} = \frac{1}{2}\sin(\beta)\sin^2(\alpha)\cdot M_0$$

Equation 3.12

$$S_{FID} = \sin(\beta)\, M_{z,FID} = \sin(\beta)\cos^2(\alpha) \cdot M_0$$

Equation 3.13

where $M_{z,STE}$ is the dephased and $M_{z,FID}$ is the in-phase longitudinal magnetisation.

Dividing these equations gives,

$$\frac{S_{STE}}{S_{FID}} = \frac{\tan^2 \alpha}{2}$$

Equation 3.14

The flip angle, α can then be calculated using,

$$\alpha = \tan^{-1}\left(\sqrt{2\, S_{STE}/S_{FID}}\right)$$

Equation 3.15

which is estimated voxel wise to provide a B_1 map, typically this is provided in terms of the percentage of nominal FA. An example DREAM B_1 map is shown in Figure 3.19.

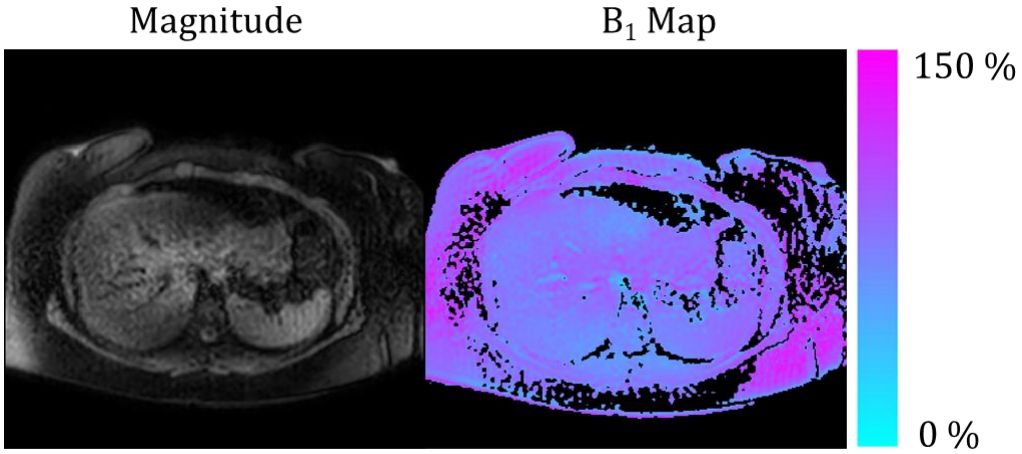

Figure 3.19 – (left) magnitude image and (right) DREAM B_1 map shown as a percentage of the nominal flip angle.

3.5 Methods

This section outlines the methods employed to study bariatric participants.

3.5.1 Study Design

In this study participants are divided into two groups, those undergoing Roux-en-Y Gastric Bypass (RYGB, Group 1) and those undergoing Sleeve Gastrectomy (SG, Group 2). Participants undertake one of the following arms:

Arm A: Primary Study. This comprises ^{1}H MRI measures of abdominal organs and ^{1}H liver MRS.

Arm B: Exploratory sub-study. This has a sub-set of ^{1}H MRI abdominal organs measures in common with Arm A as well as pilot ^{31}P liver MRS data to investigate the changes in ATP flux in response to bariatric surgery, and ^{1}H MRI measures of cardiac function and a whole body mDIXON (see Chapter 4 for detailed methods and results of the ^{31}P measures).

A list of the ^{1}H MRI and MRS measures collected in each arm are provided in **Error! Reference source not found.**, Section 3.5.5. Results of the common abdominal ^{1}H MRI and ^{1}H liver MRS measures are reported in this chapter.

The Wales REC 2 Ethics Committee approved the protocol and all amendments, and the study is registered on https://clinicaltrials.gov, study ID: NCT05092399.

Participants had to be listed for RYGB or SG bariatric surgery at the Royal Derby Hospital leading to eligibility of participants aged 18 to 70 years with a BMI ≥ 35kgm^{-2} who had type II Diabetes (T2D) or were pre-diabetic. All participants had the ability to give informed consent. Exclusion criteria included an inability to undergo a MR study, a diagnosis of liver cirrhosis, Type I Diabetes or non-diabetic and involved in other research studies. An inability to participate in MR measurements was determined to be a BMI > 60 kgm^{-2} and/or waist circumference >168 cm and/or weight over >250 kg (Ingenia scanner bed limit). Arm B had a lower BMI exclusion criterion of BMI > 50 kgm^{-2} to improve the chance of successful ^{31}P MRS acquisitions based on the estimated distance between the ^{31}P RF coil and the liver (Chapter 4). If participants were deemed eligible and able to consent to participate, their MRI screening form was emailed to the MR Physics team and any flags to taking part were raised with experienced scanner operators to assess if there were any grounds for exclusion.

3.5.2 Power and Justifications

The study was powered based on a reduction in liver FF as measured using MRI that occurred from baseline (BL) to 2 weeks on a VLCD. This was based on a previous published study by Luo *et al.* (56) on the effect of VLCD on liver FF where liver FF dropped from 16.6 ±7.8 % to 12.7 ±6.8 % in 49 participants ($P < 0.001$) (46). Assuming a normal distribution and a two-tail test, this would require a sample size of n=17 assuming a normal distribution, with a desired power of 0.8 and $p < 0.05$. Power calculations were performed using G*power (Franz Faul, Universitat Kiel,

Germany). Recruitment was thus approved for 23 people with the goal of 17 participants completing the study (assuming a ~25% dropout rate), this includes the recruitment of 6 participants to Arm B. An equal split of RYGB and SG patients was desired. The goal to recruit 6 participants to Arm B was since this is an exploratory, pilot study for which no previous study has been performed and the number was based upon the clinicians' judgment due to the difficulty in recruiting participants.

3.5.3 Study Visits

The study visits for each arm are shown in Figure 3.20, with participants attending five visits in total, the initial recruitment visit followed by four MR visits.

Visit 1 was a recruitment and screening visit. Participants were provided with the relevant Participant Information Sheet (PIS) for the arm they were being recruited to and given an overview of the protocol and their expected participation (see Appendix 9.1). A clinician (Dr Rebekah Wilmington) evaluated the participant's willingness and ability to attend all four subsequent MR visits to ensure maximum completion, and it was explained that their participation was voluntary, that it would not affect their clinical care and that they could withdraw from the study at any time. Participants filled out a MR safety form which screened for contraindications.

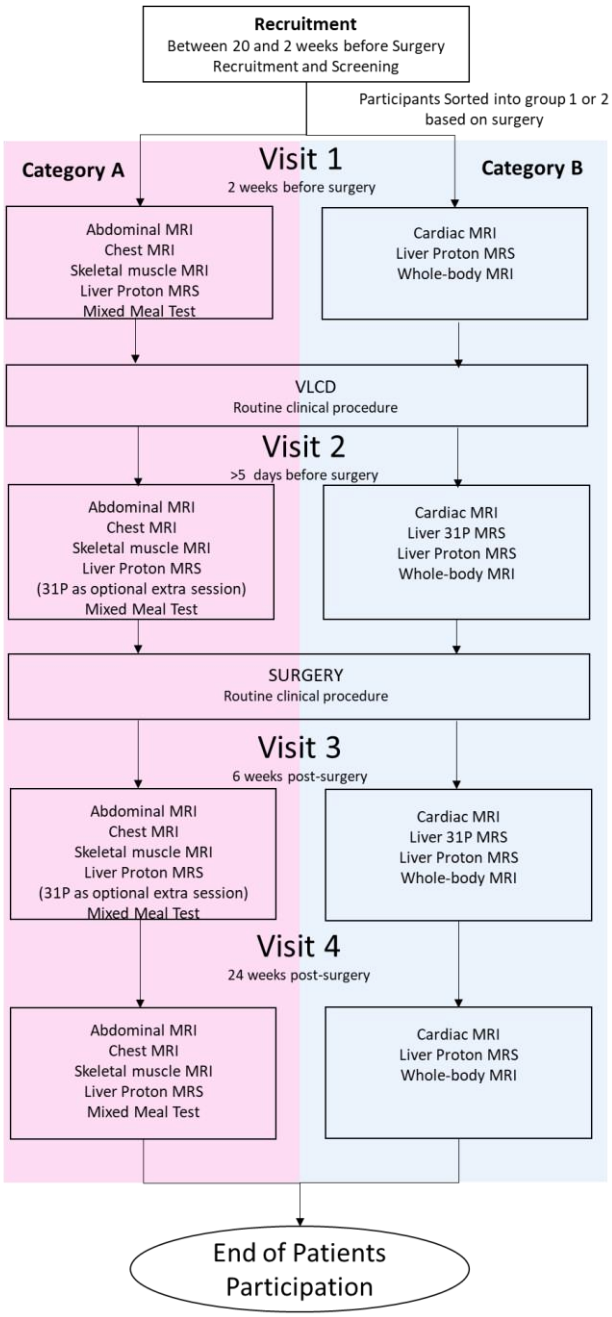

Figure 3.20 - Study visit flow chart. Participants in Group 1 (RYGB) or Group 2 (SG) are recruited to either Arm A or Arm B. Arm A collected multiparametric ^{1}H abdominal MRI and ^{1}H liver MRS measures, whilst Arm B comprised a sub-set of ^{1}H MRI measures and ^{1}H liver MRS as well as ^{31}P liver MRS and ^{1}H cardiac MRI.

Prior to each scan visit, participants were advised to avoid alcohol consumption, paracetamol, and strenuous exercise for the preceding 24 hours and caffeine for 18 hours prior, as these could affect blood markers. To reduce the fasting period, study visits were scheduled to take place in the morning. The larger body size of this participant group meant the scrubs normally provided to external participants to wear during their MR scan were not a viable option. To reduce any mental stress and improve the comfort of participants, they were informed they could wear their own clothes and were advised of what is considered MR-safe clothing. Hospital gowns were to hand if the clothing worn was not MR suitable. On the visit day, participants were greeted before being taken to the clinical room to measure their weight and height to estimate their current Body Mass Index (BMI)

$$BMI\ (kgm^{-2}) = {Weight}/{(Height)^2}$$

Equation 3.16

and Body Surface Area (BSA)

$$BSA\ (m^2) = \sqrt{{Height(cm) \cdot Weight}/{3600}}$$

Equation 3.17

and complete the CRF, which comprised boxes to confirm the participant followed instructions regarding paracetamol and alcohol use, if they were fasted, and any changes in medication, as shown in Appendix 9.3 and 9.4.

3.5.4 Clinical Measures: Mixed Meal Test and Blood Samples

3.5.4.1 Mixed Meal Test

In Arm A, for all visits a Mixed Meal Test (MMT) was performed prior to the MR scan. Subjects arrived fasted, being allowed water only. The fast was broken by the first intervention of the study morning, starting between 0900 and 0930. The participant's hand was placed in a water bath for ~5 minutes to allow time for their heart rate to normalise and for their hand to be warmed before cannulation. A trained member of staff inserted a retrograde cannula into the forearm or hand. Once canulated, the extremity was placed in a hot box set to 55°C to allow for arterial-like drawing of the blood, at each draw less than 15 ml of blood was taken and decanted into appropriate tubes for all analytes. After taking the baseline sample, the researcher gave the participant a mixed meal replacement (200 ml/300 kcal of a vanilla-flavoured Nutricia Fortisip, which was stored in the fridge and served chilled). A blood sample was taken prior to the consumption of the mixed meal with subsequent samples taken every 15 minutes for 3 hours.

3.5.4.2 Blood Measures

Measurements of plasma Glucagon, Ghrelin, Glucose, GIP and GLP-1, Insulin, C-peptide and three spare serum samples were obtained at all time points along with bile acids at baseline and T120 from the blood samples taken during the MMT. For assessment of Glucagon, Ghrelin, and C-peptide a glass pink-topped tube containing aprotinin was used (as glucagon sticks to plastic), a yellow-topped serum tube was used for insulin and GIP and spare serum samples, and a purple topped tube with

no additive was used for bile acid collection. Glucose was measured on the day using a YSI blood analyser. For GLP-1 a purple-topped plastic tube containing a DDP-IV inhibitor (inhibitor to prevent the enzyme DDP-IV from breaking down GLP-1) was needed. The DDP-IV must be frozen at -20 °C until needed and degrades each time it is frozen and thawed. DDP-IV was added to the purple tubes manually using a 10µl pipette, these were then stored in the SPMIC in a temperature-monitored freezer. The day before or morning of each study day, 13 tubes of the DDP-IV tubes were numbered for each timepoint and replaced in the freezer. The tubes were collected and placed in an insulated box on the morning of each study day to prevent thawing. This allowed for re-freezing if a last-minute cancellation or an issue with cannulation occurred. 13 glass pink tubes, 26 yellow-topped tubes and 2 purple tubes with no additives were labelled with time points. Small aliquots for each analyte were also labelled with study short title, time point and participant ID, glucagon aliquots were brown glass.

The yellow tubes were left to coagulate at room temperature for 15 minutes whilst the rest of the blood was spun in a centrifuge for 10 minutes within 10 minutes of being drawn. The plasma was then separated from the cells into appropriate aliquots and temporarily stored in a freezer at -20 °C. By the end of the following working day after the study day, the samples were transferred and stored in a -80°C freezer on the E floor of the medical school, which is locked and alarmed with CO_2 backup. The samples were periodically transferred to Royal Derby Hospital for deep

storage. Once all study-related analysis on the samples has been completed, they will be disposed of in accordance with the Human Tissue Act, 2004.

Those participants taking part in Arm B did not undertake the MMT.

3.5.5 MR Data Acquisition

Although fasted MR scanning would be ideal, the initial participants recruited to the study advised that the satiety provided by the meal replacement drink waned quickly. To ensure participants could comfortably complete the study, participants were offered a lighterlife nutritional bar after completion of the MMT. After this, participants were escorted to the MR scanner. All scans were performed on a Philips Ingenia 3T wide-bore scanner; a software patch was used to allow specialised MR sequences to be used. Details of the scans in each of the study Arms are provided in Table 3.3**Error! Reference source not found.**.

3.5.5.1 Arm A

Images were obtained using a 16 channel anterior body surface coil and the 16 channel posterior coil. Scans were collected with a large Field of View (FOV) of 450 x 450 mm to ensure full coverage in this participant group, and to ensure compliance all breath-hold (BH) scans had a duration of ~15 s.

A Survey scan was initially collected, followed by abdominal scans collected in the axial plane, with shimming covering all the internal organs. First an abdominal 6-echo mDIXON Quant scan was collected for organ volume assessment, Fat Fraction (FF_{MRI}) quantification, and T_2* mapping. The abdominal mDIXON was then used to

plan subsequent scans. Axial slices were centred over the pancreas to ensure coverage and then adjusted in foot-head if more liver coverage was needed. A MOLLI T_1 map (with liver and pancreas coverage) was collected using a physiological simulator set to 60 beat-per-minute for fixed inversion times, this sequence is used to quantify inflammation and fibrosis. To assess the field homogeneity, which is especially important in larger participants, a dual-echo FFE scan was used for B_0 mapping and a DREAM (Dual Refocusing Echo Acquisition Mode) approach for B_1 mapping, these will be used for future correction in quantitative mapping. An eThrive T_1 weighted sequence where the pancreas has high contrast (also known as a VIBE (Volumetric Interpolated Breath-hold Examination) or LAVA (Liver Acquisition with Volume Acceleration) sequence by other vendors) was collected for segmentation of the pancreas. A coronal single slice MOLLI T_1 mapping and 12-echo T_2* map was acquired centred on both kidneys.

In Arm A only, an additional Inversion Recovery Spin-Echo Echo-Planer-Imaging (IR-SE-EPI) T_1 map covering the liver, spleen and pancreas was also collected for comparison to the T_1 MOLLI data and Gradient Spin-Echo (GraSE) T_2 mapping with 10 echoes (TE = 12.9 ms, ΔTE = 12.9 ms). Magnetisation Transfer (MT, see Table 3.3 for acquisition parameter details) and Diffusion Weighted Imaging (DWI) scans (with 3 directions and b values of 0, 5, 9, 10, 20, 30, 40, 49, 50, 69, 70, 100, 105, 200, 300, 400, 500 s/mm^2) were also performed to assess liver inflammation and fibrosis. In addition, an aortic (AO) flow scan was collected to determine cardiac output. Note these results are not reported in this chapter.

^{1}H MRS of the liver and adipose tissue were collected. For the liver, a MRS voxel (20x20x20 mm^{3}) was placed in the anterior right lobe and spectra were obtained during an expiration BH to improve compliance. Since the BH was kept to a maximum of 15 s, there were 6 acquisitions collected, two Non-Water Suppressed (NWS) spectra and four Water Suppressed (WS). All acquisitions used a single voxel STEAM sequence with a train of four different TE's (15, 30, 45 and 80 ms), TR 2500 ms, 1024 data points and spectral bandwidth of 2000 Hz. Adipose MRS data was also acquired NWS with TE =14 ms, TR 2500 ms, 1024 data points and a spectral bandwidth of 2000 Hz.

3.5.5.2 Arm B

Arm B comprised a sub-set of abdominal MR measures collected in Arm A as shown in **Error! Reference source not found.**. In addition, participants had a whole body mDIXON Quant scan, as well as cardiac 2-chamber, 4-chamber and short axis cine scans collected following standard procedures. These ^{1}H measures took approximately 1-hour to collect. In Visits 3 and 4 (post-VLCD and 6 weeks PS), liver ^{31}P MRS was also collected to assess ^{31}P saturation transfer (see Chapter 4) which took an additional hour. This required changing of the RF coil, during this RF coil-change-over process, participants could get off the scanner bed and stretch or reposition to be more comfortable.

3.6 Data Analysis

3.6.1 Abdominal MRI Data Analysis Pipeline

The data was analysed using a pipeline developed within the Hepatorenal group at the Sir Peter Mansfield Imaging Centre (SPMIC).

Masks of the liver, spleen and SAT were created using nnU-NET automatic segmentation from the fat, water and T_2* mDIXON Quant images, with example masks shown in Figure 3.21. This nnU-net was developed by Stephen Lloyd-Brown at the SPMIC and was trained on 40 adult data sets across a range of BMIs (with gold standard masks generated by Dr Eleanor Cox and Dr Christopher Bradley). The pancreas was segmented from the pancreas eTHRIVE using a nnU-NET segmentation developed by Stephen Lloyd-Brown which was trained on 30 adult data sets (with gold standard masks generated by Mr Art Adam).

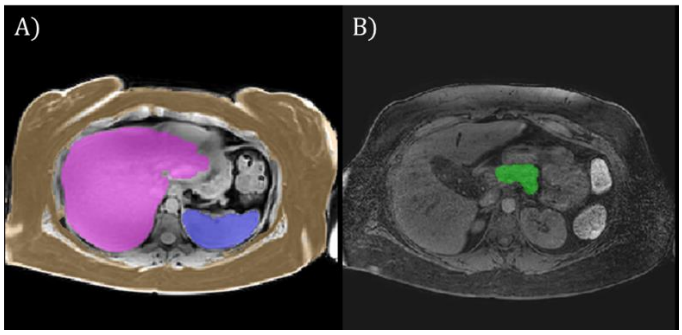

Figure 3.21 – Example slice showing (A) Spleen, liver and Subcutaneous Adipose Tissue (SAT) masks generated using an nnU-NET trained on the mDIXON Quant scan (using fat (F), water (W) and T_2 images), (B) Pancreas masks generated using an nnU-NET trained on the eThrive scan.*

Subsequent analysis was performed using a pipeline running on the high-performance cluster (HPC) (developed by Prof Sue Francis, Dr Eleanor Cox, and Martin Craig). This pipeline generated a excel spreadsheet (.xls) of results (iqmean (interquartile mean), median, mode and FWHM of measures) as well as light box images of each of the organ masks overlayed on the water DIXON image/eThrive images and of the resampled mask overlayed on the quantitative maps, to allow images to be viewed for manual quality checks.

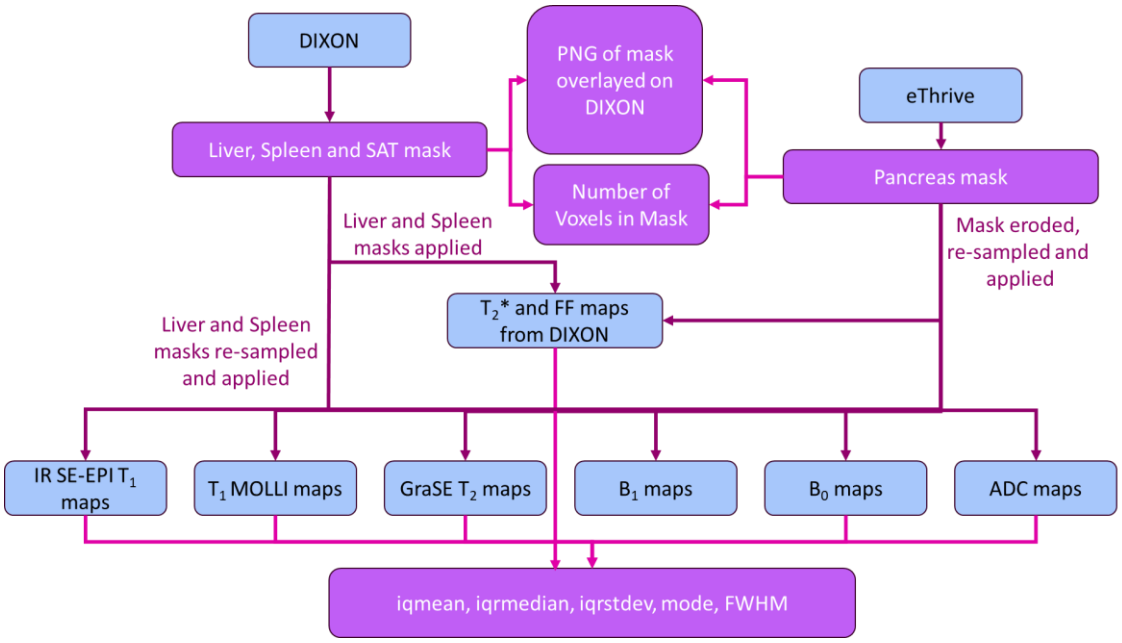

Figure 3.22 - Image Analysis Pipeline. MR data collected shown in blue and pipeline outputs shown in purple. Iqmean, iqrmeadian and iqrstdev are the interquartile mean, median and standard deviations respectively.

Masks were interrogated to provide information on the volume of the liver, pancreas, spleen and SAT. The organ masks were then re-sampled (FSL, fMRIB) and applied to the abdominal MOLLI and IR SE-EPI T_1 maps, T_2 maps, as well as the B_0

and B_1 field maps and ADC maps. Pancreas masks were eroded by 2 pixels before organ masks were used to interrogate the abdominal mDIXON T_2*, FF maps and MR relaxometry maps.

3.7.2 ^{1}H MRS data analysis

Metabolite	**Initial Guess (ppm)**	**Peak Number**
Methene or Olefinic	5.2	1
Water	4.7	2
Diallylic or Diacyl	2.8	3
Alpha-Methylene or Carboxyl	2.2	4
Allylic or alpha-Olefinic	2.0	5
Methylene	1.3	6
Methyl	0.9	7

Table 3.4 - Initial guess for peak locations used in automatic analysis of proton spectra.

Liver spectra were analysed using an automatic in-house MATLAB (2023b, Mathworks) script written by Dr Stephen Bawden, further developed by the author of this thesis. The script looped through all participants analysing the WS and NWS spectra, T_2 was calculated for fat and water individually and used to correct the FF-$_{MRS}$. An optimised zero-order phase correction written by the author of this thesis was applied to the WS and NWS spectral acquisitions before averaging. Prior knowledge (as outlined in Table 3.4 was used as initial guesses for find peaks, peaks were then fit, fits plotted and saved as images for visual controls to be performed. If the phase correction seen in these checks was not optimal, spectra were re-analysed with manual phase correction. Initial fits were performed with all fat

peaks. However, errors occurred due to failed water suppression, and so the analysis moved to using only peaks 4-7. To evaluate T_2 for fat and water, the NWS spectra were shifted according to the varying TE and a decay curve plotted.

For FF_{MRS} quantification, the signal for the fat (S_f) was calculated using,

$$S_f = {F_{ws}}\Big/{e^{\frac{-15}{T_{2-fat}}}}$$

Equation 3.18

where F_{ws} is the sum of the amplitudes of the fat peaks from the TE = 15 ms WS spectra and $T_{2\text{-}fat}$ is the T_2 of fat. FF_{MRS} was plotted as absolute values, percentage reduction from BL and compared to FF_{MRI}.

Adipose ^{1}H spectra have not yet been analysed.

3.7.3. Statistical Analysis

All endpoint measures outlined in Table 3.5 were compared across time points: BL to post-VLCD at -2 weeks, to 6 weeks PS and to 24 weeks PS, as well as post-VLCD at -2 weeks to 6 weeks PS and 24 weeks PS. All data was plotted as absolute values and percentage reductions from BL. Statistical testing was performed on all changes from BL and between each sequential timepoint.

Endpoint Measure	Organ			
	Liver	Spleen	Pancreas	Kidney
Fat Fraction mDIXON (FF_{MRI})	X	X	X	
Fat Fraction Spectroscopy (FF_{MRS})	X			
Volume	X	X	X	
T_1	X	X	X	X
T_2^*	X	X	X	X
ADC	X			

Table 3.5 - List of endpoint measures for each organ. Note T_1 IR SE-EPI and ADC are not reported in this thesis.

Results from the ^1H Spectra (FF_{MRS}) were compared to the mDIXON Quant results (FF_{MRI}), and a Bland-Altman graph was plotted. Trends were investigated in the changes in liver FF against BL liver FF, BL liver volume, and comparisons of liver FF with BMI, BSA, and T_1 MOLLI, as well as comparisons between BMI, BSA, SAT, and B_1.

For all data, statistical testing was performed using GraphPad (Prism, 10), data was tested for normality, and then a two-tail t-test was performed between BL and all subsequent time points, from post-VLCD to subsequent time points and between 6 and 24 weeks PS. For all box plots, whiskers extend from the 10^{th} to 90^{th} percentile with outliers displayed.

3.7 Results

3.7.1 Study Participants, BMI and BSA

To date, 21 participants have been recruited into the study, whilst 4 participants were withdrawn. An investigator withdrew 1 participant due to claustrophobia, and 3 participants withdrew after their first MR visit: 1 participant withdrew because they found the fasting for the MMT difficult, hence the subsequent introduction of the lighter life bar, and 2 participants withdrew due to a change of circumstance making the time commitment of the study impossible. These data sets are not included in the results shown in this thesis.

Of the 17 remaining participants, to date, 11 have completed all 4 study visits; of these, 2 are missing data from 6 weeks PS, 1 due to an adverse event following the MMT and 1 due to illness following surgery. The ongoing 6 participants at the time of writing this thesis have all completed BL, post-VLCD and 6 weeks PS. All remaining study dates are booked, with 3 participants due to complete in September 2024, 1 in October 2024 with the final visit for the final study participant booked for the start of December 2024. 6 of the 17 participants underwent RYGB and 11 of 17 underwent SG, a ratio of approximately 1:2.

On recruitment to the study, participants were expected to participate over a 28 week time period, but actual times ranged from 30 weeks to 50 weeks. On 2 occasions, participants underwent the post-VLCD Visit and then had their surgery postponed; in these instances, the post-VLCD visit was not re-performed prior to

their new surgery data as the initial data collected still accurately represented their post-VLCD changes.

3.7.1.1 BMI and BSA

As expected, a significant correlation was seen between BMI and BSA ($p < 0.0001$, $R = 0.61$) for the study participants as shown in Figure 3.23 including all time points.

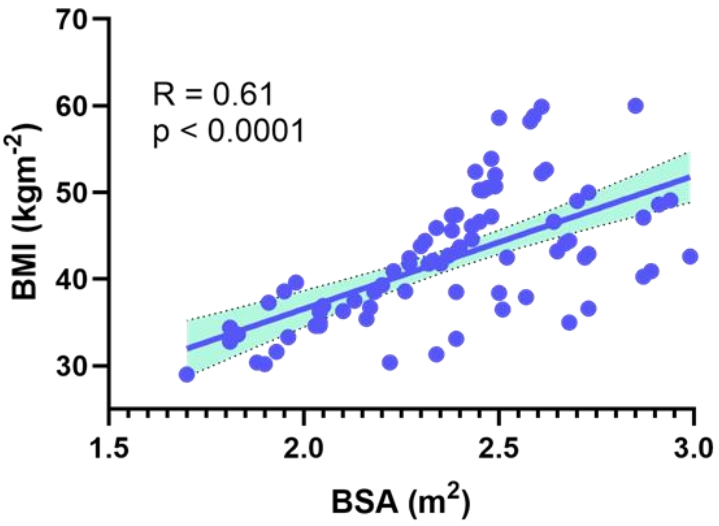

Figure 3.23 - Correlation between BMI and BSA shown for all timepoints for each of the participants, Line of best fit and 95% confidence bounds shown

Changes to BMI and BSA from recruitment across study visits over the time course of the bariatric surgery journey for each participant can be seen in Figure 3.24. No significant change was seen in either BMI or BSA from recruitment to the BL (-2 week) MR visit. However, a significant decrease in BMI was seen from recruitment to post-VLCD (0 week) ($p = 0.0052$). For BMI and BSA a significant reduction was seen from recruitment to BL, 6 weeks PS and 24 weeks PS (all $p < 0.0001$). A

significant reduction was also seen between sequential time points for BL to post-VLCD ($p < 0.0001$ for BSA and BMI), post-VLCD to 6 weeks PS ($p < 0.0001$ for BSA and BMI), from 6 to 24 weeks PS ($p = 0.0002$ and $p = 0.0009$ for BMI and BSA respectively) and also from BL to 6 and 24 weeks PS (all $p < 0.0001$). There was no significant correlation between initial BMI and the percentage reduction in BMI or BSA at any subsequent time point. BSA at the initial timepoint significantly correlated with percentage reduction at 24 weeks PS ($p = 0.04$).

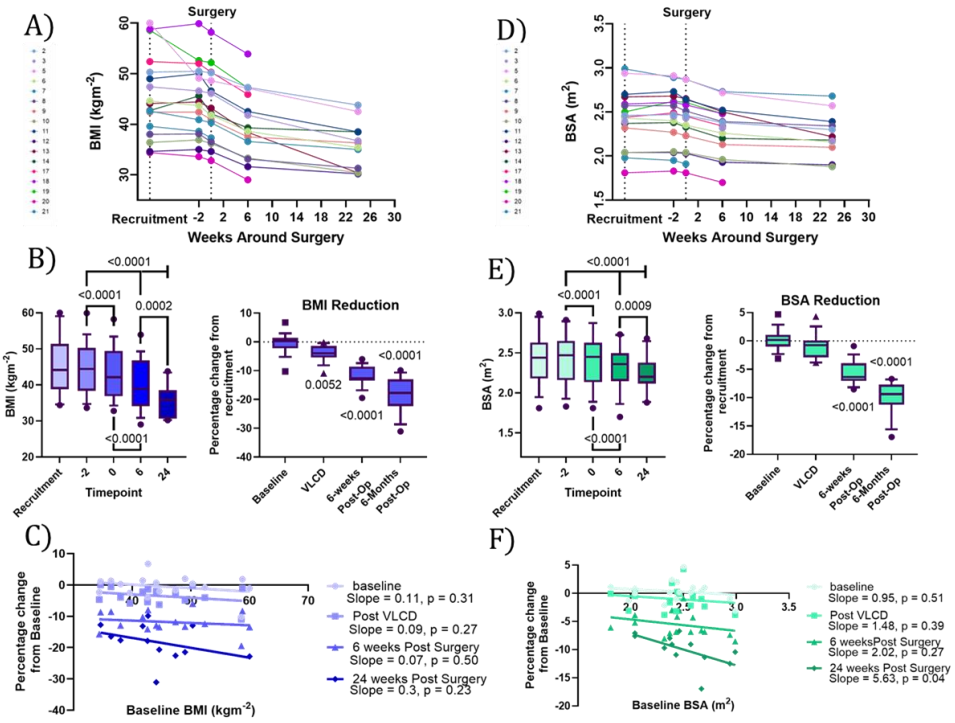

Figure 3.24 – A) BMI across study visits shown for each participant. Legend for participants shown on the left. B) Boxplot of BMI across participants for each study visit and the % reduction from recruitment. C) Trend of recruitment BMI with % reduction at subsequent time points. D) BSA across study visits shown for each participant, E) Boxplot of BSA across participants for each study visit and % reduction from recruitment, F) Trend of recruitment BSA with % reduction at subsequent time points. Significant reductions are shown above the respective boxplots

3.7.2 Abdominal MRI Endpoints

3.7.2.1 Accuracy of Automated Organ Segmentations

In total, there were 62 MRI data sets across subjects and study visits that required masks of organs to be created using the nnU-NET models. These masks were visually inspected, and if required corrected for accuracy. For the liver masks, 11 data sets required some form of correction (17 %); in 7 instances, a small section of the heart was included in the liver mask, and for 3 others a section of the liver was missing. For 1 dataset, the liver was segmented correctly; however, there was a region of hyperintensity on the T_2* map, so a second mask was manually corrected for this dataset to remove this region for quantitative analysis. For the pancreas, 12 masks were drawn manually from the mDIXON images as there was no eThrive scan acquired at early time points of the study. Of the automatically generated pancreas masks from the eThrive scan, 15 required manual correction (30 %). All spleen masks were successful, with none requiring manual correction (0 %). 8 of the SAT masks completely or partially failed and required manual correction (13 %).

Organ	Number of Masks Corrected	Change in volume (Mean ±SD %)	
		Increase	Decrease
Liver	11	6 ±6	14 ±10
Pancreas	15	24 ±7	39 ±29
SAT	8	79 ±21	-

Table 3.6 - Details of corrected organ masks, number of masks correct and the mean and standard deviation percentage change in the organ volume of these data sets after correction.

3.7.2.2 Liver

A significant reduction was seen in liver volume and liver FF_{MRI} from BL (-2 weeks) to all subsequent timepoints and from post-VLCD (0 weeks) to 6 and 24 weeks PS. Figure 3.26 shows visually the reduction in liver FF from BL to 24 weeks PS on the fat mDIXON images, with the liver changing from shades of grey to black as FF reduces.

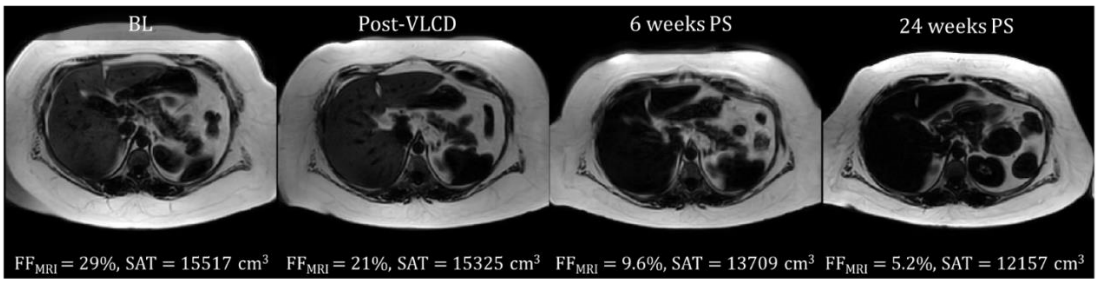

Figure 3.25 – Fat mDIXON images from an example participant across each of the 4 study visits. In the images fat is bright and water is dark. The time point and FF measured from the mDIXON scan and SAT volume are displayed below each of the respective images and shows the reduction over the course of the study.

Results of liver FF from the mDIXON data from all participants can be seen in Figure 3.26. 15 of 17 participants began with fatty livers (FF > 6.4 % (32)), and of the 12 participants scanned to date at 24 weeks PS, only 2 continue to have fatty livers. From 6 to 24 weeks PS a significant change was seen in FF_{MRI} between these time points, but for liver volume no significant change was seen. Liver T_2* significantly increased from all time points to 24 weeks PS but no significant change was seen between any other time points.

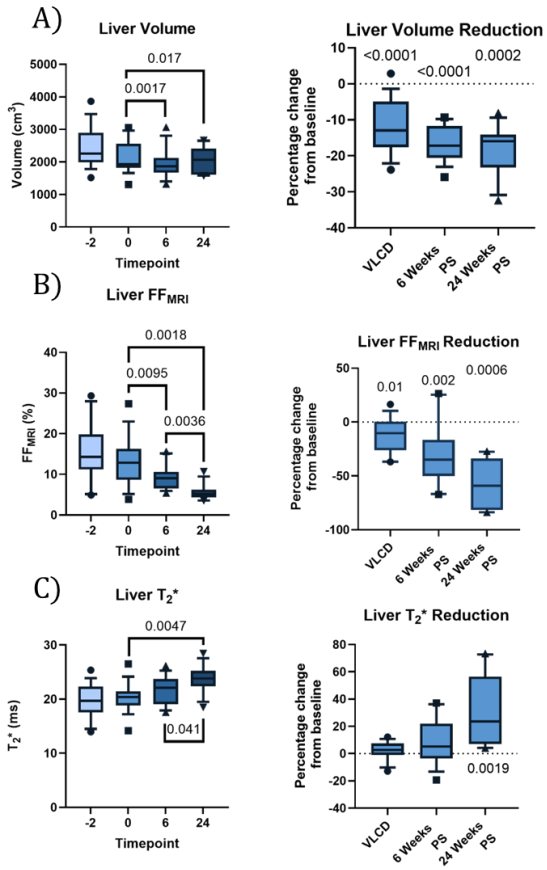

Figure 3.26 - Liver mDIXON data, box plots Left - for absolute values of A) volume, B) FF_{MRI} and C) T_2. Right - the percentage reduction from baseline. Significant values are shown above respective box plots*

Changes to liver T_2, liver T_1 MOLLI, and mean and FWHM B_0 and mean B_1 within the liver mask can be seen in Figure 3.27. No significant changes were seen in liver T_2, or the B_0 field in the liver mask. A significant decrease was seen in liver T_1 MOLLI from BL and post-VLCD to 24 weeks PS. A significant increase was seen in B_1 in the liver from post-VLCD to 24 weeks PS. No other significant changes were found in these liver measures.

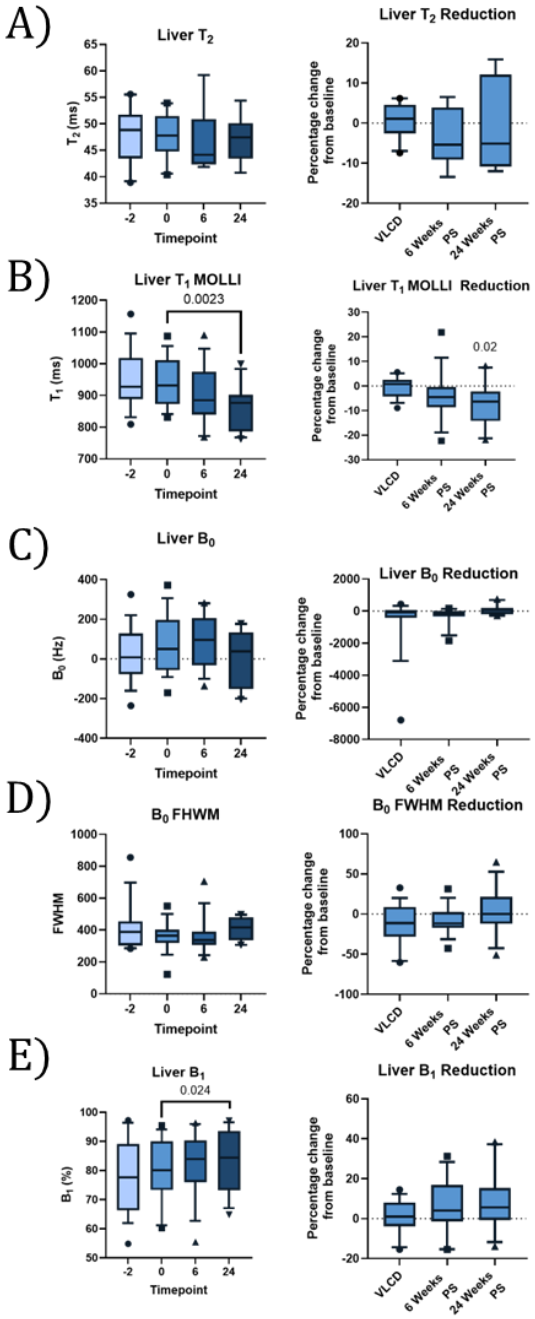

Figure 3.27 – Box plots for Liver MRI measures. Left - absolute values of A) Liver T_2, B) Liver T_1 MOLLI, and C) mean and D) FWHM B_0 in the liver, and E) B_1 within the liver for each visit. Right - percentage reduction from baseline. Significant values are shown above respective box plots

3.7.2.3 Pancreas

Results for pancreas volume, FF, T_2*, T_2 and T_1 MOLLI are shown in Figure 3.28. All participants had a fatty pancreas at BL and at 24 weeks PS (FF > 6.2 % (68)). No significant change was observed in pancreatic volume, FF or T_2. A significant increase was seen in pancreatic T_2* from 6 to 24 weeks PS but not between any other time points. A significant increase was seen in pancreas MOLLI T_1 from BL to 6 and 24 weeks PS.

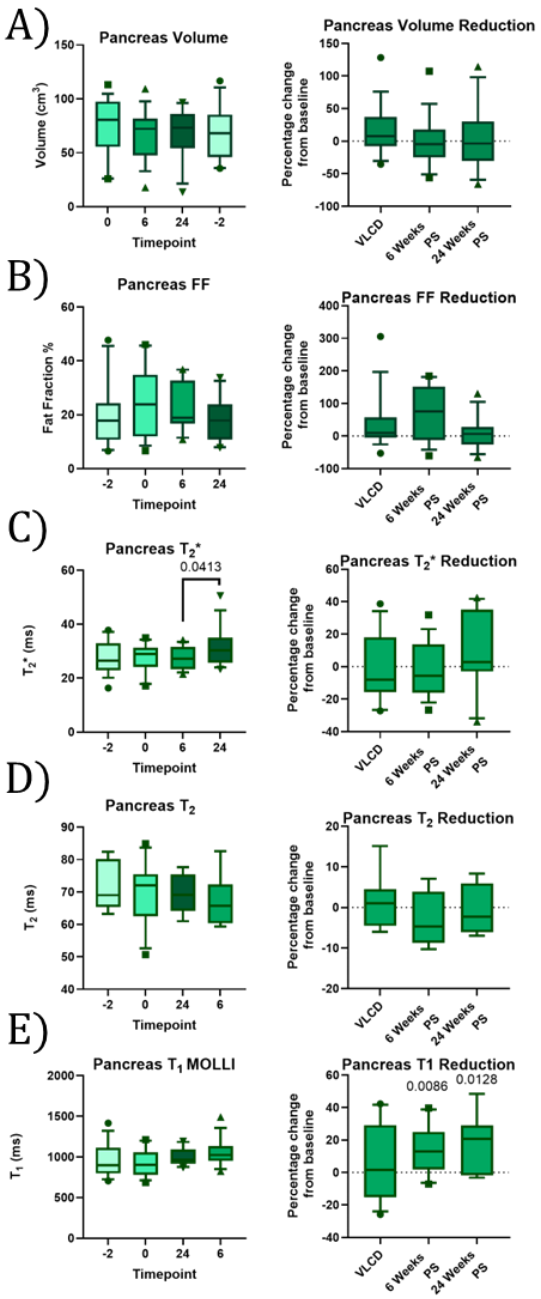

Figure 3.28 - Box plots for Pancreas MRI measures. Left - absolute values of A) Volume, B) FF_{MRI} C) T_2, D) T_2 and E) T_1 MOLLI, for each visit. Right - percentage reduction from baseline. Significant values are shown above respective box plots*

3.7.2.4 Spleen

A significant reduction was seen in splenic volume from BL and post-VLCD to 6 weeks PS, in splenic FF from BL to 6 weeks and 24 weeks PS and from 6 to 24 weeks PS, Figure 3.29. No significant change was seen in splenic T_2*, T_2 or T_1.

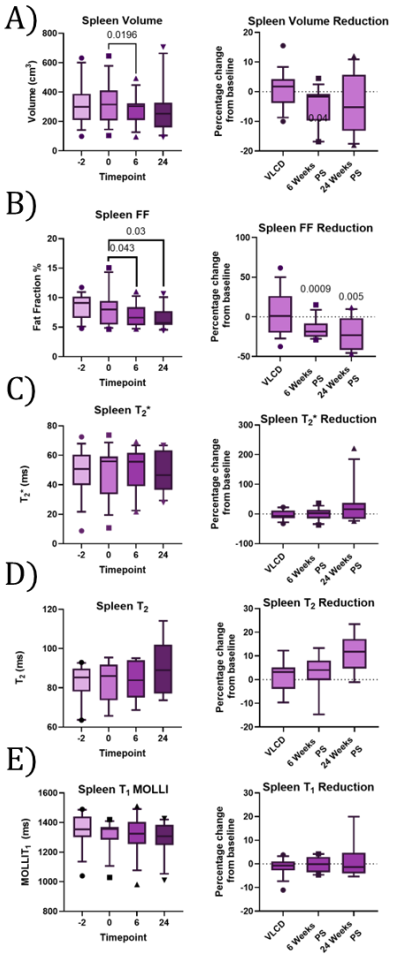

Figure 3.29 – Box plots for spleen MRI measures. Left - Absolute values for Spleen Volume, FF, T_2, T_2 and T_1. Right - percentage change from BL in these measures. Significant p values are next to respective boxplots*

3.7.2.5 Subcutaneous Adipose Tissue (SAT)

SAT volume significantly decreased from BL to 6 and 24 weeks PS (p = 0.0021 and 0.0005, respectively) as well as from post-VLCD to 6 weeks PS (p = 0.01) and from 6 to 24 weeks PS (p = 0.0056). There was no significant change in SAT volume from BL to post-VLCD at -2 weeks, as shown in Figure 3.30.

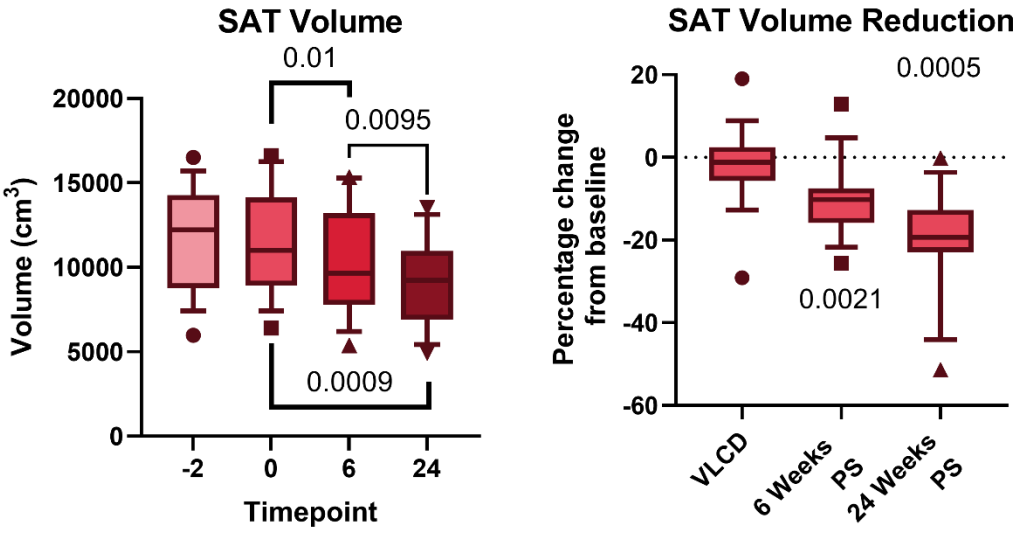

Figure 3.30 - SAT volume at each time point and the percentage reduction from BL to post VLCD (-2 weeks), 6 and 24 weeks PS

3.7.3 Comparison of Liver FF Assessed with ^{1}H MRS and ^{1}H MRI

For seven ^{1}H MRS datasets, there was a scanner failure which led to the data being corrupted; resulting in these data sets not being available for analysis, all other liver ^{1}H spectra are included in this analysis.

There was a strong agreement between the two methods (reduced number of peaks versus all peaks) of ^{1}H MRS liver fat analysis ($p < 0.0001$, $R = 0.99$) as shown in Figure 3.31. Since the use of a reduced number of fat peaks was more robust, this method was chosen for comparisons and evaluation across time points.

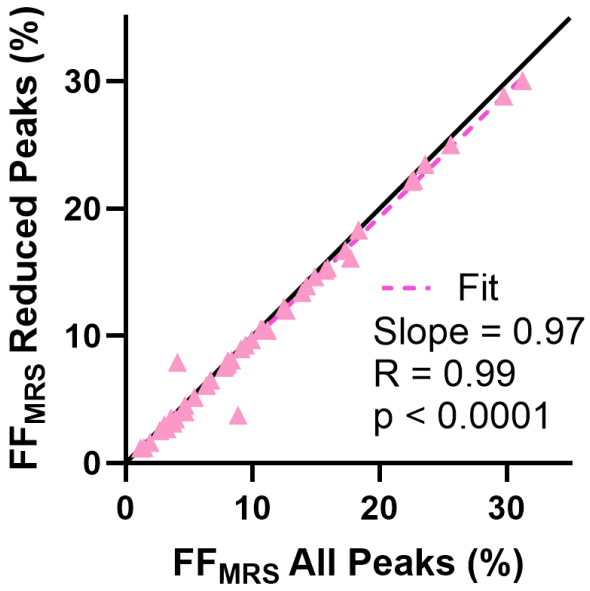

Figure 3.31 - Comparison of use of a reduced number of fat peaks versus all fat peaks in the quantification of FF_{MRS}. The dotted pink line shows the best fit ($R = 0.99$, $p < 0.0001$, slope = 0.97) with the identity line shown in black.

Figure 3.32 shows the absolute FF_{MRS} for all time points and the percentage reduction from BL across all participants. From evaluating the ^{1}H liver MRS data, 14 of 17 participants began with fatty livers (FF > 6.4 % (32)). A significant reduction in FF_{MRS} was seen from BL to all subsequent time points and from 6 to 24 weeks PS, but no significance was seen from post-VLCD (-2 weeks) to 6 weeks PS (Figure 3.21).

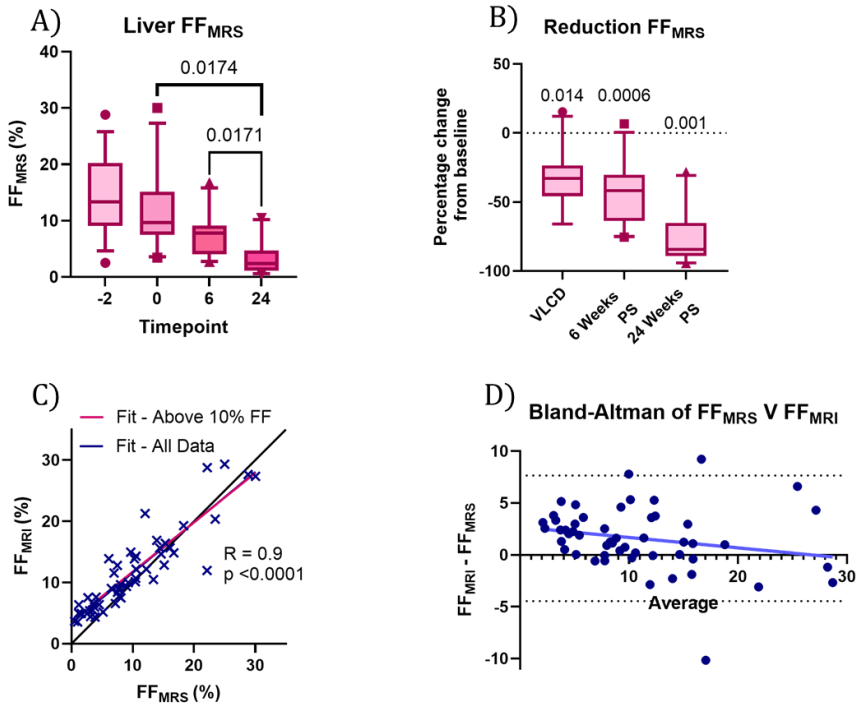

Figure 3.32 - A) Absolute liver MRS FF in %, B) Percentage reduction from baseline in liver FF_{MRS}, significant p-values are displayed above their respective box-plots and C) Comparison of liver FF_{MRS} and FF_{MRI}, fit for all data shown in blue, fit for data with MRI FF above 10 % shown in pink and identity line shown in black, D) Bland-Altman of liver FF_{MRS} versus liver FF_{MRI} with line of best fit, 95% confidence bands shown as dotted lines at -4.5 % and 7.7 %.

A significant ($p < 0.0001$, $R = 0.9$) correlation was seen between liver FF_{MRS} and liver FF_{MRI} for the full dataset, Figure 3.32C. Note the non-zero intercept with FF_{MRI} overestimating FF at low levels with clustering seen at values of FF < 10 %. When considering values of FF > 10 % for MRI a significant correlation was also seen. Figure 3.32D shows the Bland-Altman plot between FF_{MRS} and FF_{MRI}, with a bias seen for liver FF values below 10 %.

3.7.4 Assessing Changes in Individual Participants

The changes in individual participants in organ volume for liver, pancreas, spleen and SAT and BSA corrected organ volume across all time points can be seen in Figure 3.33. Changes in FF and T_2* of the liver, pancreas and spleen for individual participants across time points can be seen in Figure 3.34. Table 3.7 shows a summary of the p-values of change over the time course of the bariatric study for BMI, BSA, the liver, pancreas, spleen and SAT.

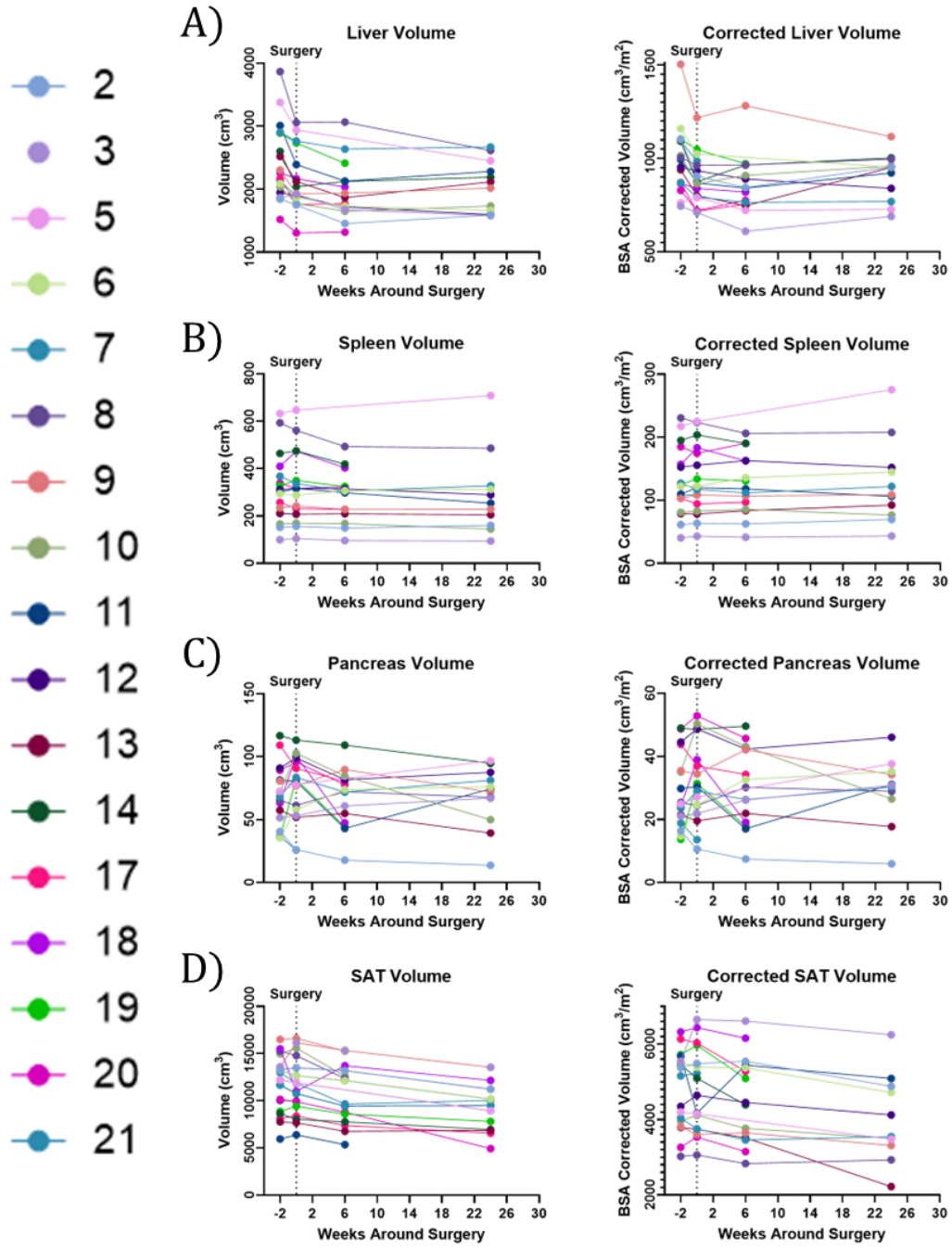

Figure 3.33 - Changes to individual participants. Left - A) liver, B) spleen, C) pancreas and D) SAT volume and Right - the BSA normalised volumes. The legend shows the colours matching the participant numbers.

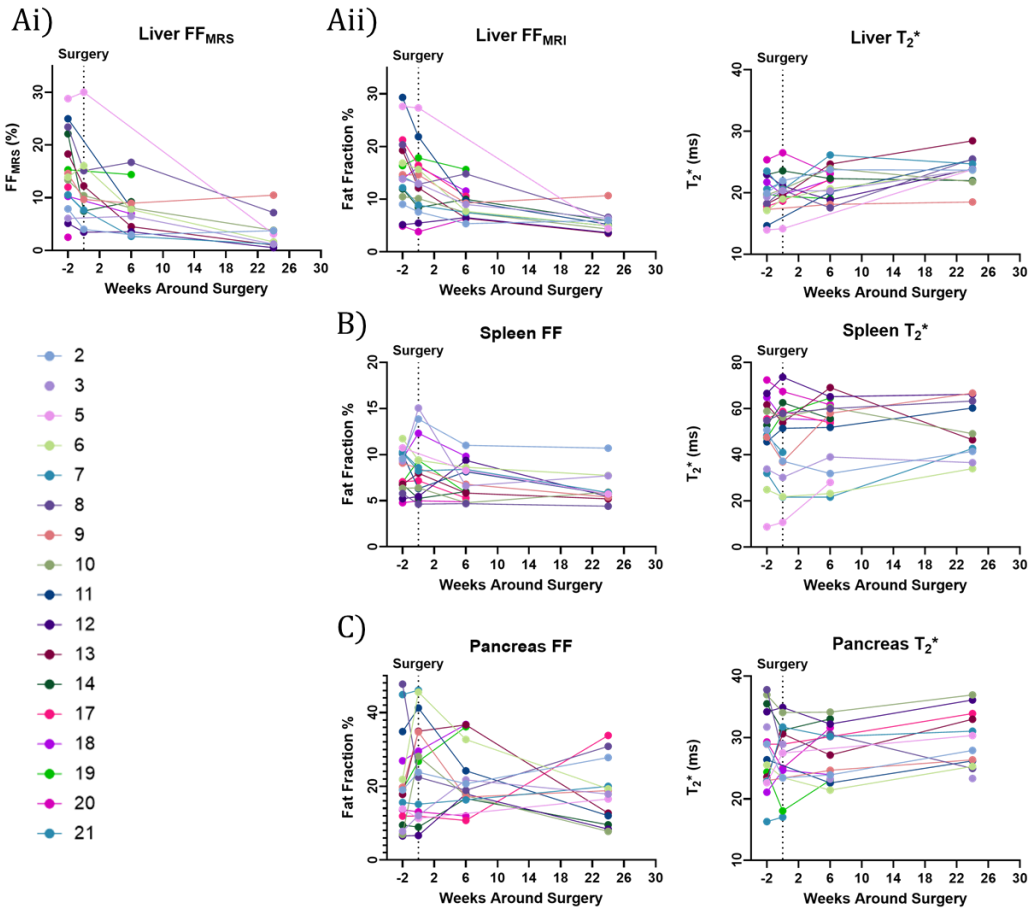

Figure 3.34 - Changes to individual participants FF for Ai) liver measured using MRS, Aii) liver measured using MRI, B) spleen, C) pancreas and Right - T_2. The legend shows the colours matching the participant numbers.*

Organ	Metric	P					
		BL-VLCD	BL – 6 weeks	BL – 24 weeks	VLCD – 6 weeks	VLCD – 24 weeks	6 weeks – 24 weeks
Liver	FF_{MRS}	0.014	0.0006	0.0010	0.092	0.017	0.017
	FF_{MRI}	0.0099	0.0020	0.0006	0.0095	0.0018	0.0036
	Volume	<0.0001	<0.0001	0.0002	0.0017	0.017	0.92
	T_2*	0.35	0.059	0.0019	0.35	0.0047	0.041
	T_1 MOLLI	0.54	0.11	0.020	0.11	0.0023	0.59
	T_2	0.59	0.81	0.46	0.57	0.88	0.46
	B_0	0.22	0.24	0.28	0.88	0.15	0.45
	B_0 FWHM	0.12	0.40	0.37	0.92	0.15	0.36
	B_1	0.82	0.11	0.078	0.82	0.023	0.70
Pancreas	FF_{MRI}	0.12	0.25	0.96	0.62	0.31	0.48
	Volume	0.16	0.53	0.87	0.052	0.37	0.55
	T_2*	0.54	0.30	0.32	0.86	0.17	0.041
	T_1 MOLLI	0.46	0.0086	0.013	0.065	0.21	0.67
	T_2	0.91	0.26	0.54	0.91	0.14	0.58
Spleen	FF_{MRI}	0.31	0.0009	0.0050	0.042	0.027	0.074
	Volume	0.76	0.040	0.34	0.019	0.30	0.31
	T_2*	0.32	0.97	0.24	0.40	0.66	0.52
	T_1 MOLLI	0.24	0.91	0.81	0.68	0.45	0.99
	T_2	0.55	0.46	0.33	0.43	0.70	0.13
SAT	Volume	0.47	0.0021	0.0001	0.011	0.0009	0.0095

P value	Colour
0.0001 >	
0.0001 – 0.0009	
0.001 – 0.009	
0.01 – 0.05	
0.051 – 0.099	
0.1 <	

Table 3.7 – Heat map of significance values for MRI data. The key for colours and p-values are shown on the right.

3.7.5 Correlations Between Endpoint Measures

Figure 3.35 shows a correlation matrix between BSA, BMI and MR endpoint measures illustrating any positive and negative relationships; what follows is then an evaluation of some of the significant correlations.

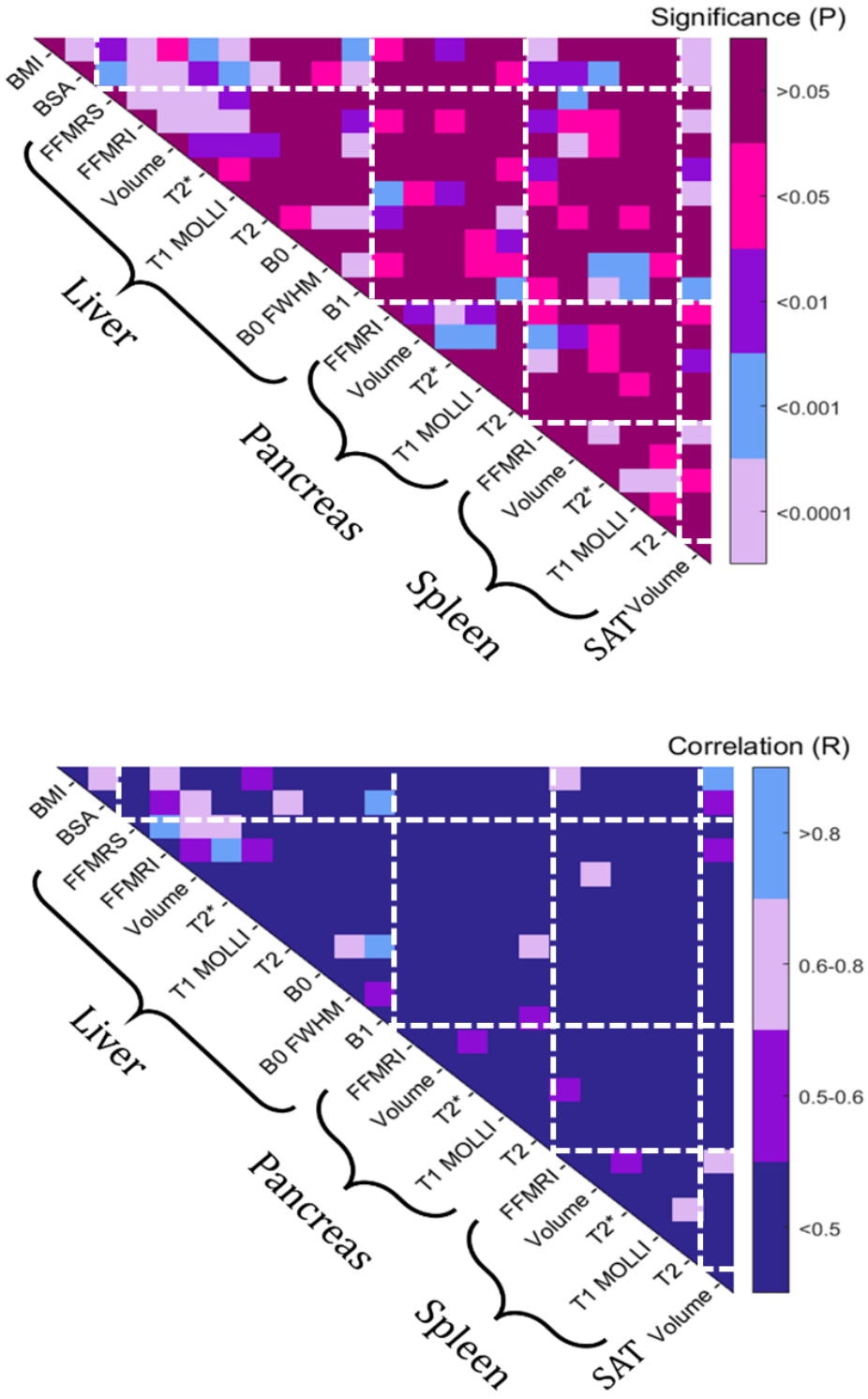

Figure 3.35- Correlation Matrice for BMI, BSA and MR measures for liver, pancreas, spleen and SAT. Top - p values, Bottom –correlation R values

BMI and BSA significantly positively correlated with liver FF_{MRI}, liver FF_{MRS}, as well as with SAT volume, as shown in Figure 3.36. Note a higher strength of correlation of BMI with SAT as compared to BSA (BMI R = 0.87, BSA R = 0.56, both $p < 0.0001$). Interestingly, there was a significant reduction in the B_1 delivery within the liver with increasing BMI and BSA, with BSA more strongly correlating with liver B_1 compared to BMI (BMI R = 0.43 p = 0.0005, BSA R = 0.80 $p < 0.0001$), see Figure 3.36C. There was no significant correlation between liver mean B_0 and BMI or BSA. However, there was a significant correlation between BSA and B_0 FHWM, with a larger distribution of B_0 measured in the liver at higher BSA (p = 0.024, R = 0.3), BMI did not significantly correlate with B_0 FWHM.

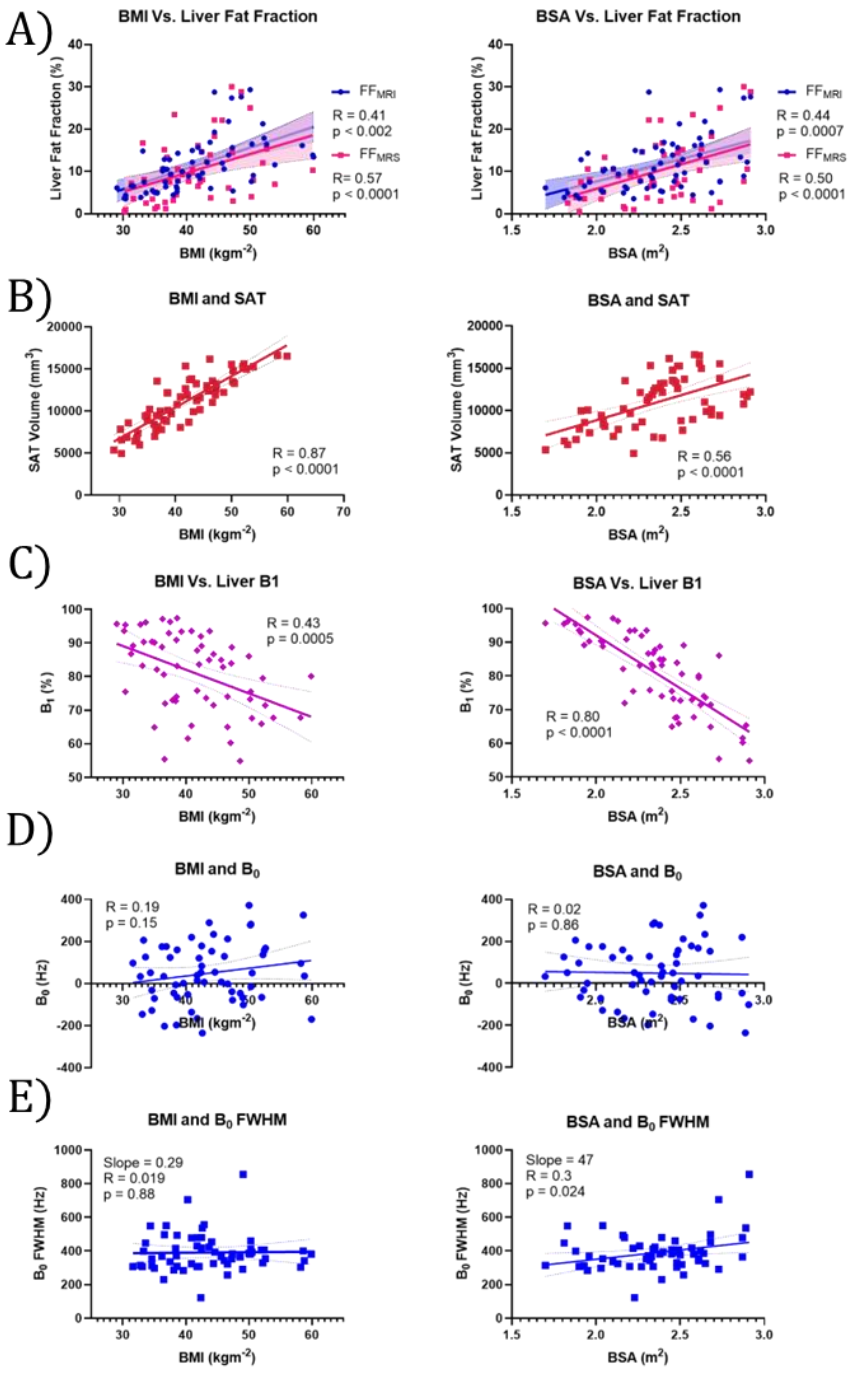

Figure 3.36 Correlation with BMI (Left) and BSA (Right) for A) Liver FF, B) SAT and C) B_1. 95% confidence lines for fits are shaded for FF and shown as dotted lines for SAT and B_1.

Both FF_{MRI} and FF_{MRS} significantly positively correlated with liver volume (both $p < 0.0001$, $R = 0.79$ and 0.59, respectively) Figure 3.37B, and MOLLI T_1 ($p < 0.0001$ $R = 0.58$ and $p = 0.0006$ $R = 0.47$, respectively), with the MOLLI T_1 being significantly increased at higher FF as shown in Figure 3.36C.

A significant correlation was seen between FF_{MRI} at BL and the percentage reduction at 6 and 24 weeks PS ($p = 0.0002$ and 0.0079, respectively), conversely no significant correlation was seen with FF_{MRS} at BL and the percentage reduction at any time point Figure 3.37A.

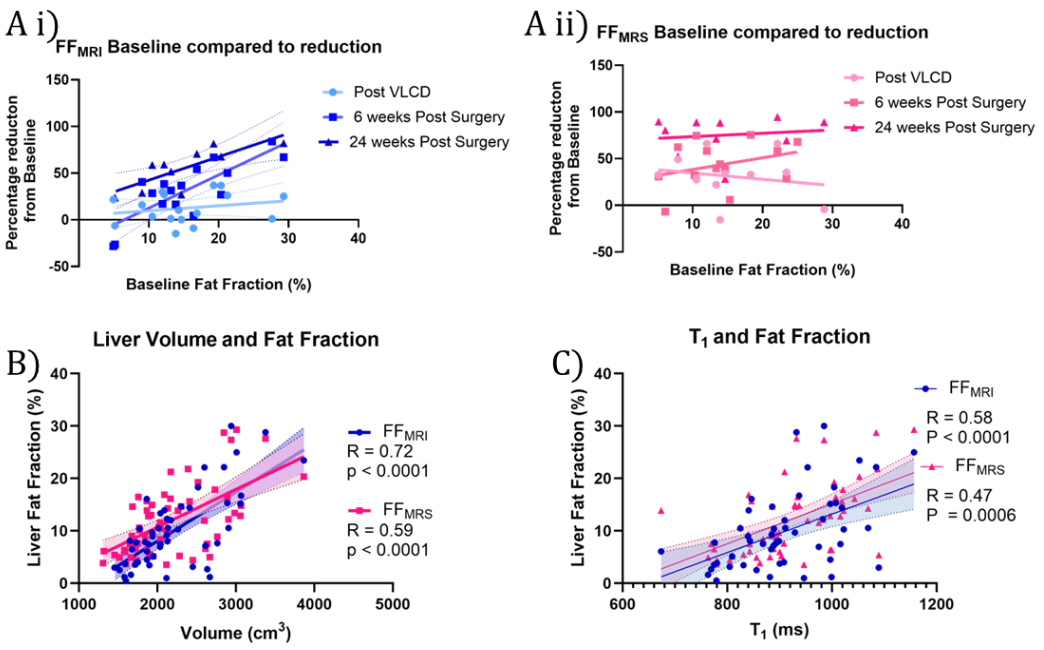

Figure 3.37 - Baseline FF compared to percentage reduction for Ai) FF_{MRI} and Aii) FF_{MRS} and the correlations between FF_{MRI}/FF_{MRS} with B) Liver Volume and C) MOLLI T_1

The T_2 measured using the GRASE scheme significantly correlated with B_1 for all organs (all $p < 0.0001$), with a lower T_2 measured for lower B1 delivery seen in subjects with higher BSA. There was no significant correlation of organ T_2 with mean or FWHM B_0.

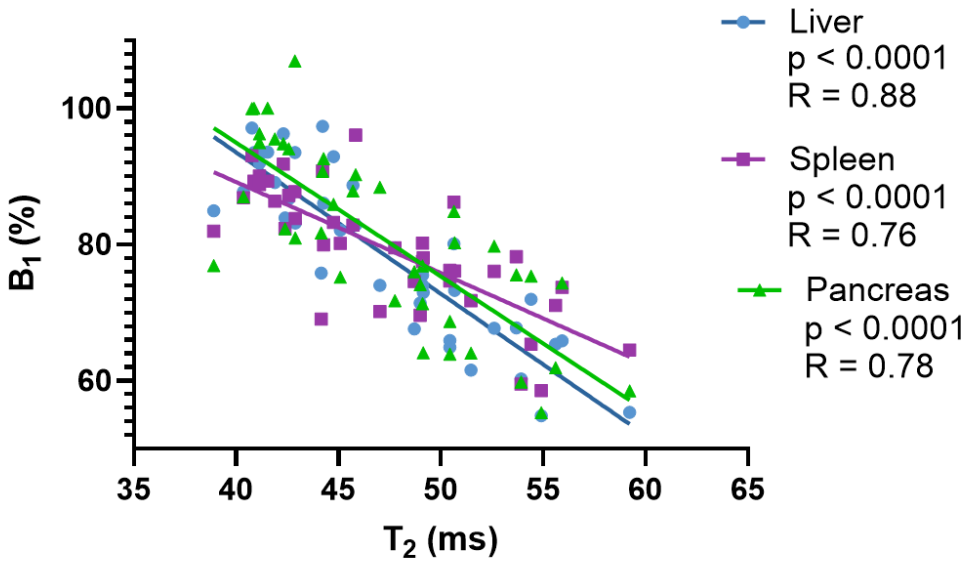

Figure 3.38 - Correlation of organ T_2 with organ matched B_1 delivered (shown as % of nominal B_1).

3.8 Discussion

This thesis chapter presents the use of MRI and MRS to study 17 participants over 4 study visits across their bariatric surgery journey. Patients on the bariatric surgery waiting list for either RYGB or SG with prediabetes or T2D were recruited into the study. Participants were split into two arms: Arm A - the main study arm, and Arm B - a pilot arm. For Arm A, participants underwent a 3-hour mixed meal test followed by a 1-hour abdominal MRI session at each visit, whilst Arm B participants had a 1-hour whole body MRI session at all visits with an additional 1-hour ^{31}P liver MRS session at visits 2 and 3. Automatic segmentations performed on the abdominal mDIXON and eThrive were used to create masks of the liver, pancreas, spleen and SAT. These masks were then used to evaluate organ volume, and liver, pancreas and spleen masks were applied to quantitative maps. Investigations of changes to participants' BMI and BSA, as well as organ and SAT volume and organ FF, T_2*, T_1 MOLLI, T_2 and B_1 and mean / FWHM B_0 in the liver across visits, were made.

3.8.1 Study Participants, BMI and BSA

The study dropout rate was low (19%, less than the allowed 25% dropout), and all withdrawals occurred after the first visit. The timeline for participation in the study was slightly longer than the estimated time of 28 weeks, with an average of 40 weeks within the study, this was due to long and unpredictable surgical waitlists. Early in the study, BL visits were organised once the participant had been given a date for their surgery; however, some participants were being offered dates as little

as 3 weeks in advance and nearly immediately after beginning the VLCD. Hence, the scheduling was altered, and the organisation of BL visits was switched to be shortly after recruitment, leaving only the post-VLCD visit to be organised on short notice. This change in recruitment strategy led to a gap from recruitment to being given a surgical date and it is this which caused the extended participation timeline.

3.8.1.1 BMI and BSA

BMI and BSA changes across timepoints were comparable ($p < 0.0001$, $R = 0.61$). No significant changes occurred in BMI or BSA from recruitment to BL. Significant reductions in both BMI and BSA were seen between all other study visits. Initial BMI had no significant effect on the percentage reduction in BMI at any other time point, whilst initial BSA was significantly linked to percentage reduction at 24 weeks PS. Hence, BSA could be a better metric for predicting weight loss outcomes from bariatric surgery.

3.8.2 Limitations in MRI and MRS Data Acquisition and Analysis

This study assessed the changes in the liver, pancreas, spleen and abdominal SAT. For the 62 MRI data sets across subjects and study visits, a small number of data was missing or excluded from the results and statistical tests, as summarised in Table 3.8.

Participant Number	Study Visit	Data set	Reason
3	2	B_1	Scan control parameter (SCP) incorrectly set
		T_1 MOLLI	Physiological simulator timing not set correctly
5	1	B_0	SCP incorrectly set so phase data inaccurate
		T_1 MOLLI	Pancreas not included in image FoV
5	3	All	Not acquired due to adverse event from MMT
9	2	FF & T_2*	Poor BH, motion preventing use of spleen data
10	1	T_1 MOLLI B_0 B_1	Not acquired due to shortage of time
11	2	T_1	Spleen not included in the image FoV
		MRS	Scanner Failure
11	4	MRS	Scanner Failure
12	3	FF	Artefacts in the spleen FF map
13	1	MOLLI T_1	Spleen not included in image FoV
17	2 3	MRS	Scanner Failure
18	2	MRS	Scanner Failure
20	2 3	MRS	Scanner Failure
21	3	All	Time point missed due to complications from surgery

Table 3.8 -Summary of the MRI data which was missing/excluded from data analysis

The MRS data was corrupted for 7 data sets, although correct at the time of acquisition. The source of the scanner failure was investigated by Philips and found to be a bug previously reported, where when the database is nearly full and surplus data purged spectroscopy data is also deleted. For the MRS data analysis, it was shown that using a reduced number of peaks to assess the FF improved the model's robustness, and so this method was used for all datasets shown.

Key to the MRI analysis was the automatic segmentation of organs and SAT using the nnU-NET model, these were visually checked and overall successful. When the liver segmentation failed this was often due to the inclusion of a section of the heart or gallbladder and a missing liver region in the liver mask, probably due to the minimal contrast and close contact between the heart and liver. In these cases, manual correction of the masks was performed, with a number of datasets and changes in organ volume outlined in Table 3.6. The spleen was segmented accurately in all cases and required no correction. For the pancreas segmentation, an eThrive scan was introduced into the protocol to improve its segmentation which was poor on the mDIXON scan. The eThrive scan provided greater contrast between the pancreas and surrounding organs than the mDIXON, however, in a few subjects the eThrive contrast was also low. This low contrast, together with the size, elongated and tortuous shape and its shape variability across subjects resulted in the pancreas being the most challenging segmentation. For failed pancreas segmentations, the pancreas was correctly identified, but regions such as the tip of the pancreas, would be identified for one visit and not for others, leading to errors in volume change across visits. The pancreas had the largest number of datasets that needed correcting and the largest change in organ volume on correction of all organs, as shown in Table 3.6. The pancreas mask was then applied to the other scans (also collected in an expiration breath hold). However, it was noted that for a few subjects, the pancreas mask created on the eThrive did not overlay well when resampled into the mDIXON space due to the difference in breath-hold position.

Figure 3.39 shows an example of this, where the pancreas mask invades the liver and some visceral fat on the mDIXON image. Future work will investigate the realignment of the eThrive and mDIXON (with ongoing work assessing FLIRT in FSL) to prevent this error. To remove any visceral fat from the masks used in this work, boundary values were set to remove those voxels with very high FF values (FF < 50%) that would likely be from visceral fat. Caution must be taken when choosing the boundaries so as not to exclude fatty tissue from the pancreas. Further work is required in this area and improvements to the accuracy of the pancreas segmentation.

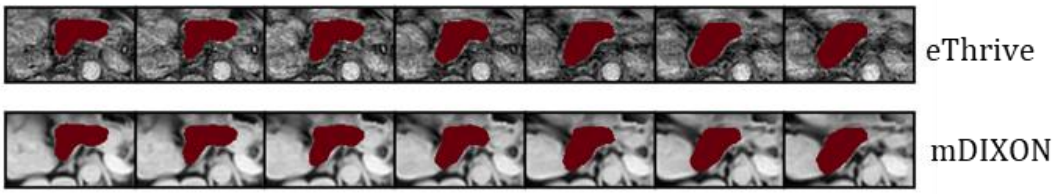

Figure 3.39 - Lightbox of pancreas mask overlayed on (top) eThrive and (bottom) mDIXON image

Unlike for the liver, spleen and pancreas organs, the SAT masks were binary in their success with the nnU-NET model failing (leading to only very small sections of SAT being identified) for 8 data sets. This is shown by the large percentage change in SAT mask volume after correction in Table 3.6. These failures seemed participant-specific, with 5 failed masks from 2 participants. It is unclear why SAT segmentations failed in these subjects as the contrast was high, and all of the SAT volume was included in the FOV; this is being investigated in future work.

3.8.3 Organ-Specific Changes over the Bariatric Surgery Journey

This section provides an overview of the key changes identified in individual organs across the study visits during the bariatric surgery journey and compares these results to literature.

3.8.3.1 Liver

Despite the short duration of the VLCD, a significant reduction was still seen in both liver volume and FF_{MRI} showing its effectiveness. No significant change was seen in liver volume from 6 to 24 weeks PS, however a significant reduction was seen in liver FF_{MRI}. Significant changes were seen to liver FF_{MRS} from BL to all subsequent time points and from 6 to 24 weeks PS but not from post-VLCD to 6 weeks PS ($p = 0.09$). These changes in liver volume occur early in the surgical journey, with the VLCD before surgery being the predominant factor for causing fat loss, after which the liver has reached normal size and fat is being replaced with healthy tissue though these effects may continue into the early PS timeline. Changes to liver volume at 24 weeks PS were comparable to those previously seen in literature, with a mean reduction of 18% ± 7% seen in this study compared to a 8% and 26% change seen by Meyer-Gerspach et al. (2019) (51) and Hedderich et al. (2017) (50) respectively. The reduction in liver FF_{MRI} from BL to 24 weeks measured in this study was slightly lower but within error of reductions seen in the literature. This study saw a mean decrease of 59% ± 20% from PS, with a 74% and 68% change seen by Meyer-Gerspach et al. (2019) (51) and Hedderich et al. (2017) (50) respectively.

Liver FF_{MRs} and FF_{MRI} correlated well. However, the FF_{MRI} appeared to overestimate FF when true values are under 10%. This bias resulted in 15 participants being classified as starting the study with fatty livers (FF > 6.4%). according to the imaging data, but only 14 started according to spectroscopy data. This bias has been shown in other studies in the literature, such as the study of Hu et al. (52), despite methods being minimally different; for example, FF_{MRS} is corrected for T_2 decay in this work, but this was not performed by Hu *et al.* Hu *et al.* suggest that the assumption that the T_2* of water and fat are equal in FF_{MRI} maps is a possible source of the overestimation and that introducing T_2* correction in FF could reduce this. As was discussed in Hu *et al*., imaging methods have some advantages over spectroscopy, requiring less expertise and allowing whole liver, spleen, and pancreas measures to be collected in a single breath-hold, whilst spectroscopy requires a minimum of a breath-hold per organ and samples only a small region making it insensitive to heterogeneous fat deposition.

Liver T_1 MOLLI showed a significant decrease from BL and post-VLCD to 24 weeks PS. It was shown by Mozes *et al.* (62) that T_1 MOLLI is increased in the presence of increased fat and so this interaction is likely the cause of this finding, this is discussed further in Section 3.8.4.

Liver T_2* significantly increased from all time points to 24 weeks PS. This may be due to a reduction in the iron content, an effect of the decrease in FF or improvements in insulin sensitivity. Previous work from Au *et al.* (69) and Kosaryan

et al. (70)did not see a link between insulin sensitivity and liver T_2* when comparing diabetic and healthy controls. However, it may be that their results are a product of inter-subject variations. Future work will investigate this link with the clinical blood measures taken in this study.

3.8.3.2 Pancreas

No significant change was seen in pancreatic volume over the study visits, Figure 3.28, with mixed trends seen on an individual participant basis, Figure 3.33. Changes seen in individuals in pancreas volume may be artefacts of accurate masking (as described in Section 3.8.2), as although any visible issues were fixed the pancreas was difficult to identify and ensure all tissue was included in the mask. No significant change was seen in pancreatic FF, and all participants had a fatty pancreas at BL and at 24 weeks PS (FF > 6.2 % (68)). This may have been impacted by errors in the mispositioning of the masks and will be further explored.

A significant increase was seen in pancreatic T_2* from 6 to 24 weeks PS. Previous literature has shown pancreas T_2* to correlate with beta cell function and insulin sensitivity, with non-diabetics having longer T_2*'s than pre-diabetic and T2D participants (69,70). Hence it has been suggested that an increase in T_2* is possibly a sign of the diabetic remission seen after bariatric surgery. No significant change was seen in pancreas T_2. A significant increase was seen in pancreas T_1 MOLLI from BL to 6 and 24 weeks PS. Previous literature from Noda *et al.* (71) has shown that pancreatic T_1 reduces as insulin sensitivity improves, assuming the improvement in

insulin sensitivity seen previously in bariatric surgery group's function (31,37) this study has inverse findings. However, T_1 MOLLI is sensitive to FF and so changes in the IR SE-EPI T_1 map which is insensitive to these effects will be explored in future work. Analysis of the blood measures taken will provide more insight into the correlation of these results with diabetic remission and improvement in insulin sensitivity. More work is needed to ensure the pancreas masks are overlayed correctly on quantitative maps and that the changes are not artefacts of the inclusion of other tissues or visceral fat.

This work used segmentations of the whole pancreas in analysis. Literature suggests that the FF is uniform across the pancreas (72), whilst T_2* has been shown to be significantly different between regions (head, body, tail), future work will explore separating the pancreas segmentations by region.

3.8.3.3 Spleen

A significant reduction in splenic volume was seen from BL and post-VLCD to 6 weeks PS but not between any other timepoints any other time points, Figure 3.29. A significant reduction in splenic FF was seen from BL to 6 and 24 weeks PS and from post-VLCD to 6 and 24 weeks PS. It is likely that the reduction in FF is the driving factor reduction in volume. No significant change was seen in splenic T_2*, T_2 or T_1 MOLLI.

One participant (Participant 5) had a considerably larger spleen volume and lower T_2* compared to other participants, FF_{MRI} were within the normal ranges, Figure

3.33. It is possible that the large increase in this participant's spleen volume at 24 weeks PS reduced the powering of the data, especially due to the lower number of data for this time point; however, upon inspection of the mask, the segmentation is correct. Once available the clinical blood data will be reviewed for this participant.

3.8.3.4 Subcutaneous Adipose Tissue

Significant reductions were seen for SAT volume from BL and post-VLCD to 6 and 24 weeks PS and from 6 to 24 weeks PS, Figure 3.30. This is likely linked to the weight loss that is seen after bariatric surgery. Percentage reductions in SAT from BL to 24 weeks PS were much lower than reported in the literature. This study showed a 20% ± 12% reduction from BL to 24 weeks PS, whilst *Hedderich et al. (2017)* (50) saw a 41% reduction in SAT volume for the same timeframe. Despite using the largest possible FOV (450 x 450 mm) for the mDIXON scan, regions of SAT were missing in the largest patients, Figure 3.25. This would lead to underestimations of the SAT volume, especially for the early visits and hence, underestimate percentage reductions. Methods used in this study included breast tissue in SAT volume estimations, this could also cause discrepancies in SAT volume between visits from differences in patient positioning. This could be mitigated in future work by reducing the region analysed to between two vertebrae in the spine, and exploring the methods suggested by Michel *et al.* (59) to overcome complete SAT estimations in datasets with insufficient size FOV to encompass the participant.

3.8.4 Correlations between MRI Measures

Figure 3.35 showed a correlation matrix between measures across visits some of them have been explored in this thesis.

BMI and BSA both significantly positively correlated with FF (FF_{MRI} and FF_{MRS}) and measured SAT volume for all timepoints, displaying the link between weight loss and reduction in liver fat and SAT volume, Figure 3.36. BMI showed a stronger correlation with SAT compared to BSA (R = 0.87 and 0.56. respectively). A negative correlation was seen for both BMI and BSA with the delivered B_1 field, however, with BSA showing the strongest correlation (BSA: R = 0.80, $p < 0.0001$, and BMI: R = 0.43 and P = 0.0005, respectively). This is likely due the BSA being a better indicator of the distance of the coil from the liver as BMI does not accurately represent weight distribution. This is an important consideration for quantitative MRI measures. No correlation was seen between mean B_0 field in the liver and BMI or BSA however the distribution of the B_0 FWHM significantly increased with BMI, suggesting improvement in shimming as the participants lose weight.

FF was significantly correlated with liver volume; it is likely that the reduction of fat is what drives liver shrinkage. FF also significantly correlated with MOLLI T_1, with a higher level of agreement seen from FF_{MRI}, this effect was explored by Mozes *et al.* (62) The IR-SE-EPI T_1 data to be analysed will highlight the degree this effect has had on the data presented. However, it is likely that the decrease seen in MOLLI T_1 is an artefact of the reduction in FF and not a true reduction in T_1. Future work will compare MOLLI T_1 with the IR-SE-EPI data acquired.

T_2 significantly correlated with B_1 for all organs (all $p < 0.0001$), this effect was explored by Li *et al. 2024* (53), and is plausibly countering any changes that may be occurring to T_2 of the organs studied. Future work will use the B_1 maps to correct quantitative imaging.

BL values of FF_{MRI} significantly correlated with the percentage reduction seen at 6 and 24 weeks PS, however, no significant correlation was seen between FF_{MRS} and percentage reduction at any time point (Figure 3.37). This may be due to variations in fat distribution throughout the liver which are not picked up by the small MRS voxel combined with inconsistencies in the voxel positioning.

3.8.5 Future Work

Steps for specific future work on the MRI measures analysed to date have been described and discussed above. Whilst some data sets from the study remain to be analysed, including the Diffusion Weighted Imaging (DWI) and Magnetisation Transfer (MT) data collected in Arm A, and future work will perform this. For the DWI data, this will include IVIM analysis in the pancreas, as this has been linked to beta cell function (54). The adipose MRS data has not been analysed and future work needs to be done to create a pipeline for this which will provide an insight into fat composition and their changes over time. Kidney T_1 MOLLI and T_2* data collected in both arms are yet to be analysed along with cardiac MRI data still including aortic flow measures from both arms and cine data from Arm B.

Pilot data on whole body mDIXON was collected in Arm B which provide a good visual aid for weight loss from participants, as shown in Figure 3.40 for a single slice at all four visits, where clear loss is seen for example around the hips. Future work will include automated segmentations of this data to estimate changes in the volume and FF of the leg and back muscles.

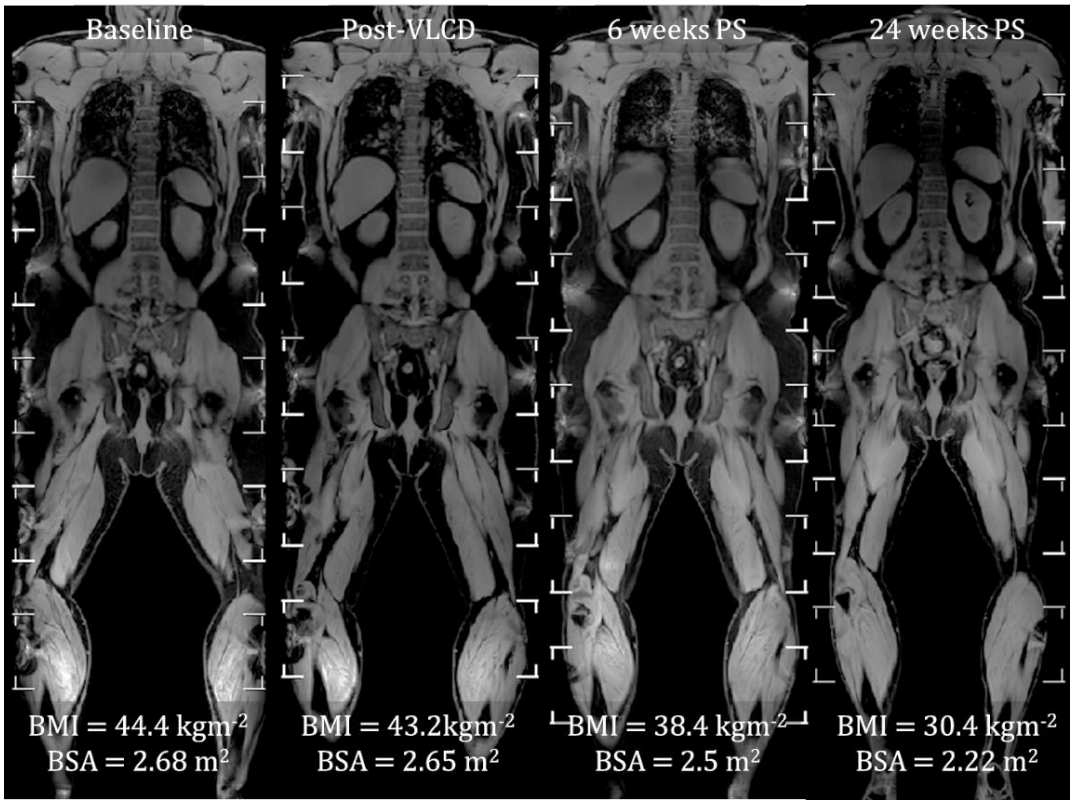

Figure 3.40 - A slice of the Whole body mDIXON scan from participant BARI 13 at all 4 time points. BMI and BSA are displayed at the bottom of the respective images.

At the time of writing this thesis the clinical blood data was not available with ELISA (Enzyme-Linked ImmunoAssay) laboratory tests to be performed. Once blood results are available, the MR measures will be linked to plasma Glucagon, Ghrelin,

Glucose, GIP and GLP-1, Insulin, C-peptide and bile acids, and changes to the Area Under the Curve (AUC) in blood measures across the surgical journey will be investigated. HbA1c values from pre-surgery and 24 weeks PS will also give insight into changes in diabetic status. Comparisons between blood measures and MRI will allow for further insights to understand the changes within the body and the mechanisms behind diabetic remission.

To date, the MR data is still blinded for the type of surgery each participant underwent. Therefore, no comparisons have been made between the two types of surgery. Of the 17 participants enrolled in this study, 6 have undergone RYGB, and 11 have undergone SG. During this study, surgical protocols changed, and the NHS now heavily favours performing SG due to the reduced risk of complications, resulting in it being more difficult to recruit participants undergoing RYGB to this work. However, Dr Rebekah Wilmington and Professor Iskandar Idris believe the ratio of participants who underwent RYGB in this study is higher than the ratio undergoing RYGB in the clinic. It should also be noted that due to the higher risk of complication RYGB is often performed on patients with less complicated health conditions which may add bias to any comparisons made between surgical outcomes.

3.9 Conclusion

In summary, this work studied changes over the bariatric surgery journey and showed significant reductions in BMI, BSA and SAT volume. In the liver, significant reductions were seen in volume, FF_{MRI} and FF_{MRS}, T_1 MOLLI from BL to 24 weeks, and significant increases in T_2* and B_1. In the pancreas, a significant increase was seen in T_2*, and in the spleen significant reductions were seen in volume and FF_{MRI} PS. There was good agreement between FF measured using MRI and MRS. Correlations were seen between BMI and BSA with FF (MRI and MRS), SAT volume, B_1 and for BSA only with B_0 FWHM. FF_{MRI} at BL correlated well with percentage reduction at 24 weeks PS but FF_{MRS} showed no correlation with percentage reduction at any time point. Liver FF (MRI and MRS) correlated with both liver volume and T_1 MOLLI.

4 The Complexities of Measuring Liver Energetics using Phosporous-31 Magnetic Resonance Spectroscopy in people with different BMIs for studies related to obesity

4.1 Overview

This Chapter explores the effect of different RF pulses on surface coil acquisition using multinuclear Magnetic Resonance Spectroscopy (MRS) particularly for the liver. Computational simulations are compared to experimental data of signal drop off with distance from the coil from non-localised (^{13}C) and localised (^{31}P) acquisitions to determine the optimal RF pulse shape. These findings are then applied to two intervention studies, which use ^{31}P Saturation Transfer (ST) experiments of ATP flux in the liver, one on the effects of consuming Inulin Propionate Ester and the other on Bariatric Surgery.

Work from this chapter has been presented as a digital poster 'Change in ATP flux after propionate ingestion in healthy volunteers Using ^{31}P MRS Saturation Transfer' at the International Society of Magnetic Resonance in Medicine, Toronto, 2023.

4.2 Introduction

As discussed in the previous (Chapter 3), rates for metabolic disorders including obesity are rising globally. Multinuclear Magnetic Resonance Spectroscopy (MRS) is a developing field that shows great promise in investigating metabolic diseases. Previous studies have used multinuclear MRS to study healthy volunteers with great success, but the transition to patient studies poses challenges. Most commercially available coils still use single-loop designs where the B_1 decay with depth into the body is a limiting factor. This is a particular problem in the study of obesity-related diseases where the Subcutaneous Adipose Tissues (SAT) may limit access to the desired organ. The purpose of this chapter is to explore the steps required to develop the experimental techniques used *in vivo* considering two studies, including the modelling of the transmit field produced and received signal collected by a single-loop coil, simulation of the excitation effects of block and Half-Passage Hyperbolic Secant (HPHS) Radio Frequency (RF) pulses and *in vivo* tests of signal changes with distance.

This chapter discusses two pilot studies to investigate changes to Adenosine TriPhosphate (ATP) flux, one on Healthy Volunteers (HV) with normal BMIs to investigate the effect of consuming an Inulin Propionate Ester (IPE) and one in patients on the effects of bariatric surgery with obese BMIs.

4.2.1.1 Inulin Propionate Ester

This chapter discusses a study on the effects of consuming an Inulin Propionate Ester (IPE) on ATP flux in the liver of HV with normal BMIs. Propionate is a short-chain fatty acid produced naturally by the fermentation of dietary fibre in the colon. Propionate and its ingestion have been linked with lower cholesterol levels, increased satiety, altered hepatic metabolism and reduction in liver lipid content, and there is some evidence that enriching colonic propionate positively affects energy homeostasis and glycaemic control (75–78). Propionate is absorbed from the colon and moves through the blood to the liver, where ~90% of propionate is metabolised, after which very little is detectable in peripheral blood. However, the mechanisms by which the human liver metabolises propionate are poorly understood; although propionate has been shown to affect both gluconeogenesis and glycolysis, metabolic pathways which produce metabolites that are used in the TCA cycle and affect ATP flux rates (78), as discussed in Chapter 1.

4.2.1.2 Bariatric Surgery

The background for the bariatric study has been covered extensively in Chapter 3. Diabetic remission has been observed in multiple bariatric surgery studies (37,45,53,79). However, the mechanisms for the improved insulin sensitivity are unknown. Previous studies from Szendroedi *et al.* (80), Kupriyanova *et al.* (81) and Schmid *et al.* (82) have shown that phosphorous metabolites are linked to insulin sensitivity, though these studies observed differences between non-diabetic, pre-

diabetic and diabetic groups. No literature was found investigating changes to phosphorous metabolites in individuals through diabetic remission. The goal of this study was to test the feasibility of Saturation Transfer (ST) experiments in obese individuals to investigate changes to phosphorus metabolites and ATP flux before and after bariatric surgery and assess the link between these markers and insulin sensitivity and diabetic remission.

4.2.2 Measuring Metabolism using ^{31}P MRS

Using phosporous-31 (^{31}P) spectroscopy it is possible to quantify the amount of Adenosine TriPhosphate (ATP) in the body. It was discussed in Chapter 1 that ATP is the body's energy currency. Measuring the concentration provides insight into a body's metabolism. This can be taken a step further, and the ATP production rate in cells can be measured using ^{31}P saturation transfer experiments as discussed in Chapter 2.

4.2.2.1 ^{31}P Experiments in Healthy Populations

Initial studies and pilot data have often been acquired using Healthy Volunteers (HV), with a recruitment criterion which was a normal Body Mass Index (BMI) which, depending on race, is defined as BMI 18.5 – 24.9 kgm^{-2} (83). Schmid *et al. 2008* (18) investigated the T_1 of phosphorous metabolites in the liver and used ^{31}P saturation transfer experiments to assess ATP flux in HV. They scanned 15 HV with a mean BMI of 22.6 kgm^{-2} using a 3 Telsa MR scanner with a 100 mm single loop surface coil. They found that Pi and γATP in the liver had T_1 values of 0.73 ±0.09 s

and 0.43 ±0.05 s, respectively, and k and flux rates of 0.30 ±0.02 s^{-1} and 29.48 ±1.79 $mMmin^{-1}$ respectively (mean ±SD).

4.2.2.2 ^{31}P Experiments in Obesity

In obesity, the distance from the coil to the liver is generally increased due to the thickness of the Subcutaneous Adipose Tissue (SAT), Figure 4.1. Nadeem *et al.* (84) found that in a cohort of 384 subjects (Age: 16 – 60 years, 32 ±10 mean ±SD, BMI: 12.1 – 61.5 kgm^{-2}, 24 ±7 mean ±SD), BMI was related to the thickness of SAT using

$$\Delta_{SAT}\ (mm) = \frac{BMI - 16.99}{0.39}$$

Equation 4.1

where Δ_{SAT} is the SAT thickness in mm at the belly button, Solga *et al.* (85) investigated factors that affected the success of liver fat measurements using ^{1}H MRS along with ^{31}P MRS in overweight and obese individuals with T2D. The intra-rater repeatability for ATP was high (intra-class correlation coefficient (ICC) 0.83-0.92), whilst the inter-rater reproducibility was good and decreased as BMI increased (average ICC = 0.65 and 0.58 for BMI <32.8 kgm^{-2} and >32.8 kgm^{-2} respectively). The intrasubject variability was said to be high and no value is quoted. They found that obesity was the largest contributor to unsuccessful ^{31}P acquisitions and that if the distance to the liver was over 60 mm, SNR was too low.

Assuming SAT thickness is uniform around the abdomen, then combining Equation 4.1 with the findings of Solga *et al.* (85), participants with a BMI over 40 kgm^{-2}

would have an SNR that is too low for analysis to be possible. Hence, the average bariatric surgery patient with a BMI of 50 kgm^{-2} would have a SAT thickness too great to produce adequate SNR (86).

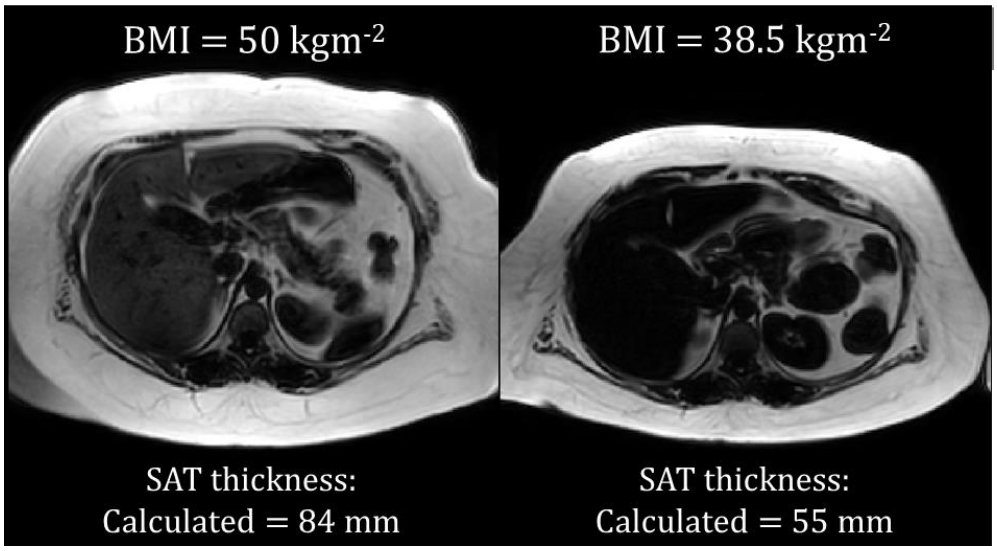

Figure 4.1 - Two data sets from a bariatric patient showing their BMI and SAT thickness as estimated using Equation 4.1 (87)

Kupriyanova *et al.* (80) investigated the changes to phosphorous metabolites in the liver from early-stage T2D to five years after diagnosis; they found that there was a 17% decrease in Pi concentrations but no change to γATP concentrations, the presence of NAFLD did not affect the Pi or γATP concentrations. It was noted that phosphorous metabolites were heavily linked to insulin sensitivity. This trend was also seen by Szendroedi *et al.* (81), who investigated the absolute concentrations of phosphorous metabolites in the liver in a T2D cohort compared to an age-weight-matched cohort and a young-healthy cohort. Kupriyanova *et al.* (80) scanned patients prone and though the reason for this was not stated, this may have been to

reduce the distance from the liver to the surface coil. They found that the T2D cohort had 26 % and 23 % lower γATP and 28 % and 31 % lower Pi concentrations than the age-weight matched and young-healthy individuals, respectively. Pi concentrations were 0.96 ±0.06 mM, 1.33 ±0.13 mM and 1.41 ±0.07 mM for T2D, age-weight matched controls and young-health individuals, respectively.

One study was found that had performed ^{31}P saturation transfer experiments in a T2D cohort. Schmid *et al*. *2011* (82) used a 3 Tesla scanner with a 100 mm single loop surface coil to scan participants supine. A 30 mm 1D ISIS sequence for ST experiments and apparent T_1 ST inversion recovery sequences were performed. Good quality data was acquired in 17 participants, 9 were T2D (BMI 26.9 ±3.4 kgm^{-2}), and 8 were HV (BMI 25.1 ±3.9 kgm^{-2}). No significant difference was seen in the exchange rate constant (k) values between T2D and HV, Table 4.1. However, a significant difference was seen in the absolute concentration of Pi (T2D = 0.96 ± 0.19 mM, HV = 1.38 ± 0.38 mM) and forward flux rate (p = 0.011 and 0.025, respectively). They found that the forward flux rate positively correlated with insulin resistance and negatively correlated with waist circumference and fasting plasma glucose. They did not report any difference in apparent T_1 between the T2D and HV cohort or their previous work (18). Although this was a T2D cohort, participants fell into the normal to overweight and not obese BMI category.

Study	Exchange Rate Constant, k (s^{-1})				Forward Flux (mMs^{-1})			
	HV	T2D	NAFLD	NASH	HV	T2D	NAFLD	NASH
Schmid *et al. 2008 (18)*	0.30 ± 0.02				0.49 ± 0.03			
Schmid *et al. 2011* (82)	0.33 ± 0.12	0.28 ± 0.07			0.47 ± 0.2	0.27 ± 0.09		
Valkovic *et al. (88)*	0.31 ± 0.03		0.30 ± 0.05	0.17 ± 0.04	0.39 ± 0.05		0.40 ± 0.06	0.18 ± 0.07
Traussnigg *et al. (89)*			0.3	0.2			0.3	0.21

Table 4.1 – Exchange rate constant (k) and forward flux values from the literature.

A study by Valkovic *et al.* (88) on obese individuals discussed the difficulty of low SNR at 3 Tesla and moved to 7 Tesla. The goal was to compare k and forward flux rates from Non-Alcoholic Fatty Liver Disease (NAFLD) and HV (n=7) with BMI ranges of 23.3–29.3 kgm^{-2} and 21.5–39.6 kgm^{-2}, respectively. The participants in the NAFLD group were later further split into NAFLD (n=6) or Non-Alcoholic SteatoHepatitis (NASH, n=10) based on liver biopsy data. Phosphorous spectra were acquired using a 100 mm coil with participants positioned laterally. A 30 mm 1D ISIS sequence with block excitation and adiabatic inversion was used. It was found that participants with NASH had significantly lower k values than both other groups and that there

was an overlap in the k values for HV and NAFLD groups. Similarly, NASH participants had significantly lower forward flux rates than other groups, with NAFLD and HV having similar rates to each other. Values for k of HV measured were similar to those reported by Schmid *et al*. *2008 and 2011*, with slightly lower forward flux rates, Table 4.1.

In a study from Traussnigg *et al.* (89) participants had either NAFLD or NASH with BMIs from each group being 27.3 ±5.2 kgm^{-2} and 31.4 ±4.1 kgm^{-2} (mean ±SD), respectively. Phosphorous spectra were acquired using a 100 mm coil with participants positioned laterally and the coil placed underneath them. Flux constant (k) values and forward flux rates significantly differed between the groups, $p=0.003$ and $p<0.001$, respectively, Table 4.1. A correlation between forward flux rate and steatosis (measured using histology) was also seen ($p=0.021$).

BMIs of the participants in the studies described above were lower than the average for bariatric surgery patients. Thus, the feasibility of ST experiments on a bariatric cohort remains questionable and requires investigation.

4.2.3 The Effects of Radio Frequency Fields on the Sensitivity of Surface Coil Signals in MRS

Surface coils are frequently used for MRS studies, but the signal from a surface coil drops off with distance from the coil, compromising MRS of organs at depth or where the SAT is thick. However, the RF pulses used can be optimised to try to reduce this effect.

In this section, the Biot-Savart model was used to simulate the RF magnetic field around a single-loop coil to produce sensitivity maps for MRS experiments using both Block and Half-Pass Hyperbolic Secant (HPHS) pulses. Experimental data collected on a small test phantom was used to test the simulation's results.

4.2.3.1 Penetration depth

Many multinuclear MRS experiments use single-loop surface coils. There are multiple possible reasons for this. Multinuclear MRS is a small field and even within expert sites, is likely to have a small user base. Single-loop coils are the simplest and cheapest to develop and build, particularly for groups which custom-build their own multinuclear coils. They can be used flexibly for various applications compared to birdcage coils. However, surface coils have disadvantages.

The B_1 drops off with distance from the coil, so single-loop coils have a penetration depth of 50-75% of their diameter (90). Current commercially available multinuclear spectroscopy coils generally range in diameter from 60 – 200 mm, with the most common being 140 or 150 mm (91,92). The effective penetration depth of the 140 mm diameter ^{31}P coil used at the Sir Peter Mansfield Imaging Centre (SPMIC) is 70 - 105 mm. Equation 4.1 predicts that the thickness of the Subcutaneous Adipose Tissue (SAT) of a bariatric patient with a BMI of 50 kgm^{-2} would be ~84 mm (84).

This would mean that only ~21 mm of muscle and liver would be accessible to this 140 mm diameter ^{31}P coil.

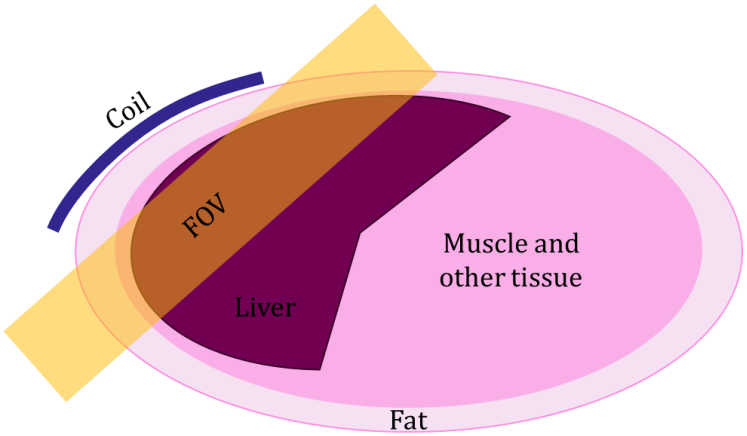

Figure 4.2 - Schematic of desired Field of View positioning for a ^{31}P MRS saturation transfer in the liver. Note that the FOV misses the edge of the liver to reduce the visible muscle volume.

For ^{31}P saturation transfer experiments, localisation techniques are used to prevent contamination of PhosphoCreatine (PCr) in the spectra from the muscle, as this reduces SNR (17,18,93). The slice selective slab should be placed perpendicular to the coil to exclude muscle from the Field Of View (FOV). Due to the human body's geometry, the liver's edge is often clipped out of the FOV (Figure 4.2). This increases the distance from the coil to the liver, which reduces SNR in the Region Of Interest (ROI) and, in particular, limits the effectiveness of the automatic B_0 shimming algorithm. The experimenter is left with a choice: to reduce the distance to FOV by including muscle and possibly improve the shim but contaminate the spectrum with signal from muscle, especially PCr which is not present in the liver, or maintain FOV

positioning requirements, which may lead to poor shimming. Initial studies showed that in larger patients, the coil failed to obtain spectra with adequate SNR, and optimisation is required to ensure adequate data was collected within this group (93).

4.2.3.2 Pulse Type

The effect of the B_1 field on the magnetisation created and the signal detected depends on the pulse type used. Here, two types of excitation pulses were investigated: block pulses and Half-Passage Hyperbolic Secant (HPHS) pulses. Block pulses are sensitive to the inhomogeneity produced by a single-loop coil, while the frequency-modulated adiabatic HPHS pulse is less sensitive to B_1 inhomogeneity.

Block pulses are produced at a single frequency, generally designed to be on-resonance with the spins that need to be excited. The Flip Angle (FA) of the pulse is directly proportional to the area under the pulse, so this makes the FA very sensitive to B_1 inhomogeneities, such as those that occur with distance from a single-loop coil. Adiabatic pulses slowly sweep across a range of amplitudes (amplitude modulation) and frequencies (frequency modulation) to tip spins evenly across a desired bandwidth. As such, the off-resonance and variable tipping angle effects of an inhomogeneous B_1 field are theoretically reduced (14,94). The most common form of adiabatic pulse used in MR follows a Hyperbolic Secant envelope and can be applied as a full passage sweep for inversion or a half-passage sweep for excitation. Despite the many potential advantages of the HPHS pulses, the studies previously

discussed often used block excitation pulses, probably due to the expertise needed for programming non-standard pulses and interpreting their response.

This chapter combines simulations of the Biot-Savart law for the magnetic field from a single-loop with RF simulations of block and HPHS pulses to investigate the optimal acquisition parameters for an obese cohort. The simulation results were then compared to data from a small phantom used to test the model at approximately discrete depths (Section 4.3.4). Each pulse type was used in turn to acquire data from two healthy subjects with different BMIs at varying distances to assess the real-world outcomes. This was used to inform the design of two liver ATP flux intervention studies. One study investigated changes to ATP flux before and after the consumption of Inulin Propionate Ester (IPE) in HV with healthy BMI's, and the other investigated changes to ATP flux before and after bariatric surgery in obese patients.

4.3 Modelling the Effects of B_1 Field Homogeneity on Multinuclear MRS

In order to quantify metabolites from multinuclear MRS experiments, the effects of B_1 inhomogeneities on the receive signal need to be corrected. This section describes the model used to simulate these effects and its experimental validation. Simulations were initially done to produce maps of the B_1 field close to the coil, which were then converted to magnetisation based on the modelled pulse response

for the block and Half Passage Hyperbolic Secant (HPHS) pulses, respectively. The received signal was then determined by scaling the magnetisation maps according to the receive sensitivity profile. To validate the simulations, MR spectra were acquired from a small test phantom at varying positions close to the coil and compared with the modelled response, Section 4.3.4. Simulations described in this section were performed for ^{13}C using a ^{13}C labelled phantom for experimental validation.

An overview of the workflow for the simulation is shown below in Figure 4.3:

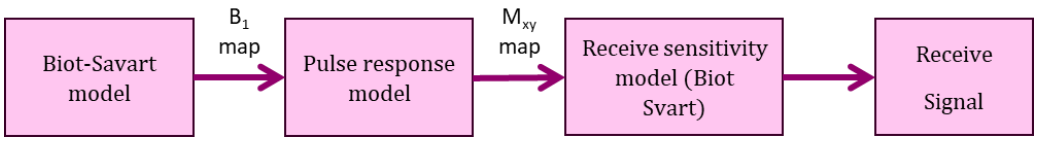

Figure 4.3 – Steps taken to calculate receive signal in simulations.

4.3.1 Modelling the B_1 near the Surface Coil

B_1 and receive sensitivity both decrease with increasing distance from the surface coil. For high resonance frequencies, the static approximation of a magnetic field is not applicable, and a full wave simulation is needed (conventional MRI above 1.5 T); however, due to the smaller gyromagnetic ratio of ^{13}C and ^{31}P, a static field approximation holds at 3 Tesla (95). Therefore, the magnetic field surrounding a single-loop surface coil can be calculated using the Biot-Savart equation:

$$d\vec{B} = \frac{\mu_0}{4\pi} \frac{I\, d\vec{l} \times \hat{r}}{r^2}$$

Equation 4.2

where $d\vec{B}$ is the field produced at point P in space by the current element $d\vec{l}$, μ_0 is the permeability of free space, I is the current around the wire, $\hat{r}$ is the unit vector pointing from the current element to P, and r is the distance to P from the current element as shown in Figure 4.4.

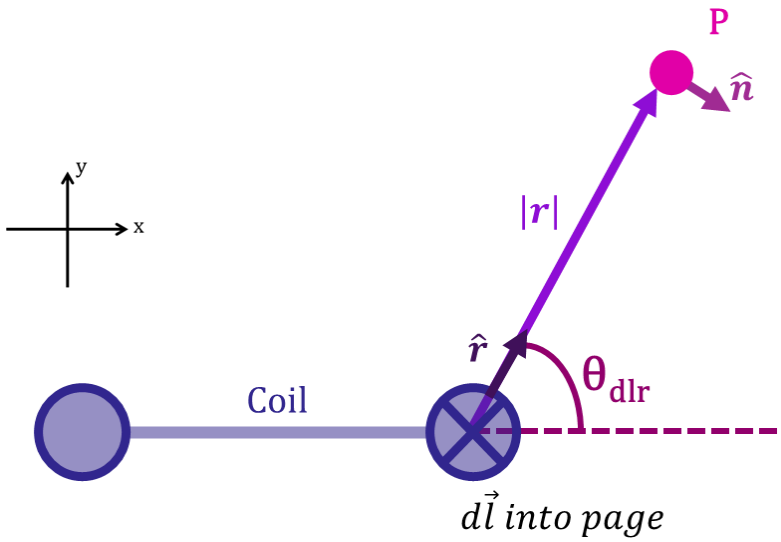

Figure 4.4 - Components of the Biot-Savart Law

Since μ_0, I and 4π are all constants, the relative magnetic field can be modelled within a given volume around the coil and scaled according to a known B_1. Hence, for equally spaced current elements, the magnetic field produced at each point in space will be proportional to the distance from the element to the point as follows:

$$d\vec{B} \propto \frac{\sin\theta_{dlr}}{r^2}\,\hat{n}$$

Equation 4.3

where $\sin\theta_{dlr}$ is the angle between $d\vec{l}$ and $\hat{r}$, and $\hat{n}$ is the unit vector perpendicular to the plane of $d\vec{l}$ and $\hat{r}$ (Figure 4.4).

Only RF magnetic field components perpendicular to the static field (B_0) are relevant to NMR excitation or detection (B_1), which can be determined by summing all the x and y components of the field at a given point over all current elements and finding the resulting vector magnitude.

Simulations were modelled using the dimensions of the Pulseteq ^{13}C coil (96,97), which had an in-plane elliptical shape and out-of-plane curvature: radius in x = 75mm, radius in y = 83 mm, curvature depth = 10 mm, Figure 4.5.

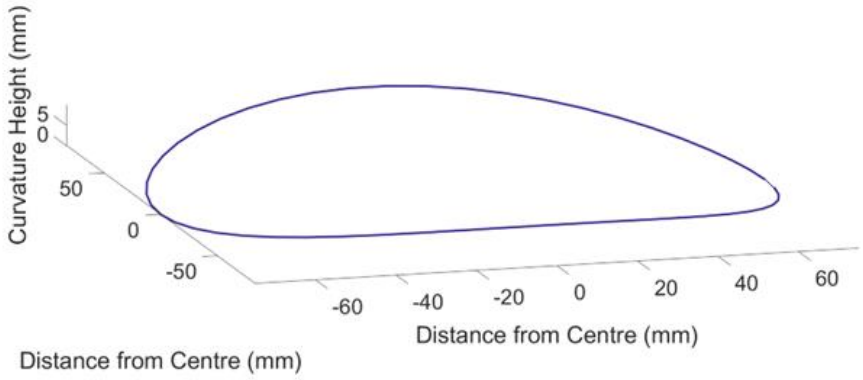

Figure 4.5 – Dimensions of the simulated coil.

Fifty current elements $d\vec{l}$ were modelled around the loop, and each element's contributions to the x and y components of the RF field at each point in space were calculated using

$$B_x = \sum_{i=1}^{50} dB_{x,i} \quad B_y = \sum_{i=1}^{50} dB_{y,i}$$

Equation 4.4

across a 100 x 100 x 100 voxel space where each voxel is 3 x 3 x 3 mm. The total field produced at each point (x,y) was then calculated using

$$B_1 = \sqrt{{B_x}^2 + {B_y}^2}$$

Equation 4.5

4.3.2 Modelling the Excitation Magnetisation for a given B_1

The transverse magnetization produced in a sample will be dependent on the B_1 values throughout the sample. Here, the response to a standard excitation block pulse and a HPHS pulse as described above was modelled.

4.3.2.1 Block pulse

For a standard on-resonance block pulse, the Flip Angle (FA) and transverse magnetisation (M_t) are determined as:

$$FA = B_1.\gamma.t_p$$

Equation 4.6

$$M_t \propto \sin(FA)$$

Equation 4.7

Hence, the maximum transverse magnetisation occurs when the flip angle is π/2 rads which approximately corresponds to the location of the maximum signal (assuming no tip angle wrapping). As such, determining the location of the maximum signal near the surface coil allows the scaling of the simulated B_1 maps to give a π/2 rads FA at that location and subsequently calculations of the transverse magnetisation. This was found empirically by acquiring repeated MRS whilst varying the position of a small test phantom and determining the location of the maximum signal, these experiments are described further in Section 4.3.4.

4.3.2.2 HPHS pulse

Due to the non-linear relationship between the HPHS pulse response and B_1, the exact B_1 at each point in space near the coil needs to be determined. Because all power optimisation adjustments were switched off during multinuclear MRS, the location of the nominal input B_1 for the π/2 rads block pulse on the scanner will correspond to the location of the nominal input B_1 for the HPHS pulse (representing the peak amplitude of the HPHS amplitude modulation). Hence, the B_1 maps can be scaled such that the location of the maximum received signal from the block pulse phantom experiment is equal to the nominal input B_1 of the HPHS pulse.

For frequency-modulated pulses such as the HPHS, the FA is not directly proportional to the B_1 amplitude, and therefore, the FA response needs to be modelled. An RF simulator in MATLAB (Mathworks 2020b) was used to determine

the transverse magnetisation response on resonance for a HPHS pulse for varying B_1, and a third-order polynomial was fitted.

The transverse magnetisation maps of the HPHS were therefore determined by applying the fitted HPHS pulse magnetization versus B_1 response curves to the scaled B_1 maps.

4.3.3 Estimating the Receive Sensitivity and Receive Signal

The receive sensitivity near the surface coil is determined by Lorentz's principle of reciprocity (98). As such, the receive signal is proportional to (and in phase with) the transmitted B_1 at any point, P, around the coils. The final receive signal maps can, therefore, be calculated as the product of the transverse magnetization maps and the B_1 field around the surface coil.

4.3.4 *Ex-vivo* Validation using a Small Test Phantom

To evaluate how well the Biot-Savart simulations worked, simulated data was compared to experimental MRS results. For the MRS experiments, a small test phantom containing ^{13}C (Figure 4.6) was placed in the centre of the coil and gradually moved away from the coil's surface. Data was then compared to a simulation of an extended cuboid designed to match the size of the phantom.

4.3.4.1 Experimental Acquisitions

Experiments were performed on the 3 Tesla Achieva using the Pulseteq ^{13}C dual-tuned surface coil, with an in-built labelled urea sample in the centre that is used as a reference for concentration values and positioning. The small test phantom used

in these experiments was a doped ^{13}C sample in a small glass vial, shown in Figure 4.6 (diameter = 10 mm, length = 30 mm).

Figure 4.6 – Photo of ^{13}C doped glycine small test phantom.

Two large bottles (containing SpectraSYN™ 4) were placed on the coil's surface to ensure that enough proton signal was present for the scanner to run. The phantoms were moved away from the coil by placing padding between them and the coil. At each location, three scans were performed: 1. a survey scan for distance measurements, 2. A non-localised block pulse (TR = 1000, NSA = 32) and 3. A non-localised HPHS pulse (TR = 1000, NSA = 128).

Distance from the coil to the sample was measured on the images using ImageJ (87), the distance recorded was the distance from the urea to the doped sample.

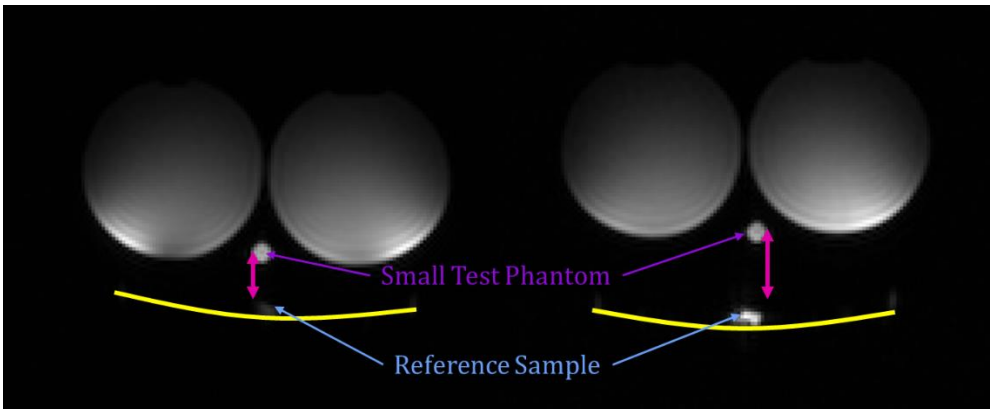

Figure 4.7 - The position of the doped carbon small test phantom (containing labelled glycine) and Urea reference sample relative to the coil, large phantoms contain SpectraSYN™ 4. Pink arrows show the perpendicular distance measured, the back of the coil is outlined in yellow.

The spectra were evaluated in JMRUI (99–101) using AMARES (Advanced Method for Accurate, Robust and Efficient Spectral fitting (102)) quantification. For the HPHS spectra, an extra Gaussian fit was used to aid in baseline correction, Figure 4.8.

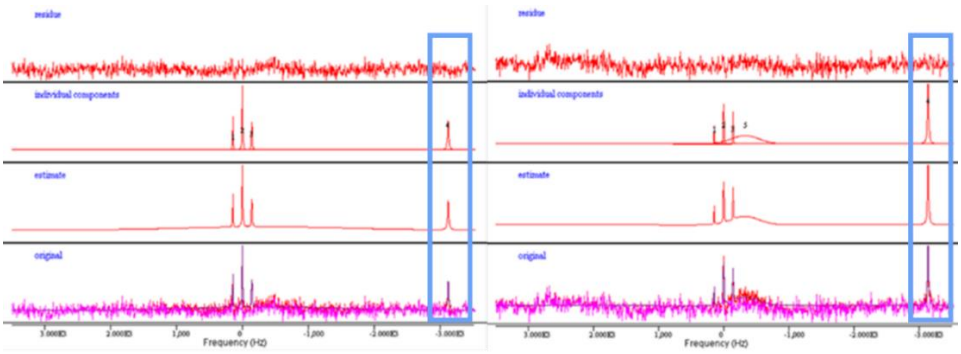

Figure 4.8 - JMRUI fits for aquisitons at 38mm from the coil. Left- Block pulse, Right- Hyperbolic secant pulse showing extra gaussian fit for basline correction. Reference peak from Urea sample are highlighted by the blue box.

The amplitudes of the triplet of peaks produced by the doped sample were summed, and divided by the amplitude of the reference peak from the urea sample within the coil,

$$S_{Norm,Exvivo} = \frac{A_1 + A_2 + A_3}{A_{Ref}}$$

Equation 4.8

where $S_{Norm,Exvivo}$ is the phantom's normalised sensitivity. $S_{Norm,Exvivo}$ was then plotted against the distance from the coil and compared to the simulated sensitivity, $S_{Norm,Sim}$.

4.3.4.2 Simulations of Extended Cuboid

To compare simulations to experimental data the signal within a VOI of similar size needed to be evaluated at varying distances from the coil. For simplicity, the small

phantom used above was represented as an extended cuboid with dimensions 10 x 10 x 30 mm in simulations, Figure 4.9.

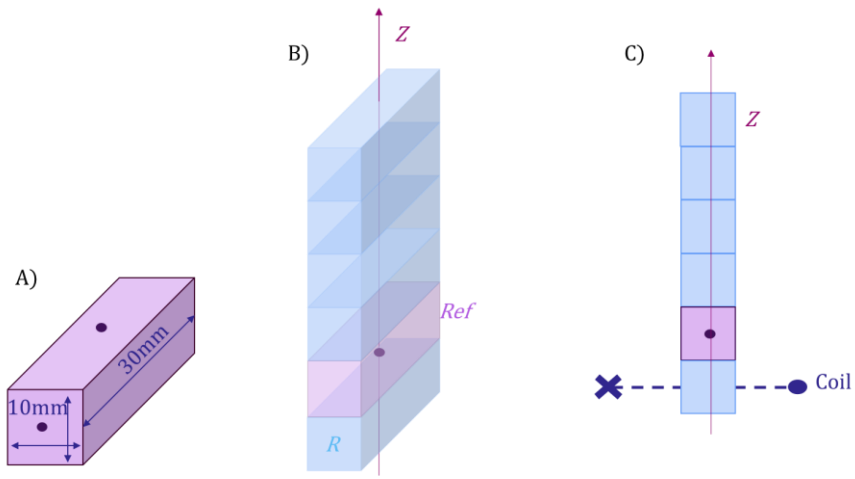

Figure 4.9 – A) Dimensions of ROI used in simulation. B) stack of 3D ROIs with respect to the point of nominal B_1 (dark circle), non-reference regions (R) are shown in blue. C) Location of the centre of the ROI's and point of nominal B_1 with respect to the coil.

The B_1 field at a point (Equation 4.5) was summed over the extended cuboid containing 275 pixels, representing the small phantom giving,

$$B_{1,ROI} = \sqrt{\left(\sum_{i=1}^{275} B_{x,i}\right)^2 + \left(\sum_{i=1}^{275} B_{y,i}\right)^2}$$

Equation 4.9

where *i* corresponds to a count across sub voxels within the VOI representing the small phantom. This region was moved stepwise along the axis of the coil, as shown in Figure 4.9. These values of B_1 were used to estimate the transverse magnetization for the block and HPHS pulse using the processes described above, and then the normalised signal was estimated to be compared to the measured values.

4.4 Optimising Readout Pulse for ^{31}P 1D ISIS Experiments

After validation, the simulation was extended for ^{31}P to determine the optimum pulse type needed for excitation in 1D ISIS Saturation Transfer (ST) experiments in participants with high BMIs. The results were confirmed using an *in vivo* experiment measuring SNR at varying distances to simulate a range of BMIs

4.4.1 Pulse Shapes Considered

The software and methods used for these simulations were identical to the previous section, adjusted to simulate the phosphorous coil's geometry and the RF readout pulses used in the 1D ISIS experiment on a wide-bore Philips Ingenia 3 Tesla MR scanner.

The phosphorous coil has a radius of 70 mm and is flexible with no fixed curvature, hence for simplicity in the simulations, no curvature was used. For the Block pulse, a 180^o pulse of width 0.485 ms was simulated so the point of maximum magnetisation would be in the centre of the B_1 profile. For the HPHS, a pulse width

of 5.42 ms with an RF limit of 59 µT was used. The bandwidth simulated was 4000 Hz (-2000 to 2000 Hz). Schematics of the pulses used can be seen in Figure 4.10.

Multinuclear MRS such as ^{31}P and ^{13}C use large spectral bandwidth with metabolites of interest often having a large range of chemical shifts. For these reasons, the off-resonance effects of excitation need to be considered. The RF pulse simulator (described in Section 4.3.2.2) was extended to evaluate the off-resonance effects across the spectral bandwidth and used to evaluate the excitation profiles for varying B_1 at the chemical shifts of Pi and γATP.

Initially, the HPHS used a frequency sweep from -1170 Hz to 0 Hz (the default on the scanner), but this showed a signal void within the spectral bandwidth, so the sweep was extended to a range of 1500, 2000, and 2500 Hz.

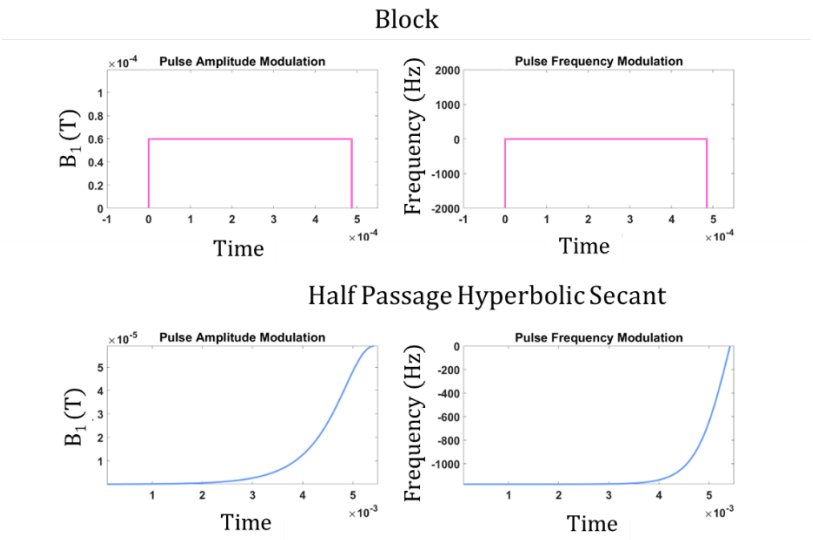

Figure 4.10 - Schematics of the (Top) Block and (Bottom) Half Passage Hyperbolic Secant pulses used in liver 1D ISIS simulations

4.4.2 Simulated 1D ISIS of the Liver

For both RF pulses, methods matched those previously described, and the coil geometry matched that of the phosphorous coil.

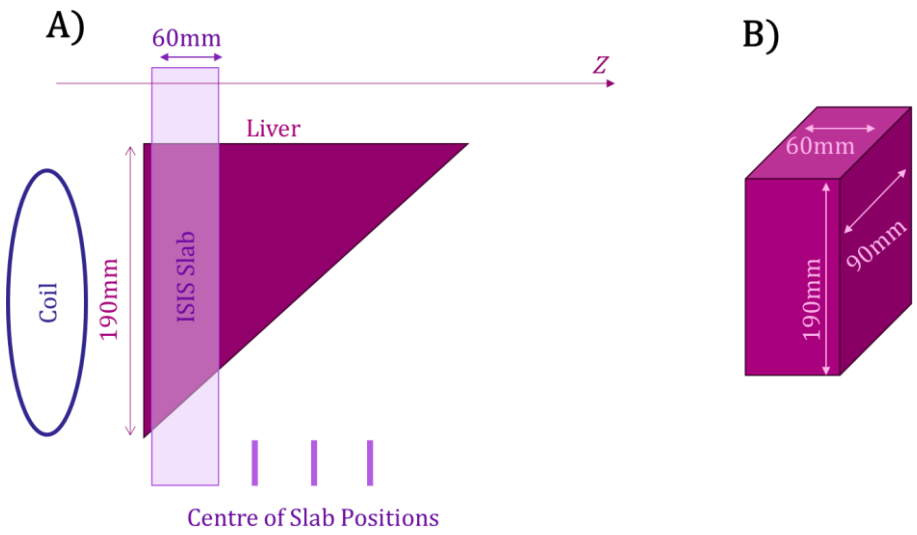

Figure 4.11 - Schematic of Liver ISIS slab simulation. (A) shows the relationship between the coil, ISIS slab and simulated liver. The centre of each ROI is shown along the bottom simulations Note the ROIs will overlap. (B) shows the dimensions of the simulated ROI.

The simulated VOI was a rectangular approximation of the intersection of a 1D ISIS slab (used in SPMIC ^{31}P experiments) with an average liver (VOI = 60 x 90 x 190 mm, Figure 4.11B) (103). The VOI was positioned at increasing distances from the coil, to match to distance from the coil to the liver for a range of BMIs (23 – 58 kgm^{-2}), approximated using Equation 4.1, and assuming 15 mm of skin and ribcage (104), Table 4.2.

Distance from coil to the centre of ROI (mm)	Approximate BMI (kgm^{-2})
30	23
57	33
81	42
120	58

Table 4.2 - Distance to the centre of ROI in ^{31}P 1D ISIS liver simulations and the corresponding BMI.

4.4.3 Investigating the Effect of Depth in *in vivo* ^{31}P MRS of the Liver

To investigate whether *in vivo* 1D ISIS data followed similar trends to simulated and *ex vivo* data. Two participants of different BMIs were scanned using the block and optimised HPHS pulses, with lard packs used to increase the distance from the coil to the liver.

4.4.3.1 Acquisition

All scans were performed on a wide-bore 3 Tesla Ingenia scanner (Philips Medical Systems, Best, the Netherlands) using a ^{31}P transmit–receive 140 mm diameter loop coil (Philips, Flex coil P-140). Two participants were scanned with BMIs of 24 and 28.7 kgm^{-2}.

At each distance, three scans were performed: a survey scan to determine the distance from the coil to the liver and two ^{31}P MRS acquisitions, including a block excitation pulse scan (FA = 180, TR = 8000 ms, NSA = 60), and an HPHS excitation

pulse scan (TR = 8000 ms, NSA = 60). All acquisitions had a bandwidth of 4000 Hz, with 2048 sample points. Acquisitions were localised, Slab thickness = 60 mm, and the FOV was positioned parallel to the coil and avoided muscle.

4.4.3.2 Analysis

To measure the distance to the edge of the liver, the slice containing the two positioning markers built into the ^{31}P coil was found, and the distance from the centre of these markers was measured perpendicularly to the edge of the liver using ImageJ (87), Figure 4.12. Each distance was measured three times on separate occasions to estimate reproducibility. The spacing between the coil markers and the edge of the coil was subtracted, and 30 mm was added (the distance from the edge of the liver to the centre of the ISIS slab) to all distances before plotting.

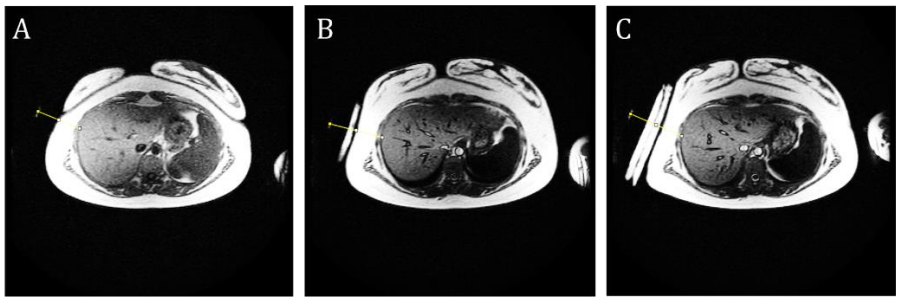

Figure 4.12 - The different images show the measured distance from the coil markers to the edge of the liver. A - shows no lard packs added. B - shows the distance with one lard pack and C - with two lard packs

The spectra were analysed using an in-house MATLAB script that averaged all NSA. The user then phase-corrected the spectra before selecting the centre of each peak, and a Gaussian was fitted to each peak.

The ratio of the inorganic phosphate (Pi) to γATP peak was calculated and used as a proxy for concentration to compare results from different pulse types and to understand any differences that appear in the Signal-to-Noise-Ratio (SNR) between participants. To compare SNR drop-off with distance, the SNR of the ratio of peaks (SNR_{Ratio}) was used in place of the SNR for either Pi or γATP. This is due to the area of individual peaks changing (due to ATP flux) whilst total area of the Pi and γATP remains relatively constant within a person. SNR_{Ratio} calculated using propagation of terms,

$$SNR_{Ratio} = 1 \Big/ \sqrt{\left(\frac{\Delta_{Pk2Pk}}{S_{Pi}}\right)^2 + \left(\frac{\Delta_{Pk2Pk}}{S_{\gamma ATP}}\right)^2}$$

Equation 4.10.

where Δ_{Pk2Pk} is the Peak-to-Peak noise in the spectra. S_{Pi} and $S_{\gamma ATP}$ are the areas under the Pi and γATP fitted peaks, respectively. SNR_{Ratio} was calculated at all distances for each participant for both pulse types and plotted against distance to evaluate change.

4.5 ^{31}P MRS in the Investigation of the effect of Interventions on Liver Function

This section describes the experimental methods used in two different intervention studies investigating changes to ATP flux in the liver: one on the effect of ingesting an Inulin Propionate Ester (IPE) on participants with normal BMIs and one on the impact of bariatric surgery of patients with Type-2-Diabetes (T2D) or pre-diabetes. In both studies, ^{31}P Saturation Transfer (ST) experiments were performed before and after an intervention, a comparison of the acquisition parameters can be seen in Table 4.3, the analysis techniques used were identical.

Intervention	Repetition Time (ms)	Averages	Excitation Pulse Angle (°)	Saturation Pulse Angle (°)	ISIS Slab Thickness (mm)
Inulin Propionate Ester	6100	200	90	100	30
Bariatric Surgery Intervention	8000	150	180	100	60

Table 4.3 – Comparison of acquisition parameters from inulin propionate ester and bariatric surgery intervention studies.

4.5.1 Inulin Propionate Ester

The procedures for this study were approved by the University of Nottingham's Medical School ethics committee. Written consent was obtained from the volunteers by the author of this thesis.

Eight Participants (Aged 24 – 38 years, no metabolic disorders) within the normal BMI range (BMI 20 – 25 kgm^{-2}) were recruited, and informed consent was obtained. On the day of the study, participants arrived having fasted from 10 pm the previous night and underwent two MRS ^{31}P ST experiments, one before (baseline) and one 180 minutes after consuming 10g of an Inulin Propionate Ester (IPE) dissolved in 100ml of water to allow time for transport to the colon (105) Figure 4.13. This study was titled the PROpionate METabobolism (PROMET) study.

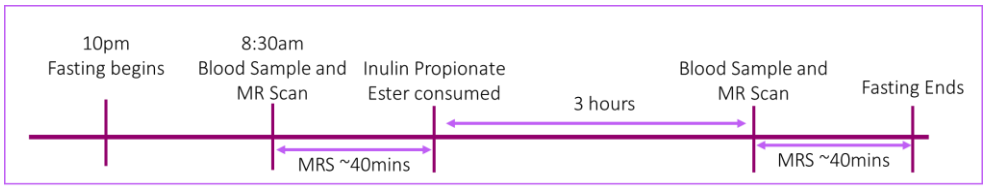

Figure 4.13 - PROMET Study Day Protocol

All scans were performed on a Philips Achieva 3 Tesla (Philips Medical Systems, Best, the Netherlands) using a ^{31}P transmit–receive 140 mm diameter loop coil (Philips, Flex coil P-140) placed over the bulk of the liver (confirmed by ^{1}H scout images). Spectra were obtained using 1D ISIS slice selective sequence (block excitation, pulse angle = 90^{0}, slab thickness = 30 mm). In two of the data sets HPHS excitation was used. Initially, a scout spectrum was acquired to determine the frequency of the

saturation pulses used in the ATP flux experiment. Subsequently, two spectra were acquired – one with saturation of the γATP peak (applied at ~ -1.5 ppm) and one with saturation targeted equidistant on the opposite side of the Pi peak (applied at ~ 13.5 ppm). Each ST experiment took approximately 20 minutes to acquire all spectra during free breathing (TR = 6100 ms, NSA = 200, saturation pulse angle = 100^0).

4.5.2 Bariatric Surgery Intervention

Two ^{31}P MRS visits occurred, one after participants completed the Very Low-Calorie Diet (VLCD) but before undergoing bariatric surgery and a second 6 weeks post-surgery, Figure 4.14. Where possible experiments occurred first thing in the morning, with participants arriving post-overnight fast. If participants could not attend morning scan sessions, measurements occurred after a minimum of an 8 hour fast, and within each participant, measurements occurred at the same time of day.

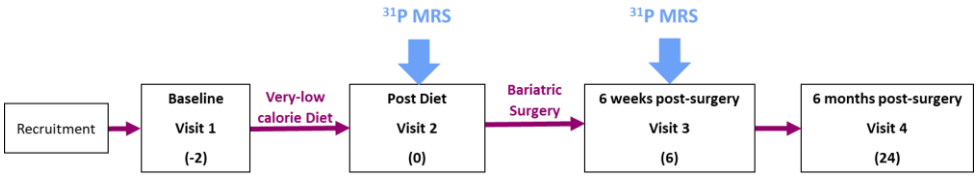

Figure 4.14 - Overview of study visits in bariatric surgery study, weeks around surgery shown in brackets. ^{31}P MRS was performed at visits 2 and 3 as shown by blue arrows.

All scans were performed on a Philips Wide Bore Ingenia 3 Tesla (Philips Medical Systems, Best, the Netherlands) using a ^{31}P transmit–receive 14-cm diameter loop coil (Philips, Flex coil P-140) placed over the bulk of the liver anteriorly as this was found to have the smallest distance to the liver when subjects were positioned supine. A short survey was performed to confirm the location of the coil with respect to the liver; if the coil was not positioned centrally, it was repositioned. Spectra were obtained using 1D ISIS slice selective sequence (excitation block pulse angle = 180^0, slab thickness = 60 mm) a larger pulse angle was used compared to the healthy volunteer study to account for the increased distance from the coil to the liver. Initially, a scout spectrum was acquired to determine the frequency of the saturation pulses to be used in the ST experiment. Subsequently, two spectra were acquired – A saturated spectra where saturation was applied to the γATP peak (approximately at -1.5 ppm) and the unsaturated spectra with saturation targeted equidistant on the opposite side of the Pi peak (approximately at 13.6 ppm). Each ST experiment took approximately 20 minutes to acquire all spectra during free breathing (TR = 8000 ms, number of averages = 150, saturation pulse angle = 100^0).

Distance measurements from the surface of the coil to the edge of the liver were made using ImageJ (87) using the same methods described in 4.4.3.2. Due to the large size of the participants in this cohort, it was not always possible to visualise the fiducials as they were too close to the bore of the MR scanner. In these instances, the coil location was identified through the indent made in the adipose tissue; a central slice was approximated, and the distance from the coil surface to

the liver was measured. Finally, the participants' BMI were used in Equation 4.1 to estimate the distance to the liver, and this was compared to the distance measured using ImageJ (87) .

4.5.3 Data Analysis

Analysis was performed using an in-house MATLAB (2023b, Mathworks) script. Spectra were phase-corrected and baseline fitted before Gaussian fits were applied to each metabolite. The quality of the saturation was estimated using

$$Saturation\ (\%) = \frac{M_0^{ATP} - M_S^{ATP}}{M_S^{ATP}} \cdot 100$$

Equation 4.11

displayed as a percentage. Pi concentrations were estimated by referencing the Pi to the γATP peak area from the unsaturated spectra and assuming literature ATP concentrations (2.5 mmol/l (Schmid et al., 2008))

$$Conc_{Pi}\ (mM) = \frac{M_{Pi}^0}{M_{ATP}^0} \times 2.5$$

Equation 4.12

the area of the unsaturated γATP peak is multiplied by three to estimate the total ATP. The αATP and βATP peaks are not used as they overlap with the Adenosine DiPhosphate peaks, which this can lead to overestimations of concentration. The exchange rate constant (k) was calculated using Equation 2.31 as described in Chapter 2, which was multiplied by Pi concentration to calculate forward flux (F_{ATP}). Values of k and F_{ATP} before and after interventions were plotted.

4.6 Results

4.6.1 Signal response to RF excitation pulse for the Carbon-13 coil

First, maps produced for each stage of the conversion from B_1 to signal maps will be examined. Then, simulated data will compare to experimental data.

4.6.1.1 Simulated Maps of B_1 and sensitivity

The B_1 profiles for the block and HPHS pulses are the same but scaled by different absolute B_1 values; the receive sensitivity maps (not shown) have the same shape but are both normalized to unity at the point of maximum signal (Figure 4.15 and 4.16). The magnetisation created by a block pulse drops off closer to the coil than for an HPHS pulse, which is mirrored in the received signal. For both the HPHS and block profiles the received signal drops off around 75 mm from the coil in z.

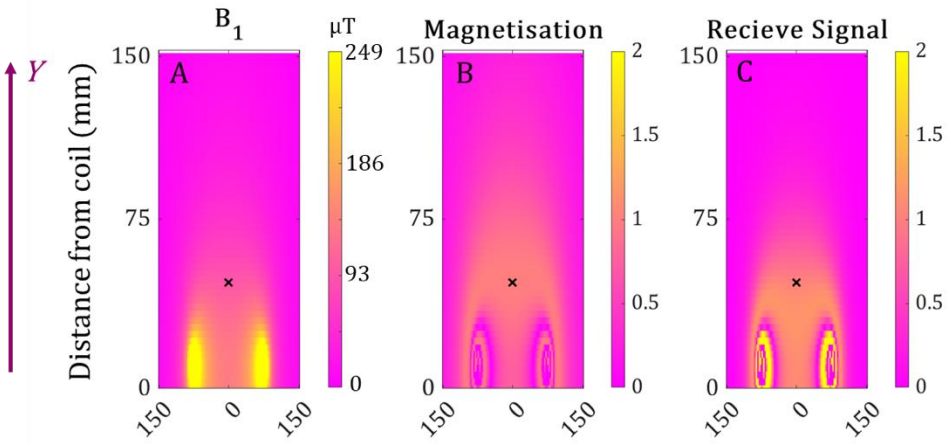

Figure 4.15 - Maps of Relative (A) B_1, (B) Magnetisation and (C) Receive Signal simulated around a 150 mm single loop coil when using a block excitation pulse.

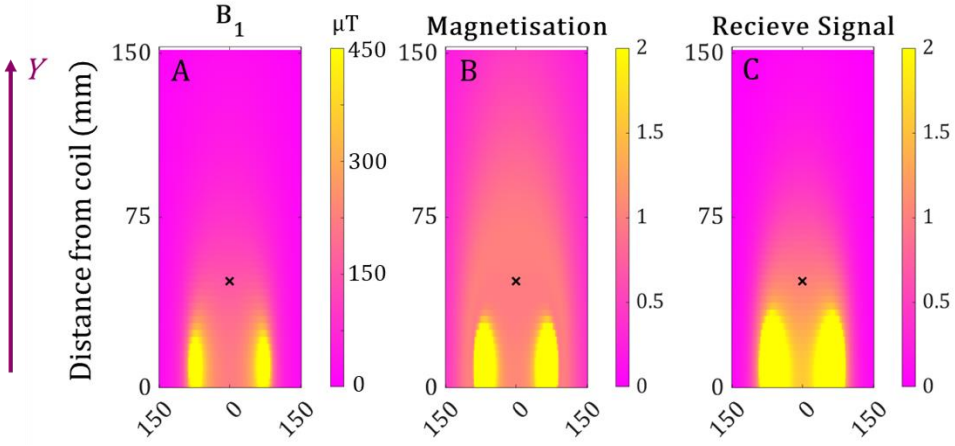

Figure 4.16 -Maps of Relative (A) B_1, (B) Magnetiaistion and (C) Receive Signal simulated around a 150 mm single loop coil when using a Half-Passage Hyperbolic Secant excitation pulse.

4.6.1.2 Comparison of Simulation and Phantom Data

The variation in simulated and measured signal with depth generally agreed well, with the differences lying within the scatter. Again, the measured data confirmed that the block pulses did not give rise to a signal close to the coil and that the signal from both pulses converged at around 50 mm from the coil.

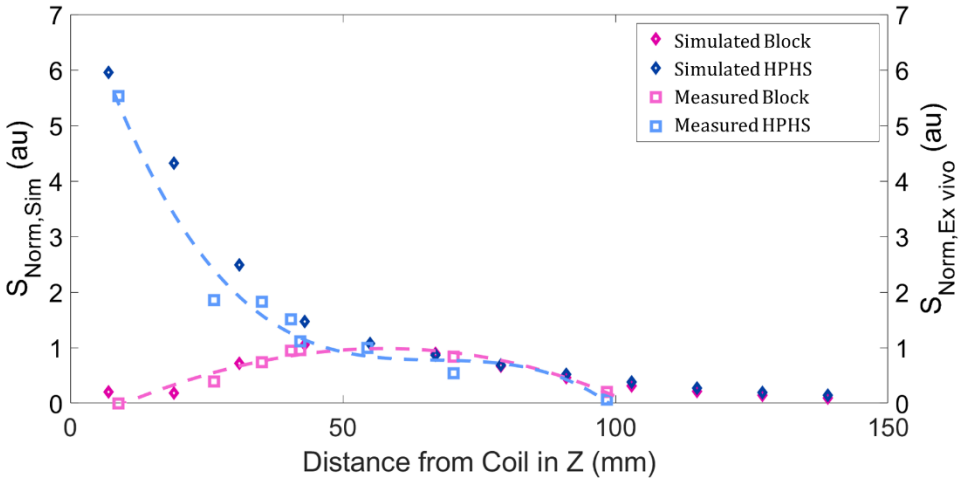

Figure 4.17 – Simulated Sensitivity ($S_{Norm,Sim}$ - diamonds) and Measured Signal ($S_{Norm,Ex\text{-}vivo}$ - squares) for block (pink) and hyperbolic secant (blue) RF pulses at increasing distances in z. The dotted lines show third-order polynomial fits for the measured data.

4.6.2 Signal response to RF excitation pulse for the ^{31}P coil

4.6.2.1 Comparison of Pulse Types

Figure 4.18 shows that the block pulse gave an even excitation profile across the range of B_1 simulated. As expected for central resonance frequencies, the spins were over-flipped close to the coil. At the resonance frequency for the Pi and γATP, the relative magnetisation increased to a maximum at B_1 = 50% (30uT) and began to fall as B_1 increased.

For the HPHS pulse, as expected, the relative magnetisation varied significantly with spectral frequencies. Relative magnetisation did not reach the maximum at the resonant frequency for Pi at any relative B_1 value, Figure 4.19.

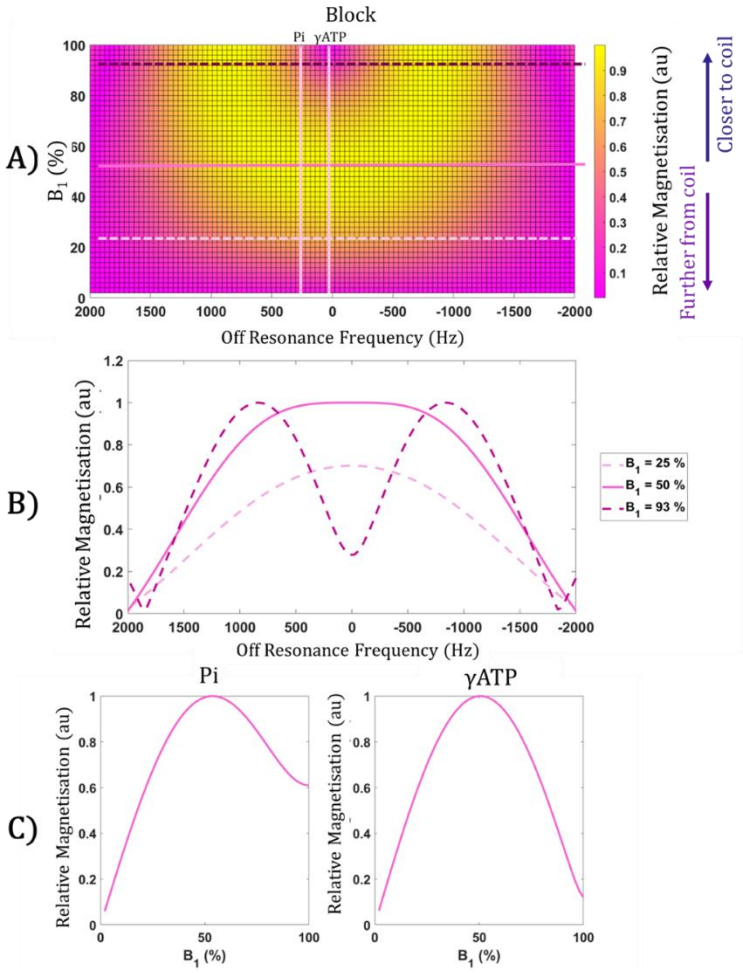

Figure 4.18 –Block Pulse - (A) map of variation in relative magnetisation with B_1 (as a percentage of the maximum B_1 = 60μT) and off-resonance frequency. The horizontal and vertical lines indicate the positions of profiles shown below, and in particular, the vertical lines indicate the resonant frequencies of inorganic phosphate (Pi) and γATP. (B) Profiles across the maps in A showing variation in magnetisation with frequency for B_1 = 25%, 50% and 93% (C) Profiles across the maps in A showing variation in magnetisation with B_1 for resonant frequencies of inorganic phosphate (Pi) and γATP.

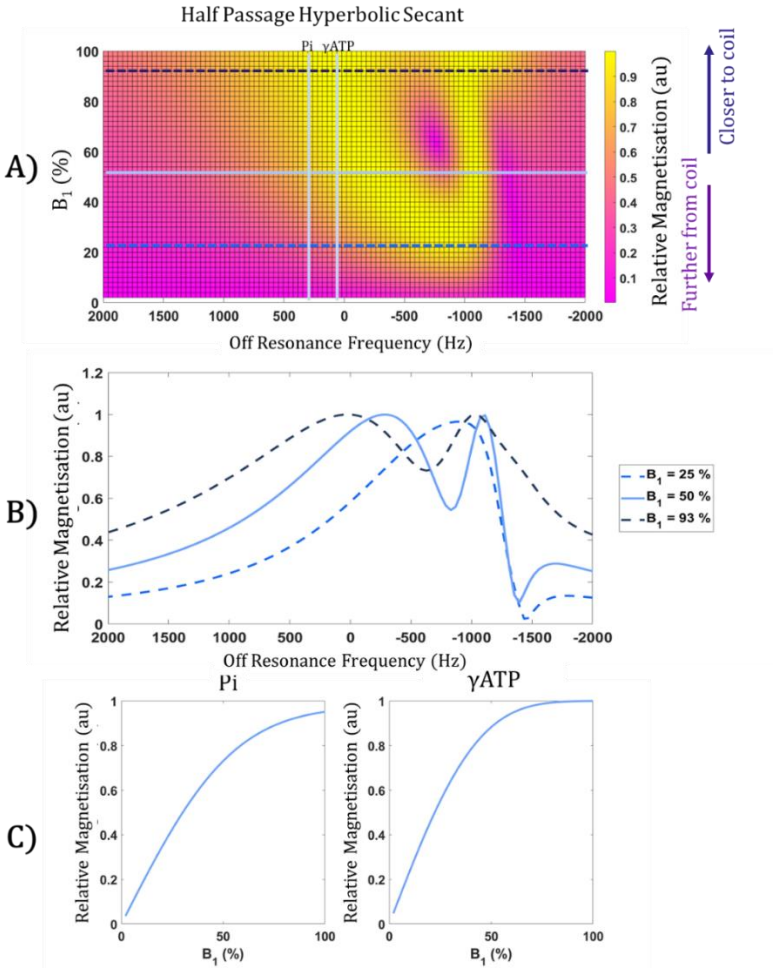

Figure 4.19 – Half-Passage Hyperbolic Secant Pulse - map of variation in relative magnetisation with B_1 (as a percentage of the maximum B_1 = 59μT) and off-resonance frequency. The horizontal and vertical lines indicate the positions of profiles shown below, and in particular, the vertical lines indicate the resonant frequencies of inorganic phosphate (Pi) and γATP. (B) Profiles across the maps in A showing variation in magnetisation with frequency for B_1 = 25%, 50% and 93% (C) Profiles across the maps in A showing variation in magnetisation with B_1 for resonant frequencies of inorganic phosphate (Pi) and γATP.

As the starting value for the frequency sweep increased, the signal void moved further off resonance, and the plots of relative magnetisation against off-resonance frequency became more even at all B_1 values (Figure 4.20). The maximum achieved relative magnetisation at the resonance frequency for Pi decreased as the range of the frequency sweep increased.

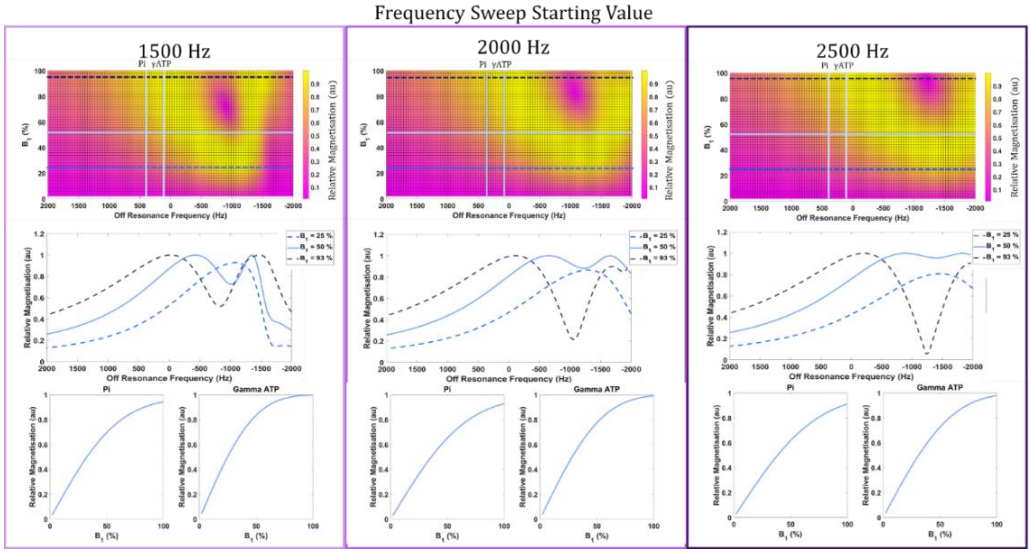

Figure 4.20 - Effect of changing the starting value of the frequency sweeps for a HPHS pulse. Top- map of magnetisation variation with B_1 and off-resonance frequency, Middle- line plots at three different B_1 values showing relative magnetisation changing with off-resonance frequency and Bottom – the change in relative magnetisation with B_1 at the frequency off the Pi and γATP Peak.

4.6.2.2 Simulations for VOIs corresponding to liver

Close to the coil, the HPHS pulse gave a much larger simulated signal than the block pulse, and as the distance from the coil increased, the simulated sensitivity for HPHS and block pulses became similar. Figure 4.21.

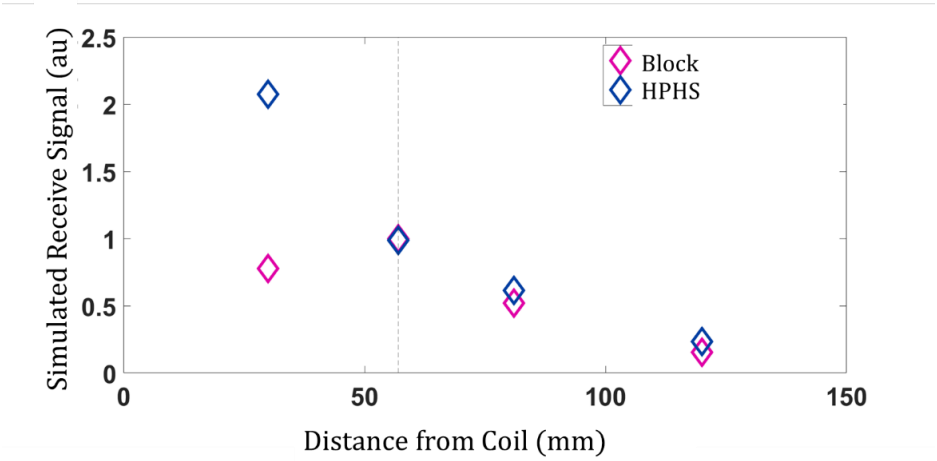

Figure 4.21 - Simulated receive signal relative to a reference region for a ROI matched to a liver slab used in 1D ISIS experiments. Blue and pink represent results for Half Passage Hyperbolic Secant and block simulations, respectively.

4.6.3 Experimentally Measured Variation in SNR with Distance *in vivo*

Spectra were all of good quality, and the fits were good upon visual inspection. The HPHS pulse introduced a dephasing of the βATP peak in the spectra, Figure 4.22.

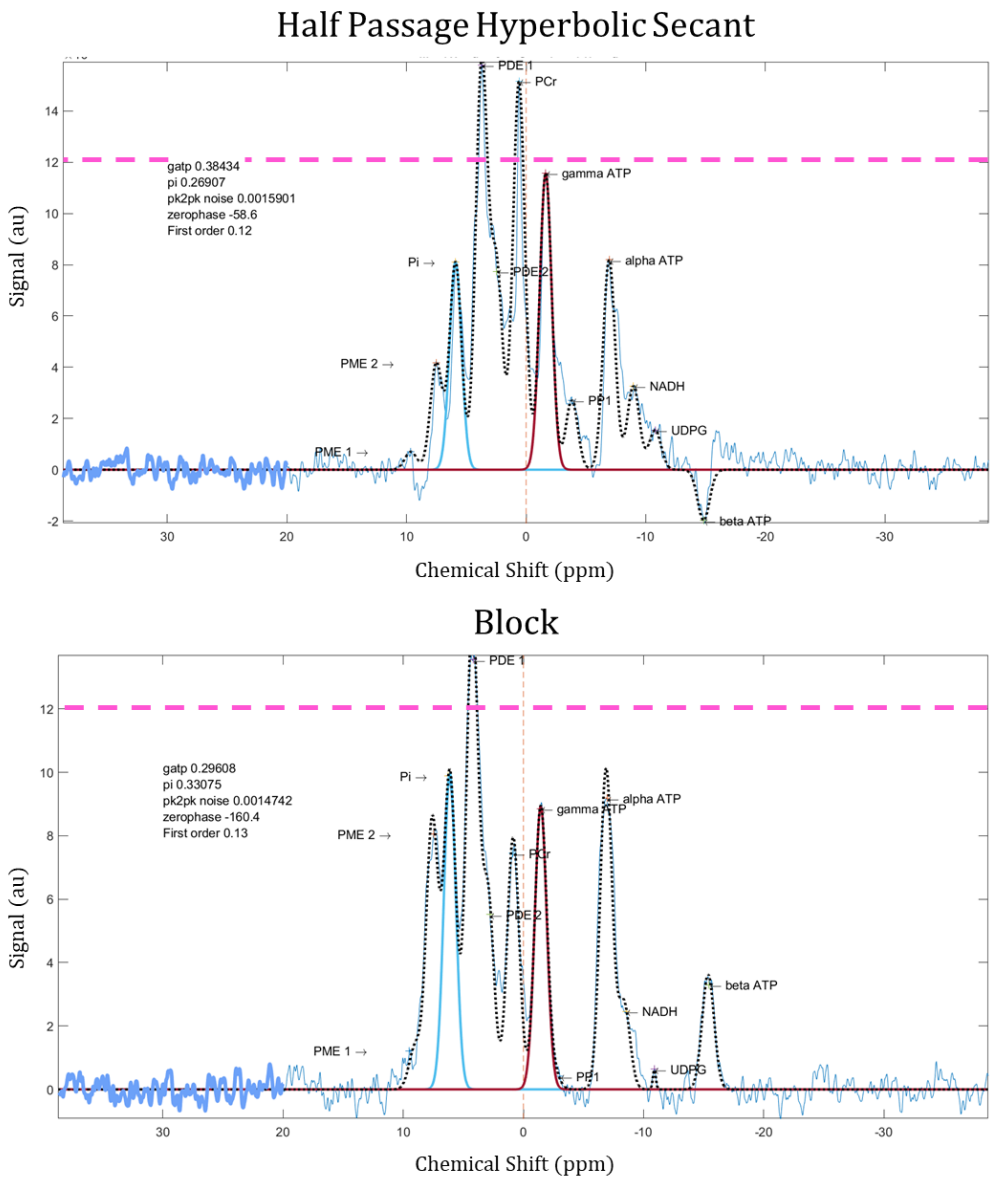

Figure 4.22 - Example fits for Top – Half Passage Hyperbolic Secant and Bottom - Block pulse acquisitions. The pink dashed line shows is drawn at the same height on both spectra to show the difference in scale of the received signal. In the bottom left of each plot, the bold blue region represents the section of noise used in SNR calculations.

The average ratio of peaks (Pi/γATP) measured using block pulse compared to the HPHS was higher, but with only two participants, no statistical significance can be determined, Figure 4.23. At all distances, the SNR_{Ratio} was higher for the HPHS than that for the block pulse. Close to the coil the difference in SNR_{Ratio} between the HPHS and block pulses is greater and the difference between the two pulses decreased as the distance to the coil increased.

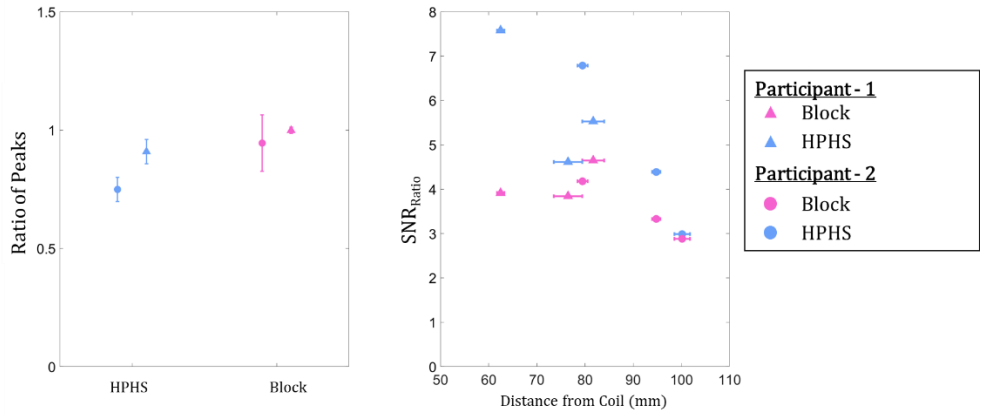

Figure 4.23 - Left – Mean and standard deviation of Pi ratio to γATP for HPHS and block excitation pulses for all distances. Right - The change in SNR_{Ratio} with distance for both excitation pulse types. For both, the slimmer participant (participant 1, BMI = 24 kgm^{-2}) is represented by triangles, and the larger (participant 2, BMI = 28.7 kgm^{-2}) is represented by circles. As with previous graphs, pink and blue represent data collected using HPHS and block excitation pulses, respectively.

4.6.4 Saturation Transfer Experiments

4.6.4.1 Inulin Propionate Ester

All participants completed the protocol and spectra had good SNR with well-resolved phosphate metabolite peaks Figure 4.24. During the ST experiment, the γATP peak was well saturated, the mean saturation percentage (reduction in γATP) was 386 ±130 %. No significant change was seen in group mean k and F_{ATP} pre- and post-IPE consumption, though individual changes varied in direction Figure 4.25. The mean and standard deviation values for Pi concentration, k and F_{ATP}, along with respective p values, can be seen in Table 4.4, no significant change ($p < 0.05$) was seen in any of the measures.

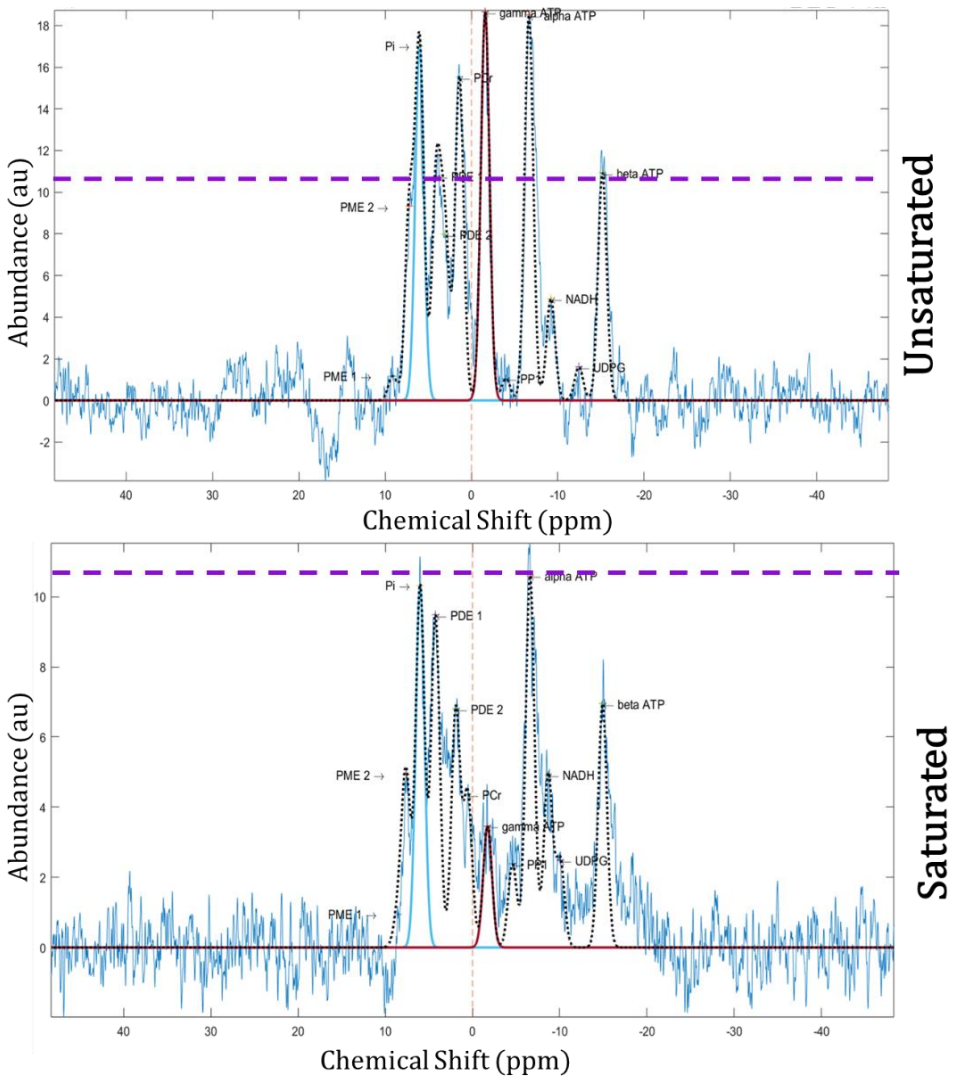

Figure 4.24 - Example of Fits for PROMET ^{31}P MRS. Top - unsaturated spectra and Bottom - Saturated Spectra. The dashed purple horizontal line is at the same abundance on both spectra to show difference in the peak heights.

Timepoint	Exchange Rate Constant, k (s^{-1})	Inorganic Phosphate Concentration (mM)	Forward Flux Rate (mMs^{-1})
Baseline	0.51 ±0.3	5.92 ±2	2.88 ±1.7
Post IPE Consumption	0.54 ±0.2	6.64 ±1	2.5 ±1.5
Significance (p-value)	0.79	0.45	0.22

Table 4.4 – Exchange rate constant, inorganic phosphate concentration and forward flux rate for the PROMET study. Measures are mean ±SD

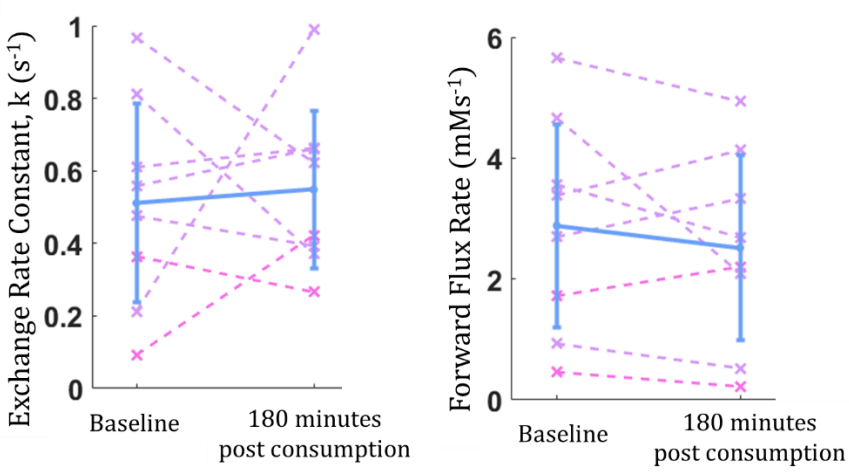

Figure 4.25 - Left - k and Right - F_{ATP} values at baseline and 180 minutes post IPE consumption. Purple and pink dashed lines represent individual participants' results from block and HPHS acquisitions, respectively. Group average and SD shown in blue

4.6.4.2 Bariatric Surgery

Of the six recruited to this study, one dataset was incomplete due to a scanner failure; all other participants had data acquired pre- and post-surgery. Spectra were all of acceptable SNR for analysis. Of the ten datasets analysed, one had equal saturation to HV (successful saturation), and for two participants, the saturation failed. Excluding the successful saturation, the average saturation percentage was 24 ±36 %. Examples of fits for each saturation instance (successful, average and failed) can be seen in Figure 4.26. The saturation quality significantly decreased with distance to the liver ($R = 0.63$, $p = 0.05$), Figure 4.27.

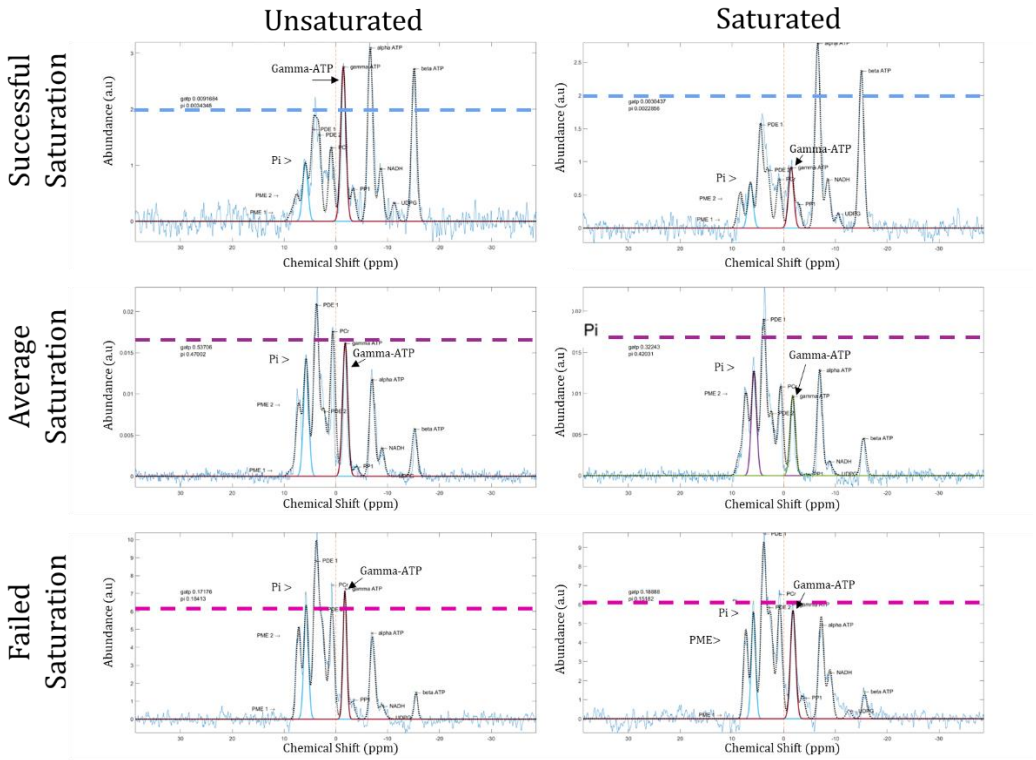

Figure 4.26 - Spectra and fits from the bariatric surgery study. Top - successful saturation of γATP peak, Middle - an example of the average saturation seen in this cohort, Bottom - a failed saturation. Areas under the peak for Pi and γATP are displayed on each graph. Dashed lines are at the same height across a row to assist in understanding the drop in signal.

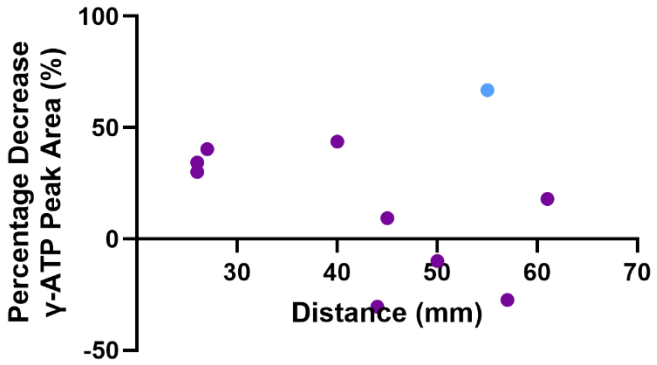

Figure 4.27 - Saturation percentage with distance. The blue point represents the dataset with successful saturation.

Pi concentrations increased by 21 ±13 % after surgery. Group mean Pi concentrations were 2.4 ±0.7 mM and 3.0 ±1 mM pre- and post-surgery, respectively. In a one-tailed t-test, a significant increase was seen in the Pi concentration from pre-surgery to post-surgery (p = 0.03), Figure 4.28.

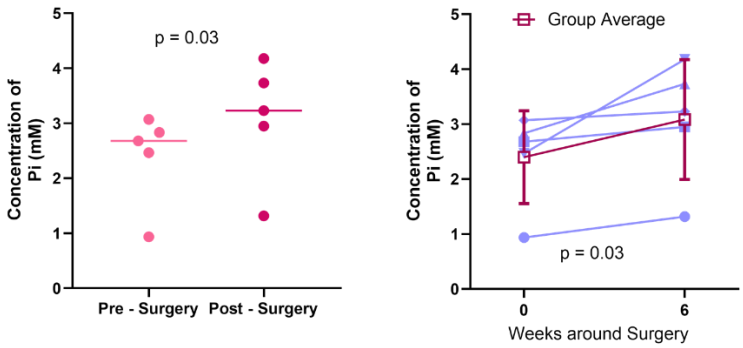

Figure 4.28 - The concentration of Pi measured pre- and post-surgery. Left- Group means are shown as horizontal lines, and the p-value is displayed above the graph. Right-paired results are shown using connecting lines, group mean, and standard deviation also displayed.

Distance estimated from Equation 4.1 correlated well with measured distance (R = 0.84, p = 0.002), a bias were distance estimated using Equation 4.1 overestimated compared to measured distance.

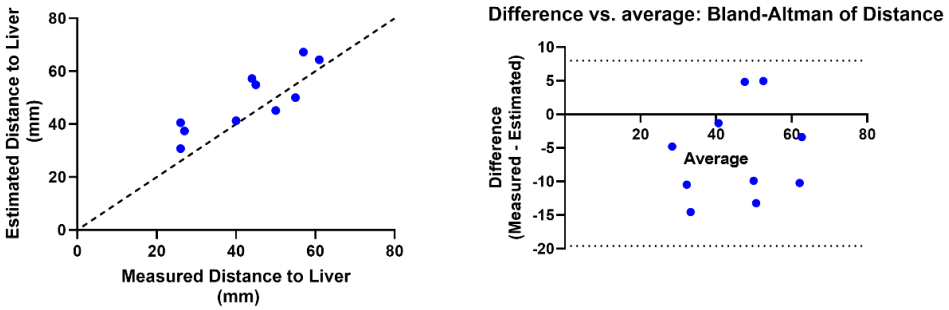

Figure 4.29 – Comparison of distance to liver estimated using Equation 4.1 and measured. Left – Plot of estimated Vs. measured distance, line of identity shown. Right- Bland-Altman showing the overestimation of the estimated distance to the liver compared to measured distance.

4.7 Discussion

The use of surface coils for multinuclear liver MRS studies is complex due to the interactions between the transmit and receive profiles and varying depths of the liver from the coil.

This chapter used simulations and experimental data to investigate the effects of different RF pulses and the B_1 drop-off on multinuclear MRS acquisitions. Initial investigations used simulations of unlocalised ^{13}C experiments and compared the results to data acquired on a small phantom. Simulations were then performed to mimic ^{31}P 1D ISIS acquisitions, and these were compared to data acquired *in vivo* on two participants. The results of these experiments were used to optimise excitation for Saturation Transfer (ST) acquisitions for two intervention studies, one performed on Healthy Volunteers (HV) with normal BMIs (BMI < 25 kgm^{-2}) and one on bariatric surgery patients with obese BMIs (BMI ≥ 35 kgm^{-2}).

4.7.1 Localised and Non-Localised Multinuclear Spectroscopy

The increased signal close to the coil from an HPHS may cause issues in non-localised acquisitions. For example, although the amount of glycogen stored in the muscle is much lower than in the liver, high receive sensitivity close to the coil may make any muscle glycogen contribute a large proportion of total signal in the spectrum. The over excitation is shown in Figure 4.8, where an extra gaussian fit was needed to account for a broad peak on the baseline of the spectra. This

additional peak is possibly from the HPHS pulse exciting the carbon in the plastic of the coil. However, the excitation produced by a block pulse can lead to over-flipping of the spins and, hence, low transverse magnetisation being created close to the coil, as seen in Figure 4.15. This could be advantageous for non-localised acquisitions such as those used in ^{13}C measurements of the liver to prevent contamination of signals from the skin, SAT and muscle in the spectra.

HPHS pulses produced a high signal close to the coil, but this dropped rapidly with distance. However, the net signal produced by the block pulses was reasonably constant over the range of depths required for liver spectroscopy in both normal (18 – 25 kgm^{-2}) and high BMI (> 35 kgm^{-2}) subjects. Therefore, in particular, if the distance from the coil to the tissue of interest is likely to vary during a subject's participation or across subjects (due to a large range of BMIs), a block pulse will provide a more consistent SNR. Also, using a block pulse allows for more direct control over the point of maximum excitation by changing the FA, as described in the following Section.

4.7.1.1 Optimised Flip Angle Block Pulse

It is possible to optimize the FA for the block RF pulse based on the distance to the VOI and the simulated signal profiles. As an example, in the bariatric study described above in Section 4.5.2, the FA was optimised to give a maximum signal of 80 mm from the coil's surface, based on the average BMI of bariatric surgery patients and Equation 4.1. However, steps could be performed to optimise the FA

per participant, based on the distance from the coil to the edge of the liver measured from MRI at the start of a given study visit, and adjusting the scaling of the B_1 map to determine the value that gives maximum signal at the required depth.

Equation 4.1 provides a useful tool for estimating subcutaneous fat thickness from BMI in participants prior to study visits, which could be useful in improving the workflow if optimisation is to be performed. However, in this work, it was found that Equation 4.1 overestimated the distance to the liver Figure 4.29. This is probably due to the participant demographic used to develop Equation 4.1 having a low BMI on average (mean 24 ± 7 kgm^{-2}) or because this study's measurements of SAT thickness were taken at the liver and not the belly button. Hence, measurements taken from survey scans should be used in FA optimisation steps.

4.7.1.2 Half-Passage Hyperbolic Secant Pulses

When using the default settings from the MR scanner, the HPHS was found to have a signal void near the centre of the B_1 profile; this could reduce the measured signal from any metabolite in the affected frequency range (-1000 to -500 Hz). Upon investigation, this depended on the frequency sweep. As the range of the frequency sweep was increased from 1170 Hz to 2500 Hz the signal void shifted further down the negative frequencies Figure 4.20. This process created a more consistent profile of relative magnetisation across the spectral bandwidth. However, the maximum achieved relative magnetisation at the resonance frequencies for the Pi and γATP

peaks was reduced, Figure 4.20. Hence, it was noted that an HPHS was unlikely to be optimal for acquisitions for these experiments.

4.7.2 Comparison of Simulations and Experimental Data

The shape of the plots for HPHS and block pulses were similar across the ^{13}C and ^{31}P simulations. In both simulations, at larger distances from the coil (> 50 mm), the simulated received sensitivity was similar for block and HPHS pulses (Figure 4.17 and Figure 4.21). At smaller distances, the simulated received sensitivity for the HPHS pulse was much larger than the block pulses due to the block pules overexciting the spins closer to the coil (Figure 4.17). For the ^{13}C experiments, the simulated received sensitivity followed the experimentally measured signal. However, it is worth noting that since the simulations assumed the maximum signal at the 90° degree point, without taking account of receive sensitivity, the B_1 scaling was adjusted to ensure that the maximum signal was achieved at the same points experimentally and in simulation.

In vivo measurements of SNR with distance performed using 1D ISIS showed similar trends to the simulations and ^{13}C phantom measurements. The measured SNR at smaller distances (closer to the coil) was much higher for HPHS pules compared to block pulses, but at larger distances (> 80 mm from the coil), the SNR was similar between HPHS and block pulses Figure 4.23. It is difficult to draw any conclusions about the difference in the ratio of peaks measured using block and HPHS pulses when the sample size is so small, but differences may be expected due to the to the

off-resonance effects (at the frequencies of the Pi and γATP) displayed in the heat maps of Figure 4.19 and Figure 4.18.

In this work, the Pi concentration is calculated using Pi and γATP ratios and literature values of concentration. Future work should investigate the use of an external reference sample for ^{31}P for evaluating absolute concentration, as was done for the ^{13}C.

One assumption made during this process was that loading on the B_1 profiles had minimal effects. This is a reasonable assumption in the case of multinuclear MRS, where a simple coil geometry is used, and tissue is present under the full sensitive region of the coil. However, the previous chapter (Chapter 3) demonstrated the effect of BMI on the B_1 profile, probably due to loading effects and interactions between tissues and the field. Future work should investigate the implication this has on simulated models.

4.7.3 Intervention Studies

4.7.3.1 Inulin Propionate Ester

This was a pilot study to investigate the effect of IPE ingestion on F_{ATP}. All peaks were well resolved and easily fitted. ST experiments were successful with γATP peaks well saturated (saturation percentage 386% ±130 %), allowing for calculations of k and F_{ATP}. No significant change was seen in group mean k and F_{ATP} values post-IPE consumption compared to baseline. Individuals showed varying directions of

change, k increased for 4 and decreased for 4 participants, and F_{ATP} increased for 3 and decreased for 5 participants post-IPE consumption Figure 4.25.

Two of the ST experiments used HPHS pulses as the participants were recruited, and experiments were performed prior to the above data being complete; future participants' data were acquired using block RF excitation pulses. Concentration, k and F_{ATP} values from the HPHS data were similar to those from block pulse Figure 4.25. Concentration values seen in this study were approximately three times higher than literature for HV (this study baseline = 5.92 ±2 mM, literature = 1.38 ± 0.38 mM (93)), k values were slightly higher than literature (this study baseline = 0.51 s^{-1}, literature ~ 0.31 s^{-1}) and F_{ATP} values were approximately six and a half times higher than literature (this study baseline = 2.88 mMs^{-1}, literature ~ 0.45) (17,18,82). The discrepancy between F_{ATP} from this study and literature is clearly a product of the increased concentration and k values measured.

Although there was no significant change in group F_{ATP}, individual participant changes varied in direction. This may be due to physiological variations between individuals, the small sample size or the experimental design. For instance, physiological differences may have led to participants metabolising the IPE at different rates. The blood data has yet to be analysed, but when it is, it might resolve this issue when the MRS results are compared to the blood measures at each time point, as information can be gained on whether participants had metabolised the IPE. It is also possible that the methodologies used in this study led

to the null result as participants arrived, fasted, and then continued to fast for a further 180 minutes. Little is known about the effect of a prolonged fast on F_{ATP}, and it is possible that F_{ATP} being maintained across this extended fast is due to the consumption of IPE. A better design to investigate the effect of IPE consumption may be to have a randomised multiday trial. Where participants arrive fasted, water only on one day and consume IPE on another, with a week washout in between. This would control the fast duration as a factor affecting F_{ATP}. It would also be possible to do multiple MRI scans around the 180 minute time point to ensure that gastric transit time is less of a factor in the results.

4.7.3.2 Bariatric Surgery

The single dataset with successful saturation was acquired early in the study prior to a scanner upgrade. Unfortunately, the upgrade then changed the scanner behaviour so that incomplete or failed saturation was seen in the remaining datasets. Removing the pre-upgrade data point from the analysis revealed a strong trend between the distance from the coil and the degree of saturation achieved Figure 4.27. The work of this chapter has focused on the importance of optimising the excitation pulse for surface coil experiments, but this result highlights the need to optimise the ST pulse too.

It was important to note that a PCr (phosphocreatine) peak is seen in the spectra, which is a metabolite not present in the liver. The presence of this peak in the spectra suggests that localisation failed as PCr is expected in muscle. It is likely to be

due to the operator moving the slab too close to the coil, as this leads to better shimming. This needs further investigation to determine the balance of this tradeoff. However, an alternative approach would be to use surface shim coils.

Percentage changes in Pi concentration were similar to the difference seen between a T2D and age-weight matched cohort from Szendroedi *et al.* (80) (this study = 21 ±13 %, Szendroedi *et al.* = 28 %). Concentrations of Pi were around double literature values (this study = 2.4 ±0.7 mM and 3.0 ±01 mM pre- and post-surgery, respectively, literature ~ 0.96 mM and ~1.4 mM for T2D and HV, respectively (80,93)). These results further the hypothesis from Szendroedi *et al.* (80), Kupriyanova *et al.* (81) and Schmid *et al.* (82) that phosphorous metabolites are linked to insulin sensitivity. Unfortunately, no blood measures were taken for this group, so this hypothesis cannot be tested in this data. A significant increase in Pi concentration was seen pre-surgery to post-surgery, from a one-tailed t-test, p = 0.03. This implies that changes to F_{ATP} may occur due to bariatric surgery, likely linked to the diabetes remission seen in bariatric surgery patients (Chapter 3). Despite the issues with ST, this study shows the feasibility of performing ST experiments on a large cohort using a single-loop surface coil if the correct optimisation is performed.

Inorganic phosphate concentrations measured in both studies described above were two to three times higher than previously measured in literature. There are likely to be multiple factors that have led to this discrepancy. A source of error may

be the fitting of the spectra. All fitting was performed using in-house MATLAB code which fitted all peaks, future work may look at optimising the prior knowledge to improve the fits of overlapping peaks, this problem can be exacerbated by motion (such as respiration, Chapter 5) and poor shimming (discussed above). From Figure 4.24 it can be seen that when the saturation pulse was applied to the γ-ATP peak the signal for the majority of the spectra is reduced, this issue is not as prevalent in Figure 4.26 due to optimisation of the bandwidth of the saturation pulse in the more recent bariatric surgery intervention study.

4.8 Conclusions

Simulators are useful tools for understanding the B_1 effects of a surface coil. In combination with an RF simulator, they are powerful tools for creating an optimised sequence. Great agreement was seen between the simulated data and experimental data from a small test phantom. Throughout the experiments, a block excitation pulse was shown to be better than an HPHS excitation pulse, due to its more consistent excitation profile and the ability to optimise the 90° point for different distances. Large deviations are seen between the literature and the data from the intervention studies in this chapter. The bariatric study further displayed the link between insulin sensitivity and ^{31}P metabolites, and the feasibility of a ^{31}P saturation transfer study in a morbidly obese cohort was shown. Future work should explore using a saturation pulse with a narrower bandwidth, explore changing the power of the saturation pulse to improve effectiveness in an obese

cohort. Work should be done to improve the fitting of the peaks within the spectra to reduce errors from overlapping peaks.

5 Influence of Free-breathing Respiration Effects on Magnetic Resonance Spectroscopy

5.1 Overview

With metabolic disorders such as Type-II-Diabetes (T2D) on the rise globally, non-invasive tools for understanding the body's metabolism, such as multinuclear Magnetic Resonance Spectroscopy (MRS), are vital for research. Many multinuclear MRS experiments require a high Number of Signal Averages (NSA) that are acquired during free breathing rather than respiratory triggered to reduce scan times. It has been suggested by previous literature that respiratory motion could lead to line-broadening effects due to the movement of tissue through B_0 field. In this chapter, ^{1}H MRS is used as an analogue of multinuclear MRS to assess the effects of respiration on spectra and corroborate the results with B_0 field effects using imaging methods.

This work was presented as a digital poster at the International Society of Magnetic Resonance in Medicine, London (2022) and Toronto (2023) as 'Investigating the effects of free-breathing on in vivo MRS in the liver at 3T' and 'Characterising the effect of free-breathing on abdominal MR Spectroscopy and impact on x-nuclei spectra' respectively.

5.2 Introduction

As a participant breathes freely, the respiratory cycle introduces motion and B_0 field shifts in the MR acquisitions, particularly for measurements collected in the abdomen. Across different points in the respiratory cycle, the volume of air in the lung changes and this can lead to susceptibility changes in surrounding tissues, altering B_0 homogeneity and causing the dephasing of signals. Abdominal MR measures are often collected using respiratory triggering or with breath-hold acquisitions to prevent movement which can appear as ghosting in images or signal contamination from tissue outside the Volume of Interest (VOI) in Magnetic Resonance Spectroscopy (MRS) data.

Multinuclear MRS of the liver using ^{13}C or ^{31}P measures are increasingly being used to understand the body's metabolic process and characterise diseases such as Diabetes (106–111). However, in multinuclear MRS, multiple averages are needed due to the low natural abundance of nuclei (see Chapter 2, Table 2.1), so spectra are typically acquired during free breathing. Although articles have discussed the issues that arise from free-breathing acquisitions, for example, Schmid et al. (2008) (7), there are no publications which quantify the impact of free-breathing on liver spectra.

This chapter describes the effect of respiratory motion on MRS measures by collecting ^{1}H MRS and B_0 field measures over the respiratory cycle. The results from ^{1}H liver MRS are then related to multinuclear liver MRS measures.

5.2.1 Measuring Respiratory Motion

During inspiration, the chest wall moves 'up and out', and the diaphragm moves down, causing the lungs to expand and the liver and other abdominal organs to move down. On expiration, the chest wall relaxes, and the diaphragm moves up, causing the lungs to shrink and the liver and abdominal organs to move up. The liver moves approximately 20 mm with each respiratory cycle, with healthy adults typically taking a breath 12 - 20 times per minute (112).

Two methods are mainly used to assess respiratory motion in MR experiments: an intrinsic navigator signal or using additional hardware such as a respiratory bellows. The respiratory bellows uses a small air-filled pillow which is strapped to the participant, often using a Velcro belt. The pressure in the bellows changes during the respiratory cycle as it is compressed between the body and a belt. A navigator signal measures the displacement of the diaphragm from the signal in an MR image, as shown in Figure 5.1. Both methods have benefits and pitfalls. The respiratory bellows can only sense changes, not an exact position, and this method can be sensitive to where the bellows is placed. For example, if it is placed on the chest wall and not over the diaphragm, it will detect less motion and, hence, be less effective. However, the respiratory bellows can obtain a continuous signal without interrupting the MR acquisition and can be used when the diaphragm is not in the imaging Field Of View (FOV).

A navigator requires an acquisition window to be performed within the imaging sequence, which will marginally extend acquisition times, to detect the position of

the tissue and, hence, trigger the acquisition to the same spatial position of the organs even with incomplete breaths. In the example respiratory trace shown in Figure 5.1, the pink arrows show breaths that are at a lower amplitude than others. In these instances, the bellows will still trigger an acquisition upon expiration despite the liver being in a different physical position.

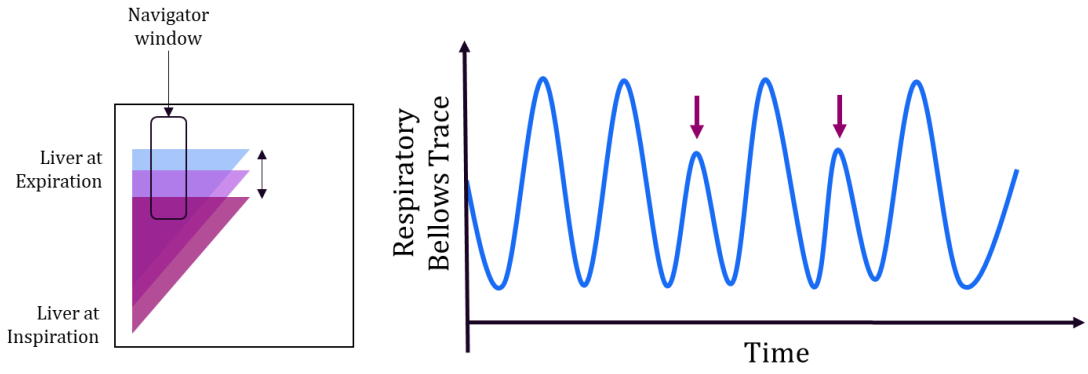

Figure 5.1 - Left - Example of navigator window positioning: blue shows the position of the liver at expiration (bottom of bellows trace), pink shows maximum inspiration (top of bellows trace) and purple shows the liver position for incomplete breaths. Right - example of respiratory bellows trace, pink arrows show incomplete breaths.

5.2.2 Correcting Respiratory Motion Effects in MRS

In Magnetic Resonance Imaging (MRI) motion results in distinct ghosting artefacts, hence motion correction has been widely researched since the 1980s (113–116). In MRS, the effects of motion are not as obvious. Nevertheless, contamination of signal from neighbouring tissues will occur if the MRS voxel is placed close to an organ boundary (partial voluming), which can lead to results differing between acquisitions dependent on the point at which they are acquired within the

respiratory cycle. This effect can be somewhat alleviated by increasing the Number of Signal Averages (NSA), as contamination is likely to occur inconsistently across repeats, hence contamination effects are minimised with high NSA (117).

Beyond motion causing differing partial voluming effects, the effect of the variation in the B_0 field in the tissue of interest across the respiratory cycle on the spectra must also be considered. Studies have looked at reducing the effects of motion in liver MRS either during the data acquisition or in post-processing. Bolan *et al*. (118) measured the frequency shift across the respiratory cycle in the breast ^{1}H MRS and MRI at 4 Tesla. They showed spectral frequency shifts of 23 ±5 Hz and a 10 - 20 Hz shift measured from B_0 maps at the centre of the breast tissue between inspiration and expiration, with larger shifts measured nearer the lung at the chest wall. On a subset of their data, they performed MRS analysis with and without frequency correction and showed that in 25% of the uncorrected data, the metabolite of interest was undetectable. Concentration values measured from corrected and uncorrected data were similar, but errors were smaller in frequency-corrected data (118).

Noworolski *et al.* (119) used post-processing to correct the effect of respiratory motion in liver MRS. The study acquired 128 Water-Suppressed (WS) and 8-Non-Water-Suppressed (NWS) single-voxel spectra (TR = 2500) on 132 subjects, split into three groups of HV, participants with Non-Alcoholic Fatty Liver Disease (NAFLD) and those who were HIV-positive. Two approaches were used to correct the effects of respiratory motion. In Approach-1, spectra were individually phase-corrected before

being frequency-shifted using the (residual) water peak. Approach 2 used individual phase correction and outlier removal, with spectra with water peaks that were more than 50% different from the median being eliminated before individual phase correction and further analysis. Spectra were averaged in both approaches, and total fat/water ratios were calculated using WS fat and NWS water estimates. They found that SNR increased on average 11-fold using individual phase correction. By removing the outlier spectra, the normalised fat/water ratios differed by more than 5% in 11% of subjects, with no significant differences in the change between groups (119).

Hock *et al.* (120) attempted to use a navigator window for respiratory gating in ^{1}H MRS at 3 Tesla. Three sequences were run: one with no navigator (no-nav, scan duration ~5 minutes), one with a navigator used after shimming and water suppression to trigger acquisitions (partial-nav, scan duration ~7 minutes), and one using a navigator to trigger the preparation steps and during data acquisition (full-nav, scan duration ~8 minutes). For experiments using the navigator, a 5 mm gating window was used with the navigator placed at the top of the liver on the edge of the diaphragm; the navigator sequence was repeated approximately 10 times per second to evaluate whether the liver was within the gating window. Results showed a significant reduction in the Full Width Half Maximum (FWHM) of the unsuppressed water peak from no-nav to partial-nav, no-nav to full-nav and from partial-nav to full-nav ($p = 0.016$, $p = 0.018$ and $p = 0.047$, respectively). The Signal to Noise Ratio (SNR) of the water and lipids peak(s) was 14 ± 8 (no-nav), 19 ± 9

(partial-nav) and 20 ± 8 (full-nav), with a significant difference from no-nav to full-nav ($p = 0.018$) (120). A 60% increase in the scan time for the full-nav compared to no-nav sequence achieved a 42% increase in SNR; if this extra scan time had instead been used to collect more averages, this would have only provided a ~26% increase in SNR (using $SNR_{increase} \approx \sqrt{NSA_2/NSA_1}$, where NSA_1 and NSA_2 are the Number of Signal Averages used in the two experiments), hence using the navigator is superior to increasing the NSA. However, this estimation of gain in SNR only applies to normally distributed noise and increasing the NSA will likely worsen line-broadening.

5.2.3 Multinuclear MRS

Multinuclear MRS has limitations of lower SNR, which stems from the inherent properties of the nuclei. For example, Phosphorous-31 (^{31}P) or Carbon-13 (^{13}C) both have lower relative sensitivity compared to ^{1}H (0.066 and 0.016 respectively, Table 2.1 in Chapter 2), and whilst ^{31}P has a similar natural abundance to ^{1}H, ^{13}C has a natural abundance of 1.108%, and both have a lower biological abundance than ^{1}H, making it very difficult to achieve sufficient SNR from a single acquisition for either of these nuclei. Therefore, in multinuclear MRS experiments, large NSA are typically performed, with ^{13}C liver glycogen measurements requiring NSA in the range of 896 – 12,800 (19,121–123) and ^{31}P liver ATP measurements requiring NSA of ~200 (124,125). Furthermore, ^{31}P has a long T_1, and hence, scans require long repetition times (TR), further increasing the scan duration. The respiratory triggering methods used in ^{1}H MRS would, therefore, not be feasible for these nuclei, as they would

result in acquisitions of over 1 hour, or it would take nearly 100 breath-holds to acquire a ^{31}P dataset. Therefore, multinuclear MRS experiments are often performed free-breathing. The effect of respiratory motion on ^{1}H MRS was discussed above, but the effect of this on multinuclear MRS has not been quantified.

To adequately assess the effect of respiratory motion on MRS, it is necessary to have spectra of good quality, high SNR, and short acquisition times. Therefore, in the work described in this chapter, ^{1}H MRS is used to study respiratory motion as an analogue for multinuclear MRS, and the spectral frequency results are corroborated with B_0 field maps.

5.3 Methods

In the experiments in this chapter, proton (^{1}H) MRS is used as an analogue for multinuclear MRS due to its high Signal-to-Noise Ratio (SNR) and short acquisition times, allowing the collection of many spectra within a single breath cycle. In post-processing, the time course of dynamic free breathing ^{1}H spectra is encoded into timepoints across the respiratory cycle using the trace from the respiratory bellows. Dynamic B_0 maps are also acquired during both free breathing ($B_0(t)$) using a phase mapping technique, as well as at inspiration and expiration breath-hold. Since imaging data is collected with a surface coil, the magnitude signal is weighted to account for variations in the B_1 profile, and this weighting is applied to dynamic B_0

maps to estimate a field offset when free-breathing, which can be compared with spectral frequency and linewidth changes.

5.3.1 Acquisition

Seven participants, aged 23 - 30 years, with Body Mass Index (BMI) ranging from 21 to 30 kgm^{-2}, were scanned on a Philips 3 Tesla Achieva system (Philips Medical). To replicate the non-localised acquisitions commonly used in multinuclear MRS experiments, MRS data were acquired using the butterfly ^{1}H quadrature loop inside the ^{13}C surface RF coil (Pulseteq, Surrey). The surface RF coil was strapped to the participant's abdomen so that it moved with them as they breathed, thus reducing potential B_1 changes contaminating the measurements of B_0 effects. The surface coil was placed centrally over the bulk of the liver, and the position was confirmed by a free breathing ^{1}H survey scan. If it were found that the surface coil was not positioned centrally over the liver, it was repositioned, and the survey repeated). During the post-processing the spectra were to be labelled by position in the respiratory cycle, the rate of acquisition of the spectra was a key consideration, and the breathing cycle needed to be continuously monitored using the respiratory bellows. For this, a respiratory belt was placed over the diaphragm and held against the participant using a Velcro strap. For each participant, a time series of free-breathing ^{1}H spectra were collected with 1800 ^{1}H spectra obtained during a ~10 minute free-breathing acquisition (non-localised, pulse acquire TR = 350 ms).

To study respiratory-induced field offsets, 1200 single slice single echo Fast-Field Echo (FFE) images with magnitude and phase data saved were obtained during free-

breathing. The slice positioning was taken perpendicular to the centre of the coil (marked with a labelled urea sample) and then optimised to ensure the large area of the liver in the Field of View (FOV). The acquisition time was 532 ms, which allowed multiple acquisitions within a breathing cycle.

Finally, standard dual-echo FFE (TE/ΔTE = 2.3/2.3 ms, 12 slices) scanner-generated B_0 maps and related magnitude images were acquired on inspiration and expiration breath-holds. These data sets were collected using the ^{1}H decoupling coil of the ^{13}C surface coil to compare to the free-breathing B_0 shifts and the Q-body coil for lung volume analysis.

5.4 Analysis

5.4.1 Free-breathing MRS and MRI Data

This section covers the data analysis of the 1800 free-breathing spectra and 1200 dynamic images.

5.4.1.1 Spectral Analysis

Spectra were phase corrected individually in JMRUI (99–101) and AMARES (Advanced Method for Accurate, Robust and Efficient Spectral fitting (102)) was used for quantification of the water peak central frequency (f_{peak}), linewidth (FWHM) and peak area (amplitude), as illustrated in Figure 5.2. The results were imported to MATLAB (MathWorks, 2020b). The time series of the water peak frequency ($f_{peak}(t)$), FWHM (FWHM(t)) and amplitude (A(t)) were generated and overlaid on the respiratory bellows signal. For one participant, the respiratory

bellows consistently failed (in this case the participant was asked to take a deep breath, and the bellows temporarily worked before failing again) leading to gaps in the respiratory bellows data; data collected in these gaps could not be encoded with the respiratory cycle and, hence, were excluded from the analysis. For each participant, a ~100 dynamic section of the respiratory bellows data without any time gaps was selected and the signals Fourier transformed to investigate the oscillation frequencies in the respiratory cycle.

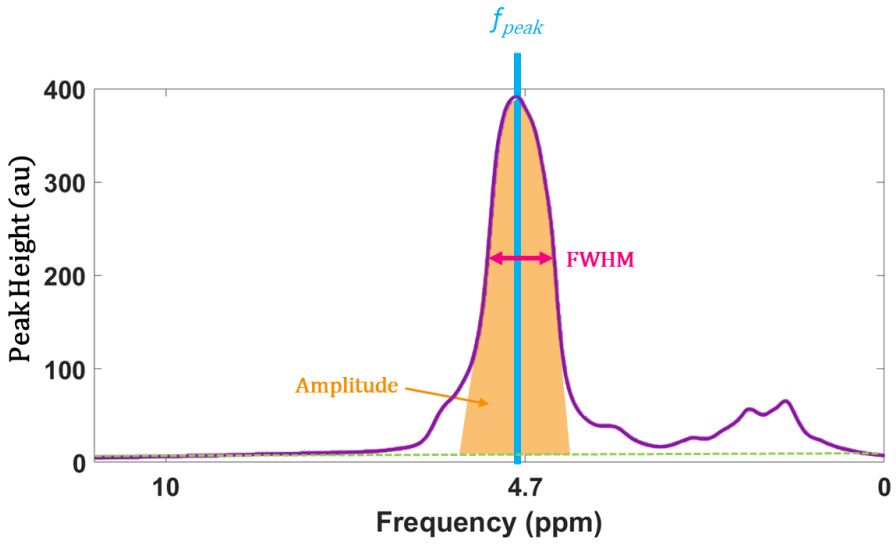

Figure 5.2 - Measurements calculated using AMARES in JMRUI shown for an example spectrum. The central frequency of the water peak (f_{peak}) is shown in blue, the FWHM in pink and the Amplitude in yellow and the approximate baseline fit is shown in green.

5.4.1.2 Image Analysis

The goal is to find the expected phase of the unlocalised data. The image analysis pipeline needed to account for the fact that the data is collected with a surface coil

by weighting the phase from the pixels within the sensitive region of the coil. The intensity of voxels in the magnitude image within the liver depending on the distance of a given voxel from the surface coil, as shown schematically in Figure 5.3. Hence, the magnitude images can be used to weight the pixels of the phase data.

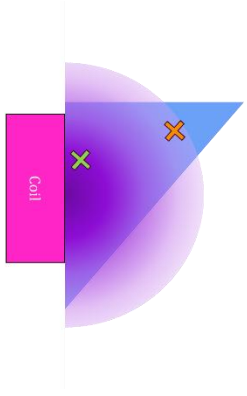

Figure 5.3 - A simplified schematic showing two different locations marked by X in the liver which is represented by the blue triangle. The purple semi-circle represents the B_1 field from the surface coil shown in pink.

The image analysis pipeline for the dynamic free-breathing magnitude and phase time series is shown in Figure 5.4.

The magnitude images (Figure 5.4A) were first normalised,

$$w(x,y,z,t) = \frac{I(x,y,z,t)}{I_{MAX}}$$

Equation 5.1

where I is the intensity value of the voxel, I_{MAX} is the maximum intensity value across the image for the entire time series and w is the normalised intensity value for that voxel (taking a value between 0 and 1). The sensitivity at each voxel in the liver and, hence, its relative contribution to the spectra is approximately equivalent

to the relative signal intensity in the magnitude images. Therefore, the normalised magnitude time series w(t) (Figure 5.4D) was used to weight the B_0 data from the liver. The free-breathing time series of phase images ($\phi(t)$, Figure 5.4B) were unwrapped (126,127) (Figure 5.4E) and a weighted phase evolution time series was then computed ($w(t)\phi(t)$,Figure 5.4F). Areas containing Subcutaneous Adipose Tissue (SAT) were masked out, by manually drawing a mask image in MRIcron (NITRC, v1.0.20190902), as they do not contribute to the water signal peak Figure 5.4C. A stack of line profiles through the liver on the weighted phase maps across dynamics was created to visually inspect the effect of respiration (Figure 5.4G).

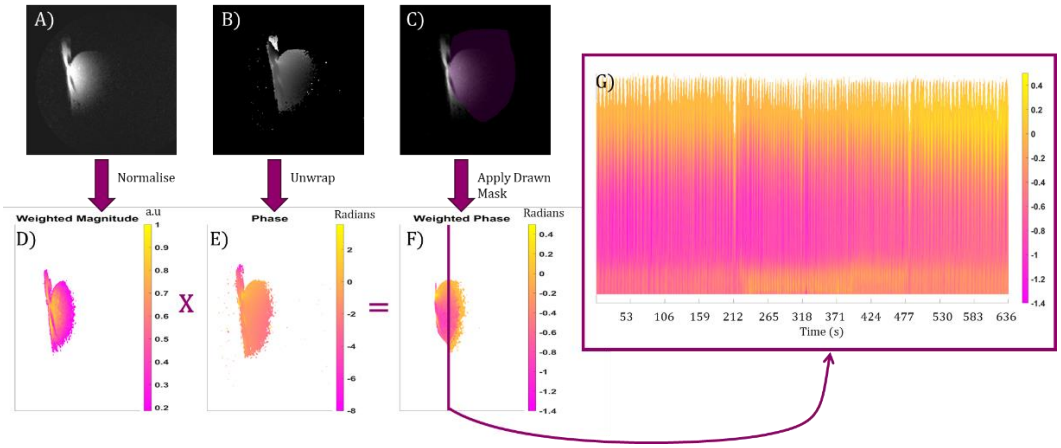

Figure 5.4 - Analysis of free-breathing imaging data showing a slice from the (A) magnitude and (B) phase timeseries. The magnitude data is (D) normalised giving $w(t)$ and multiplied by the (E) unwrapped phase ($\phi(t)$) to generate (F) a weighted phase time series before (C) a mask is applied. The purple line in (F) shows a five-pixel wide line profile used in (G) to plot the time course of the weighted phase data ($w(t)\phi(t)$) within the liver, which can be seen to be modulated by the respiratory cycle.

The maps of weighted phase evolution ($\mathrm{w(t)\phi(t)}$, Figure 5.4F) were then converted to a time series of weighted field offsets $\mathrm{B_0(t)}$ using

$$B_0(t) = \frac{\sum(w(t)\phi(t))}{TE\sum w(t)}$$

Equation 5.2

The time series $\mathrm{B_0(t)}$ was also overlaid on the time series from the respiratory bellows, to provide a comparator to the frequency shift measured from the spectral analysis. In addition, both signals were Fourier transformed.

5.4.1.3 Comparison of Imaging and Spectral Data

Spectral f_{peak}(t) and imaging B_0(t) datasets were binned into inspiration and expiration phases. From the assessment of the respiratory cycle, inspiration/expiration was defined as peaks and troughs of more than 30% above or below the mean peak height, respectively. Any points greater than two standard deviations above the mean were discarded to remove outlying deep breaths. Moving subtractions (inspiration – expiration) were used to compute the mean shifts f_{peak}(t), FWHM, amplitude and B_0(t) during free-breathing.

5.4.1.4 Assessment of Coil Position

When analysing the magnitude and phase images from the dynamic data, it became clear that the coil's position with respect to the liver was linked to the outcomes. As is seen in Figure 5.5, if the surface coil is positioned too high on the torso, the liver moves into the FOV on inspiration. However, if the surface coil is placed lower down on the torso, the liver moves out of the FOV on inspiration.

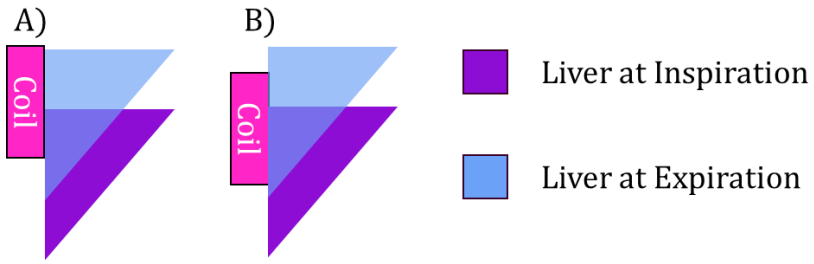

Figure 5.5 - Coil position with respect to the liver. The liver position at inspiration is shown in purple, and expiration in blue. A) shows the case when the surface coil is placed high on the torso and B) when the coil is placed low on the torso.

To assess the volume of the liver visible to the surface coil, the magnitude images were viewed in FSLeyes, FSL (FMRIB Software Library) and crosshairs placed on the image at the top of the liver dome when it was at its highest (expiration) and lowest (inspiration) point. The change in the liver volume visible to the coil was then visually estimated.

5.4.2 Breath-hold Analysis

During the time series data analysis, it was noted that respiratory amplitude varied greatly between individuals. Those B_0 maps taken using the ^1H decoupling coil were used to compare field offsets at the assumed maximum displacement, between inspiration and expiration. B_0 maps taken using the body coil were used to evaluate changes in lung volume between inspiration and expiration for each participant. Figure 5.6 shows the image analysis pipeline for the B_0 maps taken with the ^1H decoupling coil. For inspiration and expiration, the magnitude images were normalised (Equation 5.1), and a mask was applied to remove the adipose tissue

(m_w) (mask created in MRIcron, NITRC, v1.0.20190902). Phase wrapping was visible on multiple B_0 maps. To resolve this, the raw B_0 maps were reverted to phase, which were unwrapped (126,127), and the images were then converted back to B_0 maps. The unwrapped B_0 maps were multiplied by the normalised magnitude data, and finally, an average value for field offset across the map was computed,

$$B_{0,w}(VOI) = \frac{\sum(B_{0,UN} \cdot m_w)}{\sum m_w}$$

Equation 5.3

where $B_{0,UN}$ is the unwrapped data and $B_{0,w}(VOI)$ is the final computed value.

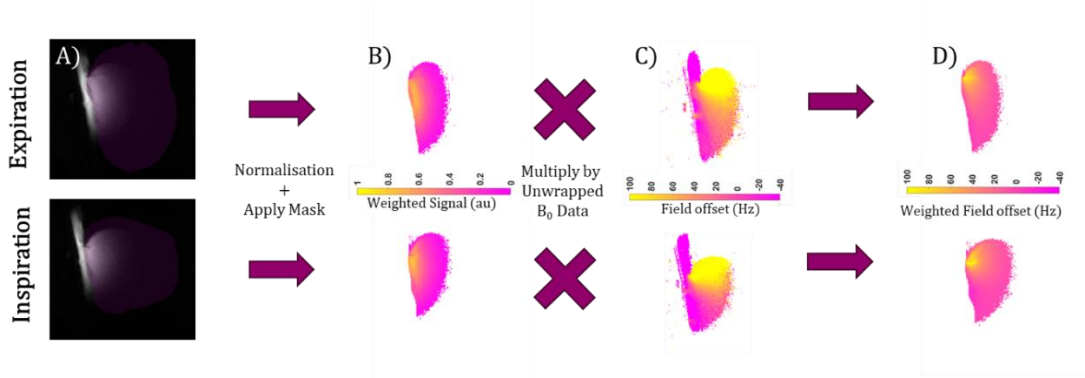

Figure 5.6 –Example analysis of the Top - expiration and Bottom - inspiration breath-hold B_0 maps taken using the ^1H decoupling coil, shown for the central slice. A) shows the masks and magnitude data used to generate B) the masked, normalised magnitude data (m_w) which is multiplied by C) the unwrapped B_0 map to generate D) the weighted field offsets.

To evaluate lung volume (V_L), the magnitude images from the Q-body expiration and inspiration breath-hold B_0 maps were segmented (3-class segmentation in FAST (FMRIB's Automated Segmentation Tool), FSL) for lung cluster identification Figure 5.7. These masks were then quantified for lung volume in MATLAB (MathWorks, 2020b). To calculate the change caused by respiration, inspiration values were subtracted from expiration values to give $\Delta B_{0,w}(\mathrm{VOI})$ and ΔV_L. As the direction of the change in B_0 is less important in this case than the magnitude $\left|\Delta B_{0,w}(VOI)\right|$ was plotted against ΔV_L.

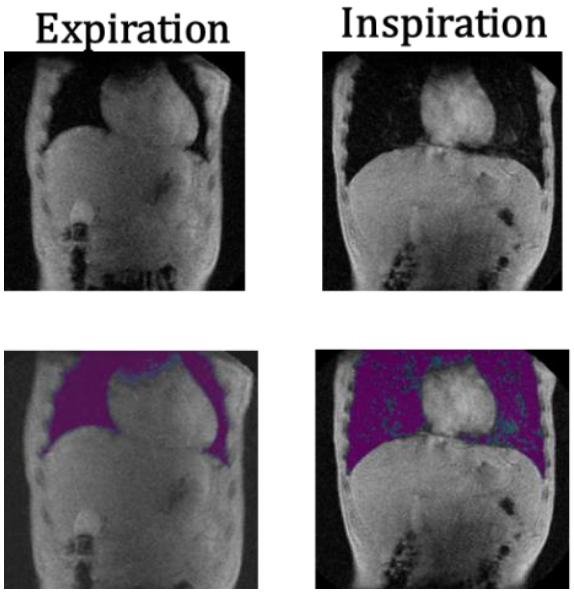

Figure 5.7 -Central slice of the multi-slice Q-body (Top) magnitude images from B_0 mapping for expiration and inspiration and (Bottom) the corresponding lung mask.

5.5 Results

Six out of the seven participants had complete data sets; for one participant (Participant 3), the respiratory bellows failed for several intervals. All spectra had good SNR (Figure 5.8) and were able to be successfully analysed in JMRUI (99–101).

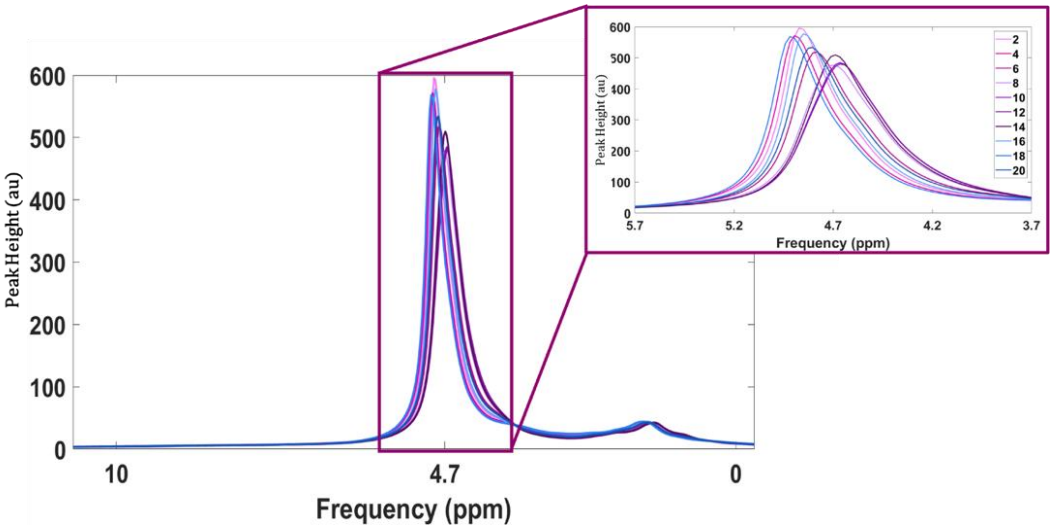

Figure 5.8 - Example of ^{1}H spectra collected during free-breathing including a close up showing the shift of the water peak. Alternate acquisitions are displayed to prevent crowding of the image, legend shows acquisition number.

5.5.1 Dynamic MRS and Imaging Data

For all participants, the time series from the respiratory bellows and water peak frequency $f_{peak}(t)$ time series were found to oscillate at a similar primary frequency as shown by the Fourier transform (Figure 5.9), and as participants breathed in f_{peak} increased. Mean free-breathing spectral shifts between expiration and inspiration ranged from 10 – 31 Hz. Figure 5.10 shows a similar correspondence of the time series of the imaging field offset with the respiratory bellow, with imaging field

offset values ranging from 6 – 31 Hz across participants. Only 3 of 7 data sets are displayed as unfortunately the physiological data files were lost due to a theft of the device they were stored on, and this data could not be retrieved from the scanner at such a later time. Figure 5.11 compares the frequency shift measured between expiration and inspiration using the spectral water peak frequency and the imaging field offset.

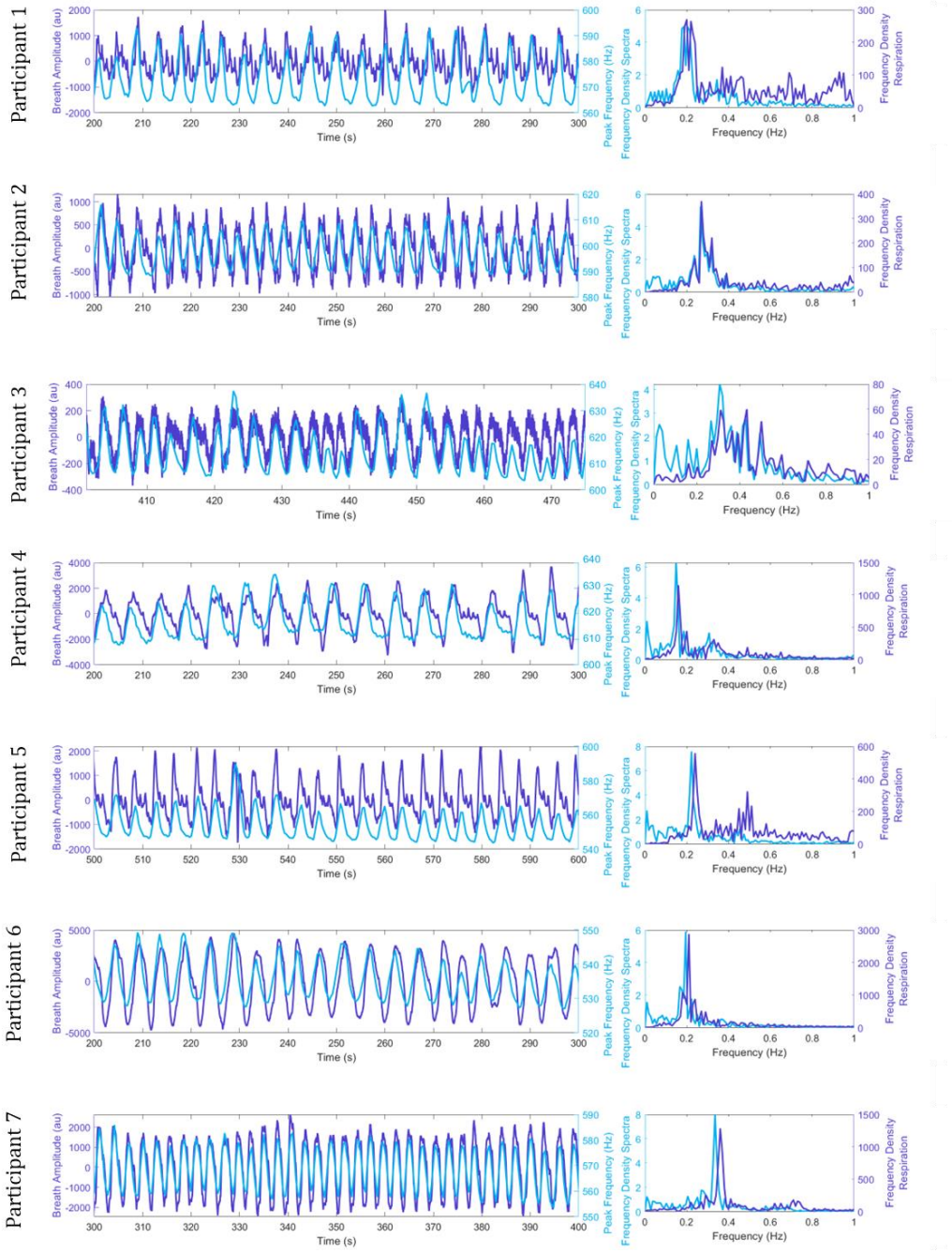

7

Figure 5.9 – Left- alignment of each participant's respiratory bellows trace and spectra water peak frequency ($f_{peak}(t)$) and (right) the Fourier transform showing matched primary frequency.

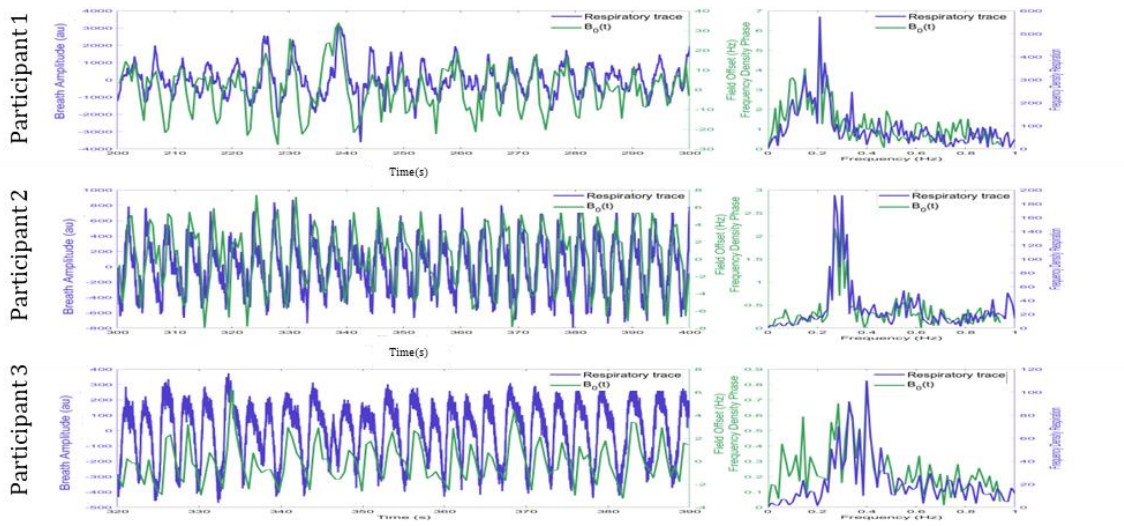

Figure 5.10 - Alignment of three participants' respiration trace and the field offset B_0 (t) measured from the dynamic imaging, the Fourier transform shows an overlap in the primary frequency. Participant one shows consistency with chaotic breathing, participant 2 shows consistency with rhythmic breathing (displayed by narrow FFT) and participant 3 shows agreement even with shallow breathing. The dynamic timings varied based on if the data monitoring window was open or closed during the acquisition. Unfortunately, the physiological data files were lost in a theft and the scanner decommissioned, hence the reduced number of participants presented.

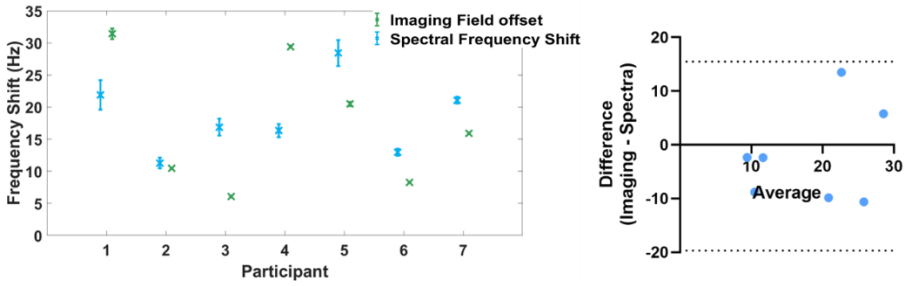

Figure 5.11 – Left - Frequency shift measured between expiration and inspiration using the imaging field offset ($B_0(t)$) and spectral water peak frequency (f_{peak}). Right – Bland-Altman showing the slight bias of spectroscopy measuring larger shifts.

Figure 5.12 and Figure 5.13 show the alignment of the FWHM and amplitude, respectively with the respiratory bellows trace and matched Fourier transforms. Figure 5.14 shows the MRS shifts in FWHM and amplitude between expiration and inspiration. Mean shifts in FWHM ranged in magnitude from 0.48 to 31 Hz, with standard deviations ranging from ±1 to ±9 Hz. For participants 1, 4, 5, and 7 FWHM shifts were negative (decrease in FWHM on inspiration compared to expiration). For participants 2, 3, and 6 shifts were positive (increase in FWHM on inspiration compared to expiration). Mean amplitude shifts ranged in magnitude from 0.14 to 2.7 au with standard deviations in shift ranging from ±0.2 to ±0.8 au. For amplitude, positive shifts (increase in amplitude on inspiration compared to expiration) were seen for participants 3, 5 and 6. In contrast, negative shifts (decrease in amplitude on inspiration compared to expiration) were seen for participants 1, 2, 4 and 7. Table 5.1 summarises for all participants the direction of the shift for in MRS

frequency shift, amplitude and FWHM as well as liver volume in the sensitive ROI of the surface coil.

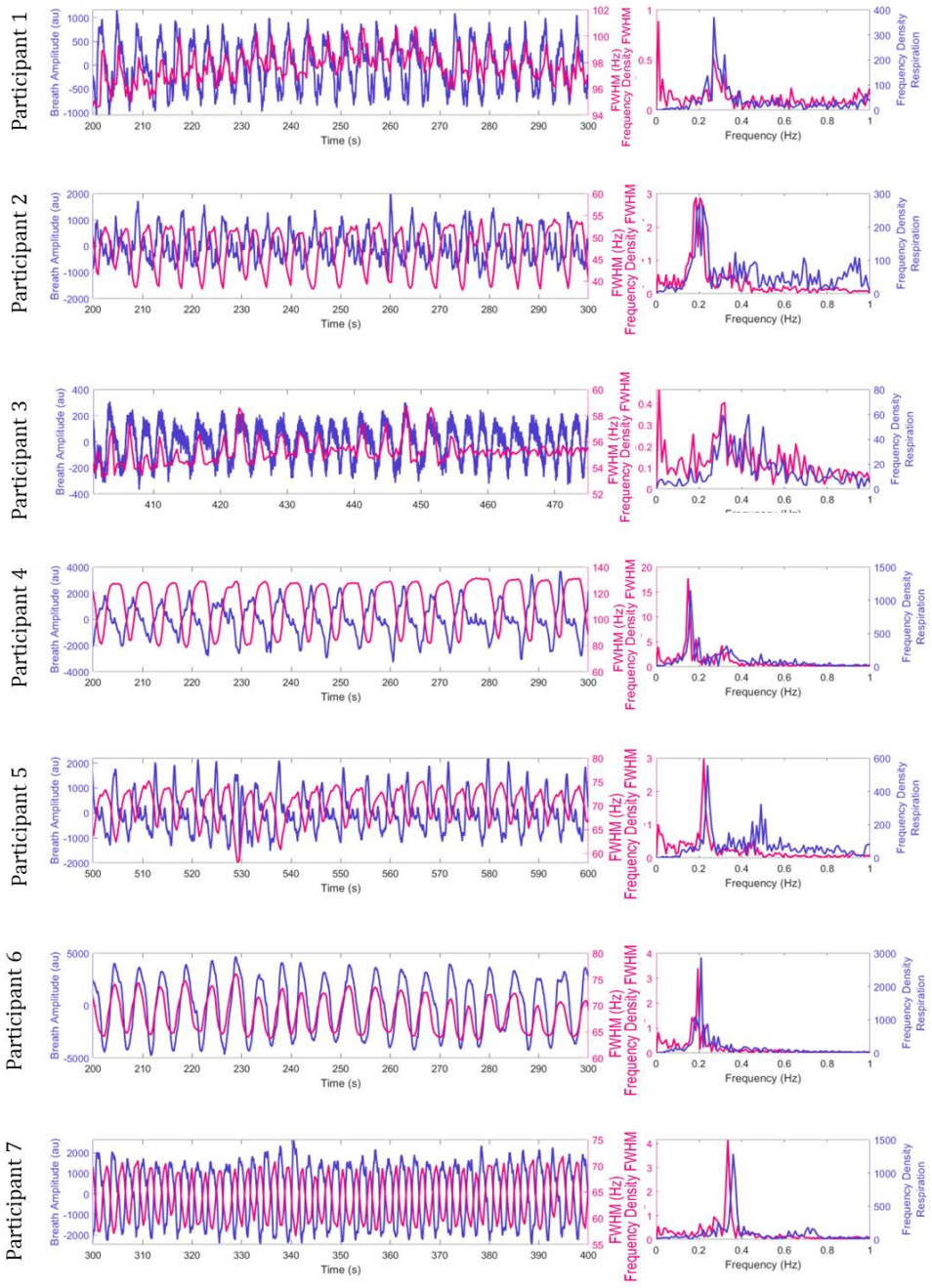

Figure 5.12 - Left- alignment of each participant's respiratory bellows trace, and spectra water peak FWHM and (right) the Fourier transform showing matched primary frequency.

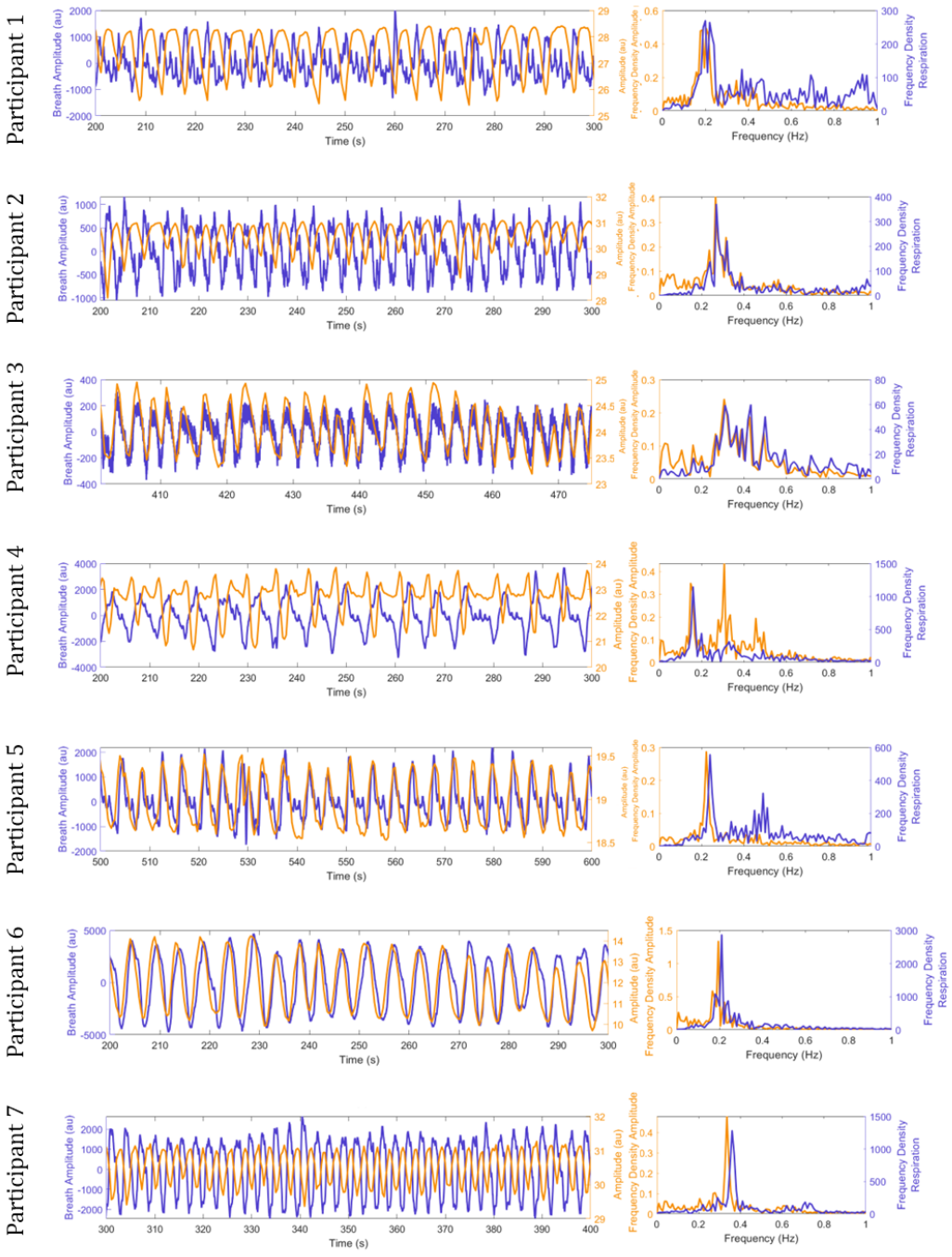

Figure 5.13 - Left- alignment of each participant's respiratory bellows trace and spectra water peak amplitude and (right) the Fourier transform showing matched primary frequency.

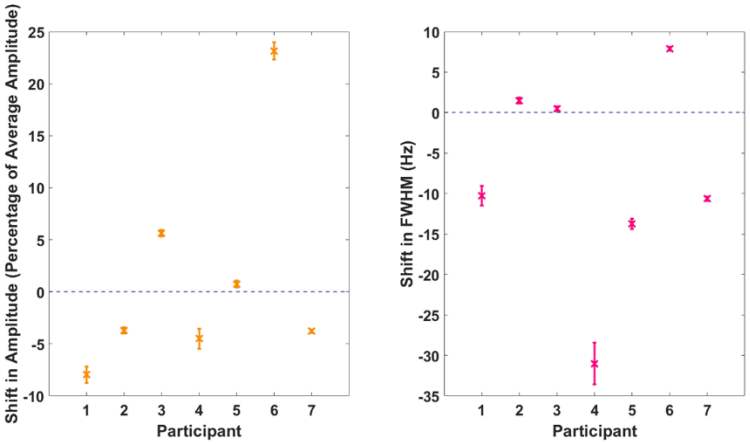

Figure 5.14—Left: Shift in the amplitude of the water peak between inspiration and expiration shown as a percentage of the average height for all peaks. Right: Shift in the FWHM of the water peak between inspiration and expiration.

Participant	Change with inspiration			
	Frequency	Amplitude	FWHM	Sensitive ROI
1	↑	↓	↓	↓
2	↑	↓	↑	↓
3	↑	↑	↑	↑
4	↑	↓	↓	↓
5	↑	↑	↓	↑
6	↑	↑	↑	↑
7	↑	↓	↓	↓

Table 5.1 - Summary of changes to MRS frequency, amplitude, FWHM and liver volume visible to the surface coil on inspiration.

5.5.2 Breath-hold Data

The B_0 maps collected on inspiration and expiration showed consistently larger field shifts than the free-breathing data, with field shifts of 16 - 113 Hz, this field shift correlated with the change in lung volume between inspiration and expiration across all participants (Figure 5.15).

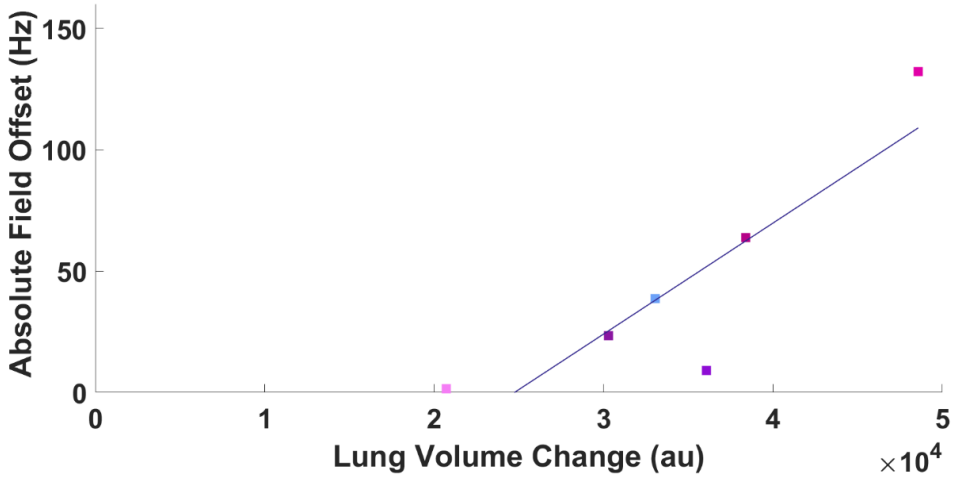

Figure 5.15 - Field shift seen in B_0 maps between expiration and inspiration breath-holds plot against the change in lung volume, with the fit having a correlation R = 0.87 and p = 0.023

5.6 Discussion

This study investigated the effect of free-breathing acquisitions in ^{1}H MRS to study the impact on the spectral shift of the water peak and compare this to imaging field offsets. All spectra had good SNR and adequate fits when assessed. Results of this work can then be used to understand the influence of free breathing in multinuclear MRS for which a large NSA of datasets must be collected to increase SNR.

5.6.1 Free-Breathing Spectral and Imaging Data

5.6.1.1 Frequency shift with Free-Breathing

The shifts in spectral resonant frequency (f_{peak}) and imaging field offsets followed the respiratory cycle with good agreement for all participants, with a maximum shift during free breathing of 31 Hz (0.24 ppm). This magnitude of change is similar to that reported by Bolan *et al*. (118) (here, field shifts range 10 – 31 Hz for Bolan *et al.* 23 ± 5 Hz). The field offsets from the created B_0 maps $(B_0(t))$ were mostly smaller than those of the spectral frequency shifts; this is likely to be caused by using a single-slice B_0 map rather than volumetric dynamic field maps. An optimal experiment would be to obtain a 3D multi-slice B_0 scan; however, this would not be able to be acquired in a short enough period to encode multiple timepoints within the respiratory cycle.

5.6.1.2 FWHM

The MRS measure of FWHM represents the linewidth of the water peak. For all participants, there was agreement between the central frequency of the Fourier transformations of the time course of FWHM and the respiratory trace; from this, it can be inferred that respiration is causing the fluctuations in the FWHM.

Participants 2, 3 and 6 whose FWHM increased with inspiration, had lower average frequency shifts in the $B_0(t)$ maps (shifts ~10 Hz), whilst participants 1, 4, 5 and 7, whose FWHM decreased with inspiration, had larger $B_0(t)$ shifts over 15 Hz (Figure 5.11). Although the amount of shift seen in the FWHM is linked to the range of phase within the FOV, the direction of the shift will predominantly be determined by any movement of the liver as the average value is dependent on the weighting of the signal from the coil sensitivity profile in these experiments.

In Table 5.1, the direction of the change for amplitude and FWHM are the same for all but two participants. It could be that for these two participants, the increase in liver volume within the FOV, which would cause the increase in amplitude, is bringing in areas of the liver that were poorly shimmed which could cause a decrease in the FWHM, as illustrated schematically in Figure 5.16.

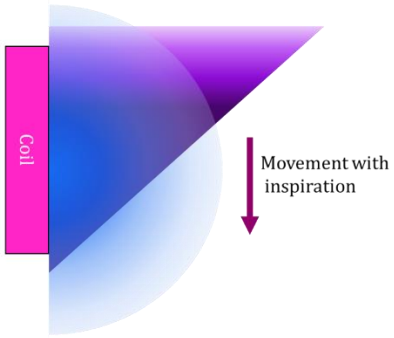

Figure 5.16 - The coil is represented in pink, and its B_1 field is in blue. For the liver (purple), darker regions are better shimmed, and the lighter region represents the areas of large field offsets. In this case, upon inspiration, the large offsets will move into the areas of higher sensitivity, which, when weighted, could introduce larger variations in FWHM.

Although placing the coil lower on the ribs may reduce the amount of the liver in the FOV, it may improve the quality of the signal, this may be beneficial in free-breathing acquisitions where a single shim is performed. This is because the top of the liver, next to the lung, often has the largest range of phase, and hence, by reducing the amount of this area in the FOV, the FWHM should be reduced with minimal loss to amplitude.

5.6.1.3 Amplitude

For some participants, the peak area (or amplitude) measured by AMARES increased with inspiration; for others, the peak area decreased with inspiration. However, for all participants, there was an agreement between the central frequency of the Fourier transformation from the spectral amplitude time series (A(t)) and respiratory trace, implying that respiration was responsible for the

fluctuations in amplitude. Amplitude changes are caused by the amount of visible signal (i.e. the liver moving in and out of the FOV) as well as intravoxel dephasing (linked to FWHM). For participants 1, 2, 4, and 7, the spectral amplitude decreased with inspiration; upon inspection of the dynamic phase images, it can be seen for these participants that the liver was moving out of the FOV.

For participants 3, 5 and 6, the spectral amplitude increased with inspiration, and it was seen that the liver was moving into the FOV with inspiration for these participants. Although the predominant effect appears to be the liver moving up or down in or out of the FOV, it can also be seen in some of the participants that the liver was being compressed due to inspiration (Figure 5.17). Due to the B_1 drop-off of the surface coil used, it is difficult to see the full morphometry of each liver. Still, some of the liver's volume is likely moving deeper into the central abdomen, reducing the available signal. Although each participant's images were visually inspected, future work should consider quantifying the change in visible signal using morphometric analysis.

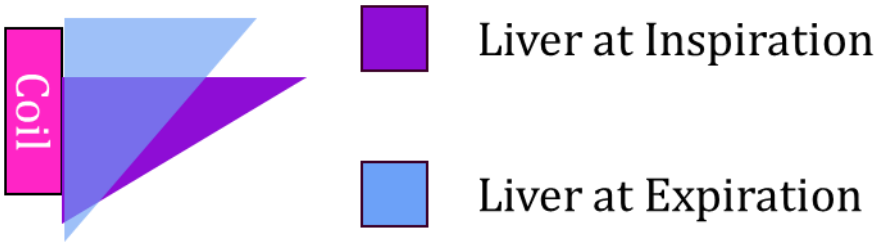

Figure 5.17 - Another case of liver movement with respiration in addition to those shown in Figure 5.5. Here on inspiration (purple) the liver moves further in from the coil and compresses, whilst on expiration (blue), the liver is closer to the coil and larger

5.6.2 Breath-hold Imaging data

The difference in the field offset between the inspiration and expiration B_0 maps correlated well with the change in lung volume. The maximum field shift seen in the breath-hold B_0 data was three times larger than the maximum shift seen in the free-breathing B_0 data. For 3 of the 7 participants, the shifts measured using breath-holds were larger than any shift measured in the dynamic data. This is probably because during the breath-hold scans, people took deeper breaths compared to free-breathing causing greater movement of the liver.

The dynamic B_0 data showed examples of deep breaths, where the shifts were larger than the rest of the time series, these data points were removed as outliers to prevent exaggerated dynamic shift estimations.

5.6.3 Implications for Multinuclear Spectroscopy

This study used ^{1}H MRS to quantify the measured effects of free breathing and this allows such effects to be related to multinuclear MRS where acquisitions are often

performed free breathing. The simplest way to understand these effects on multinuclear MRS is to convert the shift in Hz (ΔHz) caused by free breathing to a shift in the universal ppm scale (Δppm) (as the shift measured in Hz for one atomic species is not equivalent to the same Hz shift seen in another). This conversion is performed using,

$$\Delta ppm = \frac{\Delta Hz \cdot 10^6}{\gamma \cdot B_0}$$

Equation 5.4

where γ is the gyromagnetic ratio of a nuclei. Shifts seen in ^{1}H MRS in this project ranged from 10 – 31 Hz, equivalent to 0.08 – 0.24 ppm. At 3 Tesla, ^{31}P metabolite linewidths range from 0.34 - 0.73 ppm (21) and ^{13}C range from 1 – 2 ppm, meaning shifts of 0.24 ppm during free-breathing could cause significant line broadening.

5.7 Conclusion

Frequency shifts observed in this study within the liver were 10 – 31 Hz from dynamic MRS and imaging data. This shift from free breathing could cause a 0.24 ppm shift in spectra, which would cause dramatic line-broadening effects in multinuclear spectroscopy. Future work should confirm the effect of respiration on FWHM and amplitude using respiratory-triggered acquisition and frequency alignment for both ^{1}H and multinuclear applications. The spatial variations in the field map over the respiratory cycle, reported here, could be used to design dynamic shim coils.

6 Variability in Carbon-13 Magnetic Resonance Spectroscopy Measurement of Liver Glycogen in Healthy Children

6.1 Overview

The reproducibility and repeatability of liver glycogen measured in children using natural abundance Carbon-13 (^{13}C) Magnetic Resonance Spectroscopy (MRS) is yet to be established. Ensuring that the results are reproducible and repeatable and understanding the source of variability is crucial in all studies. However, since children are a complex cohort to recruit and scan, it is even more vital that the variability in the measured values is quantified. Repeatability applies to data collected in the same place with the same instrument using the same rater to analyse the data. In contrast, reproducibility refers to the degree of agreement when performed by different individuals with different instruments.

This chapter investigates the variability of Liver glycogen measurements in children and builds on previous work in adults. This work aimed to compare variations seen in children to adults, assess the impact of using different observers, and evaluate an in-house automated algorithm for analysis.

6.2 Introduction

Glycogen plays a vital role in the body as an energy storage molecule. In the postprandial state, higher blood glucose levels trigger insulin release, and the process of converting glucose to glycogen for storage begins (128). The liver and skeletal muscles store most of the body's glycogen, with the liver having the largest glycogen concentration. Liver glycogen is the only direct contributor to blood glucose regulation as skeletal muscle stores are used as local energy sources during exercise and are only used to regulate blood glucose levels in extended periods of fasting via indirect processes (129). For a more in-depth explanation of glycogen storage and production mechanisms and its role in the body, see Chapter 1. The role of glycogen storage in metabolic disorders suggests that it would be valuable to have a tool to measure changes effectively without the need for invasive biopsies, ^{13}C MRS provides such a tool.

The accuracy and repeatability of ^{13}C MRS measurements of glycogen concentration was evaluated by Taylor *et al*. (130) in 1992, where the glycogen concentration of skeletal muscle was measured using ^{13}C MRS and compared to that measured by muscle biopsies. The values from each method correlated within subjects ($p<0.0001$); seven of the eight subjects' glycogen concentrations agreed within 9.3 mM between methods (87 ±28 mM by MRS 88 ±28 mM biopsy), and the intrasubject Coefficient Of Variation (COV) was higher for biopsy than MRS. The study concluded that ^{13}C MRS could provide accurate, repeatable, non-invasive

measurements of glycogen concentrations. Since then, ^{13}C MRS has been widely used as a tool for measuring skeletal muscle and liver glycogen concentrations (97,106,123,131–133).

^{13}C glycogen measurements are challenging, particularly in the liver, due to low natural abundance, wide acquisition bandwidth and low gyromagnetic ratio. With such a wide spectral bandwidth, attempts to optimise the baseline fit for the entirety of the spectra can cause sub-optimal fitting in local regions. The low natural abundance and low relative sensitivity mean that ^{13}C spectra have low Signal-to-Noise Ratio (SNR) and the glycogen doublet is often the smallest resolved metabolite peak in the spectra, dwarfed by lipids and glycerol. Therefore, a large Number of Signal Averages (NSA) are needed to detect adequate signal, which requires the use of free breathing acquisitions (as described in Chapter 5). All these issues compound to complicate phase correction and peak fitting of ^{13}C spectra. Manual analysis from experts is generally considered necessary to ensure good fits and despite the variability introduced, manual analysis has been considered the gold standard. The measured COV of liver glycogen concentrations using non-localised MRS acquisitions in healthy adults can be seen in Table 6.1. This study looked at the reproducibility of manual analysis, comparing manual analysis from two raters with automatic analysis using previously acquired and published data of ^{13}C liver spectroscopy in children (123).

Study	Glycogen Concentration (mM)	Longitudinal Intrasubject COV (%)		Intersubject COV (%)	Number of subjects
		Fasted	Postprandial		
Stephenson *et al.* (97)		35			12
Bawden *et al.* (131)	217	32		17.5	5
Buehler *et al.* (106)	140		14.6		8

Table 6.1 - Literature values of liver glycogen concentrations and the coefficients of variation using non-localised MRS acquisitions in healthy adults.

If measurements of glycogen concentration cannot be reproduced, that is, different institutions and research centres cannot replicate the results, or if they are not repeatable, i.e. cannot be replicated by the same system on the same day, then this affects both the number of subjects needed to power future studies and the ability of ^{13}C MRS to evaluate the effectiveness of interventions.

6.2.1 Uses of Carbon-13 Magnetic Resonance Spectroscopy in Children

As children are a difficult cohort to recruit and compliance with long and complicated protocols is minimal, there is little information on the repeatability and reproducibility of data from this group. Few studies have investigated liver glycogen levels in children, and previous literature has focused on understanding Type I Diabetes (T1D) using ^{13}C MRS. Matyka *et al.* (109) investigated daytime accumulation of liver glycogen in six children aged 7 - 10 years with T1D. The healthy controls' liver glycogen concentrations post-overnight fast was 178 mM

(120-203 mM). Flück *et al.* (134) investigated fasted and fed glycogen stores in children and adolescents using 19 T1D subjects with age-matched healthy controls; liver glycogen concentrations were not quantified but given as relative values compared to an external acetone signal after coil sensitivity corrections.

There are currently no published studies investigating the variability of glycogen measures in children.

6.2.2 Sources or Variability

Although ^{13}C MRS is the only non-invasive method available to quantify liver glycogen, there are many sources of variability, arising not only from the subjects' biology (differences in physiology, compliance, and day-to-day variations) but also from the system used to collect data (field strength and RF coil) and the analysis approaches (differences in software packages and rater opinions).

6.2.2.1 Subjects

Within a group of subjects, there will be different physiologies, for instance, between sex and across age. As a person ages, their physiology will change throughout the body, including the cardiovascular, endocrine, and gastrointestinal systems (135). However, changes happen rapidly at a young age. Children aged 6 – 12 years are beginning to develop their physical and mental capabilities; in children aged 9 – 11 years, their muscles are developing to improve strength and balance, with girls maturing faster (136,137). These differences lead to intersubject variations. There are also intrasubject variations caused by many factors. Variations

in measurements taken on the same day can be caused by diurnal physiological changes or the spectral shift caused by respiration (see Chapter 5). These factors also affect measurements taken on different days but are compounded by factors such as differences in subject positioning. Also, a lack of compliance with the protocol can cause intrasubject variations, for instance, a fast not being followed or a tailored meal being fully consumed on one visit but not on another. Some of these issues can be mitigated, narrow age ranges can be used in young cohorts, deviations from protocol can be noted, and study timings can be kept consistent across visits.

6.2.2.2 The System

Inhomogeneities in the B_0 field in an MR scanner can lead to the Region Of Interest (ROI) experiencing a slightly different magnetic field if a subject is not positioned consistently, causing the spectral peak to shift. Most multinuclear MRS experiments are performed using single-loop surface coils (the B_1 fields produced by such RF coils has been discussed in depth in Chapter 4). If the surface coil is placed more laterally in one acquisition and more anteriorly in another, different amounts and types of tissue will be within the excitation volume, which will cause the signal to vary. In the case of non-localised acquisitions, this can cause differences in the measured peak areas. However, this does not pertain to samples fixed to the surface coil, such as external references. Mitigations of these effects are attempted through training operators on coil positioning, shimming of the B_0 field, and assessing coil position using survey scans.

6.2.2.3 Analysis

Software packages for spectroscopy analysis tend to be designed and optimised for data acquired in the brain. They, therefore, do not account well for the nuances of abdominal acquisitions (respiratory motion, larger volumes of interest and surface coil sensitivity) and multinuclear MRS data (low SNR, baseline corrections).

Spectral analysis requires a high level of expertise to establish an analysis protocol and train other raters to analyse data. During preprocessing, spectra need to be phase corrected, apodised, frequency aligned and baseline-subtracted, and each step may require user input to varying degrees. With so many steps, it is easy to see how variability can be introduced during preprocessing if different raters are used (inter-rater variability) or even within a rater (intra-rater variability). Having only a single rater may reduce the variation, though this is not always possible with longitudinal studies. Both inter-rater and intra-rater variations can be alleviated through automatic analysis. However, there has been a lack of standardisations in acquisition protocols, leading to many groups creating bespoke analysis packages for their data, and often, each study and the 'black box' nature of some of the automatic pipelines may lead to unexpected errors in baseline corrections and fittings. The output may often be considered unreliable and still require manual quality assurance.

The aim of this study is to investigate the repeatability and reproducibility of ^{13}C MRS measures in children, to understand the effects of changing the rater on study

results, and to evaluate the agreement between automatic and manual analysis methods.

6.3 Methods

Prepubescent children attended two study visits more than 5 days apart. At each visit, ^{13}C MRS was used to measure liver glycogen levels. Spectra were analysed, and glycogen concentrations were quantified by a newly trained rater (Rater1), an experienced rater (Rater2) and using an in-house spectral analysis algorithm written in MATLAB (MathWorks, 2020b). Each rater (excluding automatic analysis) analysed the data three times to assess intra-rater variability. Automated results were compared with the average values for each rater to determine inter-rater variability. The results within each visit were used to determine intersubject variability and between visits to determine intrasubject variability.

The procedures were approved by the University of Nottingham's Medical School ethics committee (426-1911). Written consent was obtained from the volunteers and their legal guardians. The protocol for the more extensive study is registered on www.clinicaltrials.gov (reference NCT04278209).

6.3.1 Study Design

Twenty-four healthy children aged 8-12 years participated in this study, recruited through social media and traditional media advertisements. Subjects were screened as part of a more extensive study, Astrid *et al.* (123). Inclusion criteria were normal BMI (5^{th} to 85^{th} percentile) and no health conditions; exclusion criteria included

food allergies to the test drink used in Astrid *et al.* (123). Each subject attended two visits (V1 and V2) separated by a minimum of 5-days; each visit involved consuming a tailored meal at home 3 hours before an evening session for assessment of glycogen concentrations (~2000 hrs, denoted with subscript PM) followed by an overnight fast and a morning session for assessment of glycogen concentrations (~0800 hrs, denoted with subscript AM). The timeline of participation can be seen in Figure 6.1.

Tailored meals were adjusted to each subject's dietary preferences using a 4-day diet diary; each meal provided 35% of the child's daily caloric intake (60% of energy from carbohydrates, 20% protein, and 20% fat) (123).

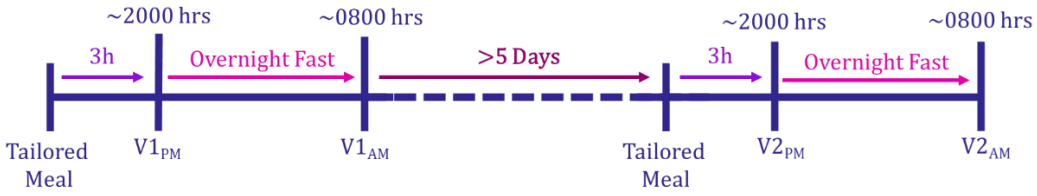

Figure 6.1 - Study participation timeline

6.3.2 Spectra Acquisition

Subjects were scanned supine, with data collected on a Philips 3 Tesla Achieva MRI system scanner (Philips Medical Systems, Best, the Netherlands) using a 150 mm rigid single-loop ^{13}C surface coil with integrated butterfly ^{1}H decoupling channels (Pulseteq, Surrey), Figure 6.2. A ^{13}C-labeled urea sample positioned in the centre of the coil was used to confirm the RF coil position and as an external reference signal

(~176ppm) to scale the measured signals. Each session lasted approximately one hour.

During each session, three scans were performed: first, a survey to ensure coil positioning, secondly a ~5 minute MRS experiment to measure the reference signal for scaling; and finally, a ~15 minute liver glycogen MRS experiment. Spectra were obtained using an unlocalised pulse-acquire sequence with narrow bandwidth and pencil beam shimming. Localisation to the liver was obtained through the RF coil's sensitivity profile. Hence, if it were found that the RF coil was not positioned centrally over the liver, it would be repositioned, and the survey scan re-run. Spectral acquisition parameters for the reference signal (long TR required due to slow T_1 recovery) and liver glycogen (shorter TR chosen due to glycogen's fast T_1 recovery, allowing for more averages within the timeframe) MRS sequences are given in Table 6.2.

MRS Purpose	TR (ms)	Flip Angle (°)	Bandwidth (Hz)	Sample points	NSA
Reference Signal	1500	25	7000	1024	20
Liver Glycogen	280	95	7000	1024	3072

Table 6.2 – MRS scan parameters

To improve compliance in this young cohort, subjects were given periscope glasses to watch a video of their choice. The video was projected onto a screen at the end of the bore from outside the magnet hall. Headphones and earplugs were provided, but it was found that the headphones compressed the glasses against the subject's

head, causing discomfort. To prevent this, participants were informed that headphones could be removed after the survey was complete for the duration of the quiet spectroscopy sequences if they kept the earplugs in their ears (Figure 6.2).

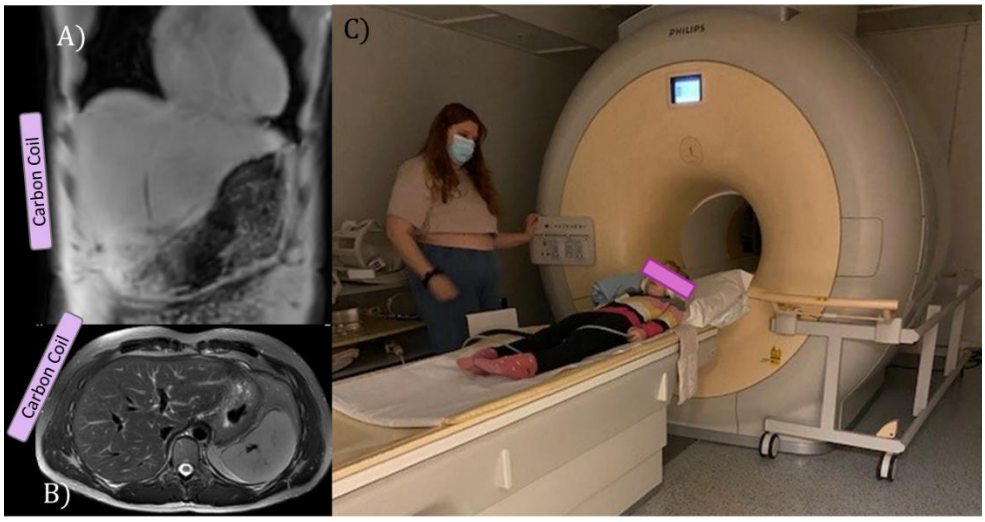

Figure 6.2 – A) and B) schematic of coil placement with respect to the liver. C) Experimental setup and subject positioning.

6.3.3 Spectral Analysis

All spectra were manually and automatically analysed using in-house MATLAB (MathWorks, 2020b) scripts. Due to the wide bandwidth of ^{13}C MRS at 3 T, first-order phase correction was required, which introduced a periodic baseline fluctuation that required correction during analysis. Both manual and automated analysis methods used a sixth-order polynomial fit for baseline correction.

6.3.3.1 Manual Analysis

Spectra were first automatically apodised (15 Hz), phase corrected to an initial estimate (-28° zero-order correction for both spectra, 1.12 degrees/ppm and 2.4 degrees/ppm first-order correction for reference and Liver glycogen spectra, respectively), and the baseline fitted based on spectral regions with no signal. Spectra were then displayed to the user for manual adjustments, as shown in Figure 6.3. Users could move the selected baseline regions to ensure no peaks were present and optimise the zero/first-order phase correction.

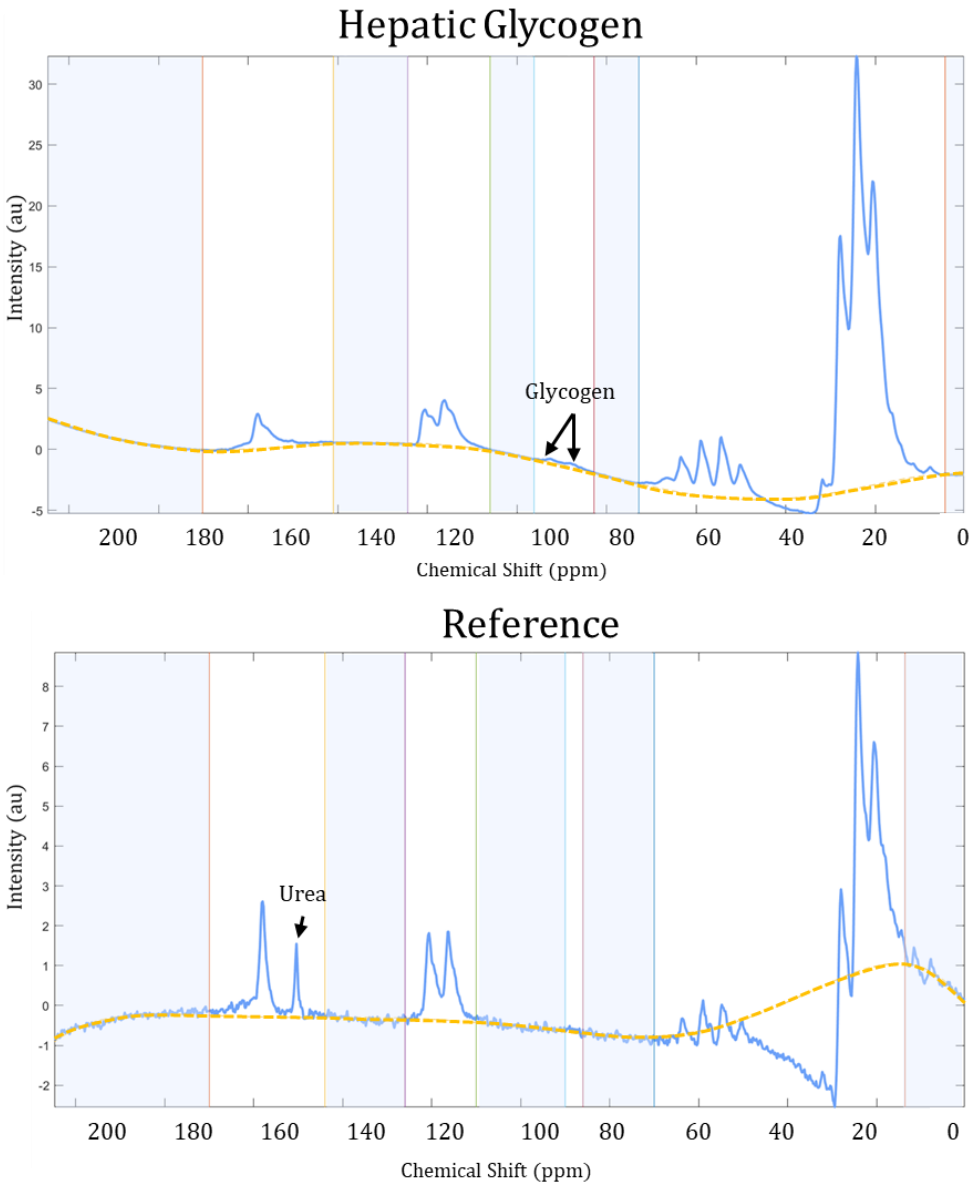

Figure 6.3 - ^{13}C spectra showing (Top) Liver glycogen and (Bottom) Reference Spectra before manual input. Coloured vertical lines and shaded regions show areas used for baseline fitting, with the baseline fit shown as a dotted yellow line on both spectra. Above each spectra are the corrections applied and the acquisition parameters, which are updated as the user modifies the spectra.

Once satisfied, depending on the analysis being performed, the user selected the centre of either the reference peak (~176 ppm) or either side of the glycogen doublet peaks (~101.5 ppm) to create a spectral region. For liver glycogen fitting, a zoomed-in window of the region appeared, and the user was prompted to select a region of baseline on either side of the doublet and select the centre of each peak. Gaussian fits were applied to the peaks, with initial linewidth estimation of 0.2 ppm (Figure 6.4). A Gaussian fit was also applied to the external reference (^{13}C Urea) signal.

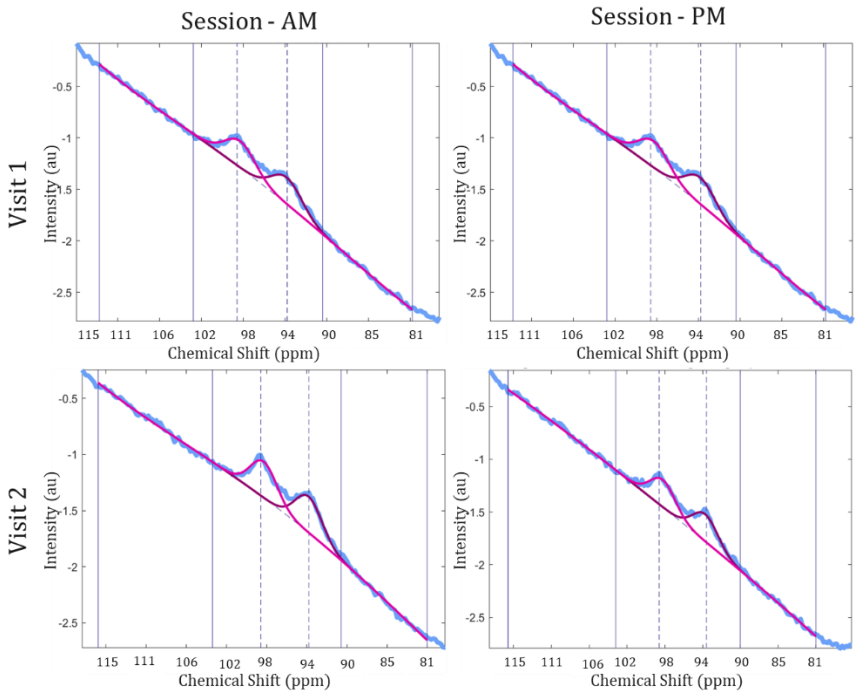

Figure 6.4 - Example fits of glycogen peaks made using manual analysis by Rater1: dashed vertical lines represent the centre of the peak selected by the rater, and solid vertical lines represent the regions chosen by the rater for baseline fitting.

6.3.3.2 Automatic Analysis

Using the automatic MATLAB (MathWorks, 2020b) script written by Dr. Stephen Bawden, initial apodisation and phase correction estimates were applied as with manual analysis. For glycogen spectra, zero-order phase corrections were adjusted by cycling through values from -90° to 90° whilst first-order corrections were cycled from -0.32 to +0.32 degrees/ppm of the starting estimate (starting estimates were 1.12 degrees/ppm and 2.4 degrees/ppm for the reference and liver glycogen spectra, respectively), finding the point of least difference between the baseline and spectral fit. Next, to find and fit the glycogen doublet, the script searches for maximum values along the ROI before searching for a baseline; these values were then used as initial estimates for Gaussian fitting.

For the external reference spectra, the script searches the region within the spectra where the external reference maximum peak is expected to be found. From the maximum, the spectra were tracked on either side to find a minimum (the baseline); these values were used as initial estimates for a Gaussian fit. As with the manual analysis (described in 6.3.3.1), the width of the peaks was automatically estimated from the fit by searching for data points on either side of the peak that returned to the baseline.

6.3.3.3 Concentration Calculations

For scaling across acquisitions, the signal from the glycogen peaks was normalised to the external reference signal. Though these relative values may be adequate for

basic variability analysis within subjects with similar loading, for the larger study, comparisons to literature and applications in the wider community, it was necessary to quantify the absolute concentration of liver glycogen. The method for conversion to concentration is outlined here. Absolute concentrations were estimated by comparison with a 200 mmol/l (mM) liver glycogen phantom (1.1 litres). Hence, liver glycogen concentration was evaluated using,

$$Gly\ (mM) = \frac{S_{in-vivo}}{S_{phantom}} \cdot \frac{\beta_{phantom}}{\beta_{in-vivo}} \cdot 200mM$$

Equation 6.1

where *S* is the scaled glycogen signal in the phantom ($S_{phantom}$) and *in vivo* ($S_{in\text{-}vivo}$). A Biot-Savart static field model (similar to that described in the Chapter 4) was used to estimate the different B_1 effects on the received signal between the phantom ($\beta_{phantom}$) and *in vivo* cases ($\beta_{in\text{-}vivo}$).

6.3.4 Repeatability and Reproducibility

Two raters performed the spectral analysis. Rater1 was the author of this thesis, who was new to the analysis methods but familiar with spectroscopy techniques. Rater2 was Dr. Stephen Bawden, who is experienced in spectral analysis, wrote the automatic analysis package, created the conversion pipeline for liver glycogen concentration used in this study, and trained Rater1. Each rater repeated each analysis three times, whilst automatic analysis was computed once.

Intra-rater reproducibility was evaluated only for the manual analysis. The average of each rater's repeats was used for inter-rater, inter-subject and intra-subject

variations. This study assesses variability in two ways: as a percentage variation (where a lower percentage is more desirable) or using the Intra-class Correlation Coefficient (ICC) computed using (IBM SPSS Statistics, V29, Armonk, NY: IBM Corp) as a value between 0 and 1, where less variation is seen as the ICC value approaches 1.

Percentage variation was calculated using two methods for inter-subject and intra-rater variations,

$$COV_{STD}\ (\%) = {}^{\sigma}/_{m}$$

Equation 6.2

where σ is the standard deviation and m is the mean of measurements. For intra-rater variations, COV_{STD} was only evaluated for manual analysis. It was calculated for every measurement at all time points, and then the values were averaged to obtain one value per rater. COV_{STD} is not recommended for use with two values as it underestimates variation (138). Instead, a method here denoted as COV_{VAR}, is suggested,

$$COV_{VAR}\ (\%) = \sqrt{\frac{1}{N}\frac{(V_1 - V_2)^2}{2m^2}}$$

Equation 6.3

where V_1 and V_2 are the glycogen concentrations from Visits 1 and 2 respectively, N is the number of subjects in the group and m is the mean glycogen concentration of the two visits. COV_{VAR} was therefore used to measure intra-subject variability.

A two-way mixed ICC calculation was also used to test intra-subject, intra-rater and inter-rater variability. All ICC values were tested for absolute agreement which reduces the ICC value if a trend of agreement is seen in the datasets even if there were systematic differences present.

6.4 Results

6.4.1 Compliance

Compliance with the MR scan protocol was good; child subjects remained still during acquisitions, reported to have complied with fasting requirements and consumed tailored meals as instructed. Spectra had good SNR, with all data sets being acceptable for analysis. Fits were of good quality; examples of the whole spectra from Figure 6.4 after corrections are shown in Figure 6.5.

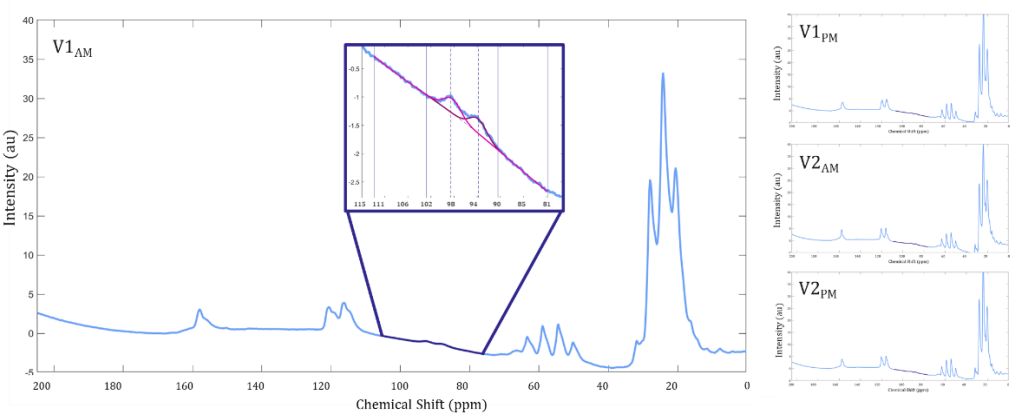

Figure 6.5 - Full spectra for one subject. Dark blue regions on spectra show the overlay of the glycogen fits shown in Figure 6.4. This is shown for the morning (AM) and the afternoon (PM) sessions for Visit 1 and Visit 2.

Liver glycogen concentrations ranged from 257-742 mM, 251-675 mM, and 263-705 mM for Rater1 and Rater2 and automatic analysis at T_{PM} and 184-538 mM, 186-508 mM, and 180-509 mM for these three measures at T_{AM} respectively (Figure 6.6).

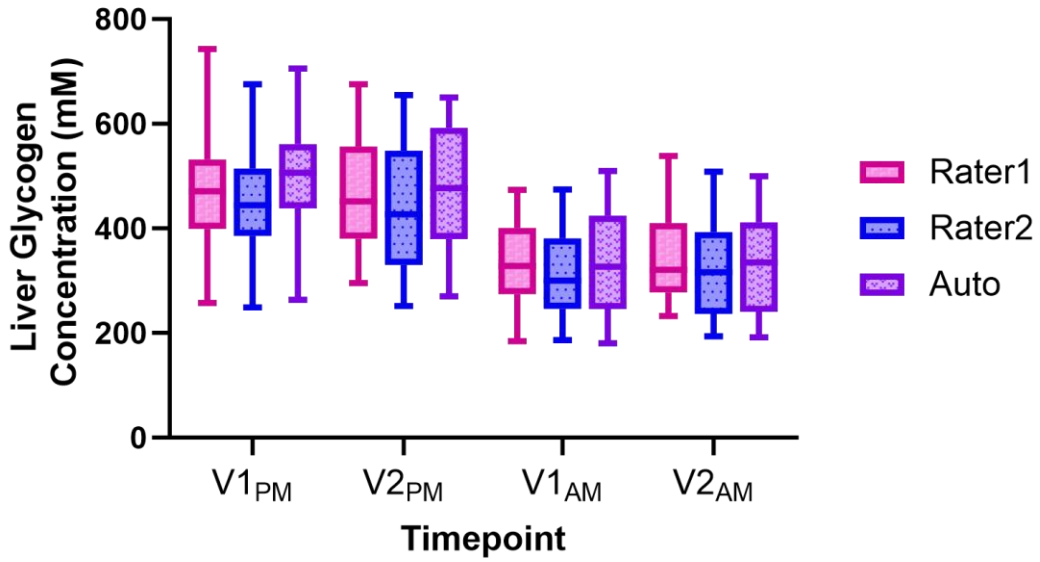

Figure 6.6 – Average Liver glycogen concentrations from both raters (Rater1 was newly trained by Rater2) and automatic analysis for all visits and time points. Whiskers show the full range of data, the box expands from the 25th to 75th percentile, and the central line represents the median value.

6.4.2 Inter- and Intra-subject Variability

The results of the variability measures can be seen in Table 6.3. Inter-subject variability ranged from 20 – 31 % depending on the rater and timepoint. Intra-subject variations were smaller, ranging from 19 – 24 % depending on the rater and timepoint.

		Visit 1		Visit 2	
		PM	AM	PM	AM
Rater1	Inter-subject (%)	23	22	24	24
Rater2	Inter-subject (%)	22	25	26	27
Automatic	Inter-subject (%)	20	23	31	27
		PM Session		AM Session	
Rater1	Intra-subject (%)	21		17	
Rater2	Intra-subject (%)	18		19	
Automatic	Intra-subject (%)	19		19	
Rater1	Intra-subject ICC	0.34		0.67	
Rater2	Intra-subject ICC	0.70		0.67	
Automatic	Intra-subject ICC	0.66		0.74	
		All Timepoints			
Rater1	Intra-rater (%)	11			
Rater2	Intra-rater (%)	5			
Automatic	Intra-rater (%)	NA			
Rater1	Intra-rater ICC	0.93			
Rater2	Intra-rater ICC	0.99			
Automatic	Intra-rater ICC	NA			
Inter-rater ICC		0.96			

Table 6.3 – Variability in measures, the first section shows the inter-subject variability for Visit 1 compared to Visit 2 for evening (PM) and morning (AM) scan sessions. The second section shows the intra-subject variability for evening (PM) sessions compared to morning (AM). The final section shows the intra- and inter-rater variability across all visits and timepoints.

6.4.3 Inter- and Intra-rater Variability

A good correlation was seen between raters and automatic analysis, Figure 6.7, with $p<0.0001$ and R values of 0.85 and 0.91 for Rater1 and Rater2, respectively. The Bland-Altman plots also seen in Figure 6.7 show little bias between across any of the rater combinations.

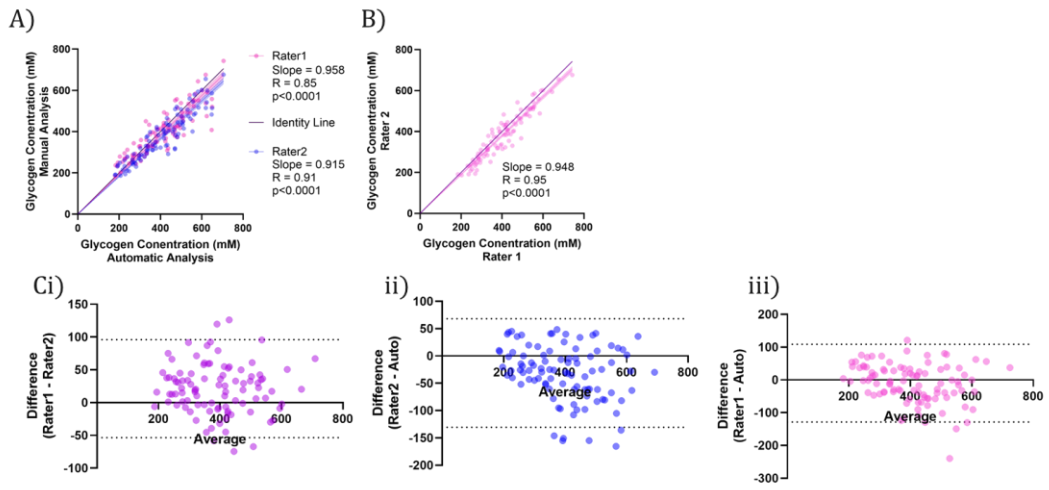

Figure 6.7 – A) Comparison of liver glycogen concentration measured by two raters to automatic analysis, Rater1 is shown in pink and Rater2 is shown in blue. B) comparison of Rater1 and Rater2 average liver glycogen concentrations for all measurements. For both identity line (purple) and line of best fit(s) plotted with intercept set to 0, shaded regions display 95% confidence bounds. C shows the bland-altmans for i) Rater1 and Rater2, ii) Rater2 and automatic analysis and iii) Rater1 and automatic analysis.

6.5 Discussion

This study investigated the repeatability and reproducibility of ^{13}C MRS (which offers the only non-invasive method to evaluate liver glycogen concentrations) in children.

6.5.1 Glycogen Concentrations

Fasted and fed liver glycogen concentrations measured in this study were larger than those found in a previous study in children by Matyka *et al.* (109) (180 - 538 mM compared to 120 - 203 Mm, respectively). However, it is hard to draw conclusions about the accuracy due to the low sample size (n = 6) and the small amount of literature on in vivo liver glycogen stores in children, which makes the expected range uncertain. ^{13}C MRS measurements in adults tend to differ across studies, and a similar variation may be expected here. This study used a longer TR than prior literature to study glycogen (TR = 280 ms compared to 150 ms previously) to ensure full relaxation of the signal. The discrepancy between this study's values for liver glycogen and previous literature in children may arise from conversion to absolute concentration, as the MR properties of the calibration phantom differ from liver tissue, causing systematic inaccuracies. This would explain why both raters and automatic analysis have high agreement (implying correct peak fitting) but disagree with the literature.

For healthy adults, literature values of liver glycogen fasted concentrations range from 146 mM up to 247 mM, and postprandial concentrations range from 170 mM to 375 mM using non-localised methods (106,131,139–141). Glycogen stores

decrease during fasted periods, with liver glycogen decreasing more rapidly than skeletal muscle. Awad *et al.* showed a 29% and 57% decrease in liver glycogen concentrations as measured with ^{13}C MRS after 12 and 24 hour fasts respectively, whilst no change was seen in calf muscle glycogen concentrations (142).

The difference between values quoted in this chapter and those quoted in Astrid *et al.* (123) are likely due to the bulk conversion factor used to obtain glycogen concentration in this chapter whilst the Astrid *et al.* used individual B_1 corrections for each subject. The discrepancy with literature does require further investigation, however, without liver biopsy data, the values of derived liver glycogen cannot be validated. Relative intra-subject changes and inter-subject variability remain accurate despite possible systematic shifts in liver glycogen concentration.

6.5.2 Subject Variability

Compliance with the MR protocol could be attributed to watching the video during the scan, as it may have prevented fidgeting from boredom. Showing a video during scanning also allowed the children to discuss their interests with researchers, which helped them feel more comfortable and relaxed in the new environment.

Intra-subject ICC values showed moderate agreement, with only one measure showing poor agreement (Rater1 T_{PM}), and variability was similar (21 ±2 %) for T_{PM} and T_{AM} across all raters. Reproducibility was better than that seen in adults for fasted measures (21% for this study compared to ~34% literature average) and worse for the post-tailored meal condition (21% for this study compared to 14% in

the literature). Tailored meals were consumed within a similar time frame before scanning in this study as literature. However, the caloric values and make-up varied considerably due to the energy requirements of subjects. Literature-tailored meals were 1/6 of the daily carbohydrate intake (50% of daily calorie intake); this study's tailored meals used mixed energy sources. Having a more varied, larger meal could have led to different eating patterns and gastric emptying, which may be the source of the larger variability seen in this study. However, the similarity in intra-subject reproducibility seen for T_{PM} and T_{AM} suggests that providing a tailored meal is adequate for ensuring reproducibility where an overnight fast may not be possible before ^{13}C MRS measurements.

The intra-subject ICC value for Rater1 T_{PM} was much lower than other measured despite the similar range seen on the boxplots. The heatmaps shown in Figure 6.8 display the larger standard deviations within participants measured by Rater1 for T_{PM} compared to T_{AM} despite the similar ranges in concentration.

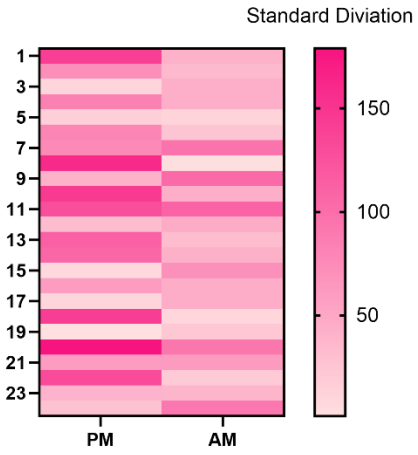

Figure 6.8 - Heatmap of standard deviations in Rater1's measurements for T_{PM} and T_{AM}

Inter-subject variations were similar to intra-subject variations, with values of inter-subject variations equal to or slightly larger than intra-subject variations, as expected.

Inter-subject reproducibility was similar across all time points and raters (23 ±3 %). No one rater had consistently larger values than another, suggesting that physiological differences between subjects may be the largest source of variability. It is not possible to compare inter-subject variation directly with inter-rater variations due to the different analysis methods. However, the intra-subject ICC values showed less agreement than the inter-rater ICC value, and intra-subject COV was smaller than inter-subject COV. From this, it can be reasoned that the effect of changing raters is smaller than the variability between subjects.

6.5.3 Rater Variability

Despite the complexity of the analysis, intra-rater ICC values display excellent agreement for Rater1 and Rater2 (0.93 and 0.99, respectively), demonstrating the robustness of the analysis method. The expertise of Rater2 compared to Rater1 is shown clearly in the data. Rater2 had a COV_{STD} less than half that of Rater1 (5% and 11%, respectively), displaying the need for adequate training and quality control measures. In a small field such as multinuclear MRS, there is a limited amount of people with the necessary expertise and time to write analysis packages, analyse data, train new raters, and quality check fits. This highlights the need for robust automatic analysis.

Across all analysers (Rater1, Rater2, and automatic analysis), the inter-rater ICC value (0.96) suggests excellent agreement. Although expertise is still needed to develop and adjust automatic analysis pipelines, it saves time and, in this study, produces similar results to manual analysis whilst removing the intra-rater variations.

The slopes in Figure 6.7 can also be used as an analogue for inter-rater agreement, with a slope of 1 implying perfect agreement between two raters. The closest agreement was seen between Rater1 and the automatic analysis (slope = 0.958, R = 0.85), followed by Rater1 with Rater2 (slope = 0.948, R = 0.95), and the least agreement was seen between Rater2 and automatic analysis (slope = 0.915, R = 0.91). Although Rater1 and automatic analysis show the highest level of agreement

when evaluating the slope of the line of best fit, this pairing also had the smallest R-value, showing a lower confidence level in the fit. This is likely due to the higher variability in the Liver glycogen values reported by Rater1.

6.5.4 Powering Future Studies

The measures of variability found in this study provide essential knowledge for designing future research in children. A sample size and a predicted effect size can be calculated from this data. For example, Kishore *et al.* investigated changes to liver glycogen following an overnight fast in both euglycemic (average blood sugar) and hypoglycaemia (low blood sugar) conditions for diabetic and healthy individuals. Participants attended a session following a 14 hour overnight fast; for the healthy individuals under euglycemic conditions, liver glycogen concentration dropped from 316 ± 14mM to 234 ± 10mM after a 120-minute fast and insulin and dextrose infusions, as measured using ^{13}C MRS (143). Based on this data, assuming a similar drop would be seen in children, a sample size of 5 would be needed to measure a statistically significant change (two-tail t-test, power = 0.8, alpha = 0.05, effective size = 2.08, calculated using G*Power). Power analysis on this study comparing T_{PM} and T_{AM} using a two-way matched pairs t-test would require a minimum sample size of 6 (assuming power = 0.8, alpha = 0.05, effective size = 1.63) i.e. you would need 6 children to get a statistically significant result when investigating the effects of an overnight fast on liver glycogen.

6.6 Conclusions

These novel MRS techniques must be made accessible to complex populations such as children. This study successfully showed the feasibility of using ^{13}C MRS to investigate liver glycogen stores in children robustly. The complete study (Astrid *et al.* (123)) showed that long fasting periods were tolerated in most cases, and the feasibility of measuring liver and muscle glycogen concentrations is critical to investigating metabolic disorders. Liver glycogen concentrations were higher than previously measured in literature for children but were not unreasonable when considered against the range of values measured in adults. Rater changes do introduce variations; however, these are minimal compared to intra-subject and inter-subject variations. Rater variations can be mitigated using automatic analysis, which showed consistent agreement with the raters. Overall, liver glycogen measurements in children were found to be reproducible across visits and raters.

7 Conclusion

This thesis optimises ^{1}H, ^{13}C and ^{31}P MRS measures and applies these methods alongside ^{1}H MRI for metabolic and functional approaches to study obesity with respect to bariatric surgery in adults and glycogen stores in children.

Chapter 3 provides one of the most comprehensive MR studies on bariatric surgery patients recorded, collecting multiparametric ^{1}H MRI and MRS data in the abdomen across their surgical journey. Measures were collected before treatment, following a Very-Low Calorie Diet (VLCD), which precedes surgery, and at 6 and 24 weeks post-surgery, and show significant changes across the surgical journey. Specifically, participants' liver, spleen and Subcutaneous Adipose Tissue (SAT) volume were shown to decrease throughout participation in the bariatric study, with significant reductions for each from baseline to 6 weeks post-surgery and from post-VLCD to 6 weeks post-surgery, whilst pancreas volume remained constant for the duration of participation. Changes in liver and spleen volume positively correlated with changes in their respective organ Fat Fraction (FF). Liver FF was measured using MRI (FF_{MRI}) and MRS (FF_{MRS}), with measures generally showing good agreement, although a bias was seen with FF_{MRI} overestimating FF < 10%. For the liver, a significant decrease in FF was shown between all timepoints (excluding FF_{MRS} from post-VLCD to 6 weeks post-surgery). Splenic FF_{MRI} decreased significantly from baseline and post-VLCD to 6 and 24 weeks post-surgery. Change in organ volume significantly correlated with BMI (for liver and SAT) and BSA (for liver, spleen, and SAT). The change in FF

significantly correlated with BMI (for liver, spleen, pancreas and SAT) and BSA (for liver, spleen and SAT).

Data from Chapter 3 also highlighted inter-dependencies in MRI measures. Liver FF (MRI and MRS) positively correlated with liver T_1 MOLLI, with a significant decrease in liver T_1 MOLLI from baseline and post-VLCD to 6 and 24 weeks post-surgery. Prior work has shown the dependence of liver T_1 MOLLI on FF, and in future work the liver T_1 MOLLI measures will be compared to the accompanying fat-suppressed inversion recovery spin-echo echo-planar T_1 measures collected in Arm A participants to determine if the changes seen are purely related to the influence of fat on the MOLLI readout, or whether additional inflammation is present which reduces across the study visits. Secondly, as the BMI and BSA of patients changed it was clear to see a negative correlation with the delivered B_1 (with the nominal B_1 field increasing across the study as participants BSA and BMI decreased). This is particularly important to quantitative MR measures, which, if not accounted for, can lead to alterations in metrics such as relaxometry. For example, here a significant correlation of organ T_2 with B_1, with higher (over-estimation) T_2 at lower B_1 due to stimulated echo effects, highlighting the need to correct for B_1 in future planned analysis.

Future work will analyse the remaining data collected in this bariatric study to evaluate if any changes occur in kidney T_1 and T_2* measures associated with renal inflammation and oxygenation changes in bariatric patients, as well as to determine whether cardiac output is altered data. On completion of the study, differences

between the two (Roux-en-Y Gastric Bypass and Sleeve Gastrectomy) surgical groups will be assessed, though this comparison may be limited by the small number of Roux-en-Y Gastric Bypass (n = 6) compared to Sleeve Gastrectomy (n = 11). On completion of blood analysis, MRI and MRS data will be compared to measures of blood glucose, Plasma GLP-1, GIP, Ghrelin and Bile Acids, C-Peptide and Insulin which may give valuable insight into the mechanisms behind diabetic remission.

In Chapter 4, the effect of block and Half-Passage Hyperbolic Secant (HPHS) RF excitation pulses for liver MRS acquisitions using a single-loop surface coil were described. Simulations were performed to evaluate the expected received signal of non-localised acquisitions and a 1D ISIS in a liver for ^{31}P; similar trends were found for empirical data from phantoms and *in vivo* measurements of SNR with distance. Block pulses were found to be robust and practical for *in vivo* use in liver spectroscopy and, hence, were used in the two intervention studies. Results from the ^{31}P MRS IPE intervention study showed no significant changes in the exchange constant (k), ATP forward Flux or inorganic phosphate (Pi) concentration before and after consuming IPE. Variations in k and ATP flux were seen across individuals, and future work will assess the correlation of the ^{31}P MRS results with blood measures of IPE. For the bariatric study, a significant increase in Pi concentration was seen after bariatric surgery, which has been previously linked to insulin sensitivity. However, saturation failed, and it was not possible to measure the k or forward flux. Future work should be aimed at developing a tool to provide the optimum saturation pulse amplitude for groups with different SAT thicknesses.

Chapter 5 explores the impact of free-breathing on the line broadening of ^{1}H liver MRS acquisitions; this is of importance to multinuclear liver MRS which must be collected free breathing due to its lower SNR requiring many signal averages as to be collected in a given time period. Using free breathing ^{1}H liver MRS, shifts in the water peak's central frequency (f_{peak}), Full-Width Half Maximum (FWHM) and amplitude were evaluated and compared to shifts measured using dynamic imaging. Frequency shifts due to respiration were shown to range from 0.08 to 0.24 ppm (10 – 31 Hz), a level which could also cause significant line broadening altering peak shapes in ^{13}C and ^{31}P spectra. For example, in Chapter 6, initial estimates of Gaussian linewidths of ^{13}C glycogen peaks were 0.2 ppm, within the level of the respiratory changes reported. This respiratory shift is also relevant to the ^{31}P MRS data collected in the bariatric surgery study which used a saturation pulse width of 20 Hz, (0.38 ppm). It is possible that if the saturation pulse is not targeting the central frequency of the chosen peak well, then during respiration the target peak will move out of the saturation window reducing its efficiency. Future work should explore the effects of respiration on the efficiency of such saturation transfer experiments. Future work using ^{1}H and multinuclear MRS should explore binning the data into inspiration and expiration phases using the respiratory cycle trace, since averaging within bins to improve SNR should provide sufficient SNR to perform peak alignment across bins before averaging inspiration and expiration data. If proven, this method could then be implemented into the automatic MRS analysis pipeline shown in Chapter 6.

Chapter 6 studies the reproducibility of ^{13}C liver glycogen stores in healthy children. Data for liver glycogen concentrations post-tailored meal and post-overnight fast from two visits were evaluated by two raters and an automatic analysis pipeline. Intra-subject reproducibility was similar to previous literature on adults and was better for fasted measures than post-tailored meals. Inter-subject variations were similar across raters, implying that the driving force for this measure is the large variability across children's metabolism. There was excellent agreement of the automatic analysis with the two raters showing promise for of such automated analysis for future longitudinal studies or clinical applications.

Pre-clinical ^{13}C MRS studies have shown interesting differences in glycogen between healthy, diabetic and non-alcoholic fatty liver-diseased models, and it would be of interest to use the methods shown in this thesis study to investigate such liver glycogen storage in humans, as well as to study longitudinal changes in a similar way to the bariatric surgery intervention study performed in Chapter 3.

In summary, this thesis has demonstrated novel research into the standardisation of ^{1}H MRS and multinuclear MRS acquisition and analysis measures, including the study of the effects of varying B_0 and B_1 fields on measures. MRS measures have been applied together with imaging at a system level to study obesity. This represents the first step in making multinuclear MRS a clinically viable tool for understanding metabolism.

8 References

1. Obesity [Internet]. [cited 2024 Aug 26]. Available from: https://www.who.int/health-topics/obesity#tab=tab_1

2. Kalra A, Yetiskul E, Wehrle CJ, Tuma F. Physiology, Liver. StatPearls [Internet]. 2023 May 1 [cited 2024 Aug 19]; Available from: https://www.ncbi.nlm.nih.gov/books/NBK535438/

3. Gong J, Tu W, Liu J, Tian D. Hepatocytes: A key role in liver inflammation. Front Immunol [Internet]. 2022 [cited 2024 Aug 19];13. Available from: /pmc/articles/PMC9890163/

4. Karpińska M, Czauderna M. Pancreas—Its Functions, Disorders, and Physiological Impact on the Mammals' Organism. Front Physiol [Internet]. 2022 Mar 30 [cited 2024 Aug 19];13. Available from: /pmc/articles/PMC9005876/

5. Spleen: Function, Location & Size, Possible Problems [Internet]. [cited 2024 Aug 26]. Available from: https://my.clevelandclinic.org/health/body/21567-spleen

6. Mebius RE, Kraal G. Structure and function of the spleen. Nature Reviews Immunology 2005 5:8 [Internet]. 2005 Aug [cited 2024 Aug 26];5(8):606–16. Available from: https://www.nature.com/articles/nri1669

7. Diabetes [Internet]. [cited 2024 Aug 20]. Available from: https://www.who.int/news-room/fact-sheets/detail/diabetes

8. Eyth E, Naik R. Hemoglobin A1C. Laboratory Screening and Diagnostic Evaluation: An Evidence-Based Approach [Internet]. 2023 Mar 13 [cited 2024 Aug 20];403–8. Available from: https://www.ncbi.nlm.nih.gov/books/NBK549816/

9. Galicia-Garcia U, Benito-Vicente A, Jebari S, Larrea-Sebal A, Siddiqi H, Uribe KB, et al. Pathophysiology of Type 2 Diabetes Mellitus. Int J Mol Sci [Internet]. 2020 Sep 1 [cited 2024 Aug 20];21(17):1–34. Available from: /pmc/articles/PMC7503727/

10. Defronzo RA. Banting Lecture. From the triumvirate to the ominous octet: a new paradigm for the treatment of type 2 diabetes mellitus. Diabetes [Internet]. 2009 Apr [cited 2024 Aug 20];58(4):773–95. Available from: https://pubmed.ncbi.nlm.nih.gov/19336687/

11. Strasser B. Physical activity in obesity and metabolic syndrome. Ann N Y Acad Sci [Internet]. 2013 [cited 2024 Aug 20];1281(1):141. Available from: /pmc/articles/PMC3715111/

12. 3 Tesla Philips Achieva MRI Scanner - The University of Nottingham [Internet]. [cited 2024 Sep 3]. Available from: https://www.nottingham.ac.uk/research/groups/spmic/facilities/3-tesla-philips-achieva-mri-scanner.aspx

13. 3 Tesla Philips Ingenia Wide Bore MRI Scanner - The University of Nottingham [Internet]. [cited 2024 Sep 3]. Available from: https://www.nottingham.ac.uk/research/groups/spmic/facilities/3-tesla-philips-ingenia-wide-bore-mri-scanner.aspx

14. Robin A de Graaf. in vivo NMR Spectroscopy Principles and Techniques. Third. Wiley; 2019. 253–279 p.

15. De Bazelaire CMJ, Duhamel GD, Rofsky NM, Alsop DC. MR Imaging Relaxation Times of Abdominal and Pelvic Tissues Measured in Vivo at 3.0 T: Preliminary Results. Radiology [Internet]. 2004 Mar 1 [cited 2024 Dec 4];230(3):652–9. Available from: https://pubs.rsna.org/doi/10.1148/radiol.2303021331

16. Mansfield P, Grannell PK. NMR “diffraction” in solids? Journal of Physics C: Solid State Phys. 1973 Nov;6:422–6.

17. Valkovič L, Chmelík M, Krššák M. In-vivo 31P-MRS of skeletal muscle and liver: A way for non-invasive assessment of their metabolism. Anal Biochem. 2017;529(January):193–215.

18. Schmid AI, Chmelík M, Szendroedi J, Krššák M, Brehm A, Moser E, et al. Quantitative ATP synthesis in human liver measured by localized 31P spectroscopy using the magnetization transfer experiment. NMR Biomed. 2008 Jun;21(5):437–43.

19. Chen C, Stephenson MC, Peters A, Morris PG, Francis ST, Gowland PA. 31P magnetization transfer magnetic resonance spectroscopy: Assessing the activation induced change in cerebral ATP metabolic rates at 3 T. Magn Reson Med. 2018;79(1):22–30.

20. Kingsley PB, Monahan WG. Correcting for Incomplete Saturation and Off-Resonance Effects in Multiple-Site Saturation-Transfer Kinetic Measurements. Journal of Magnetic Resonance. 2000;146(1):100–9.

21. Schmid AI, Chmelík M, Szendroedi J, Krššák M, Brehm A, Moser E, et al. Quantitative ATP synthesis in human liver measured by localized 31P spectroscopy using the magnetization transfer experiment. NMR Biomed [Internet]. 2008 Jun [cited 2022 Nov 7];21(5):437–43. Available from: https://pubmed.ncbi.nlm.nih.gov/17910026/

22. Tannús A, Garwood M. Adiabatic Pulses. NMR in Biomed [Internet]. 1997 [cited 2024 Aug 19];10:423–34. Available from: https://analyticalsciencejournals.onlinelibrary.wiley.com/doi/10.1002/

23. Romeijn MM, Kolen AM, Holthuijsen DDB, Janssen L, Schep G, Leclercq WKG, et al. Effectiveness of a Low-Calorie Diet for Liver Volume Reduction Prior to Bariatric Surgery: a Systematic Review. Obes Surg [Internet]. 2021 Jan 1 [cited 2024 Feb 12];31(1):350–6. Available from: https://link.springer.com/article/10.1007/s11695-020-05070-6

24. Holderbaum M, Casagrande DS, Sussenbach S, Buss C. Effects of very low calorie diets on liver size and weight loss in the preoperative period of bariatric surgery: a systematic review. Surgery for Obesity and Related Diseases. 2018 Feb 1;14(2):237–44.

25. Serafim MP, Santo MA, Gadducci AV, Scabim VM, Cecconello I, de Cleva R. Very low-calorie diet in candidates for bariatric surgery: change in body composition during rapid weight loss. Clinics [Internet]. 2019 [cited 2024 Feb 12];74. Available from: /pmc/articles/PMC6399661/

26. Chakravartty S, Vivian G, Mullholland N, Shaikh H, McGrath J, Sidhu PS, et al. Preoperative liver shrinking diet for bariatric surgery may impact wound healing: a

randomized controlled trial. Surg Obes Relat Dis [Internet]. 2019 Jan 1 [cited 2024 Feb 12];15(1):117–25. Available from: https://pubmed.ncbi.nlm.nih.gov/30471928/

27. Pre bariatric surgery diet Information for patients.

28. Jackness C, Karmally W, Febres G, Conwell IM, Ahmed L, Bessler M, et al. Very lowcalorie diet mimics the early beneficial effect of rouxen-Y gastric bypass on insulin sensitivity and β-cell function in type 2 diabetic patients. Diabetes. 2013 Sep;62(9):3027–32.

29. Lewis MC, Phillips ML, Slavotinek JP, Kow L, Thompson CH, Toouli J. Change in liver size and fat content after treatment with Optifast® very low calorie diet. Obes Surg. 2006 Jun;16(6):697–701.

30. Larson-Meyer DE, Heilbronn LK, Redman LM, Newcomer BR, Frisard MI, Anton S, et al. Effect of Calorie Restriction With or Without Exercise on Insulin Sensitivity, β-Cell Function, Fat Cell Size, and Ectopic Lipid in Overweight Subjects. Diabetes Care [Internet]. 2006 Jun 1 [cited 2024 Feb 12];29(6):1337–44. Available from: https://dx.doi.org/10.2337/dc05-2565

31. Lim EL, Hollingsworth KG, Aribisala BS, Chen MJ, Mathers JC, Taylor R. Reversal of type 2 diabetes: Normalisation of beta cell function in association with decreased pancreas and liver triacylglycerol. Diabetologia [Internet]. 2011 Oct 9 [cited 2024 Feb 12];54(10):2506–14. Available from: https://link.springer.com/article/10.1007/s00125-011-2204-7

32. Al-Mrabeh A, Hollingsworth KG, Steven S, Tiniakos D, Taylor R. Quantification of intrapancreatic fat in type 2 diabetes by MRI. PLoS One [Internet]. 2017 Mar 1 [cited 2024 Feb 12];12(4):e0174660. Available from: https://journals.plos.org/plosone/article?id=10.1371/journal.pone.0174660

33. Taylor R. Calorie restriction for long-term remission of type 2 diabetes. Vol. 19, Clinical Medicine, Journal of the Royal College of Physicians of London. Royal College of Physicians; 2019. p. 37–42.

34. Juray S, Axen K V, Trasino SE, Martínez-Hervás S, González-Navarro H. Remission of Type 2 Diabetes with Very Low-Calorie Diets—A Narrative Review. Nutrients 2021, Vol 13, Page 2086 [Internet]. 2021 Jun 18 [cited 2023 Nov 7];13(6):2086. Available from: https://www.mdpi.com/2072-6643/13/6/2086/htm

35. Steven S, Hollingsworth KG, Al-Mrabeh A, Avery L, Aribisala B, Caslake M, et al. Very Low-Calorie Diet and 6 Months of Weight Stability in Type 2 Diabetes: Pathophysiological Changes in Responders and Nonresponders. Diabetes Care [Internet]. 2016 May 1 [cited 2023 Nov 7];39(5):808–15. Available from: https://dx.doi.org/10.2337/dc15-1942

36. Vijan S, Stuart NS, Fitzgerald JT, Ronis DL, Hayward RA, Slater S, et al. Barriers to following dietary recommendations in Type 2 diabetes. Diabetic Medicine [Internet]. 2005 Jan 1 [cited 2024 Feb 12];22(1):32–8. Available from: https://onlinelibrary.wiley.com/doi/full/10.1111/j.1464-5491.2004.01342.x

37. Mullally JA, Febres GJ, Bessler M, Korner J. Sleeve Gastrectomy and Roux-en-Y Gastric Bypass Achieve Similar Early Improvements in Beta-cell Function in Obese

Patients with Type 2 Diabetes. Scientific Reports 2019 9:1 [Internet]. 2019 Feb 12 [cited 2024 Feb 12];9(1):1–7. Available from: https://www.nature.com/articles/s41598-018-38283-y

38. Peltonen M. Balancing risks and benefits of bariatric surgery for type 2 diabetes. Vol. 3, The Lancet Diabetes and Endocrinology. Lancet Publishing Group; 2015. p. 394–5.

39. Ikramuddin S, Billington CJ, Lee WJ, Bantle JP, Thomas AJ, Connett JE, et al. Roux-en-Y gastric bypass for diabetes (the Diabetes Surgery Study): 2-year outcomes of a 5-year, randomised, controlled trial. Lancet Diabetes Endocrinol. 2015 Jun;3(6):413–22.

40. Hofsø D, Fatima F, Borgeraas H, Birkeland KI, Gulseth HL, Hertel JK, et al. Gastric bypass versus sleeve gastrectomy in patients with type 2 diabetes (Oseberg): a single-centre, triple-blind, randomised controlled trial. Lancet Diabetes Endocrinol. 2019 Dec;7(12):912–24.

41. Knop FK, Taylor R. Mechanism of Metabolic Advantages After Bariatric Surgery. care.diabetesjournals.org DIABETES CARE. 2013;36(2).

42. Pucci A, Batterham RL. Mechanisms underlying the weight loss effects of RYGB and SG: similar, yet different. J Endocrinol Invest [Internet]. 2019 Feb 4 [cited 2024 Feb 12];42(2):117–28. Available from: https://pubmed.ncbi.nlm.nih.gov/29730732/

43. Glucagon-like peptide 1 | You and Your Hormones from the Society for Endocrinology.

44. Hira T, Pinyo J, Hara H. What Is GLP-1 Really Doing in Obesity? Trends in Endocrinology and Metabolism. 2020 Feb;31(2):71–80.

45. Wickremesekera K, Miller G, DeSilva Naotunne T, Knowles G, Stubbs RS. Loss of insulin resistance after Roux-en-Y gastric bypass surgery: A time course study. Obes Surg [Internet]. 2005 Apr 1 [cited 2024 Feb 15];15(4):474–81. Available from: https://link.springer.com/article/10.1381/0960892053723402

46. Luo RB, Suzuki T, Hooker JC, Covarrubias Y, Schlein A, Liu S, et al. How bariatric surgery affects liver volume and fat density in NAFLD patients. Surg Endosc. 2018 Apr;32(4):1675–82.

47. Lim EL, Hollingsworth KG, Aribisala BS, Chen MJ, Mathers JC, Taylor R. Reversal of type 2 diabetes: Normalisation of beta cell function in association with decreased pancreas and liver triacylglycerol. Diabetologia. 2011 Oct;54(10):2506–14.

48. Honka H, Koffert J, Hannukainen JC, Tuulari JJ, Karlsson HK, Immonen H, et al. The Effects of Bariatric Surgery on Pancreatic Lipid Metabolism and Blood Flow. J Clin Endocrinol Metab. 2015 May;100(5):2015–23.

49. Lehmann S, Linder N, Retschlag U, Schaudinn A, Stange R, Garnov N, et al. MRI assessment of changes in adipose tissue parameters after bariatric surgery. PLoS One [Internet]. 2018 Nov 1 [cited 2024 Feb 22];13(11):e0206735. Available from: https://journals.plos.org/plosone/article?id=10.1371/journal.pone.0206735

50. Hedderich DM, Hasenberg T, Haneder S, Schoenberg SO, Kücükoglu Ö, Canbay A, et al. Effects of Bariatric Surgery on Non-alcoholic Fatty Liver Disease: Magnetic

Resonance Imaging Is an Effective, Non-invasive Method to Evaluate Changes in the Liver Fat Fraction. Obes Surg [Internet]. 2017 Jul 1 [cited 2024 Feb 22];27(7):1755–62. Available from: https://link.springer.com/article/10.1007/s11695-016-2531-3

51. Meyer-Gerspach AC, Peterli R, Moor M, Madörin P, Schötzau A, Nabers D, et al. Quantification of Liver, Subcutaneous, and Visceral Adipose Tissues by MRI Before and After Bariatric Surgery. Obes Surg [Internet]. 2019 Sep 15 [cited 2024 Feb 16];29(9):2795–805. Available from: https://pubmed.ncbi.nlm.nih.gov/31089967/

52. Hui SCN, Wong SKH, Ai Q, Yeung DKW, Ng EKW, Chu WCW. Observed changes in brown, white, hepatic and pancreatic fat after bariatric surgery: Evaluation with MRI. Eur Radiol [Internet]. 2019 Feb 1 [cited 2024 Jul 7];29(2):849–56. Available from: https://pubmed.ncbi.nlm.nih.gov/30062524/

53. Li S, Zhang P, Di J, Han X, Tu Y, Yang D, et al. Associations of change in body fat percentage with baseline body composition and diabetes remission after bariatric surgery. Obesity. 2024 May 1;32(5):871–87.

54. Tan HC, Shumbayawonda E, Beyer C, Cheng LTE, Low A, Lim CH, et al. Multiparametric Magnetic Resonance Imaging and Magnetic Resonance Elastography to Evaluate the Early Effects of Bariatric Surgery on Nonalcoholic Fatty Liver Disease. Int J Biomed Imaging [Internet]. 2023 Jan 1 [cited 2024 Jul 7];2023(1):4228321. Available from: https://onlinelibrary.wiley.com/doi/full/10.1155/2023/4228321

55. Chiyanika C, Hui SCN, Sin DMC, Shumbayawonda E, Wong SKH, Ng EKW, et al. The effectiveness of magnetic resonance imaging (MRI) iron corrected T1 in monitoring

metabolic dysfunction-associated steatohepatitis in obesity following bariatric surgery and lifestyle modification: a prospective cohort study. Quant Imaging Med Surg [Internet]. 2024 Jul 1 [cited 2024 Jul 7];14(7):4659674–4654674. Available from: https://qims.amegroups.org/article/view/124854/html

56. Luo RB, Suzuki T, Hooker JC, Covarrubias Y, Schlein A, Liu S, et al. How bariatric surgery affects liver volume and fat density in NAFLD patients. Surg Endosc [Internet]. 2018 Apr 1 [cited 2021 Jan 19];32(4):1675–82. Available from: https://doi.org/10.1007/s00464-017-5846-9

57. Bai L, Ma M, Lin M, Cai S, Mo X, Liu G, et al. Abdominal magnetic resonance imaging assessment and quantification of pancreatic and liver adipose tissues in obesity before and after laparoscopic sleeve gastrectomy. J Radiat Res Appl Sci. 2023 Sep 1;16(3):100609.

58. Tang A, Tan J, Sun M, Hamilton G, Bydder M, Wolfson T, et al. Nonalcoholic fatty liver disease: MR imaging of liver proton density fat fraction to assess hepatic steatosis. Radiology [Internet]. 2013 May 1 [cited 2023 Nov 7];267(2):422–31. Available from: https://pubs.rsna.org/doi/10.1148/radiol.12120896

59. Michel S, Linder N, Eggebrecht T, Schaudinn A, Blüher M, Dietrich A, et al. Abdominal subcutaneous fat quantification in obese patients from limited field-of-view MRI data. Scientific Reports 2020 10:1 [Internet]. 2020 Nov 4 [cited 2024 Feb 16];10(1):1–7. Available from: https://www.nature.com/articles/s41598-020-75985-8

60. Chemical shift artifact - Questions and Answers in MRI [Internet]. [cited 2024 Jul 22]. Available from: https://mriquestions.com/chemical-shift-artifact.html

61. Dixon WT. Simple proton spectroscopic imaging. https://doi.org/101148/radiology15316089263 [Internet]. 1984 Oct 1 [cited 2024 Jul 22];153(1):189–94. Available from: https://pubs.rsna.org/doi/10.1148/radiology.153.1.6089263

62. Mozes FE, Tunnicliffe EM, Pavlides M, Robson MD. Influence of fat on liver T1 measurements using modified Look–Locker inversion recovery (MOLLI) methods at 3T. Journal of Magnetic Resonance Imaging [Internet]. 2016 Jul 1 [cited 2023 Nov 7];44(1):105–11. Available from: https://onlinelibrary.wiley.com/doi/full/10.1002/jmri.25146

63. Bencikova D, Han F, Kannengieser S, Raudner M, Poetter-Lang S, Bastati N, et al. Evaluation of a single-breath-hold radial turbo-spin-echo sequence for T2 mapping of the liver at 3T. Eur Radiol [Internet]. 2022 May 1 [cited 2024 Jul 22];32(5):3388–97. Available from: https://link.springer.com/article/10.1007/s00330-021-08439-y

64. Deng J, Larson AC. Modified PROPELLER approach for T2-mapping of the abdomen. Magn Reson Med [Internet]. 2009 Jun 1 [cited 2024 Jul 22];61(6):1269–78. Available from: https://onlinelibrary.wiley.com/doi/full/10.1002/mrm.21989

65. Vietti Violi N, Hilbert T, Bastiaansen JAM, Knebel JF, Ledoux JB, Stemmer A, et al. Patient respiratory-triggered quantitative T2 mapping in the pancreas. Journal of Magnetic Resonance Imaging [Internet]. 2019 Aug 1 [cited 2024 Jul 22];50(2):410–6. Available from: https://onlinelibrary.wiley.com/doi/full/10.1002/jmri.26612

66. Lin X, Dai L, Yang Q, Yang Q, He H, Ma L, et al. Free-breathing and instantaneous abdominal T2 mapping via single-shot multiple overlapping-echo acquisition and deep learning reconstruction. Eur Radiol [Internet]. 2023 Jul 1 [cited 2024 Jul 22];33(7):4938–48. Available from: https://link.springer.com/article/10.1007/s00330-023-09417-2

67. Nehrke K, Börnert P. DREAM—a novel approach for robust, ultrafast, multislice B1 mapping. Magn Reson Med [Internet]. 2012 Nov 1 [cited 2024 Jul 29];68(5):1517–26. Available from: https://onlinelibrary.wiley.com/doi/full/10.1002/mrm.24158

68. Singh RG, Yoon HD, Wu LM, Lu J, Plank LD, Petrov MS. Ectopic fat accumulation in the pancreas and its clinical relevance: A systematic review, meta-analysis, and meta-regression. Metabolism. 2017 Apr 1;69:1–13.

69. Au WY, Lam WWM, Chu W, Tam S, Wong WK, Liang R, et al. A T2* magnetic resonance imaging study of pancreatic iron overload in thalassemia major. Haematologica [Internet]. 2008 Jan 1 [cited 2024 Jul 29];93(1):116–9. Available from: https://haematologica.org/article/view/4694

70. Kosaryan M, Rahimi M, Darvishi-Khezri H, Gholizadeh N, Akbarzadeh R, Aliasgharian A. Correlation of Pancreatic Iron Overload Measured by T2*-Weighted Magnetic Resonance Imaging in Diabetic Patients with β-Thalassemia Major. Hemoglobin [Internet]. 2017 May 4 [cited 2024 Jul 29];41(3):151–6. Available from: https://www.tandfonline.com/doi/abs/10.1080/03630269.2017.1340306

71. Noda Y, Goshima S, Tsuji Y, Kajita K, Akamine Y, Kawai N, et al. Pancreatic extracellular volume fraction using T1 mapping in patients with impaired glucose

intolerance. Abdominal Radiology [Internet]. 2020 Feb 1 [cited 2024 Jul 29];45(2):449–56. Available from: https://link.springer.com/article/10.1007/s00261-019-02384-7

72. Li X, Yang Q, Ye H, Li S, Wang Y, Yu W. Comparison of pancreatic fat content measured by different methods employing MR mDixon sequence. PLoS One [Internet]. 2021 Nov 1 [cited 2024 Jul 29];16(11):e0260001. Available from: https://journals.plos.org/plosone/article?id=10.1371/journal.pone.0260001

73. Li H, Daniel AJ, Buchanan CE, Nery F, Morris DM, Li S, et al. Improvements in Between-Vendor MRI Harmonization of Renal T2 Mapping using Stimulated Echo Compensation. J Magn Reson Imaging [Internet]. 2024 [cited 2024 Jul 29]; Available from: https://pubmed.ncbi.nlm.nih.gov/38380700/

74. Liu P, Song Y, Zhen W, Jiang G. Intravoxel incoherent motion diffusion-weighted imaging (IVIM-DWI) of pancreas for assessment of β-cell dysfunction in hyperglycemia. In: ISMRM annual meeting [Internet]. 2024 [cited 2024 Jul 29]. Available from: https://submissions.mirasmart.com/ISMRM2024/Itinerary/PresentationDetail.aspx?evdid=1363

75. Tirosh A, Calay ES, Tuncman G, Claiborn KC, Inouye KE, Eguchi K, et al. The short-chain fatty acid propionate increases glucagon and FABP4 production, impairing insulin action in mice and humans. Sci Transl Med. 2019 Apr 24;11(489).

76. Weitkunat K, Schumann S, Nickel D, Kappo KA, Petzke KJ, Kipp AP, et al. Importance of propionate for the repression of hepatic lipogenesis and improvement of insulin

sensitivity in high-fat diet-induced obesity. Mol Nutr Food Res. 2016 Dec 1;60(12):2611–21.

77. Byrne CS, Chambers ES, Preston T, Tedford C, Brignardello J, Garcia-Perez I, et al. Effects of Inulin Propionate Ester Incorporated into Palatable Food Products on Appetite and Resting Energy Expenditure: A Randomised Crossover Study. Nutrients 2019, Vol 11, Page 861 [Internet]. 2019 Apr 16 [cited 2023 Mar 2];11(4):861. Available from: https://www.mdpi.com/2072-6643/11/4/861/htm

78. Nishina PM, Freedland RA. Effects of propionate on lipid biosynthesis in isolated rat hepatocytes. Journal of Nutrition. 1990;120(7):668–73.

79. Salem V, Demetriou L, Behary P, Alexiadou K, Scholtz S, Tharakan G, et al. Weight Loss by Low-Calorie Diet Versus Gastric Bypass Surgery in People With Diabetes Results in Divergent Brain Activation Patterns: A Functional MRI Study. Diabetes Care [Internet]. 2021 Aug 1 [cited 2024 Feb 12];44(8):1842. Available from: /pmc/articles/PMC8385466/

80. Szendroedi J, Chmelik M, Schmid AI, Nowotny P, Brehm A, Krssak M, et al. Abnormal hepatic energy homeostasis in type 2 diabetes. Hepatology [Internet]. 2009 Oct 1 [cited 2024 Mar 6];50(4):1079–86. Available from: https://onlinelibrary.wiley.com/doi/full/10.1002/hep.23093

81. Kupriyanova Y, Zaharia OP, Bobrov P, Karusheva Y, Burkart V, Szendroedi J, et al. Early changes in hepatic energy metabolism and lipid content in recent-onset type 1 and 2 diabetes mellitus. J Hepatol. 2021 May 1;74(5):1028–37.

82. Schmid AI, Szendroedi J, Chmelik M, Krššák M, Moser E, Roden M. Liver ATP Synthesis Is Lower and Relates to Insulin Sensitivity in Patients With Type 2 Diabetes. Diabetes Care [Internet]. 2011 Feb 1 [cited 2024 Jun 12];34(2):448–53. Available from: https://dx.doi.org/10.2337/dc10-1076

83. Obesity - NHS [Internet]. [cited 2024 Aug 4]. Available from: https://www.nhs.uk/conditions/obesity/

84. Nadeem B, Bacha R, Gilani SA. Correlation of Subcutaneous Fat Measured on Ultrasound with Body Mass Index. J Med Ultrasound [Internet]. 2018 Oct 1 [cited 2022 Jul 12];26(4):205. Available from: /pmc/articles/PMC6314101/

85. Solga SF, Horska A, Hemker S, Crawford S, Diggs C, Diehl AM, et al. Hepatic fat and adenosine triphosphate measurement in overweight and obese adults using 1H and 31P magnetic resonance spectroscopy. Liver International [Internet]. 2008 May 1 [cited 2024 Mar 5];28(5):675–81. Available from: https://onlinelibrary.wiley.com/doi/full/10.1111/j.1478-3231.2008.01705.x

86. Idris I. BMI of Surgery Patients. 2021.

87. Schneider CA, Rasband WS, Eliceiri KW. NIH Image to ImageJ: 25 years of image analysis. Nature Methods 2012 9:7 [Internet]. 2012 Jun 28 [cited 2022 Jul 15];9(7):671–5. Available from: https://www.nature.com/articles/nmeth.2089

88. Valkovič L, Gajdošík M, Traussnigg S, Wolf P, Chmelík M, Kienbacher C, et al. Application of localized 31P MRS saturation transfer at 7 T for measurement of ATP metabolism in the liver: Reproducibility and initial clinical application in patients

with non-alcoholic fatty liver disease. Eur Radiol [Internet]. 2014 Mar 20 [cited 2024 Jun 12];24(7):1602–9. Available from: https://link.springer.com/article/10.1007/s00330-014-3141-x

89. Traussnigg S, Kienbacher C, Gajdošík M, Valkovič L, Halilbasic E, Stift J, et al. Ultra-high-field magnetic resonance spectroscopy in non-alcoholic fatty liver disease: Novel mechanistic and diagnostic insights of energy metabolism in non-alcoholic steatohepatitis and advanced fibrosis. Liver International [Internet]. 2017 Oct 1 [cited 2024 Jun 10];37(10):1544–53. Available from: https://onlinelibrary.wiley.com/doi/full/10.1111/liv.13451

90. Receive only MR coils - Questions and Answers in MRI [Internet]. [cited 2022 Jul 12]. Available from: https://mriquestions.com/receive-only-coils.html

91. PulseTeq: Surface X-Nuclei RF Coils for Human MRI [Internet]. [cited 2024 Jun 10]. Available from: https://www.pulseteq.com/human/surface-coils/loop-coils/

92. Explore the Philips products [Internet]. [cited 2024 Jun 10]. Available from: https://www.philips.co.uk/healthcare/solutions/magnetic-resonance/coils-overview/coils-overview

93. Schmid AI, Szendroedi J, Chmelik M, Krššák M, Moser E, Roden M. Liver ATP Synthesis Is Lower and Relates to Insulin Sensitivity in Patients With Type 2 Diabetes. Diabetes Care [Internet]. 2011 Feb 1 [cited 2024 Jun 12];34(2):448–53. Available from: https://dx.doi.org/10.2337/dc10-1076

94. Bendall MR, Pegg DT. Uniform sample excitation with surface coils for in vivo spectroscopy by adiabatic rapid half passage. Journal of Magnetic Resonance (1969). 1986 Apr 1;67(2):376–81.

95. Moyher SE, Vigneron DB, Nelson SJ. Surface coil MR imaging of the human brain with an analytic reception profile correction. Journal of Magnetic Resonance Imaging [Internet]. 1995 Mar 1 [cited 2024 Sep 19];5(2):139–44. Available from: https://onlinelibrary.wiley.com/doi/full/10.1002/jmri.1880050204

96. Horstman AM, Bawden SJ, Spicer A, Darwish N, Goyer A, Egli L, et al. Liver glycogen stores via 13C magnetic resonance spectroscopy in healthy children: randomized, controlled study. Am J Clin Nutr. 2023 Apr 1;117(4):709–16.

97. Stephenson MC, Leverton E, Khoo EYH, Poucher SM, Johansson L, Lockton JA, et al. Variability in fasting lipid and glycogen contents in hepatic and skeletal muscle tissue in subjects with and without type 2 diabetes: a 1H and 13C MRS study. NMR Biomed [Internet]. 2013 Nov 1 [cited 2023 Dec 13];26(11):1518–26. Available from: https://onlinelibrary.wiley.com/doi/full/10.1002/nbm.2985

98. Hoult DI. The principle of reciprocity. J Magn Reson [Internet]. 2011 Dec [cited 2024 Sep 24];213(2):344–6. Available from: https://pubmed.ncbi.nlm.nih.gov/21889377/

99. Naressi A, Couturier C, Devos JM, Janssen M, Mangeat C, Beer R de, et al. Java-based graphical user interface for the MRUI quantitation package. Magnetic Resonance Materials in Physics, Biology and Medicine 2001 12:2 [Internet]. 2001 Jun [cited 2024 Sep 2];12(2):141–52. Available from: https://link.springer.com/article/10.1007/BF02668096

100. Stefan D, Cesare F Di, Andrasescu A, Popa E, Lazariev A, Vescovo E, et al. Quantitation of magnetic resonance spectroscopy signals: the jMRUI software package. Meas Sci Technol [Internet]. 2009 Sep 4 [cited 2024 Sep 2];20(10):104035. Available from: https://iopscience.iop.org/article/10.1088/0957-0233/20/10/104035

101. jMRUI | Software for the clinical and biomedical MRS [Internet]. [cited 2024 Sep 2]. Available from: http://www.jmrui.eu/

102. Vanhamme L, Van Den Boogaart A, Van Huffel S. Improved Method for Accurate and Efficient Quantification of MRS Data with Use of Prior Knowledge. Journal of Magnetic Resonance. 1997 Nov 1;129(1):35–43.

103. Wolf DC. Evaluation of the Size, Shape, and Consistency of the Liver. Clinical Methods: The History, Physical, and Laboratory Examinations [Internet]. 1990 [cited 2024 Jun 9]; Available from: https://www.ncbi.nlm.nih.gov/books/NBK421/

104. Holcombe SA, Kang YS, Derstine BA, Wang SC, Agnew AM. Regional maps of rib cortical bone thickness and cross-sectional geometry. J Anat [Internet]. 2019 Nov 1 [cited 2024 Jun 9];235(5):883. Available from: /pmc/articles/PMC6794212/

105. Polyviou T, MacDougall K, Chambers ES, Viardot A, Psichas A, Jawaid S, et al. Randomised clinical study: inulin short-chain fatty acid esters for targeted delivery of short-chain fatty acids to the human colon. Aliment Pharmacol Ther. 2016 Oct 1;44(7):662–72.

106. Buehler T, Bally L, Dokumaci AS, Stettler C, Boesch C. Methodological and physiological test–retest reliability of 13C-MRS glycogen measurements in liver and in skeletal muscle of patients with type 1 diabetes and matched healthy controls. NMR Biomed [Internet]. 2016 Jun 1 [cited 2023 Dec 13];29(6):796–805. Available from: https://onlinelibrary.wiley.com/doi/full/10.1002/nbm.3531

107. Stephenson MC, Leverton E, Khoo EYH, Poucher SM, Johansson L, Lockton JA, et al. Variability in fasting lipid and glycogen contents in hepatic and skeletal muscle tissue in subjects with and without type 2 diabetes: a 1H and 13C MRS study. NMR Biomed [Internet]. 2013 Nov [cited 2022 Jul 25];26(11):1518–26. Available from: https://pubmed.ncbi.nlm.nih.gov/23836451/

108. Magnusson I, Rothman DL, Katz LD, Shulman RG, Shulman GI. Increased rate of gluconeogenesis in type II diabetes mellitus. A 13C nuclear magnetic resonance study. J Clin Invest. 1992 Oct 1;90(4):1323–7.

109. Matyka K, Dixon RM, Mohn A, Rajagopalan B, Shmueli E, Styles P, et al. Daytime liver glycogen accumulation, measured by 13C magnetic resonance spectroscopy, in young children with Type 1 diabetes mellitus. Diabetic Medicine. 2001;18(8):659–62.

110. Liu Y, Mei X, Li J, Lai N, Yu X. Mitochondrial function assessed by 31P MRS and BOLD MRI in non-obese type 2 diabetic rats. Physiol Rep [Internet]. 2016 Aug 1 [cited 2024 Mar 6];4(15):e12890. Available from: https://onlinelibrary.wiley.com/doi/full/10.14814/phy2.12890

111. Befroy DE, Rothman DL, Petersen KF, Shulman GI. 31P-magnetization transfer magnetic resonance spectroscopy measurements of in vivo metabolism. Diabetes. 2012;61(11):2669–78.

112. Schär M, Kim WY, Stuber M, Boesiger P, Manning WJ, Botnar RM. The impact of spatial resolution and respiratory motion on MR imaging of atherosclerotic plaque. Journal of Magnetic Resonance Imaging [Internet]. 2003 May 1 [cited 2024 Apr 12];17(5):538–44. Available from: https://onlinelibrary.wiley.com/doi/full/10.1002/jmri.10287

113. Atkinson D, Hill DLG, Stoyle PNR, Summers PE, Clare S, Bowtell R, et al. Automatic Compensation of Motion Artifacts in MRI. Magn Reson Med [Internet]. 1999 [cited 2024 Apr 12];41:163–70. Available from: https://onlinelibrary.wiley.com/terms-and-conditions

114. Wood ML, Shivji MJ, Stanchev PL. Planar-motion correction with use of K-space data acquired in Fourier MR imaging. J Magn Reson Imaging [Internet]. 1995 [cited 2024 Apr 12];5(1):57–64. Available from: https://pubmed.ncbi.nlm.nih.gov/7696810/

115. Schultz CL, Alfidi RJ, Nelson AD, Kopiwoda SY, Clampitt ME. The effect of motion on two-dimensional Fourier transformation magnetic resonance images. Radiology [Internet]. 1984 [cited 2024 Apr 12];152(1):117–21. Available from: https://pubmed.ncbi.nlm.nih.gov/6729101/

116. Taylor AM, Jhooti P, Wiesmann F, Keegan J, Firmin DN, Pennell DJ. MR navigator-echo monitoring of temporal changes in diaphragm position: implications for MR

coronary angiography. J Magn Reson Imaging [Internet]. 1997 Jul [cited 2024 Apr 12];7(4):629–36. Available from: https://pubmed.ncbi.nlm.nih.gov/9243380/

117. Handbook of Magnetic Resonance Spectroscopy In Vivo: MRS Theory, Practice ... - Google Books [Internet]. [cited 2024 Apr 12]. Available from: https://books.google.co.uk/books?hl=en&lr=&id=KUtMDQAAQBAJ&oi=fnd&pg=PA263&dq=effect+of+respiratory+motion+on+MRS&ots=8s5i_AQNjj&sig=hecDD_diNwdG9wa3ubMa3H8no6s#v=onepage&q=effect%20of%20respiratory%20motion%20on%20MRS&f=false

118. Bolan PJ, Henry PG, Baker EH, Meisamy S, Garwood M. Measurement and correction of respiration-induced B0 variations in breast 1H MRS at 4 Tesla. Magn Reson Med [Internet]. 2004 Dec 1 [cited 2024 Apr 12];52(6):1239–45. Available from: https://onlinelibrary.wiley.com/doi/full/10.1002/mrm.20277

119. Noworolski SM, Tien PC, Merriman R, Vigneron DB, Qayyum A. Respiratory motion-corrected proton magnetic resonance spectroscopy of the liver. Magn Reson Imaging [Internet]. 2009 May [cited 2024 Apr 12];27(4):570. Available from: /pmc/articles/PMC2917604/

120. Hock A, Valkovič L, Geier A, Kuntzen T, Boesiger P, Henning A. Navigator based respiratory gating during acquisition and preparation phases for proton liver spectroscopy at 3 T. NMR Biomed [Internet]. 2014 Mar 1 [cited 2024 Apr 15];27(3):348–55. Available from: https://onlinelibrary.wiley.com/doi/full/10.1002/nbm.3069

121. Taylor R, Magnusson I, Rothman DL, Cline GW, Caumo A, Cobelli C, et al. Direct assessment of liver glycogen storage by 13C nuclear magnetic resonance spectroscopy and regulation of glucose homeostasis after a mixed meal in normal subjects. Journal of Clinical Investigation. 1996 Jan 1;97(1):126–32.

122. Casey A, Mann R, Banister K, Fox J, Morris PG, Macdonald IA, et al. Effect of carbohydrate ingestion on glycogen resynthesis in human liver and skeletal muscle, measured by 13C MRS. Am J Physiol Endocrinol Metab [Internet]. 2000 [cited 2024 Apr 16];278(1 41-1). Available from: https://journals.physiology.org/doi/10.1152/ajpendo.2000.278.1.E65

123. Astrid H, Stephen B, Abi Sp, Darwish N, Amelie G, LEonie E, et al. Hepatic glycogen replenishment in healthy children after an overnight fast: A 13C magnetic resonance spectroscopy study.

124. Spicer A, Bawden S, Gowland P, Francis S, Morrison D, Aithal G, et al. Change in ATP flux after propionate ingestion in healthy volunteers Using 31P MRS Saturation Transfer. In: ISMRM 2023 Annual Meeting Toronto. 2023. p. 3139.

125. Laufs A, Livingstone R, Nowotny B, Nowotny P, Wickrath F, Giani G, et al. Quantitative liver 31P magnetic resonance spectroscopy at 3T on a clinical scanner. Magn Reson Med [Internet]. 2014 May 1 [cited 2024 Apr 16];71(5):1670–5. Available from: https://onlinelibrary.wiley.com/doi/full/10.1002/mrm.24835

126. Burton DR, Herráez MA, Gdeisat MA, Lalor MJ. Fast two-dimensional phase-unwrapping algorithm based on sorting by reliability following a noncontinuous path. Applied Optics, Vol 41, Issue 35, pp 7437-7444 [Internet]. 2002 Dec 10 [cited

2024 Mar 13];41(35):7437–44. Available from: https://opg.optica.org/viewmedia.cfm?uri=ao-41-35-7437&seq=0&html=true

127. M. F. Kasim. Fast 2D phase unwrapping implementation in MATLAB [Internet]. https://github.com/mfkasim91/unwrap_phase/; 2017 [cited 2024 Mar 13]. Available from: https://github.com/mfkasim91/unwrap_phase/

128. Labib MH. Hypoglycaemia. Clinical Biochemistry: Metabolic and Clinical Aspects: Third Edition. 2014 Apr 24;333–48.

129. Jensen J, Rustad PI, Kolnes AJ, Lai YC. The Role of Skeletal Muscle Glycogen Breakdown for Regulation of Insulin Sensitivity by Exercise. Front Physiol [Internet]. 2011 [cited 2024 Jan 31];2. Available from: /pmc/articles/PMC3248697/

130. Taylor R, Price TB, Rothman DL, Shulman RG, Shulman GI. Validation of 13C NMR measurement of human skeletal muscle glycogen by direct biochemical assay of needle biopsy samples. Magn Reson Med [Internet]. 1992 [cited 2022 Jul 25];27(1):13–20. Available from: https://pubmed.ncbi.nlm.nih.gov/1435198/

131. Bawden SJ, Stephenson MC, Ciampi E, Hunter K, Marciani L, Spiller RC, et al. A low calorie morning meal prevents the decline of hepatic glycogen stores: a pilot in vivo 13 C magnetic resonance study. 2014 [cited 2024 Jan 31]; Available from: www.rsc.org/foodfunction

132. Bawden S, Stephenson M, Falcone Y, Lingaya M, Ciampi E, Hunter K, et al. Increased liver fat and glycogen stores after consumption of high versus low glycaemic index food: A randomized crossover study. Diabetes Obes Metab [Internet]. 2017 Jan 1

[cited 2023 Dec 13];19(1):70–7. Available from: https://onlinelibrary.wiley.com/doi/full/10.1111/dom.12784

133. Taylor R, Magnusson I, Rothman DL, Cline GW, Caumo A, Cobelli C, et al. Direct assessment of liver glycogen storage by 13C nuclear magnetic resonance spectroscopy and regulation of glucose homeostasis after a mixed meal in normal subjects. J Clin Invest. 1996 Jan 1;97(1):126–32.

134. Flück CE, Slotboom J, Nuoffer JM, Kreis R, Boesch C, Mullis PE. Normal hepatic glycogen storage after fasting and feeding in children and adolescents with type 1 diabetes. Pediatr Diabetes [Internet]. 2003 Jun 1 [cited 2023 Dec 13];4(2):70–6. Available from: https://onlinelibrary.wiley.com/doi/full/10.1034/j.1399-5448.2003.00015.x

135. Boss GR, Seegmiller JE. Age-Related Physiological Changes and Their Clinical Significance. Western Journal of Medicine [Internet]. 1981 [cited 2024 Feb 20];135(6):434. Available from: /pmc/articles/PMC1273316/?report=abstract

136. The Growing Child: School-Age (6 to 12 Years) [Internet]. [cited 2024 Feb 20]. Available from: https://www.stanfordchildrens.org/en/topic/default?id=the-growing-child-school-age-6-to-12-years-90-P02278

137. 9- to 11-year-olds: Ages and stages of youth development - MSU Extension [Internet]. [cited 2024 Feb 20]. Available from: https://www.canr.msu.edu/news/9_to_11_year_olds_ages_and_stages_of_youth_development

138. Martin Bland. frequently asked questions on the design and analysis of measurement studies. 2006 [cited 2024 Mar 7]. How should I calculate a within-subject coefficient of variation? Available from: https://www-users.york.ac.uk/~mb55/meas/cv.htm

139. Stephenson MC, Leverton E, Khoo EYH, Poucher SM, Johansson L, Lockton JA, et al. Variability in fasting lipid and glycogen contents in hepatic and skeletal muscle tissue in subjects with and without type 2 diabetes: a 1H and 13C MRS study. NMR Biomed [Internet]. 2013 Nov [cited 2023 Dec 13];26(11):1518–26. Available from: https://pubmed.ncbi.nlm.nih.gov/23836451/

140. Kacerovsky M, Jones J, Schmid AI, Barosa C, Lettner A, Kacerovsky-Bielesz G, et al. Postprandial and fasting hepatic glucose fluxes in long-standing type 1 diabetes. Diabetes [Internet]. 2011 Jun [cited 2024 Jan 31];60(6):1752–8. Available from: /pmc/articles/PMC3114392/

141. Casey A, Mann R, Banister K, Fox J, Morris PG, Macdonald IA, et al. Effect of carbohydrate ingestion on glycogen resynthesis in human liver and skeletal muscle, measured by 13C MRS. Am J Physiol Endocrinol Metab [Internet]. 2000 [cited 2023 Nov 1];278(1 41-1). Available from: https://journals.physiology.org/doi/10.1152/ajpendo.2000.278.1.E65

142. Awad S, Stephenson MC, Placidi E, Marciani L, Constantin-Teodosiu D, Gowland PA, et al. The effects of fasting and refeeding with a 'metabolic preconditioning' drink on substrate reserves and mononuclear cell mitochondrial function. Clinical Nutrition. 2010 Aug 1;29(4):538–44.

143. Kishore P, Gabriely I, Cui MH, Di Vito J, Gajavelli S, Hwang JH, et al. Role of Hepatic Glycogen Breakdown in Defective Counterregulation of Hypoglycemia in Intensively Treated Type 1 Diabetes. Diabetes [Internet]. 2006 Mar 1 [cited 2024 Feb 21];55(3):659–66. Available from: https://dx.doi.org/10.2337/diabetes.55.03.06.db05-0849

9 Appendix

9.1 Bariatric Study- MRI CRF- Arm A

The University of Nottingham

Sir Peter Mansfield Imaging Centre

Imaging CRF for Bariatric Surgery Patients.

Main study Arm

Participant Number:……..

MRI Volunteer Number: ……

Case Report Form

IRAS: 295253

Ethics: 21/WA/0387

School of Physics

Participant Number	Date of Visit	

	___/___/____ dd/mm/yyyy	Visit Day

Patch

Quilt_H Patch.

Exam Card

SPMRIUseres -> Abi ->

BAR_proton_abdo

Study Protocol

MRI Proton	Time Started: :	

Scan	Complete		Any comments
	Yes	No	
Scout Scan			
mDIXON			

Preparation tab

Echo phase determination = OFF

Plan MOLLI scan to ensure pancreas coverage in Geo4 **This will set the position of the next few scans**			
T2*			
B1 and B0 mapping			
Preparation tab **Echo phase determination = ON** **Scan tab** **GRE echo scale = -1**			
T1 mapping			
Pancreas eThrive			
General tab **Physiological Simulation = ON** **RR = 2** **Heart rate = 60** **Scan tab**			

GRE echo scale = 1			
MOLLI			
General tab **Physiological Simulation = OFF**			
Proton Spectroscopy			
Diffusion 1			
Scan tab **Dynamic Noise Scan = noRFnoGR**			
DWI reversed			
Scan tab **Dynamic Noise Scan = no**			
T2 mapping			
Magnetisation Transfer			

Preparation tab **Echo phase determination = OFF**			
Kidney T2*			
Preperation tab **Echo phase determination = ON** **General tab** **Physiological Simulation = ON** **RR = 2** **Heart rate = 60**			
Kidney MOLLI			
General tab **Physiological Simulation = OFF**			
Arterial Flow			
Optional Cardiac Card.			
End of MRI Completion time:			
Print Name Here _____			

Signed _____ Date___/____/_____

Study Researcher dd/mmm/yyyy

9.2 Participant Information Sheet-Bariatric Study – Arm A

Category A: Participant Information Sheet

Diabetes or Pre-diabetes Remission and Surgery

(Final version 4.0: 23/01/2023)

Title of Study: Effects of Very-Low Calorie Diet and Bariatric Surgery in Patients with Type 2 Diabetes Or Pre-diabetes

You are being invited to participate in a research study. It is important for you to understand why the research is being done and what it will involve before you decide whether to take part. Please read this information carefully, and discuss it freely with others should you feel necessary. If there is anything which remains unclear, or requires further explanation, please ask us. Please do not rush this decision. Thank you in advance for reading this thoroughly.

This study is occurring as part of 2 PhD students' research projects at the University of Nottingham. The Primary Investigator is Penny Gowland of the University of

Nottingham, and the Chief Investigator is Iskandar Idris of Royal Derby hospital and the University of Nottingham

What is the purpose of the study?

The purpose of the study is to develop further understanding of how the Very Low-Calorie Diet and your scheduled surgery will impact upon your diabetes or pre-diabetes. We will be assessing how, and why, these changes occur and ultimately this information will inform future research prospects and could potentially expand available treatment options. This study will be done alongside your standard treatment that you receive for your bariatric surgery. It will use Magnetic Resonance Imaging (MRI) to take pictures of your abdomen, chest and legs, and Magnetic resonance Spectroscopy to analyses the makeup of these parts of your body. Blood tests will also be done to see your response to glucose.

Why have I been Invited?

You have been invited because you either have a history of type II diabetes or pre-diabetes and are about to undergo either Sleeve Gastrectomy or Roux-en-Y Gastric Bypass surgery. We are inviting 23 participants like you to take part.

Do I have to take part?

It is entirely your decision whether you wish to take part. If you do decide to take part you will be given this information sheet to keep and be asked to sign a consent

form. If you decide to take part you are still free to withdraw at any time and without giving a reason. This would not affect your legal rights

What will happen to me if I take part?

If you wish to take part, you will undergo further screening to make sure that you don't have any metal within you, any mechanical life supporting devices such as a pacemaker or other medical implants such as cochlear implants or neurostimulators. If you know this to be the case already, please let us know as you may not be able to take part due to risks associated with the MRI machine.

If you are receiving this document, a member of your usual care team has already contacted you, over the phone about the study.

For this study you will need to take part in an hour-long screening session in person and 4 experimental sessions, each lasting around half a day. During the screening session a member of the team will check that you are suitable and you still wish to participate, answer any questions and book your first experimental session. We will do our best to align this session with your routine ERAS appointment, however this may not always be possible. The first session will be before you start your Very Low-Calorie Diet (also known as the Liver shrinkage diet), the next session will be just before your surgery, the third session will be 6 weeks after surgery and your final session will be 4 months after surgery. You will have to be fasted for these sessions to allow us to test your glucose tolerance, which will be done using blood tests. You

must be fasted for a minimum of 8 hours before you arrive. You will also need to avoid alcohol consumption and strenuous exercise in the preceding 24 hours, and consume no caffeine for 18 hours before arriving. The fasted period must include water only, the fast will be broken with your arrival at the Sir Peter Mansfield Imaging Centre at the point of the commencement of the Mixed Meal Test whereby you will be provided with a nutritional shake.To reduce the fasting period, all tests and scans will be scheduled to take place in the morning.

Please note that during the morning of the study days you will be advised not to take paracetamol.

Please also note that we will provide a nutritional bar (which also suits the calorie requirements of your Very Low Calorie Diet), this bar will be given following the completion of the Mixed Meal Test and prior to your time in the MRI scanner.

For Study Day 1, which is prior to your Very Low Calorie Diet commencing, you are welcome to bring an additional home-prepared lunch for after the MRI session if you wish to do so.

Here is a diagram to help make this process clearer:

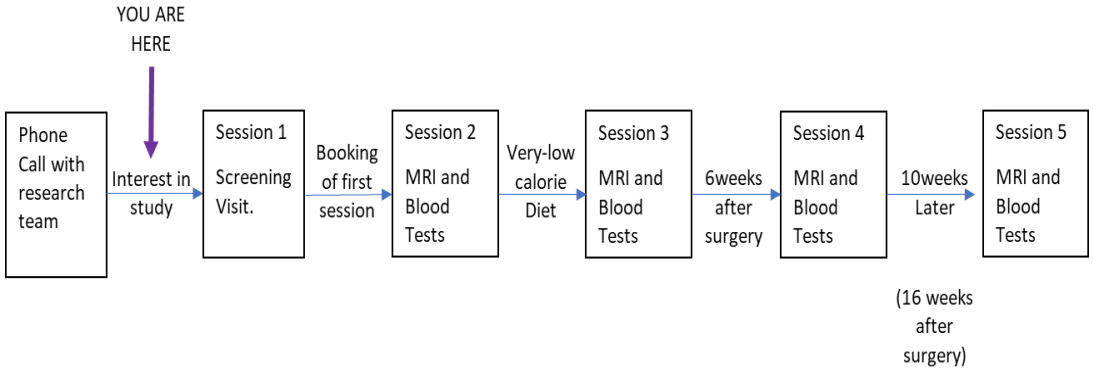

Figure 1: Diagram outlining the study.

During each of these experimental sessions we will take multiple blood samples to establish your glucose response. After all your blood tests are done you will undergo MRI scanning. We will take a picture of your legs and body, this will give us data to understand changes in the composition of your organs.

For the Blood Tests:

We will perform a mixed meal test to measure your body's response to nutrition. Prior to drinking you will have a cannula (tube) inserted into either your arm or hand to aid in drawing blood. 15ml of blood will then be taken (about a tablespoon) as a fasted measurement. You will then be given a choice in flavour of a nutria Fortisip (except chocolate) and be asked to drink all 200ml. Blood sampling will take place at 15 minutely intervals for the duration of 3 hours. Between draws the hand or arm will be placed in a warm box.

The blood samples will be taken to a lab down the corridor to be processed and stored temporarily. By the end of the following working day the samples will be transported to the medical school for longer term storage until we have collected enough samples for bulk transfer to the Royal Derby Hospital for analysis.

For the MRI and MRS:

You will be asked to remove coloured contact lenses and to change into light clothing (we have a changing facility and will provide scrubs for you to wear). You will then be taken through to the MRI scanner where a flexible pad (to collect the signal) will be placed over your body alongside a small cushion to monitor your breathing. We may put some sticky pads and wires on your chest or a small clip on your finger to measure your heartbeat. To maximise your comfort during the scan, we may place foam pads around you.

The bed will move into the scanner, you will be asked to lie very still, and the scanning will start. The scanner makes a lot of noise so you will be provided with headphones and earplugs to reduce the sound level. At all times you will be in verbal contact with the scanner operator and will be given a buzzer to press in case you want to ask the operator to come into the scanner hall.

Our scanner is larger than the average MRI scanner, but if you are very claustrophobic, that is you feel uncomfortable and panicked in a small, closed environment, you may not wish to take part in this study. You will have 1 MRI sessions just over 1 hour long, your total time in the scanner will be no longer than 1 hours and 30 minutes and you will be given breaks if needed. You can bring music or other things to listen to if you wish.

Can I ask questions about the research project?

Yes, we will to the best of our ability answer any questions which you have related to the research project.

What equipment is used?

This study uses a Magnetic Resonance Imaging (MRI) Scanner. This scanner uses a very strong magnetic field to create a detailed image of the structure of your organs, it is also the same machine we use for the Magnetic Resonance Spectroscopy. This does not involve any X-rays or other ionising radiation. We will also use a cannula to collect blood samples during the study session, rather than putting in new needles every time as this reduces the risk of infection.

What are the possible risks of taking part?

MRI is considered to be a safe imaging technique. There are no known risks or side effects except that in less than 5% of people you might experience a very slight twitching or tingling in the hands or feet (caused by peripheral nerve stimulation).

This is not dangerous but may be disconcerting. The scan can be stopped if this occurs and has become uncomfortable. In some very rare cases, being in the magnetic field may induce temporary dizziness. In the event you experience any of these, you are free to withdraw from the study should you wish to. Although there is no evidence to suggest it is dangerous, as a precaution we will not include any women who are pregnant, or who have a reason to believe they may be.

Going near to the strong magnets that are used in MRI machines can be dangerous if someone has a pacemaker (as it can alter the way it works) or someone has metal clips (that are sometimes used in surgical procedures) inside them; the clips can move if they are around soft tissue such as around blood vessels or in the brain. To avoid this risk, we will ask you about any surgical procedures that you may have had, or any metal implants inside your body and it is important that this information is disclosed to researchers. You will not be recruited for this study if there is a chance that you have metal inside your body. Please note, fixed metal braces (retainers) are not a problem.

The scanner can be loud when it collects images and this sound varies depending on the type of image we are collecting. You will be given headphones and earplugs to help reduce this sound. If you are very claustrophobic, that is you feel uncomfortable and panicked in a small, closed environment, it may be best for you to decide not to take part in this study at all. Remember, you can withdraw from the study at any point without giving a reason, this will not affect your standard care.

Contacting Your GP – Abnormalities in Scans

The Sir Peter Mansfield Magnetic Resonance Centre is **not** a clinical diagnostic facility and the scans we collect are **not** the same as scans collected by doctors for medical purposes. The pictures will **not** usually be looked at by a radiologist (a doctor qualified to find abnormalities in scans), so this test does **not** replace any

tests that your doctor thinks might be needed. It is therefore unlikely that we would detect anything unusual or irregular on the images, even if they were present. However, if we suspect that there is something abnormal on your scan, we will ask a specialist to review it. If we did find anything abnormal on your scan the investigator would arrange for an appropriately qualified doctor, from the NHS Trust to look at them. That specialist doctor would contact your GP to explain the situation, so that your GP could then advise you.

What are the benefits of taking part?

We cannot promise the study will help you but the information we get from this study may help inform future studies and help us better understand and improve treatment of diabetes and pre-diabetes. You will have the knowledge that you have made a contribution to our understanding of science and may gain some general better understanding of your own body. However, there are no direct health benefits for you by taking part in this study.

Will my travel expenses be covered?

For your research participation there will be a total inconvenience fee of £80 comprised of £20 for each experimental session. This money is to assist with expenses incurred as part of your participation, such as travel expenses. Car parking vouchers can be provided in addition to this, so that you don't incur any parking expenses if you are travelling by car.

If you live over 20 miles away from the University of nottingham main campus we are able to cover for standard milage for attending experimental sessions.

What happens at the end of this study?

The results of this study may be used for educational purposes, for scientific publications, to inform clinical practice or for further studies, or a combination of all four. Scans are anonymised when they are collected and will presented in such a way that volunteers cannot be identified wherever they are used.

Can I withdraw from the study and what happens if I do?

Yes.
Your participation is voluntary and you are free to withdraw at any time, without giving any reason, and without your legal rights being affected. If you withdraw we will no longer collect any information about you or from you but we will keep the information about you that we have already obtained as we are not allowed to tamper with study records and this information may have already been used in some analyses and may still be used in the final study analyses. To safeguard your rights, we will use the minimum personally identifiable information possible.

Who knows I am taking part?

Members of the study team at the University of Nottingham will know that you are taking part in the study and authorised individuals from the sponsor or its affiliates who see personal data when monitoring the conduct of the research. All other data are identified only by a code (as described further down in 'Anonymised Research Data'), so anyone outside of the study team looking at this information cannot identify you directly.

We will not contact your GP to inform him/her that you are going to take part in this study. However, as previously mentioned, if we did find anything abnormal on your scan the investigator would arrange for an appropriately qualified doctor to look at them, who will then contact your GP to discuss a care plan if needed.

What will happen to the study Results?

The collective results from the study will be discussed with research collaborators at Leicester University, Glenfield hospital, Medical Research Council, Biomedical Research Centre and presented national or international conferences to allow findings to be shared with other researchers. Results will also be used to design future research.

Your coded data may be shared with journals, experts or other scientists to verify the quality of results or to allow our data to be used as part of larger studies in the future. However, you will not be identified in any shared data, report or publication. Your data will also be used for Abi Spicer's and Rebekah Wilmington's PhD theses. You are welcome and invited to request a copy of the results, just ask a member of the team!

Confidentiality – Who will have access to the data?

We will follow ethical and legal practice and all information about you will be handled in confidence.

If you join the study, we will use information collected from you [and your medical records] during the course of the research. This information will be kept **strictly confidential**, stored in a secure and locked office, and on a password protected database at the University of Nottingham. Under UK Data Protection laws the University is the Data Controller (legally responsible for the data security) and the Chief Investigator of this study (Prof Iskandar Idris) is the Data Custodian (manages

access to the data). This means we are responsible for looking after your information and using it properly. Your rights to access, change or move your information are limited as we need to manage your information in specific ways to comply with certain laws and for the research to be reliable and accurate. To safeguard your rights we will use the minimum personally – identifiable information possible.

You can find out more about how we use your information and to read our privacy notice at:

https://www.nottingham.ac.uk/utilities/privacy.aspx.

The data collected for the study will be looked at and stored by authorised persons from the University of Nottingham who are organising the research. They may also be looked at by authorised people from regulatory organisations to check that the study is being carried out correctly. All will have a duty of confidentiality to you as a research participant and we will do our best to meet this duty.

Where possible information about you which leaves the Sir Peter Mansfield Imaging Centre will have your name and address removed and a unique code identifier will be used so that you will not be recognised from this data. However, sometimes we need to ensure that we can recognise you to link the research data with your medical records so in these instances we will need to know your name and date of birth. We will also need this information if we need to follow up your medical records as part

of the research, where we may need to ask the Government services that hold medical information about you (such as NHS Digital, the Office for National Statistics, among others) to provide this information to us. By signing the consent form you agree to the above.

Your contact information will be kept by the University of Nottingham for 12 months after the end of the study so that we are able to contact you about the findings of the study and possible follow-up studies (unless you advise us that you do not wish to be contacted).

This information will be kept separately from the research data collected and only those who need to will have access to it. All other data (research data) will be kept securely for 7 years. After this time there will be secure disposal of your data. During this time all precautions will be taken by all those involved to maintain your confidentiality, only members of the research team given permission by the data custodian will have access to your personal data.

In accordance with the University of Nottingham's, the Government's and our funders' policies we may share our research data with researchers in other Universities and organisations, including those in other countries, for research in health and social care. Sharing research data is important to allow peer scrutiny, re-use (and therefore avoiding duplication of research) and to understand the bigger picture in particular areas of research. Data sharing in this way is usually anonymised

(so that you would not be identified) but if we need to share identifiable information we will seek your consent for this firstly and ensure it is secure.

Data collected during the study will be looked at and stored by authorised persons from the University of Nottingham, Royal Derby Hospital and Glenfield Hospital who are organising the research. Only a limited number of people involved in this research are allowed to see your personal records at this institution.

In addition, authorised persons from the Medical Research Council, the University of Nottingham and the Biomedical Research Council (the sponsors) or its representatives will also look at the data collected during the study, including your personal data held at the University of Nottingham. This is required to allow auditing and/or monitoring of the information to check that the research is being carried out correctly. Access to personal data will be by arrangement with the lead investigator at the University of Nottingham and we will make sure your data is kept strictly confidential until it is destroyed. Moreover, your identity will not be disclosed in any reports arising from the research, or documents that leave the study centre.

Anonymised Research data

Research data includes all the measurements that we make on you in the course of the study, for example, age, height, weight, MR images, dietary intake. To help maintain your privacy, you will be assigned an identification code (for example P01 for participant number 1), and this code will be used instead of your name on all study documents. We will save all the MRI images/recordings and electronic

research data using this code, so that none of the data will have your real name or other individual identifiers associated with them.

The data will be stored at the University for 10 years after publication or public release of the research findings.

We would like your permission to use this anonymised data (including the MR images) in future studies, and to share your data with other researchers in other universities and organisations both inside and outside the UK for research in health and social care. Sharing research data is important to allow other scientists to check our methods, avoid unnecessary duplication of experiments, and allow studies to be combined thereby providing more general answers to scientific questions. Personal information that could identify you will not be shared with other researchers and will never be included when results are made public.

Identifiable Personal Data

Identifiable, personal data (such as name and address) will be stored confidentially in a locked cabinet within a locked office and in a secure location at the Sir Peter Mansfield Imaging Centre. This data will be on a password protected secure database that is only accessible by a very limited number of administrative staff who have no access to the scientific data whatsoever. This information will be held by the Chief Investigator (Dr Iskandar Idris) and the Sir Peter Mansfield imaging Centre.

The Sir Peter Mansfield Imaging Centre enters all participant data onto a secure database, which is password protected and supported/maintained by Information

Services at the University. Any paperwork, such as paper consent/screening forms are locked in fireproof cabinets with only limited people having access.

The research team at the University of Nottingham will access this personal data whilst the project is being carried out to enable them to contact you. This identifiable, personal information will be kept separately from the coded research data and will not leave the study site.

Documents that contain personal information, will be kept securely by the research team at the University of Nottingham for 10 years after the end of the study.

You have the right to view and access your personal data and have the right to erase, limit the processing of it, or lodge an objection on the processing of this identifiable data.

If you are happy for us to do so, we may use your personal data to contact you after the study is finished to let you know the results and possible follow-up studies.

How will the University keep my data Private?

Under UK Data Protection laws the University is the Data Controller for the data and documents held at their site, and Dr Iskandar Idris is the Data Custodian (manages access to the data). This means we are responsible for looking after your information and using it properly. Your rights to access, change or move your information are limited as we need to manage your information in specific ways to comply with certain laws and for the research to be reliable and accurate. To safeguard you and your rights we always use the personally – identifiable information as little as possible. You can find out more about how we use

information and to read our privacy notice at:

https://www.nottingham.ac.uk/utilities/privacy.aspx/

Who reviewed the study?

All research involving people is looked at by an independent group of people, called a Research Ethics Committee, to protect your interests. This study has been reviewed and given a favourable opinion by the Faculty of Medicine and Health Sciences Research Ethics Committee (Reference number:21047). This research study has been given a favourable opinion by Wales REC 4

Who is organising the study?

This study is a collaboration between the Royal Derby Hospital, The University of Nottingham and Glenfield Hospital in Leicester as part of a PhD student project.

This study is organised by Professor Iskandar Idris (Royal Derby Hospital, University of Nottingham UoN). Other Members of the team include: Miss Abi Spicer (UoN), Dr Rebekah Wilmington (UoN), Dr Stephen Bawden (UoN), Professor Guruprasad Aithal (UoN), Professor Susan Francis (UoN), Professor Penny Gowland (UoN) and Professor Gerry Mcann (University of Leicester, Glenfield Hospital).

This study was co-funded by Medical Research council, the University of Nottingham and the Biomedical Research Council.

What if something goes wrong?

If you have a concern about any aspect of this project, please speak to the researchers Abi Spicer (abi.spicer@nottingham.ac.uk +447714239831) or Rebekah Wilmington (Rebekah.wilmington@nottingham.ac.uk) or Penny Gowland (penny.gowland@nottingham.ac.uk +44 (0) 115 95 14754), or the Chief Investigator Iskandar Idris (iskandar.idris@nottingham.ac.uk) , who will do their best to answer your query. The researchers should acknowledge your concern within 24hrs and give you an indication of how they intend to deal with it.

If you remain unhappy and wish to complain formally, you can do this by contacting the FMHS Research Ethics Committee Administrator, c/o The University of Nottingham, Faculty PVC Office, B Floor, Medical School, Queen's Medical Centre Campus, Nottingham University Hospitals, Nottingham, NG7 2UH. E-mail: FMHS-ResearchEthics@nottingham.ac.uk. If you do not feel comfortable contacting the Research Ethics Committee Administrator then an alternative would be to contact the Patient Advice and Liaison Service (PALS) for Nottingham University Hospitals who can provide you with confidential advice, support and information on health-related matters. Contact PALS on 08001830204 or email PALS@nuh.nhs.uk.

Do you have any further questions?

If you have any further questions, please ask the person who gave you this information sheet or contact Abi abi.spicer@nottingham.ac.uk .

This research study has been given a favourable opinion by Wales REC 4

Thank you for considering taking part in this study. Our research depends entirely on the goodwill of potential volunteers such as you. If you require any further information, we will be pleased to help in any way we can.

9.3 Screening and Study Day CRF – Bariatric Study Arm A

Sir Peter Mansfield Imaging Centre

Screening and test visit CRF for

Bariatric Surgery Patients.

31P Arm

Participant Number:……..

MRI Volunteer Number: ……

Case Report Form

IRAS: 295253

Ethics: 21/WA/0387

School of Physics

INSTRUCTIONS FOR COMPLETION OF CRFS

- The Case Report Forms (CRF) are to be completed in **black ballpoint pen** only. All entries must be printed and legible.
- Ensure that the participant ID is consistent throughout the document.
- Each part of the CRF is to be completed as indicated.
- Dates are to be written as follows: 24 /FEB/2022
  dd mmm yyyy
  Day Month Year
- Times are to be written using the 24h clock configuration as follows:- 00 : 00 (Midnight)
  Hours Minutes
- When an answer to a question is required, mark the box corresponding to the response:

Example: "YES" YES ☑ NO ☐

Example: "NO" YES ☐ NO ☑

The following abbreviations are to be used:-

ND = Not Done, NA = Not Applicable, NK = Not Known

- If comments are required, print them clearly and briefly in English using capital letters.
- Corrections are to be made by striking out the erroneous data with a **single line** in such a way that the **original entry remains legible.** The correct datum is then written clearly alongside the erroneous datum. Do NOT use correction fluid.
- All **corrections are to be dated** and **initialled**. A reason must be given for each correction or missing datum.
- If a whole page is to be changed, the page is to be **struck out with a diagonal black line** and a copy inserted in the CRF, dated and initialled.
- Ensure that all boxes are completed. If a participant discontinues early, ensure that the Header information for all of the remaining pages is completed and a single line drawn through each uncompleted page.
- The Principal Investigator must sign and date the Study Completion page to certify completeness of the CRF.
- Only those members of staff trained and responsible for completing the specified duties may complete the CRF.
- Members of staff trained and the specified duties are listed in the site personnel list, with identification if initials and signature.

Principal Investigator	_____ (PRINT NAME HERE)	Study Researcher MRI scanning	_____ (PRINT NAME HERE)
Study Researcher Product manufacture	_____ (PRINT NAME HERE)	Study Researcher etc	_____ (PRINT NAME HERE)

Participant Number	Date of Visit	Screening Visit
☐☐☐	___/___/____ dd/mm/yyyy	

Participants Demographic					
Date of Birth	___/___/____ dd/mm/yyyy	Age years □□			
Height Weight Waist Circumference	□□□.□ □□□.□ □□□.□	Body Mass Index (BMI) □□/m□			
Diabetic Medication Type/Brand Name		Advice Given			
HbA1c / date taken					
Inclusion Criteria (If the answer is **NO** please comment below)					
Is the Patient listed for Roux-en-Y Gastric Bypass or Sleeve Gastrectomy at Derby Hospital?	Yes		No		
Is the Patients BMI over or equal to 35kg/m^2	Yes		No		
Is the Patient between the ages of 18 and 70 years?	Yes		No		

Does the Patient have type 2 diabetes or Prediabetes?	Yes		No	
Can the Patient give informed consent?	Yes		No	
Exclusion Criteria (If the answer is **YES** please comment below)				
Is the Patients BMI greater than 50kg/m^2	Yes		No	
Does the Patient have Liver Cirrhosis?	Yes		No	
Does the Patient have any MR contraindications?	Yes		No	
Using waist Circumference or the MR hoop, is the patient **unlikely** to fit in the MR scanner?	Yes		No	

Print Name Here _____

Signed _____ Date___/____/_____

Study Researcher dd/mmm/yyyy

Participant Number	Date of Visit	Visit Day 1
	___/___/____ dd/mm/yyyy	

Test Day 1		
Height	□□□.□	Body Mass Index (BMI)
Weight	□□□.□	□□.□

Has the Participant Started their VLCD?	Yes		No	
If Yes, how many days have they been on it?	days □□□			

The study visit cannot proceed unless all questions below are answered YES				
Is the Participant in a fasting state?	Yes		No	
Has the Participant avoided alcohol and Paracetamol in the last 24 hours?	Yes		No	
Has the Participant avoided strenuous exercise for the last 24hours?	Yes		No	
Can the Participant fit on the bed with room for surface coils?	Yes		No	
Is the participant happy to proceed?	Yes		No	
Study Protocol				
Did the Participant Complete the MRI?	Yes		No	

Adverse Effects				
Any Adverse Events since the Participants last visit?	Yes		No	
Any medication changes Since the last visit?	Yes		No	
Comments:				

Print Name Here _____

Signed _____ Date___/____/_____

Study Researcher dd/mmm/yyyy

Participant Number	Date of Visit	Visit Day 2
	___/___/____ dd/mm/yyyy	

Test Day 1					
Height Weight	□□□.□ □□□.□	Body Mass Index (BMI) □□.□			
Has the Participant Started their VLCD?		Yes		No	
If Yes, how many days have they been on it?		days □□□			

The study visit cannot proceed unless all questions below are answered YES				
Is the Participant in a fasting state?	Yes		No	
Has the Participant avoided alcohol and Paracetamol in the last 24 hours?	Yes		No	
Has the Participant avoided strenuous exercise for the last 24hours?	Yes		No	
Can the Participant fit on the bed with room for surface coils?	Yes		No	
Is the participant happy to proceed?	Yes		No	
Study Protocol				
Did the Participant Complete the MRI?	Yes		No	

Adverse Effects				
Any Adverse Events since the Participants last visit?	Yes		No	
Any medication changes Since the last visit?	Yes		No	
Comments:				

Print Name Here _____

Signed _____ Date___/____/_____

Study Researcher dd/mmm/yyyy

Participant Number	Date of Visit	Visit Day 3
☐☐☐	___/___/____ dd/mm/yyyy	

Test Day 1		
Height Weight	☐☐☐.☐ ☐☐☐.☐	Body Mass Index (BMI) ☐☐.☐

Has the Participant Started their VLCD?	Yes		No	
If Yes, how many days have they been on it?	days ☐☐☐			

The study visit cannot proceed unless all questions below are answered YES				
Is the Participant in a fasting state?	Yes		No	
Has the Participant avoided alcohol and Paracetamol in the last 24 hours?	Yes		No	
Has the Participant avoided strenuous exercise for the last 24hours?	Yes		No	
Can the Participant fit on the bed with room for surface coils?	Yes		No	
Is the participant happy to proceed?	Yes		No	
Study Protocol				
Did the Participant Complete the MRI?	Yes		No	

Adverse Effects				
Any Adverse Events since the Participants last visit?	Yes		No	
Any medication changes Since the last visit?	Yes		No	
Comments:				

Print Name Here _____

Signed _____ Date___/____/_____

Study Researcher dd/mmm/yyyy

Participant Number	Date of Visit	Visit Day 4
	___/___/____ dd/mm/yyyy	

Test Day 1		
Height	□□□.□	Body Mass Index (BMI)
Weight	□□□.□	□□.□

Has the Participant Started their VLCD?	Yes		No	
If Yes, how many days have they been on it?	days □□□			

The study visit cannot proceed unless all questions below are answered YES				
Is the Participant in a fasting state?	Yes		No	
Has the Participant avoided alcohol and Paracetamol in the last 24 hours?	Yes		No	
Has the Participant avoided strenuous exercise for the last 24hours?	Yes		No	
Can the Participant fit on the bed with room for surface coils?	Yes		No	
Is the participant happy to proceed?	Yes		No	
Study Protocol				
Did the Participant Complete the MRI?	Yes		No	

Adverse Effects				
Any Adverse Events since the Participants last visit?	Yes		No	
Any medication changes Since the last visit?	Yes		No	
Comments:				
Print Name Here _____ Signed _____ Date___/____/_____ Study Researcher dd/mmm/yyyy				
Participant Number [ ][ ][ ]	Date of Visit ___/___/____ dd/mm/yyyy		Study Status	

Did the Participant complete the study? If no, complete below	Yes		No	

Date of withdrawal: ___/____/_____

dd/mmm/yyyy

At whose Request did the Participant withdraw?

- ☐ Participant
- ☐ Investigator
- ☐ Sponsor
- ☐ Participants GP
- ☐ Other (Specify) _____

Primary Reason for withdrawal due to…

- ☐ Problems tolerating MRI
- ☐ Failure to comply with requirements of protocol
- ☐ Serious illness
- ☐ Withdrawal of consent

☐	Other (Specify) _____

Print Name Here _____

Signed _____ Date___/____/_____

Study Researcher dd/mmm/yyyy

Participant Number	Date of Visit	Investigation Statement
☐☐☐	___/___/____ dd/mm/yyyy	

Investigation Statement

To the best of my knowledge, I can confirm that I have made every reasonable effort to ensure that the data presented in this Case Report Form are true, complete and accurately reflect the study conduct.

Print Name Here _____

Signed _____ Date___/____/_____ Study Researcher dd/mmm/yyyy

9.4 Screening and Study Day CRF – Bariatric Study Arm B

The University of Nottingham

Sir Peter Mansfield Imaging Centre

Screening and test visit CRF for

Bariatric Surgery Patients.

31P Arm

Participant Number:……..

MRI Volunteer Number: ……

Case Report Form

IRAS: 295253

Ethics: 21/WA/0387

School of Physics

INSTRUCTIONS FOR COMPLETION OF CRFS

- The Case Report Forms (CRF) are to be completed in **black ballpoint pen** only. All entries must be printed and legible.
- Ensure that the participant ID is consistent throughout the document.
- Each part of the CRF is to be completed as indicated.
- Dates are to be written as follows: 24 /FEB/2022 (dd mmm yyyy, Day Month Year)
- Times are to be written using the 24h clock configuration as follows:- 00 : 00 (Midnight) (Hours Minutes)
- When an answer to a question is required, mark the box corresponding to the response:

Example: "YES" YES ☑ NO ☐

Example: "NO" YES ☐ NO ☑

The following abbreviations are to be used:-

ND = Not Done, NA = Not Applicable, NK = Not Known

- If comments are required, print them clearly and briefly in English using capital letters.
- Corrections are to be made by striking out the erroneous data with a **single line** in such a way that the **original entry remains legible.** The correct datum is then written clearly alongside the erroneous datum. Do NOT use correction fluid.
- All **corrections are to be dated** and **initialled**. A reason must be given for each correction or missing datum.
- If a whole page is to be changed, the page is to be **struck out with a diagonal black line** and a copy inserted in the CRF, dated and initialled.
- Ensure that all boxes are completed. If a participant discontinues early, ensure that the Header information for all of the remaining pages is completed and a single line drawn through each uncompleted page.
- The Principal Investigator must sign and date the Study Completion page to certify completeness of the CRF.
- Only those members of staff trained and responsible for completing the specified duties may complete the CRF.
- Members of staff trained and the specified duties are listed in the site personnel list, with identification if initials and signature.

Principal Investigator	_____ (PRINT NAME HERE)	Study Researcher MRI scanning	_____ (PRINT NAME HERE)
Study Researcher Product manufacture	_____ (PRINT NAME HERE)	Study Researcher etc	_____ (PRINT NAME HERE)

Participant Number	Date of Visit	Screening Visit
☐☐☐	___/___/____ dd/mm/yyyy	

Participants Demographic					
Date of Birth	___/___/____ dd/mm/yyyy	Age years ☐☐			
Height Weight Waist Circumference	☐☐☐.☐ ☐☐☐.☐ ☐☐☐.☐	Body Mass Index (BMI) ☐☐/m☐			
Diabetic Medication Type/Brand Name		Advice Given			
HbA1c / date taken					
Inclusion Criteria (If the answer is **NO** please comment below)					
Is the Patient listed for Roux-en-Y Gastric Bypass or Sleeve Gastrectomy at Derby Hospital?	Yes		No		
Is the Patients BMI over or equal to 35kg/m^2	Yes		No		
Is the Patient between the ages of 18 and 70 years?	Yes		No		

Does the Patient have type 2 diabetes or Prediabetes?	Yes		No	
Can the Patient give informed consent?	Yes		No	
Exclusion Criteria (If the answer is **YES** please comment below)				
Is the Patients BMI greater than 50kg/m^2	Yes		No	
Does the Patient have Liver Cirrhosis?	Yes		No	
Does the Patient have any MR contraindications?	Yes		No	
Using waist Circumference or the MR hoop, is the patient **unlikely** to fit in the MR scanner?	Yes		No	

Print Name Here _____

Signed _____ Date___/____/_____

Study Researcher dd/mmm/yyyy

Participant Number	Date of Visit	Visit Day 1
☐☐☐	___/___/____ dd/mm/yyyy	

Test Day 1				
Height	☐☐☐.☐	Body Mass Index (BMI)		
Weight	☐☐☐.☐	☐☐.☐		
Has the Participant Started their VLCD?		Yes		No
If Yes, how many days have they been on it?		days ☐☐☐		

The study visit cannot proceed unless all questions below are answered YES				
Is the Participant in a fasting state?	Yes		No	
Has the Participant avoided alcohol and Paracetamol in the last 24 hours?	Yes		No	
Has the Participant avoided strenuous exercise for the last 24hours?	Yes		No	
Can the Participant fit on the bed with room for surface coils?	Yes		No	
Is the participant happy to proceed?	Yes		No	
Study Protocol				
Did the Participant Complete the MRI?	Yes		No	

Adverse Effects				
Any Adverse Events since the Participants last visit?	Yes		No	
Any medication changes Since the last visit?	Yes		No	
Comments:				

Print Name Here _____

Signed _____ Date___/____/_____

Study Researcher dd/mmm/yyyy

Participant Number	Date of Visit	Visit Day 2
☐☐☐	___/___/____ dd/mm/yyyy	

Test Day 1		
Height	☐☐☐.☐	Body Mass Index (BMI)
Weight	☐☐☐.☐	☐☐.☐

Has the Participant Started their VLCD?	Yes		No	
If Yes, how many days have they been on it?	days ☐☐☐			

The study visit cannot proceed unless all questions below are answered YES				
Is the Participant in a fasting state?	Yes		No	
Has the Participant avoided alcohol and Paracetamol in the last 24 hours?	Yes		No	
Has the Participant avoided strenuous exercise for the last 24hours?	Yes		No	
Can the Participant fit on the bed with room for surface coils?	Yes		No	
Is the participant happy to proceed?	Yes		No	
Study Protocol				
Did the Participant Complete the MRI?	Yes		No	

Adverse Effects				
Any Adverse Events since the Participants last visit?	Yes		No	
Any medication changes Since the last visit?	Yes		No	
Comments:				

Print Name Here _____

Signed _____ Date___/____/_____

Study Researcher dd/mmm/yyyy

Participant Number	Date of Visit	Visit Day 3
☐☐☐	___/___/____ dd/mm/yyyy	
Test Day 1		

Height	□□□.□	Body Mass Index (BMI)
Weight	□□□.□	□□.□

Has the Participant Started their VLCD?	Yes		No	
If Yes, how many days have they been on it?	days ☐☐☐			

The study visit cannot proceed unless all questions below are answered YES				
Is the Participant in a fasting state?	Yes		No	
Has the Participant avoided alcohol and Paracetamol in the last 24 hours?	Yes		No	
Has the Participant avoided strenuous exercise for the last 24hours?	Yes		No	
Can the Participant fit on the bed with room for surface coils?	Yes		No	
Is the participant happy to proceed?	Yes		No	
Study Protocol				
Did the Participant Complete the MRI?	Yes		No	

Adverse Effects				
Any Adverse Events since the Participants last visit?	Yes		No	
Any medication changes Since the last visit?	Yes		No	
Comments:				

Print Name Here _____

Signed _____ Date___/____/_____

Study Researcher dd/mmm/yyyy

Participant Number	Date of Visit	Visit Day 4
	___/___/____ dd/mm/yyyy	

Test Day 1		
Height	□□□.□	Body Mass Index (BMI)
Weight	□□□.□	□□.□

Has the Participant Started their VLCD?	Yes		No	
If Yes, how many days have they been on it?	days □□□			

The study visit cannot proceed unless all questions below are answered YES				
Is the Participant in a fasting state?	Yes		No	
Has the Participant avoided alcohol and Paracetamol in the last 24 hours?	Yes		No	
Has the Participant avoided strenuous exercise for the last 24hours?	Yes		No	
Can the Participant fit on the bed with room for surface coils?	Yes		No	
Is the participant happy to proceed?	Yes		No	
Study Protocol				
Did the Participant Complete the MRI?	Yes		No	

Adverse Effects				
Any Adverse Events since the Participants last visit?	Yes		No	
Any medication changes Since the last visit?	Yes		No	
Comments				
Print Name Here _____ Signed _____ Date___/____/_____ Study Researcher dd/mmm/yyyy				

Participant Number ☐☐☐	Date of Visit ___/___/____ dd/mm/yyyy	Study Status			
Did the Participant complete the study? If no, complete below		Yes		No	
Date of withdrawal: ___/____/_____ dd/mmm/yyyy At whose Request did the Participant withdraw? ☐ Participant					

	Investigator
	Sponsor
	Participants GP
	Other (Specify) _____

Primary Reason for withdrawal due to…

	Problems tolerating MRI
	Failure to comply with requirements of protocol
	Serious illness
	Withdrawal of consent
	Other (Specify) _____

Print Name Here _____

Signed _____ Date___/____/_____

Study Researcher dd/mmm/yyyy

Participant Number	Date of Visit	Investigation Statement
	___/___/____ dd/mm/yyyy	

Investigation Statement

To the best of my knowledge, I can confirm that I have made every reasonable effort to ensure that the data presented in this Case Report Form are true, complete and accurately reflect the study conduct.

Print Name Here _____

Signed _____ Date___/____/_____

Study Researcher dd/mmm/yyyy

9.5 Bariatric Study UoN ethics Application

DIFFERENTIAL EFFECTS OF VERY LOW-CALORIE DIET (VLCD), ROUX-EN-Y-GASTRIC BYPASS AND SLEEVE GASTRECTOMY ON PANCREATIC, LIVER, MUSCLE AND HEART FAT DEPOSITION AND METABOLISM IN PEOPLE WITH TYPE 2 DIABETES OR PRE-DIABETES: AN MRI STUDY

Final Version 9.0 28/08/2024

Short title:	Effects of VLCD and Bariatric Surgery in Patients with Type 2 Diabetes
Acronym:	BARIATRICMRI
Trial Registration:	www.clinicaltrials.gov 21047
IRAS Project ID:	295253
Trial Sponsor:	University of Nottingham
Sponsor reference:	*21047*
Funding Source:	Medical Research Council, University of

Nottingham, Biomedical Research Council

TRIAL / STUDY PERSONNEL AND CONTACT DETAILS

Sponsor:	University of Nottingham
Contact name	Ms Angela Shone Research and Innovation University of Nottingham East Atrium Jubilee Conference Centre Triumph Road Nottingham NG8 1DH Email: sponsor@nottingham.ac.uk
Chief investigator:	
	Iskandar Idris Professor of Diabetes & Metabolic Medicine & Honorary Consultant Physician Phone: Email: mdzii@exmail.nottingham.ac.uk

Add the name and contact details of the medical expert if different to the CI.

Co-investigators: Penny Gowland, Professor of Physics, University of Nottingham, ppzpag@exmail.nottingham.ac.uk

Susan Francis, Professor of Physics, University of Nottingham, ppzstf@exmail.nottingham.ac.uk

Stephen Bawden, Research Fellow, University of Nottingham, mszsjb@exmail.nottingham.ac.uk

Guruprasad Aithal, Professor of Hepatology, University of Nottingham, mszag3@exmail.nottingham.ac.uk

Abi Spicer, PhD student in Physics, University of Nottingham, abi.spicer@nottingham.ac.uk

Rebekah Wilmington, PhD student in Medicine and Health, University of Nottingham,

Rebekah.wilmington@nottingham.ac.uk

Gerry McCann, Professor of Cardiac Imaging, Honorary Consultant Cardiologist,

University of Leicester,

gpm12@leicester.ac.uk

Trial / Study Statistician: Stephen Bawden

Phone:

Email: Stephen.bawden@nottingham.ac.uk

SYNOPSIS

Title	DIFFERENTIAL EFFECTS OF VERY LOW CALORIE DIET (VLCD), ROUX-EN-Y-GASTRIC BYPASS AND SLEEVE GASTRECTOMY ON PANCREATIC, LIVER, MUSCLE AND HEART FAT DEPOSITION AND METABOLISM IN PEOPLE WITH TYPE 2 DIABETES: AN MRI STUDY
Acronym	BARIATRICMRI
Short title	Effects of VLCD and Bariatric Surgery in Patients with Type 2 Diabetes
Chief Investigator	Prof Iskandar Idris

Objectives	To investigate the effects of 2 weeks of Very Low Calorie Diet (VLCD) prior to bariatric surgery on liver fat. To investigate the effects of 2 weeks of Very Low Calorie Diet (VLCD) prior to bariatric surgery on physiological changes to the skeletal and cardiac muscle To investigate if bariatric surgery causes additional physiological and metabolic changes within the liver, pancreas and muscle compared to the VLCD. To investigate if Roux-en-Y Gastric Bypass (RYGB) causes differential changes in pancreatic and hepatic fat deposition, cardiac and skeletal muscle metabolism compared to Sleeve Gastrectomy (SG). These differences will relate to differences in the changes in glucose metabolism and mechanism of diabetes and pre-diabetes remission between the two surgical groups. The effects of VLCD on blood analytes: plasma glucagon, ghrelin, glucose , GIP, GLP-1, serum insulin and c-peptide. The effects of bariatric surgery on blood analytes: plasma glucagon, ghrelin, glucose, GIP, GLP-1, serum insulin and cpeptide.

	The effects of RYGB vs SG on blood analytes: plasma glucagon, ghrelin, glucose, GIP, GLP-1, serum insulin and c-peptide
Trial Configuration	A parallel study design will be used. With each arm representing a type of surgery. A secondary smaller parallel study will also exist with 2 arms, also each representing a surgery type. Patients will be allocated a surgery type using routine clinical procedure.
Setting	Bariatric Unit at Royal Derby Hospital Sir Peter Mansfield Imaging centre, University of Nottingham
Sample size estimate	Power calculations were performed using G*power (Franz Faul, Universitat Kiel, Germany) assuming a normal distribution, with a desired power of 0.8 and $p < 0.05$.

	Powering on changes due to VLCD, In Luo et al. liver fat fraction dropped from 16.6 ±7.8 % to 12.7 ± 6.8 % in 49 patients (P < 0.001) (1). Assuming

	a normal distribution and using these values, a one-tail test would find a significant drop in a sample size of n=17 participants. Accounting for a percentage drop of 22%, we will need to recruit n=21 participants to fulfil this target.
Number of participants	For the main study, Category A, we will scan n= 17 participants, with an approximate equal number of participants in Group 1 (~ 9 participants undergoing RYGB) and Group 2 (~8 participants undergoing SG). A pilot study, Category B, will recruit with n=6 participants. This will be used to investigate the effects of the VLCD, SG and RYGB on cardiac muscle. This will comprise 50% RYGB (Group 3) and 50% SG patients (Group 4).

Eligibility criteria	Inclusion: Being listed for RYGB or SG bariatric surgery at the Royal Derby Hospital. Inclusion BMI is based on eligibility for Bariatric surgery as per routine (standard) practice (BMI ≥35) Age range 18 to 70-year-old Type-II diabetes (defined as HbA1c 48mmol/mol or over) or pre-diabetes (defined as HbA1c 42-47 mmol/mol) The ability to give informed consent Exclusion: Not suitable for either RYGB or SG as determined by the MDT meeting BMI>60 Category B: BMI> 50 4. Liver cirrhosis. If they are deemed unfit for an MRI via the standard safety screeni ng form. If their waist circumference is too large for them to safely fit inside the bore of the MRI with coils in place. Participation in other research projects

Description of interventions	There are NO research interventions, this study is observing a patient's response to clinical interventions. The below describes our methods of observation. *First Contact:* Patients who are listed for surgery by the Bariatric surgical Tier 4 MDT team will be telephoned by one of the main care team, who may also be a member of the research team, to enquire if they are interested in participating in the study. If so, they will be emailed the PIS and a screening session booked Session 1 - Screening: Between 6 months and 2 weeks before surgery. Screening includes for their ability to undergo MRI, determined by a questionnaire and a replica of the MRI bore for size comparison. If eligible and consent is provided, their details will be kept by the research team to be contacted to attend the University of Nottingham (UoN) research unit based at the Royal Derby Hospital.

	There are 2 groups being considered in this study, participants undergoing RYGB (Group 1) and participants undergoing SG (Group 2). These groups will participate in either of the following sets of observations: *Category A* – Primary Study. Participants who will take part to investigate the primary and secondary outcomes. *Category B* – Exploratory sub-study. Participants will take part to investigate the primary outcome but also a pilot set of data for 31P liver MRS measures. *All study sessions:* All participants will be asked to attend a session at the Sir Peter Mansfield Imaging Centre (SPMIC) on the UoN main campus. They will also have to avoid alcohol consumption and strenuous exercise in the preceding 24 hours, alongside omitting caffeine for 18 hours. Participants have been advised to drink only water

	during that fasting period. Paracetamol should not be taken on the morning of the study day: before or during the Mixed Meal Test. Category A: The participant(s) must be fasted for 8hours. They will receive an MRI and MRS scan, a Blood Test and a liquid mixed meal test (MMT). The mixed meal test is not a part of routine care and is used to examine the change in participants' responses to a meal after each clinical intervention (VLCD and Surgery). Blood samples will be taken by a trained member of staff and transferred to the Royal Derby Hospital for testing, this is to obtain Glucose, Ghrelin, C-peptide, glucagon, Glucagon inhibitory polypeptide (GIP) and total glucagon-like peptide-1 (GLP-1). Category B: Participants will only receive MRI and MRS scans. *Session 2:*

	Between 3 and 1 day prior to the commencement of the VLCD. *Category A:* The MRI protocol for this session includes scans of the chest, abdomen as well as proton MR spectroscopy (MRS) of the liver. Participants will be in the scanner for no longer than 1 hour. *Category B:* The MRI protocol for this session includes scans of the chest, abdomen and skeletal muscle (thigh). Liver proton (^{1}H) and phosphorus (^{31}P) MR Spectroscopy will be performed. Participants will be offered a break after being in the scanner for 1 hour with a maximum time in the scanner of 2 hours and 30 minutes. Between Session 2 and 3 participants will undergo a Very Low Calorie Diet (VLCD) as part of their routine care. *Session 3:* Between 3 and 1 day prior to the participants bariatric surgery. *Category A*: As for session 2. Participants who

	opt into the additional scans will have a second visit date to undergo 31P liver MRS.

	Category B: Proton (^{1}H) and phosphorus (^{31}P) liver MR Spectroscopy will be performed. Participants will be offered a break after being in the scanner for 1 hour with a maximum time in the scanner of 2 hours and 30 minutes. *Surgery:* Roux-en-Y Gastric Bypass (RYGB): Follows standard clinical practice. Sleeve Gastrectomy (SG): Follows standard clinical practice. *Session 4:* 6 weeks post Bariatric Surgery. *Category A:* As for Session 3. *Category B:* As for Session 2 *Session 5:* 6 months post Bariatric Surgery. *Category A:* As for Session 2 *Category B:* As for Session 2
Duration of study	Start Date: December 2021 End Date: December 2025

	Each participant will be in the study for 18 weeks (2 weeks prior to surgery and 16 post-surgery)
Outcome measures	Primary outcome: Change in liver fat deposition from the VLCD (-2 weeks to –2 days) Secondary Measures: Musculoskeletal fat, whole body fat fraction, ATP flux at -2 days and +6 weeks for SG and RYGB groups. Liver and abdominal organs fat and musculoskeletal fat at +6 weeks and +6 months for SG and RYGB groups BMI between all-time points for both groups Pancreatic fat at -2 days and +6 weeks for SG and RYGB groups. Liver fat deposition at -2 days and +6 weeks for SG and RYGB groups. Change from baseline to 2 weeks on VLCD on blood analytes: plasma glucagon, ghrelin, glucose, GIP, GLP-1, serum insulin and c-peptide. Change from baseline and change from 2 weeks on VLCD to 6 weeks post-bariatric surgery on blood analytes: plasma

	glucagon, ghrelin, glucose, GIP, GLP-1, serum insulin and c-peptide. Change from baseline and change from 2 weeks on VLCD to 6 months post-bariatric surgery on blood analytes: plasma glucagon, ghrelin, glucose, GIP, GLP-1, serum insulin and cpeptide. Difference in changes due to RYGB with regards to SG on blood analytes: plasma glucagon, ghrelin, glucose, GIP, GLP-1, serum insulin and c-peptide at 6 weeks post-surgery.

	• Difference in changes due to RYGB with regards to SG on blood analytes: plasma glucagon, ghrelin, glucose, GIP, GLP-1, serum insulin and c-peptide at 6 months post-surgery.
Statistical methods	In Luo et al. liver fat fraction dropped from 16.6 ±7.8 to 12.7 ±6.8 in 49 participants ($P < 0.001$) (1). Assuming a normal distribution and using these values, a two-tail test would find a significant drop in a sample size of n=17 participants.

	Looking on to the secondary outcomes comparing RYGB to SG we aim to recruit at least 8 participants from each respective group. A dropout rate of 22% is anticipated, therefore we would need to recruit 21 participants to see 17 through to completion. For our Group 3 and Group 4 participants, all data is pilot data and so has not been powered, instead we chose a number that was reasonably recruitable.

ABBREVIATIONS

AE Adverse Event

ATP Adenosine triphosphate

BMI Body Mass Index

CI Chief Investigator overall

CRF Case Report Form

DMC Data Monitoring Committee

ERAS Enhanced Recovery After Surgery

GCP Good Clinical Practice

GIP Glucagon inhibitory polypeptide

GLP-1 Glucagon-Like Peptide-1 (GLP-1)

ICF Informed Consent Form

MRI Magnetic Resonance Imaging

MRS Magnetic Resonance Spectroscopy

NHS National Health Service

PI Principal Investigator at a local centre

PIS Participant Information Sheet

REC Research Ethics Committee

R&D Research and Development department

RYGB Roux-en-Y Gastric Bypass

SAE Serious Adverse Event

SG Sleeve Gastrectomy

SPMIC Sir Peter Mansfield Imaging Centre

T2D Type II Diabetes

UoN University of Nottingham

VLCD Very Low-Calorie Diet

TABLE OF CONTENTS

TRIAL / STUDY BACKGROUND INFORMATION AND RATIONALE

Obesity rates are climbing worldwide. This has led to a corresponding rise in obesity related complications such as type 2 diabetes (T2D), pre-diabetes and cardiovascular diseases with their inherent mortality, risk for functional decline, hospitilisation and loss of independence, especially in morbidly obese subjects. Over the last decade, bariatric surgery has emerged as a safe and proven method for better, more sustained weight loss versus exercise and dietary measures. The most commonly performed bariatric surgery in the UK and worldwide are: Roux-en-Y gastric bypass (RYGB) and sleeve gastrectomy (SG) operations.

In addition to bariatric surgery, all patients undergo a period of Very Low-Calorie diet (VLCD) to reduce the size of the liver prior to bariatric surgery. VLCD has also been shown to independently reduce blood glucose levels and in some cases, induce diabetes remission by removal of fatty acids (triacylglycerol) from the pancreas and liver (2).

Both surgical procedures have been shown to achieve a large and sustained improvement in weight loss with improvements in insulin sensitivity, improved beta cell function and associated with high resolution rate in T2D or achievement of normoglycaemia in prediabetic states (3–5). SG surgery involves the removal of 80% of the stomach whilst RYGB involves the anastomosis of lower oesophagus with distal small bowel, which means that food ‘skips’ the stomach, duodenum and upper small intestine (See figure 1).

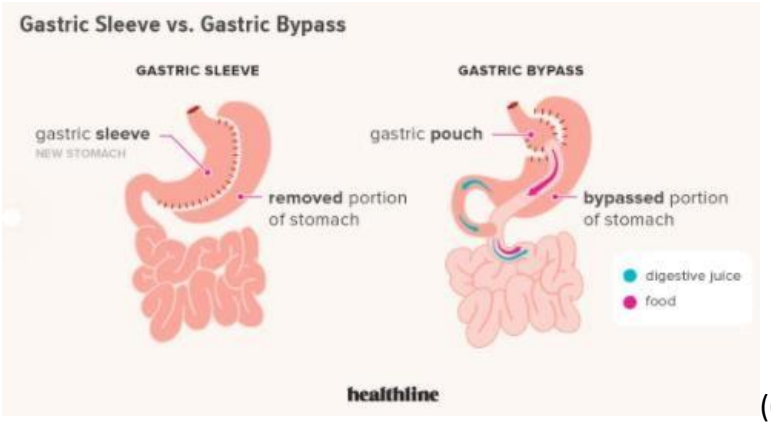

(6)

Figure 1 – The difference between Sleeve gastrectomy and Gastric bypass

Metabolic effects of surgery can be observed early and long term. However, the observation that the rapid rate of glucose lowering is disproportionate to degree of weight loss suggests that bariatric surgery reverses the fundamental pathophysiological defects of glucose dysregulation seen with type 2 diabetes or pre-diabetes- independent of weight loss.

Current Research has focused on the use of MRI to investigate the physical changes to fat deposition and using this as a marker of improvements from the VLCD and surgery (1,2,7,8). Focusing on Liver fat MRI- proton density fat-fraction (PDFF) measurements were taken prior to the surgery and at 1,6 and 12-months post-surgery. It was found that for 49 (26 for RYGB, 20 for SG and 3 for Gastric banding)

participants, the PDFF showed a statistically significant reduction (P<0.001) between baseline and post VLCD (16.6 ± 7.8 vs. 12.7 ± 6.8, ±SD), a 23% reduction, and post VLCD to 1 month post-surgery (12.7 ± 6.8 vs. 7.3 ± 4.1, ±SD), a 42% reduction for the whole group (1). However, these do not record the point at which a patient starts to show diabetes remission.

We are therefore interested to explore the effects of VLCD and different bariatric surgery procedures to changes in the physical deposition of fat in organs which regulate glucose metabolism (i.e. in the liver, pancreas, muscle) in the earlier (6 weeks) and intermediate (4 months) period after bariatric surgery, where rate of weight loss at this stage are similar between the two procedures. Increased understanding of the changes in these important metabolic organs, will increase our understanding of mechanism for an improved glycaemic profile including diabetes remission following bariatric surgery or return to euglycaemia from pre-diabetic states, their effects on weight loss or changes in gut hormones levels. Magnetic Resonance imaging (MRI) and Magnetic Resonance spectroscopy (MRS) are non-invasive, non-ionising techniques. MRI can be used to investigate the body's physiology and MRS can be used to investigate the body's metabolic processes, so by combining these two methods we are able to investigate the process of fat reduction and glycaemic improvement by diabetes remission, or return to euglycaemic state from pre-diabetes, post gastric surgery without performing any secondary invasive procedures.

TRIAL / STUDY OBJECTIVES AND PURPOSE

PURPOSE

The purpose of this project is to investigate the effects of a Very Low Calorie Diet (VLCD) followed by two different bariatric surgical procedures, Roux-en-Y Gastric Bypass (RYGB) and Sleeve gastrectomy (SG) on skeletal muscle, liver and pancreatic fat deposition, ATP flux as well as cardiac function

PRIMARY OBJECTIVE

The effects of VLCD on liver fat.

SECONDARY OBJECTIVES

The effects of VLCD on cardiac function

The effects of VLCD on skeletal muscle, liver and pancreatic and other abdominal organs fat, volume T2, T2* and T1

The effect of Bariatric Surgery on skeletal muscle, liver and pancreatic and other abdominal organs fat and volume T2, T2* and T1 .

The effects of Bariatric Surgery on Liver ATP flux.

The effects of RYGB or SG on Liver ATP and cardiac function

The effects of RYGB or SG on skeletal muscle, liver, and pancreatic and other abdominal organs fat and volume T2, T2* and T1

The effects of VLCD on blood analytes: plasma glucagon, ghrelin, glucose , GIP, GLP-1, serum insulin and c-peptide.

The effects of bariatric surgery on blood analytes: plasma glucagon, ghrelin, glucose, GIP, GLP-1, serum insulin and c-peptide.

The effects of RYGB vs SG on blood analytes: plasma glucagon, ghrelin, glucose, GIP, GLP1, serum insulin and c-peptide.

DETAILS OF PRODUCT(S)

A liquid mixed meal test

Description

Fortisip – a meal replacement drink, used in the mixed meal test

Fortisip Bottle Fortisip Bottle is a nutritionally complete, milk shake style nutritional drink for the management of disease related malnutrition. Fortisip Bottle is high in energy (1.5kcal/ml) and can be used to supplement the diet of those unable to meet their nutritional requirements from other foods, or as a sole source of

nutrition. Fortisip Bottle is ready to drink and is available in 8 flavours: Neutral, Vanilla, Chocolate, Toffee/Caramel, Banana, Orange, Strawberry, and Tropical.. Fortisip Bottle is best served chilled and Fortisip Bottle Neutral may be added to sweet and savoury foods. Fortisip Bottle is gluten and lactose free.

Manufacture

Nutricia Fortisip

Packaging and labelling

Ingredients: Water, maltodextrin, milk protein, sucrose, vegetable oils, tri potassium citrate, emulsifier (soy lecithin), flavour, magnesium chloride, acidity regulator (citric acid), tri calcium phosphate, carotenoids (contains soy) (b-carotene, lutein, lycopene), choline chloride, calcium hydroxide, potassium hydroxide, sodium L-ascorbate, ferrous lactate, zinc sulphate, colour (curcumin), magnesium hydroxide, nicotinamide, retinyl acetate, copper gluconate, DL-a-tocopheryl acetate, sodium selenite, manganese sulphate, calcium D-pantothenate, chromium chloride, D-biotin, cholecalciferol, thiamin hydrochloride, pteroylmonoglutamic acid, pyridoxine hydrochloride, cyanocobalamin, sodium molybdate, riboflavin, sodium fluoride, potassium iodide, phytomenadione.

Storage, dispensing and return

Store in a cool, dry place (5-25°C). Shake well before use. Once opened, close the bottle and store in a refrigerator for a maximum of 24 hours.

Fortisip Bottle is ready to drink and is best served chilled. Shake well before opening. Fortisip Bottle Neutral may be added to sweet and savoury foods.

Placebo

No Placebo will be used

Known Side Effects

For enteral use only. ACBS approved, can be prescribed on form FP10 (GP10 in Scotland) for the following indications: short bowel syndrome; intractable malabsorption; pre-operative preparation of undernourished patients; inflammatory bowel disease; total gastrectomy; dysphagia; bowel fistulae; disease related malnutrition. Not suitable for patients with galactosaemia.

A nutritional bar –

This patient group can struggle with fasting. To address this a nutritional bar will be provided to participants following their MMT prior to the MRI scan to sustain them until they get home.

Description

High in protein bar, packed with vitamins and minerals

Manufacture

Lighterlife

Packaging and Labelling:

Ingredients: milk chocolate 15,2% (sugar, cocoa butter, whole milk powder, cocoa mass, emulsifier (soy lecithin), flavours), rice syrup, milk protein, hydrolysed wheat gluten, soy protein, wheat starch, humectant (glycerol), butterscotch pieces 4,5% (sugar, glucose syrup, milk fat), soy granules, minerals (dipotassium phosphate, trimagnesium citrate, potassium chloride, ferric(III)diphosphate, zinc oxide, copper(II) gluconate, sodium fluoride, manganese sulphate, chromium(III)chloride, sodium selenite, sodium molybdate, potassium iodide), sweetener 3,3% (erythritol), rice crisp (rice flour, wheat gluten, sugar, wheat malt, glucose, salt), peanuts 2,1%, sunflower oil, colouring agent (calcium carbonate), flavours, vitamins (vitamin C (ascorbic acid), nicotinamide, vitamin E (tocopheryl acetate), calcium pantothenate,

vitamin B2 (riboflavin), vitamin B6 (pyridoxine hydrochloride), vitamin B1 (thiamin hydrochloride), vitamin A (retinyl acetate), folic acid, vitamin K, biotin, vitamin D (cholecalciferol), vitamin B12 (cyanocobalamine)).

Storage, Dispensing and Return Store in a cool, dry place.

Placebo

No placebo will be used

Known Side Effects

For exteral use only. May contain nuts, sesame. Suitable for vegetarians. The soya in this product is from a non-genetically modified source

TRIAL / STUDY DESIGN

TRIAL / STUDY CONFIGURATION

This will be a multi-centre, non-randomised parallel group study, with Participants undergoing procedures at both the Sir Peter Mansfield Imaging Centre (SPMIC) at the University of Nottingham (UON) and the Royal Derby hospital.

All Participants will undergo the same VLCD for a minimum of 2 weeks as part of their standard clinical care but will then be split into 2 treatment groups, one undergoing RYGB and one undergoing SG. Allocation for surgery type will be according to routine clinical practice. Surgery will be performed at the Royal Derby Hospital.

All groups will receive Magnetic Resonance Imaging (MRI) and Magnetic Resonance Spectroscopy (MRS) scans, and a fasting mixed meal test will be done at the SPMIC.

Primary endpoint

Change to the Liver fat volume from baseline to 2 weeks on the VLCD as measured using MRI.

Secondary endpoint

Change from baseline to 2 weeks on VLCD on cardiac function as measured using MRI. Change from baseline to 2 weeks on of VLCD on skeletal muscle, liver and pancreatic and other abdominal organs fat and volume as measured using MRI.

Change from baseline and change form 2weeks on VLCD to 6 weeks post-bariatric-surgery on skeletal muscle, liver and pancreatic and other abdominal organs fat and volume. Change from baseline and change form 2weeks on VLCD to 6 weeks post-bariatric-surgery on Liver ATP flux.

Change from baseline and change form 2weeks on VLCD to 6months post-bariatric-surgery on skeletal muscle, liver and pancreatic and other abdominal organs fat and volume. Change from baseline and change form 2weeks on VLCD to 6months post-bariatric-surgery on Liver ATP flux.

Difference in changes due to RYGB with regards to SG on Liver ATP and cardiac function at 6weeks post-surgery

Difference in changes due to RYGB with regards to SG on Liver ATP and cardiac function at 6months post-surgery

Difference in changes due to RYGB with regards to SG on skeletal muscle, liver, and pancreatic and other abdominal organs fat and volume at 6weeks post-surgery

Difference in changes due to RYGB with regards to SG on skeletal muscle, liver, and pancreatic and other abdominal organs fat and volume at 6months post-surgery

Change from baseline to 2 weeks on VLCD on blood analytes: plasma glucagon, ghrelin, glucose, GIP, GLP-1, serum insulin and c-peptide.

Change from baseline and change from 2 weeks on VLCD to 6 weeks post-bariatric surgery on blood analytes: plasma glucagon, ghrelin, glucose, GIP, GLP-1, serum insulin and cpeptide.

Change from baseline and change from 2 weeks on VLCD to 6 months post-bariatric surgery on blood analytes: plasma glucagon, ghrelin, glucose, GIP, GLP-1, serum insulin and cpeptide.

Difference in changes due to RYGB with regards to SG on blood analytes: plasma glucagon, ghrelin, glucose, GIP, GLP-1, serum insulin and c-peptide at 6 weeks post-surgery. Difference in changes due to RYGB with regards to SG on blood analytes: plasma glucagon, ghrelin, glucose, GIP, GLP-1, serum insulin and c-peptide at 6 months post-surgery.

Safety endpoints

Stopping rules and discontinuation

Participants may withdraw from the study for:

Failure of participant in the group to attend a session.

If the progress of their recovery is delayed increasing the MRI risk factor Withdrawal of consent:

In the event of withdrawal, we will aim to replace with a new participant for the same group i.e. RYGB/SG. Participants may be withdrawn from the trial either at their own request or at the discretion of the Investigator. The participants will be made aware that this will not affect their future care. Participants will be made aware (via the information sheet and consent form) that should they withdraw the data collected to date cannot be erased and may still be used in the final analysis.

TRIAL/STUDY MANAGEMENT

The Chief Investigator has overall responsibility for the study and shall oversee all study management.

The data custodian will be the Chief Investigator.

DURATION OF THE TRIAL / STUDY AND PARTICIPANT INVOLVEMENT

Study Duration: Recruitment will start by December 2021 and end in December 2025.

Participant Duration: Each participant will be in the study for 2 weeks prior to their surgery and for 26 weeks after. Giving a total of 28 weeks.

End of the Trial

The end of the study will be 16 weeks after the final study session of the last participant.

SELECTION AND WITHDRAWAL OF PARTICIPANTS

Recruitment

Participants will be recruited from Royal Derby Hospital. This is the regional centre for bariatric surgery for East Midlands, and also accepts some referrals from outside of the East Midlands. In addition, participants will be identified from those who have been listed for surgery by the Bariatric surgical Tier-4 MDT team. This list is held by the bariatric surgery administrative team. The initial approach will be from a member of the patient's usual care team (which may include the investigator), and information about the trial will be on display in the relevant clinical areas. This will likely happen when the patient is listed for surgery via telephone.

The investigator or their nominee, e.g. from the research team or a member of the participant's usual care team, will inform the participant (other individual or other body with appropriate jurisdiction), of all aspects pertaining to participation in the study. Participants who lack the ability to give informed consent will not be included in the study.

If needed, the usual hospital interpreter and translator services will be available to assist with discussion of the trial, the participant information sheets, and consent

forms, but the consent forms and information sheets will not be available printed in other languages.

It will be explained to the potential participant that entry into the trial is entirely voluntary and that their treatment and care will not be affected by their decision. It will also be explained that they can withdraw at any time, but attempts will be made to avoid this occurrence. It will be explained that in the event of their withdrawal their data collected so far cannot be erased and we will seek consent to use the data in the final analyses where appropriate.

Category A:

At session 2. Participants who tolerate the MRI well and have a BMI<50 will be given the opportunity to take part in 2 additional MR sessions for 31P liver MR spectroscopy at the same study time points as Session 3 (post-VLCD/pre-surgery) and Session 4 (6-weeks-postsuregery). Due to the need for the MMT to be consistently performed at the same time of day for each study visit, we are unable to offer these extra 31P liver MRS scan sessions on the same dayas their other MR scans for that study visit time. Due to the spontaneous movement of surgery dates offers may be withdrawn based on MRI availability, the main study arm will be prioritised in bookings.

Category B has been given a lower BMI cut off. This is due to the difficulty in gaining adequate signal for ATP flux from the liver at large distances.

Eligibility criteria

Inclusion criteria

Being listed for RYGB or SG bariatric surgery at the Royal Derby Hospital.

Inclusion BMI is based on eligibility for Bariatric surgery as per routine (standard) practice (BMI ≥35)

Age range 18 to 70-year-old.

Ability to give informed consent

Type II Diabetes (T2D) or pre-diabetes

Exclusion criteria

Patients who are not fit or not suitable for RYGB operation, according to the MDT meeting described above.

BMI>60

Category B participants: BMI>50

Not suitable for MRI scanning (as decided by a MRI safety screening form) Liver Cirrhosis

Type I Diabetes

Non-diabetic

Involvement in other Research Studies

Expected duration of participant participation

Study participants will be participating in the study for 18 weeks.

Removal of participants from therapy or assessments/Participant Withdrawal

Participants may withdraw from the study for:

Withdrawal of consent

Failure of participant to attend a study session.

In the event of withdrawal, we will aim to replace with a new participant for the same group i.e. RYGB/SG.

If Participants become pregnant over the course of the study they will be removed from the study.

Participants may be withdrawn from the trial either at their own request or at the discretion of the Investigator. The participants will be made aware that this will not affect their future care. Participants will be made aware (via the information sheet

and consent form) that should they withdraw the data collected to date cannot be erased and may still be used in the final analysis.

Informed consent

Patient who are listed for bariatric surgery will be contacted over the phone by a member of their main care team (who may also be a member of the research team) and will be informed of the study and their interest in participating will be established. If the patient is interested in participating in the study a screening session will be booked.

Attempts will be made so the screening session and the ERAS (Enhanced Recovery After Surgery) session occur on the same day. Informed consent will be taken at the screening session by a trained member of the research team.

All participants will provide their written informed consent. The Informed Consent Form will be signed and dated by the participant before they enter the trial. The Investigator will explain the details of the trial and provide a Participant Information Sheet, ensuring that the participant has sufficient time to consider participating or not. The Investigator will answer any questions that the participant has concerning study participation.

Informed consent will be collected from each participant before they undergo any interventions (including physical examination and history taking) related to the study. One copy of this will be kept by the participant, one will be kept by the Investigator, and a third will be retained in the patient's hospital records.

Should there be any subsequent amendment to the final protocol, which might affect a participant's participation in the trial, continuing consent will be obtained using an amended Consent form which will be signed by the participant.

TRIAL / STUDY TREATMENT AND REGIMEN

There are 2 groups being considered in this study, participants undergoing RYGB (Group 1) and participants undergoing SG (Group 2). Participants in these groups will participate in either of the following sets of observations:

Category A – Primary Study. The focus of Catergory A is the abdominal organs, especially the liver's reaction to the clinical interventions. Participants who will take part to investigate the primary and secondary outcomes.

Category B – Exploratory sub-study. Due to similarities in protocol and recruitment a smaller group (category B) was created. There had to be 2 separate groups due to the lengthy nature of the MR scans. Participants will take part to investigate the

primary outcome but also a pilot set of data for 31P liver MRS measures. The purpose of category B is to allow us to pilot an investigation into the effects of the RYGB and SG on the energy flux.

Initially participants recruited will be entered into category A. This means that they will be used to investigate the primary and most of the secondary outcomes. Recruitment for Category A and B will be simutaneous with participants whose BMI is below 50 being offered both protocols during their screening visit. Once 6 participants have been recruited to category B this option will be removed and recruitment paused. Recruitment will ressume if a participant has to be removed or drops out of the study.

Figure 2 – Study Session interventions, Category A interventions are shown in blue.

Category B interventions are shown in Green.

All other interventions are identical within a category, as explained by the following schematic (figure 3):

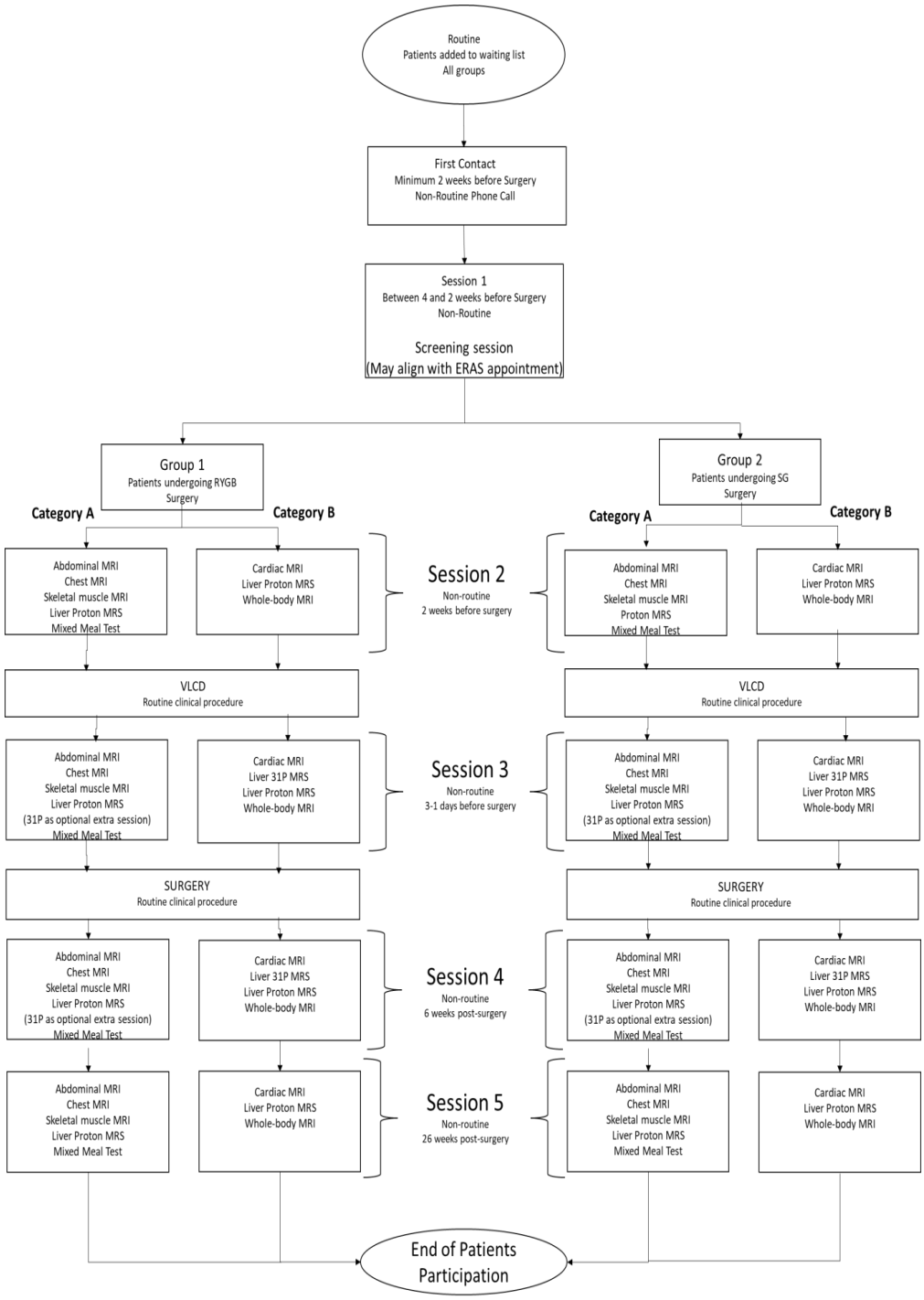

Figure 3: Flow of study sessions for each group.

More Detail on each session is given below:

First Contact: Non-routine

Patient who are listed for bariatric surgery will be contacted by a member of their main care team (who may also be a member of the research team) over the phone and will be informed of the study and their interest in participating will be established.

During this contact participants will be asked their availability and booked in for the screening session, attempts will be made for this to be the same day as their ERAS appointment.

Session 1 - Screening:

6 months to 2 weeks prior to surgery – non-routine appointment – All Groups: Non-Routine: Carried out by a member of the research team: Participants who are interested in the study will be asked to lie down and a replica of the MRI bore will be placed over them to ensure they can fit into a scanner, if so participants will complete the MRI screening test, as this is a safety-critical element of the eligibility criteria. All other eligibility criteria will be performed as part of routine care. The Participants will be provided with the PIS and their willingness and ability to attend all 4 sessions will be evaluated to ensure maximum completion of participants in

the study. If participants are eligible and consent to participate, their information will be passed on to the rest of the research team to be contacted further.

The CI will be in charge of obtaining informed consent. If unavailable, another trained member of the research team may take their place.

At all following study sessions (All Non-routine):

Participants will have been advised to avoid alcohol consumption and strenuous exercise for the preceding 24 hours, and caffeine for 18 hours prior to the undertaking of the test. To reduce the fasting period all tests and scans will be scheduled to take place in the morning. The fasting period will allow water only. The fast will be broken at the point of the Mixed Meal Test which is the first intervention of the study morning. Participants will visit the SPMIC on the UoN main campus. Participants will be greeted by a member of the research team. Participants will be asked to remove all jewellery and change into paper scrubs, provided by the centre, and directed to a changing room where they can leave their belongings. The participant will then be screened using a standard secondary screening form.

Category A: The participants will need to be fasted prior to the study for a minimum of 8 hours. Participants will be taken into a clinical room adjacent to the MRI suite. Here they will be met by a trained member of staff, who will insert a cannula into

their arm or hand. Less than 15ml of blood will be drawn and decanted into appropriate tubes to allow for all analytes.

There should be minimal distress from the procedure as this process is similar to what the participants will have experienced as part of their routine care at a GP surgery or hospital. Sharp pain is common during the procedure but well tolerated. Bruising is a known complication of the venepuncture but can be minimised with compression of the site postprocedure. The extremity will be placed in a hot box to allow for arterial like drawing of the blood.

Participants will then undergo a Mixed Meal Test (MMT) (200ml 300kcal). The MMT will be a Nutricia, Fortisip, this will be stored in the fridge and a flavour of their choice (except chocolate which is not suitable for this process) will be served to the participants chilled. Each bottle is 200ml and this is the standard size of the mixed meal (200ml 300kcal).Once the participant has consumed the mixed meal the bloods will been drawn every 15 minutes for 3hours.

The blood will be spun in a centrifuge for 10minutes within 10 minutes of being drawn. This will be done in an appropriate lab at the SPMIC. The plasma will then be separated from the cells and stored in a -20degree freezer temporarily. By the end of the following working day after the study day the samples will be transferred to the medical school to be stored at 80°C freezer on E floor of the medical school which is locked & alarmed with CO_2 back up.

The samples will be transferred to Royal Derby Hospital for analysis after all data collection has been completed. Samples will be removed from the -80°C freezer and couriered in a labelled igloo containing dry ice to laboratories in Derby Medical School. The shipment will contain a complete inventory of all samples, along with the name of the person responsible for sending and receiving the samples. These samples will be stored in a -80°C freezer in this facility until analysis. Once all study-related analysis on the samples have been completed, they will be disposed of in accordance with the Human Tissue Act, 2004.

Following the MMT the participant will be offered a lighterlife nutritional bar and opportunity to use toilet facilities and will then proceed to have their MRI scan. The participants will then be led into the magnet hall and asked to lie on the bed, ear protection and headphones will be provided and then surface coils will be placed on the patient. The participants will then be moved into the bore of the scanner and the researcher will leave the room and scanning will begin.

Category B: Participants will only receive MRI and MRS scans using similar procedures to category A above.

Category A:

Session 2, 3, 4and 5:

Participants will undergo MRI scans of their chest, abdomen. These scans will be used to determine the health of tissue. MRI scans will take around 30-40 minutes. A proton MRS scan of the Liver which will require a different surface coil to be used, this scan will take around 15 minutes.

At session 2. Participants who tolerate the MRI well and have a BMI<50 will be offered 2 additional sessions at the same study time points as Session 3 (post-VLCD/pre-surgery) and 4 (6-weeks-post-suregery). Offers will also be based on MRI availability.

These will each be a 1h (no longer than 1h30) 31P liver MRS scan on an additional day.

Following session 5, we will access NHS records to review for an up-to-date HbA1c result to allow us to assess for glycaemic control at this phase; it is expected to form part of clinical standard practice to monitor for improved glycaemic control following bariatric surgery.

Category B:

Session 2 and 5:

Participants will undergo MRI scans of their chest, abdomen and thighs. These scans will be used to determine the health of tissue. MRI scans will take around 30-40 minutes. A proton MRS scan will take around 15 minutes. Participants will undergo physiological scans of the heart which will take approximately 15minutes.

Following session 5, we will access NHS records to review for an up-to-date HbA1c result to allow us to assess for glycaemic control at this phase; it is expected to form part of clinical standard practice to monitor for improved glycaemic control following bariatric surgery.

Sessions 3 and 4:

Participants will undergo MRI scans of their chest, abdomen. These scans will be used to determine the health of tissue. MRI scans will take around 30-40 minutes. A proton MRS scan will take around 15 minutes. Participants will undergo physiological scans of the heart which will take approximately 15minutes. Phosphorus (31P) MRS will also be performed on the patient's livers, this requires a specialised coil and will take 60 minutes. It is likely participants will need to take a break to stretch and be out of the scanner mid-session due to the long scan times.

Compliance

Compliance will be determined as attendance at every visit.

Criteria for terminating trial.

The majority of the study is performed at a single focal centre (SPMIC) so termination at this centre will result in termination of the whole study. No participants are required to attend sessions at the Royal Derby Hospital so termination here will not result in termination of the Study, rather a new location to analyse the blood samples will be found and the protocol updated accordingly. Termination will be considered if it becomes clear that the study is resulting in an unacceptably high incidence of significant side effects from the study protocol (drink, blood sampling and MRI). However, this is of minimal likelihood as all study protocol interventions are well tolerated. Nonetheless, termination will also be considered if during the course of the study it becomes apparent that the majority of participants are not able to achieve acceptable levels of compliance with the MRI scanning protocols. Responsibility for the decision to terminate the study will fall upon the Chief Investigator.

It will be explained to all participants that any research data obtained until the point of termination will be stored as per the ICH/GCP guidelines, and in accordance with the University of Nottingham Research Code of Conduct and Research Ethics.

TRANSPORT AND STORAGE OF THE TISSUES

The blood samples will be walked to a lab close to the clinical room within the SPMIC. By the end of the following working day after the study day the samples will be transferred to the Queens Medical Centre, medical school to be stored at -80°C freezer on D floor which is locked & alarmed with CO_2 back up.

The samples will be transferred to Royal Derby Hospital for analysis after all data collection has been completed.

Samples will be removed from the -80°C freezer and couriered in a labelled igloo containing dry ice. The shipment will contain a complete inventory of all samples, along with the name of the person responsible for sending and receiving the samples.

Samples will be stored in a linked anonymised format and labelled using a combination of study reference, unique study identifier and cross referenced with location code numbers to permit accurate linkage to study data and the consent

form (as per Human Tissue Act requirement). Samples for NHS pathology analysis will be labelled in accordance with local NHS procedures. All blood samples will be stored in aliquots in -80 degrees' centigrade freezer in our department of Metabolic & Molecular Physiology, University of Nottingham, Derby.

The master database will be held by the primary researcher (in a password encrypted file. The analysis of samples will take place at the University of Nottingham (Derby) within the Department of Metabolic & Molecular Physiology.

Once Analysis is complete samples will be destroyed in accordance with the Human Tissue Act, 2004.

LABORATORY ANALYSES

All analyses will be undertaken within the Clinical, Metabolic and Molecular Physiology Laboratories (~400m2) based in the Medical School at the Royal Derby Hospital Campus. All laboratory procedures are well-established in-house and the procedures validated and published in peer-reviewed journals.

Plasma Glucagon, Ghrelin, Glucose, GIP and GLP-1, and serum Insulin and C-peptide will be measured using Multiplex ELISA technique.

All samples will be stored appropriately in -80°C and -20°C freezers in line with HTA guidelines; all -80°C freezers are monitored constantly by an alarm system (Notion Pro) and linked to the University of Nottingham Alarm system. In the event of a

freezer failure, senior lab staff members are notified by email and text and procedures are put in place to relocate the samples to backup freezers within the Medical School.

All analyses will be undertaken by trained staff, who have been signed off as being competent, with reference to standard operating procedures for each of the analyses. All laboratory equipment is maintained in line with manufacturers' recommendations, with routine maintenance and servicing being performed by trained laboratory staff.

STATISTICS

Methods

Statistical analysis will be undertaken using SPSS (IBM Corp. IBM SPSS Statistics for Windows. Armonk, NY: IBM Corp) with a significance level of $p<0.05$. The group assignment of the data will be blinded by an independent investigator and analysed for blind review before group comparisons are made.

Primary measure:

Effects of the VLCD diet will be statistically analysed using a whole group means difference test (matched pairs t-test) for normally distributed data and Wilcoxon signed-rank test for non-normally distributed data.

Secondary Measure:

Additional effects of bariatric surgery will be statistically analysed in each group separately (SG and RYGB) using a one-way repeated measures ANOVA test. A statistically significant effect will be followed up with individual matched pair t-tests for normally distributed data and a wilcoxon sign ranked test for non-normally distributed data at each time point.

The effect of the different surgery types will be statistically analysed using a two-way repeated measures ANOVA test comparing surgery type and time. A significant interaction between surgery type and time will be followed up by an independent group t-test at each time point for normally distributed data and wilcoxon sign ranked test for non-normally distributed data.

Sample size and justification

We are aiming for 17 completed participants for the study for arm A. The number was justified based on our on-going study in this area, as well as previous published study on the effect of VLCD on liver fat deposition. In Luo et al. liver fat fraction

dropped from 16.6 ±7.8 to 12.7 ±6.8 in 49 Participants (P < 0.001) (Luo RB, Suzuki T, Hooker JC, Covarrubias Y, Schlein A, Liu S, et al. How bariatric surgery affects liver volume and fat density in NAFLD Participants. Surg Endosc [Internet]. 2018 Apr 1 [cited 2021 Jan 19];32(4):1675–82. Available from: https://doi.org/10.1007/s00464-017-5846-9). Assuming a normal distribution and using these values, a two-tail test would find as significant drop in a sample size of n=22. Power calculation were performed using G*power (Franz Faul, Universitat Kiel, Germany) assuming a normal distribution, with a desired power of 0.8 and p < 0.05.

For arm B we are aiming for 6 Participants. This is an exploratory, pilot study. No previous study has been performed. The number was based upon the judgment of clinicians due to the difficulty in recruiting Participants, the limitation on their size and the time they will need to be in the scanner.

Assessment of efficacy

This is an observational physiological study to understand the mechanism of glycaemic improvement including diabetes remission, or return to euglycaemia from a pre-diabetic state, following bariatric surgery, undertaken during routine clinical care. This is therefore not an efficacy study and hence no assessment of efficacy will be conducted.

Assessment of safety

This study will not be assessing safety endpoints. However, safety of participants is of utmost priority to our research department and will be actively monitored throughout the course of the study. These will be documented in the participant's case report form and in the trial master file. There will also be a database specifically designated to the documentation of adverse events and safety concerns. This database will be reviewed regularly by the Chief Investigator and Co-Investigators. If a high occurrence of intolerance to MRI scanning protocol, this will be discussed and potential alterations to the protocol that will improve this will be made. If the occurrence becomes unacceptably high then the study will be terminated before completion. We do not anticipate this as the MRI protocol is non-invasive and usually well tolerated.

Procedures for missing unused and spurious data

This is a small physiology research study; therefore missing data would have a significant impact on the validity of the results obtained. As such, every effort will be made to ensure the amount of missing data is kept to a minimum. Study visits will be performed by researchers who have a full and complete understanding of every aspect of the study. There will be a detailed proforma with clear instructions regarding the data be collected at each timepoint. In addition, any samples requiring storage prior to analyses will be duplicated and stored in separate freezers.

With these measures in place, we will endeavour to ensure that fewer than 10% of the complete data set will be missing. If this is achieved, the data will be analysed using standard statistical techniques as described above. However, if despite these measures there is greater than 10% missing data, this will be discussed directly with the supporting statistician and the procedure for dealing with this will then depend on the extent of data that is missing. Definition of populations analysed All data sets will be analysed.

ADVERSE EVENTS

The occurrence of an adverse event as a result of participation within this study is not expected and as such no adverse event data will be collected

Reporting of adverse events

There are no research interventions as we will be using non-invasive MRI and minimally invasive blood sampling techniques, both of which are well tolerated. Therefore no adverse event reporting will be undertaken.

Trial Treatment / Intervention Related SAEs

A serious adverse event that is unexpected in its severity and seriousness *and* deemed directly related to/or suspected to be related to the trial treatment or intervention shall be reported to the ethics committee that gave a favourable opinion as stated below.

The event shall be reported immediately of knowledge of its occurrence to the Chief Investigator.

The Chief Investigator will:

Assess the event for seriousness, expectedness and relatedness to the trial treatment or intervention.

Take appropriate medical action, which may include halting the trial and informing the Sponsor of such action.

If the event is deemed related to the trial treatment or intervention shall inform the REC using the reporting form found on the NRES web page within 7 days of knowledge of the event.

Shall, within a further eight days send any follow-up information and reports to the REC.

Make any amendments as required to the study protocol and inform the REC as required

Participant removal from the study due to adverse events

Any participant who experiences an adverse event may be withdrawn from the study at the discretion of the Investigator.

ETHICAL AND REGULATORY ASPECTS

ETHICS COMMITTEE AND REGULATORY APPROVALS

The trial will not be initiated before the protocol, informed consent forms and participant and

GP information sheets have received approval / favourable opinion from the Research Ethics Committee (REC), the respective National Health Service (NHS) or other healthcare provider's Research & Development (R&D) department, and the Health Research Authority (HRA) if required. Should a protocol amendment be made that requires REC approval, the changes in the protocol will not be instituted until the amendment and revised informed consent forms and participant information sheets (if appropriate) have been reviewed and received approval / favourable opinion from the REC and R&D departments. A protocol amendment intended to eliminate an apparent immediate hazard to participants may be

implemented immediately providing that the REC are notified as soon as possible and an approval is requested. Minor protocol amendments only for logistical or administrative changes may be implemented immediately; and the REC will be informed.

The trial will be conducted in accordance with the ethical principles that have their origin in the Declaration of Helsinki, 1996; the principles of Good Clinical Practice, and the UK Department of Health Policy Framework for Health and Social Care, 2017.

INFORMED CONSENT AND PARTICIPANT INFORMATION

The process for obtaining participant informed consent will be in accordance with the REC guidance, and Good Clinical Practice (GCP) and any other regulatory requirements that might be introduced. The investigator or their nominee and the participant shall both sign and date the Informed Consent Form before the person can participate in the study.

The participant will receive a copy of the signed and dated forms and the original will be retained in the Trial Master File. A second copy will be filed in the participant's medical notes and a signed and dated note made in the notes that informed consent was obtained for the trial.

The decision regarding participation in the study is entirely voluntary. The investigator or their nominee shall emphasise to them that consent regarding study participation may be withdrawn at any time without penalty or affecting the quality or quantity of their future medical care, or loss of benefits to which the participant is otherwise entitled. No trial-specific interventions will be done before informed consent has been obtained.

The investigator will inform the participant of any relevant information that becomes available during the course of the study, and will discuss with them, whether they wish to continue with the study. If applicable they will be asked to sign revised consent forms.

If the Informed Consent Form is amended during the study, the investigator shall follow all applicable regulatory requirements pertaining to approval of the amended Informed Consent Form by the REC and use of the amended form (including for ongoing participants).

RECORDS

Case Report Forms (CRF)

Each participant will be assigned a trial identity code number, allocated at randomisation if appropriate, for use on CRFs other trial documents and the electronic database. The documents and database will also use their initials (of first and last names separated by a hyphen or a middle name initial when available) and date of birth (dd/mm/yy).

CRFs will be treated as confidential documents and held securely in accordance with regulations. The investigator will make a separate confidential record of the participant's name, date of birth, local hospital number or NHS number, and Participant Trial Number (the Trial Recruitment Log), to permit identification of all participants enrolled in the trial, in accordance with regulatory requirements and for follow-up as required

CRFs shall be restricted to those personnel approved by the Chief or local Principal Investigator and recorded in the 'Trial Delegation Log.'

All paper forms shall be filled in using black ballpoint pen. Errors shall be lined out but not obliterated by using correction fluid, and the correction shall be inserted, initialled and dated. The Chief or local Principal Investigator shall sign a declaration ensuring accuracy of data recorded in the CRF.

Sample Labelling

Each participant will be assigned a trial identity code number for use on the samples, consent forms and other study documents and the electronic database. The documents and database will also use the study acronym and sequential study number. For example, with a hypothetical 22nd study volunteer called "John Doe", the pseudonymisation would resemble "RYGBSG22", where "RYGBSG" represents the study's abbreviations and "22" represents the volunteer's ID. This will act as the 'name' for the study.

The SPMIC will also generate a unique volunteer number for each MRI visit, this will be used to identify the scans to each participant.

Source documents

Source documents shall be filed at the investigator's site and may include but are not limited to, consent forms, current medical records, laboratory results and records. A CRF may also completely serve as its own source data. Only trial staff as listed on the Delegation Log shall have access to trial documentation other than the regulatory requirements listed below.

Direct access to source data / documents

The CRF and all source documents, including progress notes and copies of laboratory and medical test results shall made be available at all times for review by the Chief Investigator,

Sponsor's designee and inspection by relevant regulatory authorities (e.g. Department of Health, Human Tissue Authority).

DATA PROTECTION

All trial staff and investigators will endeavour to protect the rights of the trial's participants to privacy and informed consent, and will adhere to the Data Protection Act, 2018. The CRF will only collect the minimum required information for the purposes of the trial. CRFs will be held securely, in a locked room, or locked cupboard or locked cabinet. Access to the information will be limited to the trial staff and investigators and relevant regulatory authorities (see above). Computer held data including the trial database will be held securely and password protected. All data will be stored on a secure dedicated web server. Access will be restricted by user identifiers and passwords (encrypted using a one way encryption method).

Information about the trial in the participant's medical records / hospital notes will be treated confidentially in the same way as all other confidential medical information.

Electronic data will be backed up every 24 hours to both local and remote media in encrypted format.

QUALITY ASSURANCE & AUDIT

INSURANCE AND INDEMNITY

Insurance and indemnity for trial participants and trial staff is covered within the NHS

Indemnity Arrangements for clinical negligence claims in the NHS, issued under cover of HSG (96)48. There are no special compensation arrangements, but trial participants may have recourse through the NHS complaints procedures.

The University of Nottingham as research Sponsor indemnifies its staff with both public liability insurance and clinical trials insurance in respect of claims made by research subjects.

TRIAL CONDUCT

Trial conduct may be subject to systems audit of the Trial Master File for inclusion of essential documents; permissions to conduct the trial; Trial Delegation Log; CVs of trial staff and training received; local document control procedures; consent procedures and recruitment logs; adherence to procedures defined in the protocol (e.g. inclusion / exclusion criteria, correct randomisation, timeliness of visits); adverse event recording and reporting; accountability of trial materials and equipment calibration logs.

The Academic Supervisor, or where required, a nominated designee of the Sponsor, shall carry out a site systems audit at least yearly and an audit report shall be made to the Trial Steering Committee.

TRIAL DATA

Monitoring of trial data shall include confirmation of informed consent; source data verification; data storage and data transfer procedures; local quality control checks

and procedures, back-up and disaster recovery of any local databases and validation of data manipulation. The Academic Supervisor (Penny Gowland), or where required, a nominated designee of the Sponsor, shall carry out monitoring of trial data as an ongoing activity.

Entries on CRFs will be verified by inspection against the source data. A sample of CRFs (10% or as per the study risk assessment) will be checked on a regular basis for verification of all entries made. In addition the subsequent capture of the data on the trial database will be checked. Where corrections are required these will carry a full audit trail and justification.

Trial data and evidence of monitoring and systems audits will be made available for inspection by REC as required.

RECORD RETENTION AND ARCHIVING

In compliance with the ICH/GCP guidelines, regulations and in accordance with the University of Nottingham Research Code of Conduct and Research Ethics, the Chief or local Principal Investigator will maintain all records and documents regarding the conduct of the study. These will be retained for at least 10 years or for longer if

required. If the responsible investigator is no longer able to maintain the study records, a second person will be nominated to take over this responsibility.

The research team at the University of Nottingham will access this personal data whilst the project is being carried out to enable them to contact you. This identifiable, personal information will be kept separately from the coded research data and will not leave the study site.

The Trial Master File and trial documents held by the Chief Investigator on behalf of the

Sponsor shall be finally archived at secure archive facilities at the University of Nottingham. This archive shall include all trial databases and associated meta-data encryption codes. Identifiable, personal data (such as name and address) will be stored confidentially in a locked cabinet within a locked office and on a password protected secure database that is only accessible by a very limited number of administrative staff who have no access to the scientific data whatsoever. This information will be held by the Chief Investigator (Dr Iskandar Idris) and the Sir Peter Mansfield imaging Centre.

The Sir Peter Mansfield Imaging Centre enters all participant data onto a secure database, which is password protected and supported/maintained by Information

Services at the University. Any paperwork, such as paper consent/screening forms are locked in fireproof cabinets with only limited people having access.

DISCONTINUATION OF THE TRIAL BY THE SPONSOR

The Sponsor reserves the right to discontinue this trial at any time for failure to meet expected enrolment goals, for safety or any other administrative reasons. The Sponsor shall take advice from the Trial Steering Committee and Data Monitoring Committee as appropriate in making this decision.

STATEMENT OF CONFIDENTIALITY

Individual participant medical information obtained as a result of this study are considered confidential and disclosure to third parties is prohibited with the exceptions noted above. Participant confidentiality will be further ensured by utilising identification code numbers to correspond to treatment data in the computer files.

Such medical information may be given to the participant's medical team and all appropriate medical personnel responsible for the participant's welfare.

If information is disclosed during the study that could pose a risk of harm to the participant or others, the researcher will discuss this with the CI and where appropriate report accordingly.

Data generated as a result of this trial will be available for inspection on request by the participating physicians, the University of Nottingham representatives, the REC, local R&D Departments and the regulatory authorities.

PUBLICATION AND DISSEMINATION POLICY

No identifiable material will be used in any report or publication.

The results from the study will be discussed with research collaborators at Leicester University, Glenfield hospital, Medical research council, biomedical research council and presented at a national or international conference to allow findings to be shared with other researchers. Results will also be used to design future research.

Coded data may be shared with journals, experts, or other scientists to verify the quality of results. However, no identifiable material will be used in any report or publication. We intend to publish our results throughout the trial and up to 24 months after the end date of the study.

The results will also be used as part of Abi Spicer's and Dr Rebekah Wilmington's PhD theses in agreement with the MRC and UoN.

USER AND PUBLIC INVOLVEMENT

We have spoken to a previous bariatric patient who now works for Derby hospital. We discussed what adjustments would be needed, such as a special size of scrubs, chairs and access to bathrooms. This was done to improve our understanding of bariatric patient struggles and ensure patients are more comfortable when they visit.

STUDY FINANCES

Funding source

This study is funded in partnership by the medical research council, University of Nottingham as part of a PhD project and by the biomedical research council.

Participant stipends and payments

Participants will be paid to participate in the trial. For each participant there will be a total inconvenience fee of £80 comprised of £20 for each in-person session. This is to aid in expenses incurred as part of visitation, such as travel expenses. However, car parking vouchers can be provided.

For those participants who reside more than 20 miles away from the main study site (University Park, Nottingham),we will offer enhanced inconvenience allowance which will cover the equivalent of standard mileage costs (i.e. 45 pence per mile).

SIGNATURE PAGES

Signatories to Protocol:

Chief Investigator: (name)____Iskandar Idris

Signature:____  __

Date: __6/2/23_____

Co- investigator: (name) _____Penny Gowland_____

Signature:_____ Penny Gowland _____

Date: 13-2-23_____

Co- investigator: (name) _____Susan Francis_____

S.T. Francis

Signature:_____ _____

Date: __22-2-23_____

Co- investigator: (name) _____Abi Spicer_____

Signature:_____  __

Date: _____22-2-23_____

Co- investigator: (name) _____Rebekah Wilmington_____

Signature:_____  _____

Date: ____22-2-23_____

Co- investigator: (name) _____ Guruprasad Aithal _____

Signature:_____ _  _____

Date: _____22-2-23_____

Co- investigator: (name) _____Gerry McCann_____

Signature:_____ _____

Date: _____22-3-23_____

Co- investigator: (name) _____Stephen Bawden_____

Signature:_____ _____

Date: _____22-2-23____

Trial Statistician: (name)_____Stephen Bawden_____

Signature:_____ 

_____

Date: ____22-2-23_____

REFERENCES

Luo RB, Suzuki T, Hooker JC, Covarrubias Y, Schlein A, Liu S, et al. How bariatric surgery affects liver volume and fat density in NAFLD patients. Surg Endosc [Internet].

2018 Apr 1 [cited 2021 Jan 19];32(4):1675–82. Available from: https://doi.org/10.1007/s00464-017-5846-9

Lewis MC, Phillips ML, Slavotinek JP, Kow L, Thompson CH, Toouli J. Change in liver size and fat content after treatment with Optifast® very low calorie diet. Obes Surg [Internet]. 2006 Jun 1 [cited 2021 Jan 19];16(6):697–701. Available from: https://link.springer.com/article/10.1381/096089206777346682

Peltonen M. Balancing risks and benefits of bariatric surgery for type 2 diabetes. Vol.

3, The Lancet Diabetes and Endocrinology. Lancet Publishing Group; 2015. p. 394–5.

Ikramuddin S, Billington CJ, Lee WJ, Bantle JP, Thomas AJ, Connett JE, et al. Roux-en-Y gastric bypass for diabetes (the Diabetes Surgery Study): 2-year outcomes of a 5-year, randomised, controlled trial. Lancet Diabetes Endocrinol. 2015 Jun 1;3(6):413–22.

Hofsø D, Fatima F, Borgeraas H, Birkeland KI, Gulseth HL, Hertel JK, et al. Gastric bypass versus sleeve gastrectomy in patients with type 2 diabetes (Oseberg): a

single-centre, triple-blind, randomised controlled trial. Lancet Diabetes Endocrinol. 2019 Dec 1;7(12):912–24.

Gastric Sleeve vs. Gastric Bypass: Differences, Pros, Cons [Internet]. [cited 2021 Jan 22]. Available from: https://www.healthline.com/health/gastric-sleeve-vs-gastric-bypass

Lim EL, Hollingsworth KG, Aribisala BS, Chen MJ, Mathers JC, Taylor R. Reversal of type 2 diabetes: Normalisation of beta cell function in association with decreased pancreas and liver triacylglycerol. Diabetologia [Internet]. 2011 Oct 9 [cited 2021 Feb 18];54(10):2506–14. Available from: https://link.springer.com/article/10.1007/s00125011-2204-7

Honka H, Koffert J, Hannukainen JC, Tuulari JJ, Karlsson HK, Immonen H, et al. The Effects of Bariatric Surgery on Pancreatic Lipid Metabolism and Blood Flow. J Clin Endocrinol Metab [Internet]. 2015 May 1 [cited 2021 Jan 21];100(5):2015–23. Available from: https://academic.oup.com/jcem/article/100/5/2015/2829724

9.6 Bariatric Study IRAS application

Welcome to the Integrated Research Application System

IRAS Project Filter

The integrated dataset required for your project will be created from the answers you give to the following questions. The system will generate only those questions and sections which (a) apply to your study type and (b) are required by the bodies reviewing your study. Please ensure you answer all the questions before proceeding with your applications.

Please complete the questions in order. If you change the response to a question, please select 'Save' and review all the questions as your change may have affected subsequent questions.

Please enter a short title for this project (maximum 70 characters)
Effects of VLCD and Bariatric Surgery in Patients with Type 2 Diabetes

1. Is your project research?

(●) Yes ( ) No

2. Select one category from the list below:

( ) Clinical trial of an investigational medicinal product

( ) Combined trial of an investigational medicinal product and an investigational medical device

( ) Clinical investigation or other study of a medical device

( ) Other clinical trial to study a novel intervention or randomised clinical trial to compare interventions in clinical practice

(●) Basic science study involving procedures with human participants

( ) Study administering questionnaires/interviews for quantitative analysis, or using mixed quantitative/qualitative methodology

( ) Study involving qualitative methods only

( ) Study limited to working with human tissue samples (or other human biological samples) and data (specific project only)

( ) Study limited to working with data (specific project only)

( ) Research tissue bank

( ) Research database

If your work does not fit any of these categories, select the option below:

( ) Other study

2a. Will the study involve the use of any medical device without a UKCA/CE UKNI/CE Mark, or a UKCA/CE UKNI/CE marked device which has been modified or will be used outside its intended purposes?

( ) Yes (●) No

2b. Please answer the following question(s):

a) Does the study involve the use of any ionising radiation? ( ) Yes (●) No

b) Will you be taking new human tissue samples (or other human biological samples)? (●) Yes ( ) No

c) Will you be using existing human tissue samples (or other human biological samples)? ( ) Yes (●) No

d) Will the study involve any other clinical procedures with participants (e.g. MRI, ultrasound, physical examination)? (•) Yes ( ) No

3. In which countries of the UK will the research sites be located? *(Tick all that apply)*

- [x] England
- [ ] Scotland
- [ ] Wales
- [ ] Northern Ireland

3a. In which country of the UK will the lead NHS R&D office be located:

- (•) England
- ( ) Scotland
- ( ) Wales
- ( ) Northern Ireland
- ( ) This study does not involve the NHS

4. Which applications do you require?

- [x] IRAS Form
- [ ] Confidentiality Advisory Group (CAG)
- [ ] Her Majesty's Prison and Probation Service (HMPPS)

Most research projects require review by a REC within the UK Health Departments' Research Ethics Service. Is your study exempt from REC review?

( ) Yes (•) No

5. Will any research sites in this study be NHS organisations?

(•) Yes ( ) No

5a. Are all the research costs and infrastructure costs (funding for the support and facilities needed to carry out the research e.g. NHS support costs) for this study provided by a NIHR Biomedical Research Centre (BRC), NIHR Applied Research Collaboration (ARC), NIHR Patient Safety Translational Research Centre (PSTRC), or an NIHR Medtech and In Vitro Diagnostic Co-operative (MIC) in all study sites?

Please see information button for further details.

( ) Yes (•) No

Please see information button for further details.

5b. Do you wish to make an application for the study to be considered for NIHR Clinical Research Network (CRN) Support and inclusion in the NIHR Clinical Research Network Portfolio?

Please see information button for further details.

( ) Yes (•) No

The NIHR Clinical Research Network (CRN) provides researchers with the practical support they need to make clinical studies happen in the NHS in England e.g. by providing access to the people and facilities needed to carry out research "on the ground".

If you select yes to this question, information from your IRAS submission will automatically be shared with the NIHR CRN. ***Submission of a Portfolio Application Form (PAF) is no longer required.***

6. Do you plan to include any participants who are children?

○ Yes ◉ No

7. Do you plan at any stage of the project to undertake intrusive research involving adults lacking capacity to consent for themselves?

○ Yes ◉ No

Answer Yes if you plan to recruit living participants aged 16 or over who lack capacity, or to retain them in the study following loss of capacity. Intrusive research means any research with the living requiring consent in law. This includes use of identifiable tissue samples or personal information, except where application is being made to the Confidentiality Advisory Group to set aside the common law duty of confidentiality in England and Wales. Please consult the guidance notes for further information on the legal frameworks for research involving adults lacking capacity in the UK.

8. Do you plan to include any participants who are prisoners or young offenders in the custody of HM Prison Service or who are offenders supervised by the probation service in England or Wales?

○ Yes ◉ No

9. Is the study or any part of it being undertaken as an educational project?

◉ Yes ○ No

Please describe briefly the involvement of the student(s):
The student will be aiding in the design of the research. Will be conducting the majority of the research and will be analysing data (MRI/MRS)

9a. Is the project being undertaken in part fulfilment of a PhD or other doctorate?

◉ Yes ○ No

10. Will this research be financially supported by the United States Department of Health and Human Services or any of its divisions, agencies or programs?

○ Yes ◉ No

11. Will identifiable patient data be accessed outside the care team without prior consent at any stage of the project (including identification of potential participants)?

○ Yes ◉ No

Integrated Research Application System
Application Form for Basic science study involving procedures with human participants

The Chief Investigator should complete this form. Guidance on the questions is available wherever you see this symbol displayed. We recommend reading the guidance first. The complete guidance and a glossary are available by selecting Help.

Please define any terms or acronyms that might not be familar to lay reviewers of the application.

Short title and version number: (maximum 70 characters - this will be inserted as header on all forms)
Effects of VLCD and Bariatric Surgery in Patients with Type 2 Diabetes

PART A: Core study information

1. ADMINISTRATIVE DETAILS

A1. Full title of the research:

DIFFERENTIAL EFFECTS OF VERY LOW CALORIE DIET (VLCD), ROUX-EN-Y-GASTRIC BYPASS AND SLEEVE GASTRECTOMY ON PANCREATIC, LIVER, MUSCLE AND HEART FAT DEPOSITION AND METABOLISM IN PEOPLE WITH TYPE 2 DIABETES: AN MRI STUDY

A2-1. Educational projects

Name and contact details of student(s):

Student 1

Title	Forename/Initials	Surname
Miss	Abi	Spicer

Address	Sir Peter Mansfield Imaging Centre (SPMIC) University Park Nottingham
Post Code	NG7 2RD
E-mail	abi.spicer@nottingham.ac.uk
Telephone	07714239831
Fax	

Give details of the educational course or degree for which this research is being undertaken:

Name and level of course/ degree:
PhD in Physics

Name of educational establishment:
University of Nottingham

Student 2

Title	Forename/Initials	Surname
Dr	Rebekah L J	Wilmington

Address	Room 5032, School of Graduate Entry Medicine and Health Sciences Faculty of Medicine and Health Sciences

	University of Nottingham, Royal Derby Hospital Centre
Post Code	DE22 3DT
E-mail	rebekah.wilmington@nottingham.ac.uk
Telephone	07704739792
Fax	

Give details of the educational course or degree for which this research is being undertaken:

Name and level of course/ degree:
PhD in Medicine and Health

Name of educational establishment:
University of Nottingham

Name and contact details of academic supervisor(s):

Academic supervisor 1

	Title	Forename/Initials	Surname
	Professor	Penny	Gowland
Address	Sir Peter Mansfield Imaging Centre (SPMIC)		
	University Park		
	Nottingham		
Post Code	NG7 2RD		
E-mail	penny.gowland@nottingham.ac.uk		
Telephone	0115 951 4754		
Fax			

Academic supervisor 2

	Title	Forename/Initials	Surname
	Professor	Susan	Francis
Address	Sir Peter Mansfield Imaging Centre (SPMIC)		
	University Park		
Post Code	NG7 2RD		
E-mail	susan.francis@nottingham.ac.uk		
Telephone	01159566518		
Fax			

Academic supervisor 3

	Title	Forename/Initials	Surname
	Prof	Iskandar	Idris
Address	MRC Musculoskeletal, Physiology and Ageing		
	School of Medicine, University of Nottingham		
	Royal Derby Hospital, Derby		
Post Code	DE22 3DT		
E-mail	iskandar.idris@nottingham.ac.uk		
Telephone	01332724605		
Fax			

Please state which academic supervisor(s) has responsibility for which student(s):
Please click "Save now" before completing this table. This will ensure that all of the student and academic supervisor details are shown correctly.

Student(s)	Academic supervisor(s)
Student 1 Miss Abi Spicer	☑ Professor Penny Gowland ☐ Professor Susan Francis ☐ Prof Iskandar Idris
Student 2 Dr Rebekah L J Wilmington	☐ Professor Penny Gowland ☐ Professor Susan Francis ☑ Prof Iskandar Idris

A copy of a current CV for the student and the academic supervisor (maximum 2 pages of A4) must be submitted with the application.

A2-2. Who will act as Chief Investigator for this study?

- ○ Student
- ○ Academic supervisor
- ◉ Other

A3-1. Chief Investigator:

	Title	Forename/Initials	Surname
	Dr	Iskadar	Idris
Post	Associate Professor		
Qualifications	BMedSci, BMBS, FRCP, DM		
ORCID ID			
Employer	University of Nottingham		
Work Address	MRC Musculoskeletal Physioogy and Ageing School of Medicine, University of Nottingham Royal Derby Hospital Derby		
Post Code	DE22 3DT		
Work E-mail	Iskandar.Idris@nottingham.ac.uk		
* Personal E-mail			
Work Telephone	01332724605		
* Personal Telephone/Mobile			
Fax			

** This information is optional. It will not be placed in the public domain or disclosed to any other third party without prior consent.*
A copy of a current CV (maximum 2 pages of A4) for the Chief Investigator must be submitted with the application.

A4. Who is the contact on behalf of the sponsor for all correspondence relating to applications for this project?
This contact will receive copies of all correspondence from REC and HRA/R&D reviewers that is sent to the CI.

	Title	Forename/Initials	Surname
	Ms	Angela	Shone
Address	Research and Innovation		
	University of Nottingham,		
	East Atrium, Jubilee Conference Centre		
Post Code	NG8 1DH		
E-mail	sponsor@nottingham.ac.uk		
Telephone	0115 8467906		
Fax			

A5-1. Research reference numbers. *Please give any relevant references for your study:*

Applicant's/organisation's own reference number, e.g. R & D (if available):	N/A
Sponsor's/protocol number:	21047
Protocol Version:	N/A
Protocol Date:	
Funder's reference number (enter the reference number or state not applicable):	N/A
Project website:	N/A

Registry reference number(s):
The UK Policy Framework for Health and Social Care Research sets out the principle of making information about research publicly available. Furthermore: Article 19 of the World Medical Association Declaration of Helsinki adopted in 2008 states that "every clinical trial must be registered on a publicly accessible database before recruitment of the first subject"; and the International Committee of Medical Journal Editors (ICMJE) will consider a clinical trial for publication only if it has been registered in an appropriate registry. Please see guidance for more information.

International Standard Randomised Controlled Trial Number (ISRCTN):

ClinicalTrials.gov Identifier (NCT number):

Additional reference number(s):

Ref.Number Description	Reference Number

A5-2. Is this application linked to a previous study or another current application?

○ Yes ◉ No

Please give brief details and reference numbers.

2. OVERVIEW OF THE RESEARCH

To provide all the information required by review bodies and research information systems, we ask a number of specific questions. This section invites you to give an overview using language comprehensible to lay reviewers and members of the public. Please read the guidance notes for advice on this section.

A6-1. Summary of the study. *Please provide a brief summary of the research (maximum 300 words) using language easily understood by lay reviewers and members of the public. Where the research is reviewed by a REC within the UK Health Departments' Research Ethics Service, this summary will be published on the Health Research Authority (HRA) website following the ethical review. Please refer to the question specific guidance for this question.*

A promising recently-investigated and effective conservative approach to T2DM is through very-low-calorie diets (VLCD). Some studies have shown that the diabetic status of some patients can be reversed through VLCD. However, in patients undergoing bariatric surgery it is still debated whether it is the diet or the surgery that often follows this that

causes diabetes remission.
The purpose of this project is to investigate the effects of a Very Low-Calorie Diet (VLCD) followed by two different bariatric surgical procedures, Roux-en-Y Gastric Bypass (RYGB) and Sleeve gastrectomy (SG) on skeletal muscle, liver and pancreatic fat deposition, ATP flux as well as cardiac function in Type 2 diabetes patients.
The two surgical procedures result in different metabolic and physical changes in the body. We will investigate if these surgical procedures cause differences in the diabetes remission process.
The Patients recruited to this study will be those already undergoing bariatric surgery as part of their standard care and who have type 2 diabetes.
Using Magnetic Resonance Imaging (MRI) and Magnetic Resonance Spectroscopy (MRS) and mixed meal tests (MMT), at various points through their surgical journey, (before and after the VLCD, 6 weeks post-surgery, and 4 months post-surgery) we will investigate the aforementioned changes.
This will give us an insight into how surgery and diet affect Type 2 diabetes status in those undergoing bariatric surgery.
The study procedures that are not a part of standard care (MRI, MRS, MMT) will be performed at the Sir Peter Mansfield Imaging Centre, University Park, University of Nottingham.

A6-2. Summary of main issues. *Please summarise the main ethical, legal, or management issues arising from your study and say how you have addressed them.*

Not all studies raise significant issues. Some studies may have straightforward ethical or other issues that can be identified and managed routinely. Others may present significant issues requiring further consideration by a REC, R&D office or other review body (as appropriate to the issue). Studies that present a minimal risk to participants may raise complex organisational or legal issues. You should try to consider all the types of issues that the different reviewers may need to consider.

The main issue related to the study is the increased burden on patients already undergoing surgery, however we have sought to minimise this in the following ways

Recruitment will take place through liaising with patients on the waiting list for bariatric surgery, and will be focused on local patients (within the vicinity of the Royal Derby Hospital) to ease the burden of the participants traveling to the study sessions.
All patients will be given an inconvenience fee, for each participant, there will be a total inconvenience fee of £80 comprised of £20 for each in-person session. This money is to assist with expenses incurred as part of their participation such as travel expenses. Travel expenses will not be offered for visits incurred as a result of participation. However, car parking vouchers will be provided.

3. PURPOSE AND DESIGN OF THE RESEARCH

A7. Select the appropriate methodology description for this research. *Please tick all that apply*:

- [ ] Case series/ case note review
- [ ] Case control
- [x] Cohort observation
- [ ] Controlled trial without randomisation
- [ ] Cross-sectional study
- [ ] Database analysis
- [ ] Epidemiology
- [x] Feasibility/ pilot study
- [ ] Laboratory study
- [ ] Metanalysis
- [ ] Qualitative research
- [ ] Questionnaire, interview or observation study
- [ ] Randomised controlled trial
- [ ] Other (please specify)

A10. What is the principal research question/objective? *Please put this in language comprehensible to a lay person.*

The effects of a 2 week Very low-calorie diet (VLCD) performed prior to bariatric surgery on the percentage of liver fat as determined using Magnetic Resonance Imaging.

A11. What are the secondary research questions/objectives if applicable? *Please put this in language comprehensible to a lay person.*

The effects of VLCD on cardiac ATP changes and cardiac function, determined by the ventricular wall thickness.
The effects of VLCD on skeletal muscle, liver, and pancreatic fat percentages.

The effect of Bariatric Surgery (RYGB or SG) on skeletal muscle, liver, and pancreatic fat percentage.
The effects of Bariatric Surgery on Liver ATP flux.
The differential effects of RYGB and SG on liver ATP flux and cardiac function, determined by the left ventricular wall mass.
The differential effects of RYGB and SG on skeletal muscle, liver, and pancreatic fat percentage.

A12. What is the scientific justification for the research? *Please put this in language comprehensible to a lay person.*

Obesity rates continue to increase worldwide. This has led to a corresponding rise in obesity-related negative health issues complications such as Type 2 diabetes mellitus (T2D) and cardiovascular disease, with their inherit risks of increased mortality, functional decline, hospitalization and loss of independence, especially inthose who are classified as morbidly obese.
Over the last decade, bariatric surgery has emerged as a safe and proven method for better, more sustained weight loss when compared with exercise and dietary strategies. The most commonly performed bariatric surgery in the UK and worldwide are: Roux-en-Y gastric bypass (RYGB) and sleeve gastrectomy (SG) operations.

In addition to bariatric surgery, all patients undergo a period of Very Low-Calorie diet (VLCD) to reduce the size of the liver prior to bariatric surgery. VLCD has also been shown to independently reduce blood glucose concentration and in some cases, induce T2D remission by removal of fatty acids (triacylglycerol) from the pancreas and the liver (2)

Both surgical procedures (RYGB and SG) have been shown to achieve a large and sustained improvement in weight loss with improvements in insulin sensitivity, improved beta cell function and associated with high-resolution rate in T2D (3–5). SG surgery involves the removal of 80% of the stomach whilst RYGB involves the anastomosis of lower oesophagus with distal small bowel, which means that food ‘skips’ the stomach, duodenum and upper small intestine.

Metabolic effects of surgery can be observed early (in the first 6 weeks) and long term (years after surgery). However, the observation that the rapid rate of glucose lowering at the early stages is disproportionate to the degree of weight loss seen after surgery. This suggests that bariatric surgery reverses the fundamental pathophysiological defects of T2D independent of weight loss.

Current research has focused on the use of MRI to investigate the physical changes to fat deposition and used this a tool to mark improvements from the VLCD and bariatric surgery (1,2,7,8). Focusing on liver fat MRI- proton density fat-fraction (PDFF) measurements have been taken prior to the surgery and at 1,6 and 12-months post-surgery. It was found that for 49 (26 for RYGB, 20 for SG and 3 for Gastric banding) participants, PDFF showed a statistically significant 23% reduction ($P<0.001$) between baseline and post VLCD (16.6 ± 7.8 vs. 12.7 ± 6.8, ±SD), and post VLCD to 1 month post-surgery a 42% reduction (12.7 ± 6.8 vs. 7.3 ± 4.1, ±SD) for the whole group (1). However, these do not record the point at which a patient starts to show T2D remission.

We are therefore wish to explore the impact of VLCD and different bariatric surgery procedures on the physical deposition of fat in organs which regulate glucose metabolism (i.e. in the liver, pancreas, muscle) both in the earlier (6 weeks) and intermediate (4 months) period after bariatric surgery, where rate of weight loss have been shown to be similar between the two surgical procedures. Increased understanding of the changes observed in these important metabolic organs, will: increase our understanding of mechanism underpinning T2D remission following bariatric surgery; their effects on weight loss; and effect on gut hormones related to appetite, glucose regulation and gastrointestinal function.
Magnetic Resonance imaging (MRI) and Magnetic Resonance spectroscopy (MRS) are non-invasive, non-ionising techniques. MRI can be used to investigate the body’s physiology and MRS can be used to investigate the body’s metabolic processes, so by combining these two methods we are able to investigate the process of fat reduction and T2D remission post gastric surgery without performing any secondary invasive procedures.

A13. Please summarise your design and methodology. *It should be clear exactly what will happen to the research participant, how many times and in what order. Please complete this section in language comprehensible to the lay person. Do not simply reproduce or refer to the protocol. Further guidance is available in the guidance notes.*

We have separated this study into 2 groups for the main study (Category A) and a smaller arm of the study for cardiac MRI and MRS (Category B). All participants will be asked to attend a session at the Sir Peter Mansfield Imaging Centre (SPMIC) on the UoN main campus.
Initially all participants recruited will be entered into category A. This means that they will be used to understand the primary outcomes. Once 17 participants have been recruited (not necessarily completed) into category A, potential participants will be given the option to enter into category A or B or both (since category B is a less intense protocol). Once all 6 particpants have been recruited to category B this option will be removed and recruitment paused. Recruitment will ressume if a participant has to be removed or drops out of the study.
The focus of Catergory A is the abdominal organs, especially the liver's recation to the clinical interventions. This is our primary focus of the study and application. However, due to the similaritys in protocol and recruitment a smaller arm (category B) was created. These had to be 2 sperate arms due the the lengthy nature of the MR scans. The purpose of category B is to allow us to pilot an investigation into the effects of the VLCD, RYGB and SG on the cardiac muscle

Flow Chart of sessions:
--> [successful screening]
--> Session 1
--> [booking first session]
--> Session 2 (2 weeks pre-surgery)
--> [VLCD]
--> Session 3 (3-1 day pre-surgery)
--> [Surgery, SG or RYGB]
--> Session 4 (6 weeks post surgery)
--> Session 5 (16 weeks post surgery)

- See attached file for more detailed flow chart.

Screening:

Patients who are listed for surgery by the Bariatric surgical Tier 4 MDT team, will be approached by one of the usual care team (who may also be a member of the research team) during the ERAS session (Enhanced Recovery After Surgery). This will occur approximately 6 months before surgery. If they wish to participate in the study they will be screened for suitability and willingness to undergo MRI. If eligible and consent is provided, their details will be kept by the research team to be contacted for further appointments to attend the University of Nottingham (UoN) research unit based at the Royal Derby Hospital.

Participants who are interested in the study will be asked to lie down and a replica of the MRI bore will be placed over them to ensure they can fit into a scanner, if so Participants will complete the MRI screening test, as this is a safety-critical element of the eligibility criteria. All other eligibility criteria will be known as part of the routine care. The Participants will be provided with the PIS and their willingness and ability to attend all 4 sessions will be evaluated to ensure maximum completion of Participants in the study. If Participants are eligible and consent to participate their information is passed on to the rest of the research team to be contacted further.

The CI will be in charge of obtaining informed consent. If unavailable another trained member of the research team may take their place.

FOR ALL CATEGORY A SESSIONS:
The participants will receive an MRI and MRS scan a Mixed meal test (MMT) at every session. Blood samples will be taken by a trained member of staff and transferred to the Royal Derby Hospital for testing, this is to obtain postprandial glucose, insulin, C-peptide, glucagon, total and intact glucagon-like peptide-1 (GLP-1), glucose-dependent insulinotropic polypeptide (GIP).

Mixed meal Protocol:
The participants will need to be fasted prior to the Mixed Meal Test (MMT) for a minimum of 8 hours. Participants will also need to be advised that they must avoid alcohol consumption and strenuous exercise for the preceding 24 hours, alongside avoiding caffeine for 18 hours prior to the undertaking of the test. To reduce fasting period all tests and scans will be scheduled for the morning.

Participants will visit the SPMIC on the UoN main campus. During their visit participants will undergo a mixed meal test (200ml 300kcal).

Participants will be taken into a clinical room adjacent to the MRI suite. Here they will be met by a trained member of staff, who will insert a cannula into their arm or hand.
2ml of blood will then be drawn into a P800 sample tube.
There should be minimal distress from the procedure as this process is similar to what the participants will have experienced as part of their routine care at a GP surgery or hospital. Sharp pain is common during the procedure but well tolerated. Bruising is a known complication of the venepuncture but can be minimised with compression of the site post-procedure. The extremity will be placed in a hot box to allow for arterial like drawing of the blood.
The mixed meal will be a Nutricia, Fortisip, this will be stored in the fridge and a flavour of their choice will be served to the participants chilled (exceot chocolate which is not suitable for this process). Each bottle is 200ml and this is the standard size of the mixed meal (200ml 300kcal).
Once the participant has consumed the mixed meal the bloods will been drawn every 15 minutes for 3hours.

The blood needs to be spun in a centrifuge for 10minutes within 30 minutes of being drawn. This will be done in an appropriate lab at the SPMIC. The plasma will then be separated from the cells and stored in a -20degree freezer temporarily. By the end of the following working day after the study day the samples will be transferred to the medical school to be stored at -80°C freezer on D floor of the medical school which is locked & alarmed with CO2 back up.

The samples will be transferred to Royal Derby Hospital for analysis after all data collection has been completed. Samples will be removed from the -80°C freezer and couriered in a labelled igloo containing dry ice to laboratories in Derby Medical School. The shipment will contain a complete inventory of all samples, along with the name of the person responsible for sending and receiving the samples. These samples will be stored in a -80°C freezer in this facility until analysis. Once all study-related analysis on the samples has been completed, they will be disposed of in accordance with the Human Tissue Act, 2004.

Session 1- same protocol for Category A and B:
A member of the research team will reach out to the patient 2 weeks prior to the commencement of their VLCD in order to confirm they are still interested in participating, book in the first study session and answer any questions they may have.

Session 2: Between 3 days and 1 day prior to the commencement of the VLCD.
Category A: Participants will undergo standard physiological scans of their chest, abdomen, and upper legs. These scans will be used to determine the health of tissue. Physiology scans will take around 30-40 minutes. A proton MRS scan of the Liver which will require a different surface coil to be used, this Scan will take around 15 minutes.

Category B: Participants will undergo physiological scans of the heart which will take approximately 15minutes, these Participants will also undergo Proton MRS of the heart which will take approximately 30 minutes and will use the physiological scans for positioning. Participants will also undergo 31P MRS, this scan will require a specialised coil and will take around 70 minutes.

Session 3: Between 3 and 1 day prior to the patients Bariatric Surgery.
Category A: Participants will undergo standard physiological scans of their chest, abdomen, and upper legs. These scans will be used to determine the health of tissue. Physiology scans will take around 30-40 minutes. A proton MRS scan of the Liver which will require a different surface coil to be used, this Scan will take around 15 minutes.
Phosphorus (31P) MRS will also be performed on the patient's livers, this requires a specialised coil and will take 60 minutes. It is likely Participants will need to take a break to stretch and be out of the scanner mid-session due to the long scan times.

Category B: Participants will undergo physiological scans of the heart which will take approximately 15minutes, these Participants will also undergo Proton MRS of the heart which will take approximately 30 minutes and will use the physiological scans for positioning. Participants will also undergo 31P MRS, this scan will require a specialised coil and will take around 70 minutes.

Surgery:
Roux-en-Y Gastric Bypass (RYGB): Follows standard clinical practice.
Sleeve Gastrectomy (SG): Follows standard clinical practice.

Session 4:6 weeks post Bariatric Surgery.
Category A: Participants will undergo standard physiological scans of their chest, abdomen, and upper legs. These scans will be used to determine the health of tissue. Physiology scans will take around 30-40 minutes. A proton MRS scan of the Liver which will require a different surface coil to be used, this Scan will take around 15 minutes.
Phosphorus (31P) MRS will also be performed on the patient's livers, this requires a specialised coil and will take 60

minutes. It is likely Participants will need to take a break to stretch and be out of the scanner mid-session due to the long scan times.

Category B: Participants will undergo physiological scans of the heart which will take approximately 15minutes, these Participants will also undergo Proton MRS of the heart which will take approximately 30 minutes and will use the physiological scans for positioning.

Session 5: 16 weeks post Bariatric Sugery.
Category A: Participants will undergo standard physiological scans of their chest, abdomen, and upper legs. These scans will be used to determine the health of tissue. Physiology scans will take around 30-40 minutes. A proton MRS scan of the Liver which will require a different surface coil to be used, this Scan will take around 15 minutes.
Session 3 and 4:

Category B: Participants will undergo physiological scans of the heart which will take approximately 15minutes, these Participants will also undergo Proton MRS of the heart which will take approximately 30 minutes and will use the physiological scans for positioning.

A14-1. In which aspects of the research process have you actively involved, or will you involve, patients, service users, and/or their carers, or members of the public?

- [x] Design of the research
- [ ] Management of the research
- [ ] Undertaking the research
- [ ] Analysis of results
- [ ] Dissemination of findings
- [ ] None of the above

Give details of involvement, or if none please justify the absence of involvement.
We have spoken to a previous patient who has undergone bariatric surgery, who also liaises with a wider group of patients who have undergone bariatric surgery in Derby. This discussion have provided us with useful insight about appropriate timing of study protocols, tolerability of MRI scanning as well as general insight about what adjustments would be needed, such a special size of scrubs, chairs and access to bathrooms. This was done to improve our understanding of bariatric patients struggles and ensure patients are more comfortable when they visit.

4. RISKS AND ETHICAL ISSUES

RESEARCH PARTICIPANTS

A15. What is the sample group or cohort to be studied in this research?

Select all that apply:

- [x] Blood
- [ ] Cancer
- [x] Cardiovascular
- [ ] Congenital Disorders
- [ ] Dementias and Neurodegenerative Diseases
- [x] Diabetes
- [ ] Ear
- [ ] Eye

- ☐ Generic Health Relevance
- ☐ Infection
- ☐ Inflammatory and Immune System
- ☐ Injuries and Accidents
- ☐ Mental Health
- ☐ Metabolic and Endocrine
- ☑ Musculoskeletal
- ☐ Neurological
- ☑ Oral and Gastrointestinal
- ☐ Paediatrics
- ☐ Renal and Urogenital
- ☐ Reproductive Health and Childbirth
- ☐ Respiratory
- ☐ Skin
- ☐ Stroke

Gender:	Male and female participants
Lower age limit: 18	Years
Upper age limit: 70	Years

A17-1. Please list the principal inclusion criteria (list the most important, max 5000 characters).

Being listed for RYGB or SG bariatric surgery at the Royal Derby Hospital.
Inclusion BMI is based on eligibility for Bariatric Surgery as per routine (standard) practice (BMI 35 or greater)
Age range 18 to 70-year-old.
Ability to give informed consent
Type II Diabetes (T2D)

A17-2. Please list the principal exclusion criteria (list the most important, max 5000 characters).

Patients who are not fit or not suitable for RYGB operation, according to the MDT meeting described above.
BMI>60
Not suitable for MRI scanning (as decided by a MRI safety screening form)
Liver Cirrhosis
Type I Diabetes
Non-diabetic
Involvement in other Reserach Studies

Pregnancy is an exclusion criteria for bariatric surgery so by proxy is nd exclusion to this study

RESEARCH PROCEDURES, RISKS AND BENEFITS

A18. Give details of all non-clinical intervention(s) or procedure(s) that will be received by participants as part of the research protocol. *These include seeking consent, interviews, non-clinical observations and use of questionnaires.*

Please complete the columns for each intervention/procedure as follows:

1. Total number of interventions/procedures to be received by each participant as part of the research protocol.
2. If this intervention/procedure would be routinely given to participants as part of their care outside the research, how many of the total would be routine?
3. Average time taken per intervention/procedure (minutes, hours or days)

4. Details of who will conduct the intervention/procedure, and where it will take place.

Intervention or procedure	1	2	3	4
Consent Taking Including an explanation of the study and protocol	1	0	20mins	The Chief Investigator (or an alternative nominated colleague)
Bore Measurements, Patients will be ask to lie down and a replica of the bore will be placed over then to ensure they can fit into the scanner	1	0	5mins	The student (or an alternative nominated colleague)
Screening, including a discussion of medical background	1	0	20mins	The Student (or an alternative nominated colleague)
Booking in the first session and answering questions via phone call	1	0	30mins	The student (or an alternative nominated colleague)

A19. Give details of any clinical intervention(s) or procedure(s) to be received by participants as part of the research protocol. *These include uses of medicinal products or devices, other medical treatments or assessments, mental health interventions, imaging investigations and taking samples of human biological material. Include procedures which might be received as routine clinical care outside of the research.*

Please complete the columns for each intervention/procedure as follows:

1. Total number of interventions/procedures to be received by each participant as part of the research protocol.
2. If this intervention/procedure would be routinely given to participants as part of their care outside the research, how many of the total would be routine?
3. Average time taken per intervention/procedure (minutes, hours or days).
4. Details of who will conduct the intervention/procedure, and where it will take place.

Intervention or procedure	1	2	3	4
Magnetic Resonance Imaging/ Magnetic Resonance Spectroscopy	4	0	2h	The Student (or an other trained, nominated member of the research team) Sir Peter Mansfield imaging Centre, University of Nottingham, Main campus
Venous Blood sampling	1	1	3min	Performed by registered nurse or nominated clinical/phlebotomy representative
Mixed meal test (not for all participants) (15minute interval blood sampling via canulae)	4	0	3h	Trained Nurse (or an other trained, nominated member of the research team) Sir Peter Mansfield imaging Centre, University of Nottingham, Main campus
General examination (including assessment of height, weight, blood pressure, heart rate, cardiac and respiratory systems).	1	1	15m	Chief Investigator (or clinical fellow representative)

A21. How long do you expect each participant to be in the study in total?

Recruitment will start at 6months prior to their surgery. And So the time from recruitment/consent to the end of participation is 10months.
However, each patient will be actively involved in the study for 20weeks.

A22. What are the potential risks and burdens for research participants and how will you minimise them?

For all studies, describe any potential adverse effects, pain, discomfort, distress, intrusion, inconvenience or changes to lifestyle. Only describe risks or burdens that could occur as a result of participation in the research. Say what steps would be taken to minimise risks and burdens as far as possible.

Patients are required to attend 4 physical and 1 remote session(s) outside of their routine care. These will be 4weeks before their surgery (for the remote session) and at 2 weeks, 2days pre- and 6weeks, and 4 months post-surgery. To help with the burden of attending all these sessions we will employ flexibility (within the required time points) in arranging study dates and times with our participants, pending Scanner availability.

With respect to potential risks, the following are present but are minimal with respect to overall morbidity. Our department has experience in undertaking similar studies:

Regular sampling of venous blood will be undertaken throughout the day to assess multiple aspects of lipid/glucose metabolism. This will be done through a single venous cannulae, inserted at a peripheral site. The cannulae will be inserted with an aseptic technique by a trained member of staff. Risks include thrombophlebitis and infection. As only two cannulae are anticipated to be inserted over the course of the study, there is minimal risk of vein sclerosis. Appropriate insertion and an aseptic technique will minimise the risk of thrombophlebitis and infection.

Participants will be given a verbal and written explanation of the study requirements, with the participant providing written informed consent and completing a health screen questionnaire prior to participation.

As part of the preparation for the Mixed Meal Test, the participant will need to be fasted for a minimum of 8 hours. The burden of this will be explained to the patient and we will attempt to mitigate this by ensuring that all patients have their tests and scans performed as morning sessions. As part of recruitment, explanation as to standard practice regarding the fasting requirement will be provided to the participants before the session commences to allow adequate preparation.

MRI
The MRI scan does not emit any ionising radiation, nor it not known be harmful to the participants. Pillows and cushions may be used for comfort and holding position purposes. The participant may find the MRI to be loud however, each participant will be provided with ear plugs and headphones to help counteract the noise. Should the participant experience any discomfort or stress then the participants are able to stop and withdraw from the study at any point by pressing the safety button they are handed during the scans.

Safety screening should eliminate any risk to health for participants. The bore scanner of the MRI scan is confined and therefore, there is a possibility of a feeling of claustrophobia and associated anxiety. The time spend scanning will be kept to a minimum and participants will be regularly updated of time via intercom. Participants will be constantly monitored by at least one of the experimenters for any signs of discomfort or distress during the scan. Padding will be used to prevent holding the body in any unnatural positions. This will also prevent contact with the bore of the MRI scanner or the coils where this is not built-in.

There is a chance of an incidental finding if this is the case, the experimenters will continue with the scan and discreetly discuss with a more experienced member of the team to verify that it requires review by a clinician. If confirmed, the scans and participants information will be forwarded to the appropriate clinician for review. The clinician will the contact the participants GP if necessary. There is a further chance that a suspected finding will be clinically relevant.

A24. What is the potential for benefit to research participants?

We cannot promise the study will help you but the information we get from this study may help inform future studies and help us better understand and improve the treatment of disease. There are, however, no direct health benefits to you of taking part in this study.

RECRUITMENT AND INFORMED CONSENT

In this section we ask you to describe the recruitment procedures for the study. Please give separate details for different study groups where appropriate.

A27-1. How will potential participants, records or samples be identified? Who will carry this out and what resources will be used?*For example, identification may involve a disease register, computerised search of social care or GP records,*

or review of medical records. Indicate whether this will be done by the direct care team or by researchers acting under arrangements with the responsible care organisation(s).

Participants will be identified from the waiting list of patients undergoing bariatric surgery at Royal Derby Hospital. Identification of potential participants will be done by the usual care team, who are the clinicians involved in the routine care of these patients.

Patients will be contacted and a Participant Information Sheet (PIS) will be discussed and discuss the study in detail.

A27-2. Will the identification of potential participants involve reviewing or screening the identifiable personal information of patients, service users or any other person?

◉ Yes ○ No

Please give details below:
Chief Investigator, who is a member of the clinical team looking after the patient, and other clinical team members will identify potential participants meeting the eligibility criteria from patients that they are seeing in the clinic. Thus, whilst there will be screening of patients' identifiable data, this will be minimal and only performed by the members of the clinical team directly involved in the care of the individual.

A27-3. Describe what measures will be taken to ensure there is no breach of any duty of confidentiality owed to patients, service users or any other person in the process of identifying potential participants.*Indicate what steps have been or will be taken to inform patients and service users of the potential use of their records for this purpose. Describe the arrangements to ensure that the wishes of patients and service users regarding access to their records are respected. Please consult the guidance notes on this topic.*

Chief Investigator, who is a member of the clinical team looking after the patient, and other clinical team members will identify potential participants meeting the eligibility criteria from patients that they are seeing in the clinic. Thus, whilst there will be screening of patients' identifiable data, this will be minimal and only performed by the members of the clinical team directly involved in the care of the individual who will have seen this information even if the study did not exist.

A27-4. Will researchers or individuals other than the direct care team have access to identifiable personal information of any potential participants?

○ Yes ◉ No

A28. Will any participants be recruited by publicity through posters, leaflets, adverts or websites?

○ Yes ◉ No

A29. How and by whom will potential participants first be approached?

Approximately 6months prior to surgery – routine appointment – All Groups:
Patient who are listed for bariatric surgery will attend their ERAS (enhanced recovery after surgery) session and will be approached by a member of their main care team (who may also be a member of the research team) and will be informed of the study and their interest in partaking will be established.

A30-1. Will you obtain informed consent from or on behalf of research participants?

◉ Yes ○ No

If you will be obtaining consent from adult participants, please give details of who will take consent and how it will be done, with details of any steps to provide information (a written information sheet, videos, or interactive material). Arrangements for adults unable to consent for themselves should be described separately in Part B Section 6, and for children in Part B Section 7.

If you plan to seek informed consent from vulnerable groups, say how you will ensure that consent is voluntary and fully informed.

Details of the trial will be explained to the patient, and where appropriate, also to their relative/representative, and a Participant Information Sheet will be provided, ensuring that those involved have sufficient time to consider participating or not. The Chief Investigator/researcher/surgeon will answer any questions that the participant or their representative have concerning study participation.

The Researcher will collect informed consent from each participant before they undergo any interventions related to the study, and continuing agreement/verbal consent will be obtained from the patient prior to carrying out any study sessions. If the participant's health or cognition deteriorates and agreement to study procedures can no longer be obtained, these procedures will not be carried out. However, unless the patient (or their nominee) requests to withdraw from the study, we will continue to collect patient-related outcome data from their medical notes and analyse any blood samples that had been collected prior to the deterioration.

If you are not obtaining consent, please explain why not.

Please enclose a copy of the information sheet(s) and consent form(s).

A30-2. Will you record informed consent (or advice from consultees) in writing?

◉ Yes ○ No

A31. How long will you allow potential participants to decide whether or not to take part?

Patients will be first approached at their routine ERAS (enhanced recovery after surgery) 6 months before their surgery but we will not book in their first session until 20 weeks after that.
However, we will ask for confirmation of participation 1 week after the first contact. If they remain undecided, their details will be noted on a spreadsheet within our internal university server for later contact.

A32. Will you recruit any participants who are involved in current research or have recently been involved in any research prior to recruitment?

○ Yes
◉ No
○ Not Known

A33-1. What arrangements have been made for persons who might not adequately understand verbal explanations or written information given in English, or who have special communication needs?*(e.g. translation, use of interpreters)*

Individuals who lack the capacity to make decisions or provide informed consent will not be included in this study.

Individuals whose primary language is not English and their ability to communicate in English prevents the acquisition of informed consent will be provided with a formal hospital translator (per Royal Derby Hospital services). However, versions of the written consent form will have to be provided in their preferred non-English language, should this transpire.

A35. What steps would you take if a participant, who has given informed consent, loses capacity to consent during the study? *Tick one option only.*

○ The participant and all identifiable data or tissue collected would be withdrawn from the study. Data or tissue which is not identifiable to the research team may be retained.
◉ The participant would be withdrawn from the study. Identifiable data or tissue already collected with consent would be retained and used in the study. No further data or tissue would be collected or any other research procedures carried out on or in relation to the participant.
○ The participant would continue to be included in the study.

◯ Not applicable – informed consent will not be sought from any participants in this research.

◯ Not applicable – it is not practicable for the research team to monitor capacity and continued capacity will be assumed.

Further details:

If you plan to retain and make further use of identifiable data/tissue following loss of capacity, you should inform participants about this when seeking their consent initially.

CONFIDENTIALITY

In this section, personal data means any data relating to a participant who could potentially be identified. It includes pseudonymised data capable of being linked to a participant through a unique code number.

Storage and use of personal data during the study

A36. Will you be undertaking any of the following activities at any stage (including in the identification of potential participants)? *(Tick as appropriate)*

- ☐ Access to medical records by those outside the direct healthcare team
- ☐ Access to social care records by those outside the direct social care team
- ☑ Electronic transfer by magnetic or optical media, email or computer networks
- ☐ Sharing of personal data with other organisations
- ☐ Export of personal data outside the EEA
- ☐ Use of personal addresses, postcodes, faxes, emails or telephone numbers
- ☐ Publication of direct quotations from respondents
- ☐ Publication of data that might allow identification of individuals
- ☐ Use of audio/visual recording devices
- ☑ Storage of personal data on any of the following:
  - ☑ Manual files (includes paper or film)
  - ☐ NHS computers
  - ☐ Social Care Service computers
  - ☐ Home or other personal computers
  - ☑ University computers
  - ☐ Private company computers
  - ☐ Laptop computers

Further details:
Source data will be psuedo-anonymised, being identified by a unique code which can be traced to the individual via a name to code log. The former records will be held securely and separately to the name to code log (Study Recruitment Log).

MRI images will be identified by the patient's unique code and stored on the hard drive intrinsic to the equipment. These images will be transferred to a password protected University or NHS computer for analysis via an encrypted USB storage device. The name to code log will not be held electronically on these computers.

All Blood samples collected during the study will be identified by the participants' unique study codes and those analysing these samples will have no access to the name to number log and would have had no contact with the patients. Data generated from this sample analysis will be collated in a password protected study database for comparative analysis by members of the study team who were not involved with sample analysis.

Articles arising from the study will report only group level data; no data at the individual level, including case studies, will be presented.

A37. Please describe the physical security arrangements for storage of personal data during the study?

Electronic data will be stored within password-protected computers, present within a password-protected database (secure internal network), in the University of Nottingham's Postgraduate Centre offices.
Physical data (paperback) will be filed within locked drawers in the locked offices of the Clinical Physiology department of Royal Derby Hospital (same offices as above).
The Sir Peter Mansfield Imaging Centre enters all participant data onto a secure database, which is password protected and supported/maintained by Information Services at the University. Any paperwork, such as paper consent/screening forms are locked in fireproof cabinets with only limited people having access.

A38. How will you ensure the confidentiality of personal data?*Please provide a general statement of the policy and procedures for ensuring confidentiality, e.g. anonymisation or pseudonymisation of data.*

Each participant will be assigned a trial identity code number for use on case report forms (CRF), other trial documents and the electronic database. The documents and database will also use the study acronym and sequential study number. For example, with a hypothetical 22nd study volunteer called "John Doe", the pseudonymisation would resemble "RYGBSG22", where "RYGBSG" represents the study's abbreviations and "22" represents the volunteer's ID.

All trial staff and investigators will protect the rights of the trial's participants to privacy and informed consent in accordance with the Data Protection Act 2018. The CRF will only collect the minimum required information for the purposes of the trial. CRFs will be held securely, in a locked room, or locked cupboard or cabinet. Access to the information will be limited to the trial staff and investigators and relevant regulatory authorities. The computer-held data, including the trial database, will be held securely and will be password-protected. All data will be stored on a secure & dedicated web server. Access will be restricted by user identifiers and passwords (encrypted using a one-way encryption method)

A40. Who will have access to participants' personal data during the study? *Where access is by individuals outside the direct care team, please justify and say whether consent will be sought.*

The chief investigator and lead research member will have exclusive access to participant personal data throughout the study. This will be encrypted with password access and stored separately from other CRF's in the department. All other research members will use the anonymised unique reference number in relation to any data from the study. Written consent will be taken from all participants to grant the lead researcher access to personal data to check study protocol and administrate the study. Written consent will be taken to allow the use of anonymised data for analysis and presentation of the study in various venues. The CRF and all source documents, including progress notes and copies of laboratory and medical test results shall be made available at all times for review by the Chief Investigator, Sponsor's designee and inspection by relevant regulatory authorities (including the Department of Health).

Storage and use of data after the end of the study

A41. Where will the data generated by the study be analysed and by whom?

The data will be generated at the Sir Peter Mansfield Imaging Centre, University of Nottingham, Nottingham and Glenfield Hospital, Leicester.

The data will be analysed at both the Sir Peter Mansfield Imaging Centre based on the University of Nottingham main campus and the Clinical, Metabolic and Molecular Physiology Laboratories based in the University of Nottingham Medical School at the Royal Derby Hospital Campus.

This will be done by a member of the research team.

A42. Who will have control of and act as the custodian for the data generated by the study?

Title	Forename/Initials	Surname
Dr	Iskandar	Idris

Post	Associate Professor & Honorary Consultant in metabolic disease
Qualifications	BMedSci, BMBS, FRCP (UK), DM
Work Address	University of Nottingham Medical school Derby
Post Code	DE22 3DT
Work Email	iskandar.idris@nottingham.ac.uk
Work Telephone	01332724605
Fax	

A43. How long will personal data be stored or accessed after the study has ended?

- ○ Less than 3 months
- ○ 3 – 6 months
- ○ 6 – 12 months
- ○ 12 months – 3 years
- ◉ Over 3 years

If longer than 12 months, please justify:
Seven years, if the volunteer provides consent for this. Otherwise, it will be removed in keeping with the GDPR.

All anonymised data will be retained for 7 years after the study has been completed. To comply with regulations, the consent forms containing patient name must be retained for inspection during this time. Therefore, the name to number recruitment log will also need to be retained to facilitate this linkage. After 7 years, anonymised and patient data will be destroyed.

A44. For how long will you store research data generated by the study?

Years: 7
Months: 0

A45. Please give details of the long term arrangements for storage of research data after the study has ended.*Say where data will be stored, who will have access and the arrangements to ensure security.*

Research Code of Conduct and Research Ethics, The trial master file and trial documents held by the Chief Investigator, on behalf of the Sponsor, will be archived at a secure archive facility at the University of Nottingham. This archive shall include all trial databases and associated meta-data encryption codes. Personal data will be destroyed after it is no longer necessary to contact a participant.

In compliance with the DH Research Governance Framework guidelines, the Human Tissue Act and in accordance with the University of Nottingham Code of Research Conduct, the Chief Investigator (Dr Iskandar Idris) will maintain all records and documents of the study. These will be retained for 7 years after the study finishes. If the responsible investigator is not able to maintain the study records for this time, a second person will be nominated to take over this responsibility.

The study documents held by the Chief Investigator shall be archived at secure facilities at the University of Nottingham. This archive shall include anonymised paper records, source data and all study databases (which will be encrypted and password protected), with associated meta-data encryption codes held separately by the PIs. After the study has been completed, access to the anonymised data sets for further research purposes will be granted only after agreement from the Chief Investigators has been obtained. Only data sets from participants who have given prior

consent for their data to be used for future research purposes will be made available, and to facilitate this, a separate database will be generated which contains the anonymised data from only those who have consented to this future data use.
Where prior consent to sample storage has been obtained from participants, any relevant material will be stored under the Human Tissue act (HTA) and to comply with HTA regulations, the consent forms and name to unique study code log (containing identifiable personal data) will need to be retained and accessed by HTA inspectors. These documents will be held separately to archived anonymised data/documents and will not be accessible for those undertaking future research on the anonymised data.

INCENTIVES AND PAYMENTS

A46. Will research participants receive any payments, reimbursement of expenses or any other benefits or incentives for taking part in this research?

◉ Yes ○ No

If Yes, please give details. For monetary payments, indicate how much and on what basis this has been determined.
Volunteers will be given an inconvenience fee of £20 per in-person session in excess of usual care, totalling £80. They will also be provided with car parking vouchers. This money is to assist with expenses incurred as part of their participation such as travel expenses.

A47. Will individual researchers receive any personal payment over and above normal salary, or any other benefits or incentives, for taking part in this research?

○ Yes ◉ No

A48. Does the Chief Investigator or any other investigator/collaborator have any direct personal involvement (e.g. financial, share holding, personal relationship etc.) in the organisations sponsoring or funding the research that may give rise to a possible conflict of interest?

○ Yes ◉ No

NOTIFICATION OF OTHER PROFESSIONALS

A49-1. Will you inform the participants' General Practitioners (and/or any other health or care professional responsible for their care) that they are taking part in the study?

○ Yes ◉ No

If Yes, please enclose a copy of the information sheet/letter for the GP/health professional with a version number and date.

PUBLICATION AND DISSEMINATION

A50-1. Will the research be registered on a public database?

The UK Policy Framework for Health and Social Care Research sets out the principle of making information about research publicly available. Furthermore: Article 19 of the World Medical Association Declaration of Helsinki adopted in 2008 states that "every clinical trial must be registered on a publicly accessible database before recruitment of the first subject"; and the International Committee of Medical Journal Editors (ICMJE) will consider a clinical trial for publication only if it has been registered in an appropriate registry. Please see guidance for more information.

◉ Yes ○ No

Please give details, or justify if not registering the research.
This study will be listed on Clinicaltrials.gov.

Please ensure that you have entered registry reference number(s) in question A5-1.

A51. How do you intend to report and disseminate the results of the study?*Tick as appropriate:*

- [x] Peer reviewed scientific journals
- [x] Internal report
- [x] Conference presentation
- [x] Publication on website
- [ ] Other publication
- [ ] Submission to regulatory authorities
- [ ] Access to raw data and right to publish freely by all investigators in study or by Independent Steering Committee on behalf of all investigators
- [ ] No plans to report or disseminate the results
- [x] Other (please specify)

In addition to the above, a written report for this study will be submitted as part of the student's (Abi Spicer) Ph.D. thesis.
No patient-identifiable information will be contained within this report.

A52. If you will be using identifiable personal data, how will you ensure that anonymity will be maintained when publishing the results?

No patient-identifiable data will be contained in either the data analysis, the results, the discussion or conclusion of any written reports based on the conducted study. If sample-specific data is discussed or cited, the sample-specific code will instead be cited (e.g. "RYGBSG22" per the example cited in A38).

A53. How and when will you inform participants of the study results?

If there will be no arrangements in place to inform participants please justify this.
Patients will be informed of the study results, without any patient-specific data, per request by email.

5. Scientific and Statistical Review

A54-1. How has the scientific quality of the research been assessed?*Tick as appropriate:*

- [ ] Independent external review
- [ ] Review within a company
- [x] Review within a multi−centre research group
- [ ] Review within the Chief Investigator's institution or host organisation
- [x] Review within the research team
- [ ] Review by educational supervisor
- [ ] Other

Justify and describe the review process and outcome. If the review has been undertaken but not seen by the researcher, give details of the body which has undertaken the review:
This study has been reviewed several times since its' inception by senior members of the research team in multiple departments and institutions.

This includes the department of physics and astronomy and Medicine at the University of Nottingham and the department of Cardiovascular Science at the University of Leicester.

For all studies except non-doctoral student research, please enclose a copy of any available scientific critique reports, together with any related correspondence.

For non-doctoral student research, please enclose a copy of the assessment from your educational supervisor/ institution.

A56. How have the statistical aspects of the research been reviewed? *Tick as appropriate:*

- ☐ Review by independent statistician commissioned by funder or sponsor
- ☐ Other review by independent statistician
- ☐ Review by company statistician
- ☐ Review by a statistician within the Chief Investigator's institution
- ☐ Review by a statistician within the research team or multi−centre group
- ☑ Review by educational supervisor
- ☐ Other review by individual with relevant statistical expertise
- ☐ No review necessary as only frequencies and associations will be assessed – details of statistical input not required

In all cases please give details below of the individual responsible for reviewing the statistical aspects. If advice has been provided in confidence, give details of the department and institution concerned.

	Title	Forename/Initials	Surname
	Dr	Stephen	Bawden
Department	Physics and astronomy		
Institution	University of Nottingham		
Work Address	Sir Peter Mansfield imaging centre		
	Nottingham		
Post Code	NG7 2RD		
Telephone			
Fax			
Mobile			
E-mail	stephen.bawden@nottingham.ac.uk		

Please enclose a copy of any available comments or reports from a statistician.

A57. What is the primary outcome measure for the study?

The effects of VLCD on liver fat as measured with MRI and MRS

A58. What are the secondary outcome measures? *(if any)*

The effects of VLCD on cardiac ATP and cardiac function
The effects of VLCD on skeletal muscle, liver and pancreatic fat
The effect of Bariatric Surgery on skeletal muscle, liver and pancreatic fat.
The effects of Bariatric Surgery on Liver ATP flux.
The effects of RYGB or SG on Liver ATP and cardiac function
The effects of RYGB or SG on skeletal muscle, liver, and pancreatic fat

A59. What is the sample size for the research? *How many participants/samples/data records do you plan to study in total? If there is more than one group, please give further details below.*

Total UK sample size:	29
Total international sample size (including UK):	0
Total in European Economic Area:	0

Further details:
Participants within and around Derby and Leicester will be recruited.
23 for arm A and 6 for arm B.

A60. How was the sample size decided upon? *If a formal sample size calculation was used, indicate how this was done, giving sufficient information to justify and reproduce the calculation.*

We are aiming for 17 participants for the study for arm A. Power calculation were performed using G*power (Franz Faul, Universitat Kiel, Germany) assuming a normal distribution, with a desired power of 0.8 and $p < 0.05$.
Powering on changes due to VLCD, In Luo et al. liver fat fraction dropped from 16.6 ±7.8 to 12.7 ±6.8 in 49 patients ($P < 0.001$) (1). Assuming a normal distribution and using these values, a one-tail test would find as significant drop in a sample size of n=17.
Percentage drop out will be around 22% meaning we will need to recruit 23 patients to fulfil this target.

For arm B we are aiming for 6 patients. This is an exploratory, pilot study. No previous study has been performed. The number was based upon the judgment of clinicians due to the difficulty in recruiting patients and the limitation on their size and the time they will need to be in the scanner.

A61-1. Will participants be allocated to groups at random?

○ Yes ◉ No

A62. Please describe the methods of analysis (statistical or other appropriate methods, e.g. for qualitative research) by which the data will be evaluated to meet the study objectives.

Statistical analysis will be undertaken using SPSS (IBM Corp. IBM SPSS Statistics for Windows. Armonk, NY: IBM Corp) with a significance level of $p<0.05$. The group assignment of the data will be blinded by an independent investigator and analysed for blind review before group comparisons are made.

Primary measure:
Effects of the VLCD diet will be statistically analysed using a whole group means difference test (matched pairs t-test) for normally distributed data and Wilcoxon signed-rank test for non-normally distributed data.

Secondary Measure:
Additional effects of bariatric surgery will be statistically analysed in each group separately (SG and RYGB) using a one-way repeated measures ANOVA test. A statistically significant effect will be followed up with individual matched pair t-tests for normally distributed data and a wilcoxon sign ranked test for non-normally distributed data at each time point.

The effect of the different surgery types will be statistically analysed using a two-way repeated measures ANOVA test comparing surgery type and time. A significant interaction between surgery type and time will be followed up by an independent group t-test at each time point for normally distributed data and wilcoxon sign ranked test for non-normally distributed data.

6. MANAGEMENT OF THE RESEARCH

A63. Other key investigators/collaborators. *Please include all grant co−applicants, protocol co−authors and other key members of the Chief Investigator's team, including non-doctoral student researchers.*

	Title	Forename/Initials	Surname
	Professor	Guruprasad	Aithal
Post Qualifications	Professor of Hepatology		
Employer	University of Nottingham		
Work Address	Medical School		

	Nottingham
Post Code	NG7 2RD
Telephone	
Fax	
Mobile	
Work Email	guru.aithal@nottingham.ac.uk

Title	Forename/Initials	Surname
Dr	Iskandar	Idris

Post Qualifications	Associate Professor
Employer	University of Nottingham
Work Address	MRC Musculoskeletal Physioogy and Ageing School of Medicine, University of Nottingham Royal Derby Hospital
Post Code	DE22 3DT
Telephone	
Fax	
Mobile	
Work Email	iskandar.idris@nottingham.ac.uk

Title	Forename/Initials	Surname
Dr	Gerry	McCann

Post Qualifications	Professor of Cardiology
Employer	University of Leicester
Work Address	Glenfield Hospital Leicester
Post Code	LE3 9QP
Telephone	
Fax	
Mobile	
Work Email	gpm12@leicester.ac.uk

Title	Forename/Initials	Surname
Dr	Stephen	Bawden

Post Qualifications	Research Fellow
Employer	University of Nottingham
Work Address	Sir Peter Mansfield imaging centre Derby
Post Code	DE22 3DT
Telephone	
Fax	
Mobile	
Work Email	stephen.bawden@nottingham.ac.uk

	Title	Forename/Initials	Surname
	Dr	Bethan	Phillips
Post Qualifications	Professor		
Employer	University of Nottingham		
Work Address	MRC Musculoskeletal, Physiology and Ageing School of Medicine, University of Nottingham Royal Derby Hospital, Derby		
Post Code	DE22 3DT		
Telephone			
Fax			
Mobile			
Work Email	beth.phillips@nottingham.ac.uk		

A64. Details of research sponsor(s)

A64-1. Sponsor

Lead Sponsor

Status:
- ○ NHS or HSC care organisation
- ◉ Academic
- ○ Pharmaceutical industry
- ○ Medical device industry
- ○ Local Authority
- ○ Other social care provider (including voluntary sector or private organisation)
- ○ Other

If Other, please specify:

Commercial status: Non-Commercial

Contact person

Name of organisation	University of Nottingham
Given name	Angela
Family name	Shone
Address	Research and Innovation
Town/city	Nottingham
Post code	NG8 1DH
Country	United Kingdom
Telephone	0115 8467906
Fax	
E-mail	sponsor@nottingham.ac.uk

Legal representative for clinical investigation of medical device (studies involving Northern Ireland only)

Clinical Investigations of Medical Devices that take place in Northern Ireland must have a legal representative of the sponsor that is based in Northern Ireland or the EU

Contact person

Name of organisation
Given name
Family name
Address
Town/city
Post code
Country
Telephone
Fax
E-mail

A65. Has external funding for the research been secured?

Please tick at least one check box.

- [x] Funding secured from one or more funders
- [x] External funding application to one or more funders in progress
- [ ] No application for external funding will be made

What type of research project is this?

- ○ Standalone project
- ○ Project that is part of a programme grant
- ○ Project that is part of a Centre grant
- ◉ Project that is part of a fellowship/ personal award/ research training award
- ○ Other

Other – please state:

Please give details of funding applications.

Organisation	Medical Research Council
Address	Polaris House North Star Avenue Swindon
Post Code	SN2 1FL
Telephone	01793 416200
Fax	
Mobile	
Email	corporate@mrc.ukri.org

Funding Application Status: ◉ Secured ○ In progress

Amount: £8'750

Duration
Years: 3
Months: 6

If applicable, please specify the programme/ funding stream:

What is the funding stream/ programme for this research project?
PhD studentship

Organisation University of Nottingham
Address Research and Innovation

Post Code NG8 1DH
Telephone
Fax
Mobile
Email sponsor@nottingham.ac.uk

Funding Application Status: (•) Secured ( ) In progress

Amount: £8'750

Duration
Years: 3
Months: 6

If applicable, please specify the programme/ funding stream:

What is the funding stream/ programme for this research project?
PhD Studentship

Organisation Biomedical Research Council
Address Queens Medical centre nottingham

Post Code NG7 2UH
Telephone
Fax
Mobile
Email

Funding Application Status: (•) Secured ( ) In progress

Amount: £25'000

Duration
Years: 1
Months: 4

If applicable, please specify the programme/ funding stream:

What is the funding stream/ programme for this research project?

GI and Liver Theme

A66. Has responsibility for any specific research activities or procedures been delegated to a subcontractor (other than a co-sponsor listed in A64-1) ? *Please give details of subcontractors if applicable.*

○ Yes ◉ No

A67. Has this or a similar application been previously rejected by a Research Ethics Committee in the UK or another country?

○ Yes ◉ No

Please provide a copy of the unfavourable opinion letter(s). You should explain in your answer to question A6-2 how the reasons for the unfavourable opinion have been addressed in this application.

A68-1. Give details of the lead NHS R&D contact for this research:

	Title	Forename/Initials	Surname
		Teresa	Grieve
Organisation	University of Nottingham Medical School at Derby		
Address	Research and Development		
	Derby Hospitals NHS Foundation Trust		
	Royal Derby Hospital		
Post Code	DE22 3DT		
Work Email	dhft.researchgov@nhs.net		
Telephone	01332724710		
Fax			
Mobile			

Details can be obtained from the NHS R&D Forum website: http://www.rdforum.nhs.uk

A69-1. How long do you expect the study to last in the UK?

Planned start date: 01/12/2021
Planned end date: 31/12/2023
Total duration:
Years: 2 Months: 0 Days: 31

A70.

Definition of the end of trial, and justification in the case where it is not the last visit of the last subject undergoing the trial

The end of the study will be 16 weeks after the final study session of the last participant. This is to allow for all samples collected to be analysed and disposed of.

A71-1. Is this study?

○ Single centre
◉ Multicentre

A71-2. Where will the research take place? *(Tick as appropriate)*

- [x] England
- [ ] Scotland
- [ ] Wales
- [ ] Northern Ireland
- [ ] Other countries in European Economic Area

Total UK sites in study 2

Does this trial involve countries outside the EU?

○ Yes ◉ No

A72. Which organisations in the UK will host the research?*Please indicate the type of organisation by ticking the box and give approximate numbers if known:*

☐ NHS organisations in England	
☐ NHS organisations in Wales	
☐ NHS organisations in Scotland	
☐ HSC organisations in Northern Ireland	
☐ GP practices in England	
☐ GP practices in Wales	
☐ GP practices in Scotland	
☐ GP practices in Northern Ireland	
☐ Joint health and social care agencies (eg community mental health teams)	
☐ Local authorities	
☐ Phase 1 trial units	
☐ Prison establishments	
☐ Probation areas	
☐ Independent (private or voluntary sector) organisations	
☑ Educational establishments	1
☐ Independent research units	
☑ Other (give details)	1
PIC Site	
Total UK sites in study:	2

A73-1. Will potential participants be identified through any organisations other than the research sites listed above?

◉ Yes ○ No

A73-2. If yes, will any of these organisations be NHS organisations?

◉ Yes ○ No

If yes, details should be given in Part C.

A73-3. Approximately how much time will these organisations expect to spend on screening records and/or provision of information to potential participants, and how will the costs of these activities be funded?

Approximately 1-2 hours per week, however, the staff at Royal Derby Hospital involved in the projects hold contracts with the University of Nottingham and so their time is covered by this.

A76. Insurance/ indemnity to meet potential legal liabilities

***Note:* in this question to NHS indemnity schemes include equivalent schemes provided by Health and Social Care (HSC) in Northern Ireland**

A76-1. What arrangements will be made for insurance and/or indemnity to meet the potential legal liability of the sponsor(s) for harm to participants arising from the management of the research? *Please tick box(es) as applicable.*

Note: Where a NHS organisation has agreed to act as sponsor or co-sponsor, indemnity is provided through NHS schemes. Indicate if this applies (there is no need to provide documentary evidence). For all other sponsors, please describe the arrangements and provide evidence.

☐ NHS indemnity scheme will apply (NHS sponsors only)

☑ Other insurance or indemnity arrangements will apply (give details below)

The University of Nottingham as research Sponsor indemnifies its staff with both public liability insurance and clinical trials insurance in respect of claims made by research subjects.

Please enclose a copy of relevant documents.

A76-2. What arrangements will be made for insurance and/ or indemnity to meet the potential legal liability of the sponsor(s) or employer(s) for harm to participants arising from the design of the research? *Please tick box(es) as applicable.*

Note: Where researchers with substantive NHS employment contracts have designed the research, indemnity is provided through NHS schemes. Indicate if this applies (there is no need to provide documentary evidence). For other protocol authors (e.g. company employees, university members), please describe the arrangements and provide evidence.

☐ NHS indemnity scheme will apply (protocol authors with NHS contracts only)

☑ Other insurance or indemnity arrangements will apply (give details below)

The University of Nottingham as research Sponsor indemnifies its staff with both public liability insurance and clinical trials insurance in respect of claims made by research subjects.

Please enclose a copy of relevant documents.

A76-3. What arrangements will be made for insurance and/ or indemnity to meet the potential legal liability of investigators/collaborators arising from harm to participants in the conduct of the research?

Note: Where the participants are NHS patients, indemnity is provided through the NHS schemes or through professional indemnity. Indicate if this applies to the whole study (there is no need to provide documentary evidence). Where non-NHS sites are to be included in the research, including private practices, please describe the arrangements which will be made at these sites and provide evidence.

☐ NHS indemnity scheme or professional indemnity will apply (participants recruited at NHS sites only)

☑ Research includes non-NHS sites (give details of insurance/ indemnity arrangements for these sites below)

The University of Nottingham as research Sponsor indemnifies its staff with both public liability insurance and clinical trials insurance in respect of claims made by research subjects.

Please enclose a copy of relevant documents.

A78. Could the research lead to the development of a new product/process or the generation of intellectual property?

◯ Yes ◉ No ◯ Not sure

9. Has the study been the subject of a scientific review/opinion (Expert Panel)?

◯ Yes ◉ No

If yes, please provide a copy of the review as part of your application.

Part B: Section 5 – Use of newly obtained human tissue(or other human biological materials) for research purposes

1. What types of human tissue or other biological material will be included in the study?

Blood Samples

2. Who will collect the samples?

Samples will be collected by a trained member of staff who is assisting the research team.

3. Who will the samples be removed from?

- [x] Living donors
- [ ] The deceased

4. Will informed consent be obtained from living donors for use of the samples? *Please tick as appropriate*

In this research?

(●) Yes ( ) No

In future research?

( ) Yes (●) No ( ) Not applicable

If answering No in either case, please justify:

We do not intent to use the samples in future research and so consent will not be taken for such circumstance.

6. Will any tissues or cells be used for human application or to carry out testing for human application in this research?

( ) Yes (●) No

8. Will the samples be stored: *[Tick as appropriate]*

In fully anonymised form? *(link to donor broken)*

( ) Yes (●) No

In linked anonymised form? *(linked to stored tissue but donor not identifiable to researchers)*

(●) Yes ( ) No

If Yes, say who will have access to the code and personal information about the donor.

The Chief investigator will retain the linkage of the participant name to the unique study code, but this information will not be available to researchers carrying out the analysis.

In a form in which the donor could be identifiable to researchers?

( ) Yes (●) No

9. What types of test or analysis will be carried out on the samples?

Plasma Glucagon, Ghrelin, Glucose and GLP-1, and serum Insulin and C-peptide will be measured using Multiplex ELISA technique.

10. Will the research involve the analysis or use of human DNA in the samples?

○ Yes ◉ No

11. Is it possible that the research could produce findings of clinical significance for donors or their relatives?

○ Yes ◉ No

12. If so, will arrangements be made to notify the individuals concerned?

○ Yes ○ No ◉ Not applicable

13. Give details of where the samples will be stored, who will have access and the custodial arrangements.

The blood samples will be walked to a lab close to the clinical room withing the SPMIC. By the end of the following working day after the study day the samples will be transferred to the Queens Medical Centre, medical school to be stored at -80°C freezer on D floor of the which is locked & alarmed with CO2 back up.

The samples will be transferred to Royal Derby Hospital for analysis after all data collection has been completed. Samples will be removed from the -80°C freezer and couriered in a labelled igloo containing dry ice. The shipment will contain a complete inventory of all samples, along with the name of the person responsible for sending and receiving the samples.

Samples will be stored in a linked anonymised format and labelled using a combination of study reference, unique study identifier and cross referenced with location code numbers to permit accurate linkage to study data and the consent form (as per Human Tissue Act requirement). Samples for NHS pathology analysis will be labelled in accordance with local NHS procedures. All blood samples will be stored in aliquots in -80 degrees' centigrade freezer in our department of Metabolic & Molecular Physiology, University of Nottingham, Derby.
The master database will be held by the primary researcher (in a password encrypted file.
The analysis of samples will take place at the University of Nottingham (Derby) within the Department of Metabolic & Molecular Physiology.

Once Analysis is complete samples will be destroyed in accordance with the Human Tissue Act, 2004.

14. What will happen to the samples at the end of the research? *Please tick all that apply and give further details.*

☐ Transfer to research tissue bank

(If the bank is in England, Wales or Northern Ireland the institution will require a licence from the Human Tissue Authority to store relevant material for possible further research.)

☐ Storage by research team pending ethical approval for use in another project

(Unless the researcher's institution holds a storage licence from the Human Tissue Authority, or the tissue is stored in Scotland, or it is not relevant material, a further application for ethical review should be submitted before the end of this project.)

☐ Storage by research team as part of a new research tissue bank

(The institution will require a licence from the Human Tissue Authority if the bank will be storing relevant material in England, Wales or Northern Ireland. A separate application for ethical review of the tissue bank may also be submitted.)

☐ Storage by research team of biological material which is not "relevant material" for the purposes of the Human Tissue Act

- [x] Disposal in accordance with the Human Tissue Authority's Code of Practice
- [ ] Other
- [ ] Not yet known

Please give further details of the proposed arrangements:

Once all study-related analysis on the blood samples have been completed, they will be disposed of in accordance with the Human Tissue Act, 2004.

PART C: Overview of research sites

Please enter details of the host organisations (Local Authority, NHS or other) in the UK that will be responsible for the research sites. *For further information please refer to guidance.*

Investigator identifier	Research site	Investigator Name
IN2	○ NHS/HSC Site ◉ Non-NHS/HSC Site	Forename: Penny Middle name: Family name: Gowland Email: Penny.gowlang@nottingham.ac.uk Qualification (MD...): PhD Country: United Kingdom

Institution name: University of Nottingham
Department name: Physics
Street address: Sir Peter Mansfield imaging centre
Town/city: Nottingham
Post Code: NG7 2RD
Country: United Kingdom

Participant Identification Centres

PIC Type	Centre	Individual(s)
◉ NHS (England) ○ NHS (outside England) ○ Non-NHS	UNIVERSITY HOSPITALS OF DERBY AND BURTON NHS FOUNDATION TRUST	Iskandar Idris E-mail: iskandar.idris@nottingham.ac.uk